
Bridging the scales: model-driven integrative interpretation of archaeological and geophysical data.

Dissertation

zur Erlangung des Doktorgrades

der Mathematisch-Naturwissenschaftlichen Fakultät
Der Christian-Albrechts-Universität zu Kiel

Vorgelegt von
Erica Corradini

Kiel
Im Juni 2020

Referent:
Koreferent:
Tag der mündlichen Prüfung:

Prof. Dr. Wolfgang Rabbel
Prof. Dr. Berit Valentin Eriksen
05-10-2020

to my family

Zusammenfassung

Die geophysikalische Prospektion in Mooregebieten wird wegen der kritischen, instabilen Umgebung und des reichhaltigen, kulturellen Erbes häufig diskutiert. Im Rahmen des interdisziplinären Sonderforschungsbereiches (SFB)1266 'TransformationsDimensionen' befasst sich die vorliegende Dissertation mit der Rekonstruktion der prähistorischen Landschaftstransformation zur Zeit der menschlichen Besiedlung. Das Ziel ist, das Potential konventioneller, geophysikalischer Vermessungsmethoden (spezifischer Widerstand, Bodenradar und Seismik) als Werkzeug für die Standortsuche und Landschaftsuntersuchung in Mooren zu untersuchen. Es werden zwei Fallstudien vorgestellt, in denen multi-geophysikalische Untersuchungen durchgeführt und durch archäologische Ausgrabungen und stratigraphische Informationen validiert wurden.

Toteislöcher sind Reliquien der Eisschmelze in ehemaligen Gletscherlandschaften, welche heute insbesondere in Südsandinavien und Norddeutschland verbreitet sind. Im Jahr 2017 führte das Horsens Museum (Dänemark) in Tyrsted eine Rettungsgrabung an einigen Toteislöcher durch. Diese Ausgrabung zeigte eine Feuer Steinansammlung und ein bearbeitetes Rentiergeweih aus der spät paläolithischen Bromme Kultur (12.000-11.000 BCE). Bis heute ist das Inventar der organischen Artefakte aus der Bromme Kultur wegen des Mangels an organischen Überresten und des allgemeinen Mangels an stratigraphischen Beobachtungen weitgehend unbekannt. Die verfügbaren Daten konzentrieren sich auf die Chronozonen des (späten) Allerød und der frühen jüngeren Dryas, aber leider sind die meisten dieser Datierungen nur vorläufig. Daher ist diese Verbindung in einem späten Gletscher Horizont bei Tyrsted einzigartig und hat das Potenzial, neue Informationen in der aktuellen archäologischen Debatte zu liefern. Im Rahmen dieser Arbeit wurde ein kleines Toteisloch (Standort 8) mit Bodenradar, elektromagnetischer Induktion und Geoelektrik untersucht, um die Ausdehnung des Merkmals abzuschätzen. Scherwellenreflexion und Refraktionsseismik konnten die gesamte Form und das Bodensediment des ehemaligen Sees erfassen. Außerdem wurde ein seismischer Reflektor sichtbar, der mit dem Übergang zwischen den Sedimenten des Allerød und der jüngeren Dryas in Verbindung gebracht werden kann. Die Erkennung des Bromme-Horizontes ist so möglich. Im Anschluss an die nicht-invasive Untersuchung wurde ein Ort für eine offene Ausgrabung ausgewählt, um die geophysikalischen Ergebnisse zu validieren und einen direkten Vergleich mit der Stratigraphie zu ermöglichen. Diese Ergebnisse erlauben es den Archäologen, wichtige Ausgrabungsgebiete zu identifizieren. Sie können sich auf die Untersuchung der Sedimentschichten des Allerød und der jüngeren Dryas konzentrieren, um die bisher gesammelten Datierung Informationen über den Bromme-Horizont zu verbessern.

An der mesolithischen Jäger-Sammler-Siedlung von Duvensee (10000-6500 BCE) wurde ebenfalls eine multi-methodologische Untersuchung durchgeführt, um die ehemalige Landschaft während der menschlichen Besiedlung zu rekonstruieren. Bodenradar, Geoelektrik und Seismik wurden zusammen mit Kernbohrungen, DP-EC logs und Bodenanalysen durchgeführt. Es stellte sich heraus, dass jede dieser Methoden in der Lage ist, zwischen Sedimenten mit unterschiedlicher Korngröße zu unterscheiden, insbesondere zwischen Torf, Seesedimenten (Gyttjas und Ton) und basalen Gletschersandablagerungen. Bodenradar lieferte zudem den Standort von fünf ehemaligen, kleinen Sandhügeln, welche Inseln im prähistorischen See bildeten. Auf diesen Inseln wurden Ansammlungen von mesolithischen Lagern gefunden. In dieser Arbeit werden Tiefenkarten der drei wichtigsten Grenzflächen der Sedimentfazies sowie ein 3D-Modell der zeitlichen Entwicklung des Duvensee-Moores, das mit dem zeitlichen Muster der

früheren archäologischen Funde übereinstimmt, präsentiert Bodenradar ist sogar in der Lage, zwischen stark und wenig zersetzten Torf schichten zu trennen, was auch unter Berücksichtigung von Widerstandsveränderungen bei der ERT-Computation deutlich wird. Für jedes Sediment wurden Werte bezüglich des spezifischen elektrischen Widerstands, der dielektrischen Permittivität und der Scherwellengeschwindigkeit bestimmt, die zu Verfügung stehen, um die Untersuchung von Feuchtgebieten zu erweitern und zu verbessern. Seismische Geschwindigkeiten können mit Porosität und Permeabilität korreliert werden. Sowohl die in dieser Studie vorgestellten geophysikalischen Messungen als auch die Sedimentanalysen können nützlich sein, um die Akkumulation von Seesedimenten in Feuchtgebieten abzubilden. Diese Studie leistet somit einen Beitrag zur aktuellen Debatte um Feuchtgebiets- und Kulturerbe management.

Die vorliegende Dissertation kommt zu dem Schluss, dass die geophysikalische Prospektion zur Moorgebiet Archäologie als Instrument zur Standorterkennung und Landschaftsinterpretation beiträgt. Zukünftige Forschungen sollten darauf abzielen, unser Verständnis der Beziehung zwischen den Eigenschaften des Moorbodens und deren geophysikalischer Reaktion weiter zu verbessern sowie ein umfassenderes Programm von geophysikalischen Prospektionen, interdisziplinären Feldarbeiten und archäologischen Interpretationen zu fördern.

Abstract

Geophysical prospecting in wetland environments is continuously under debate because of the critical unstable environment, but at the same time the richness in cultural heritage. This thesis is part of the interdisciplinary project SFB 1266 of the CRC 'Scales of transformation' at Kiel University, which focuses on reconstructing the prehistoric landscape transformation during human occupation. It aims to examine the potential for conventional geophysical survey methods (resistivity, ground penetrating radar and seismics) as site prospection and landscape investigation tools in peatland environments. Two case studies are presented in which multi-geophysical investigations have been performed and validated by archaeological excavations and stratigraphic information.

Kettle holes are common ice decay features in formerly glacial landscapes like those in Southern Scandinavia and Northern Germany. In 2017 the Horsens Museum (Denmark) carried out a rescue excavation at Tyrsted which revealed Late Palaeolithic flint of the Bromme type (12.000-11.000 BCE) and worked reindeer antlers. Nowadays, the organic artefact inventory from the Bromme culture is largely unknown due to the scarcity of organic remains and the general lack of proper stratigraphic observations. The available dates concentrate in the (late) Allerød and early Younger Dryas chronozones, but unfortunately most of these dating are tentative only. Therefore, this connection in a Late Glacial horizon at Tyrsted is unique and it has the potential to provide new information in the current archaeological debate. The aim is to investigate a small kettle hole (site 8) using ground penetrating radar (GPR), electromagnetic induction (EMI) and electrical resistivity tomography (ERT) to estimate the extension of the feature. Shear wave reflection and refraction seismics (SH Seismics) were able to detect the whole shape and the bottom sediment of the former lake. Furthermore a seismic event is visible which can be associated to the transition between the Allerød and Younger Dryas sediment making the detection of the Bromme horizon possible. After the non invasive investigation, a location for an open excavation has been chosen in a way to groundtruth the geophysical results allowing the direct comparison with the stratigraphy. These results allow the archaeologists to identify key excavation areas focused on the investigation of the Allerød and Younger Dryas layers in a way to improve the dating information about the Bromme horizon collected so far.

At the Mesolithic hunter-gatherers site of Duvensee (10000-6500 BCE) a multi methodological investigation has been carried out too, aiming to reconstruct the ancient landscape during human occupation. GPR, ERT and SH-Seismic have been performed together with corings, DP-EC logs and soil analyses as well for ground-truthing. It turned out that each method is able to distinguish between sediments that differ in grain size, in particular between peat, lake sediment (gyttjas and clay) and basal glacial sand deposits. GPR delivered the location of five former small sand hills that formed islands in the prehistoric lake where clusters of Mesolithic camps have been found. This study delivers depth maps of the three most important sedimentary facies interfaces and a 3D model of the spatio-temporal development of the Duvensee bog which agrees with the spatio-temporal pattern of the previous archaeological finds. GPR is even able to separate between high and low decomposed peat layers which is also clear considering resistivity variations in the ERT computation. From the association between geophysical properties and soil analyses (e.g. water content and organic matter) different gyttjas were distinguished and seismic velocity was correlated to bulk density. Values concerning electrical resistivity, dielectric permittivity, and shear

wave velocity have been determined for each sediment and are therefore available to complete and improve the investigation of wetland environments. Both geophysical measurements and sediment analyses presented in this study can finally be useful to map lake sediments in wetland environments offering a potential to shape the common debate regarding wetland heritage management.

This thesis concludes that geophysical prospection contributes to wetland archaeology as a tool for site detection and landscape interpretation. Future research should aim to further our understanding of the relationship between geophysical response and peatland soil properties, alongside a more extensive program of surveys and ground-truthing work to improve survey methodologies and archaeological interpretations.

Contents

1. Introduction	3
1.1 Motivation and objective.....	3
1.2 Archaeo-Geophysics in wetlands	5
1.3 Interpretation of the surveys based on ground-truthing	7
1.4 Structure of the thesis	8
2. Publications	10
2.1 List of publications.....	10
2.2 Contributions.....	10
2.3 Other Contributions.....	11
3. Summary and conclusions	13
4. Outlook	15
4.1 Ideas for Tyrsted	15
4.2 Ideas for Duvensee.....	16
4.2.1 Detecting roasting hearths	16
4.2.2 Quantitative interpretation with a priori information.....	17
4.2.3 Ameliorating the methodology	18
5. Publications	27
A.1 Paper I.....	29
A.2 Paper II	71
A.3 Paper III.....	87

Chapter 1

Introduction

1.1 Motivation and objective

From prehistoric to historic times wetland margins, lake shorelines, kettle holes and coasts are important zones in geoarchaeological research (Brown, 1997; Utsi, 2004) in particular because of the excellent anaerobic preservation conditions for palaeoecological proxy-parameters, archaeological remnants and organic compounds (Menotti and O'Sullivan, 2013).

Wetland environments have frequently been exploited by humans; some wetlands are incredibly rich in natural resources, home to a myriad of plant and animal species that would have been very useful to Palaeolithic, Mesolithic hunter-gatherers groups and all communities that have followed.

The Late Palaeolithic and the Mesolithic are two archaeological periods divided by the onset of warmer climatic conditions at the start of the interglacial, 11,700 years ago. These two cultural periods would have witnessed modifications in the vegetation composition and structure against a background of climatic amelioration and short-term climatic variability. The interaction between Late Palaeolithic and Mesolithic groups and the environment is inadequately understood in northern Europe, and could have included exploitation of specific species and landscape modification.

However, the Late Glacial period is characterized by extremely rare human traces (Borup and Nielsen, 2017; Eriksen et al., 2018) compared with the very rich finds from the Mesolithic and onwards (Clarke et al., 1999; Conneller, 2004; Utsi, 2004; Bokelmann, 2012; Groß et al., 2018).

For example, throughout southern Scandinavia, Late Palaeolithic finds are almost exclusively known in the form of lithic inventories, many of which come from sites lacking a proper stratigraphy. Thus, the organic artefact inventory from the Bromme culture is largely unknown and the absolute dating of this culture is a research desideratum (Eriksen, 2002).

In Mesolithic contexts there is evidence for hunting and fishing, such as arrow points and bows; structures like fireplaces, tools, and other, more ritual aspects of human interaction with the landscape from the United Kingdom (Clarke et al., 1999; Utsi, 2004; Conneller, 2004) to northern Germany (Van de Noort & O'Sullivan, 2006; Groß et al., 2018; Groß et al., 2019).

The problem is that most of these finds only come to light as they are being destroyed, as chance finds during extraction operations, rescue excavations or amatorial research. These sites are largely invisible to conventional prospection techniques such as fieldwalking, aerial photography, and topographical survey.

On dryland sites, the first step in preserving and investigating the Archaeological Heritage is to apply non-destructive methods wherever possible (Tricks et al., 2018). Geophysical surveys can indeed reveal

location, geometry and physical properties of archaeological features invisible at the surface, helping to place them within a landscape context (Gaffney and Gater, 2003).

However, wetlands geophysical surveys present some complications that are caused by difficult exploration conditions, e.g. water inflow or the groundwater impact (Doran, 2013), which can be highly expensive and time consuming. Today, systematic corings followed by test pits, is the most common procedure used in archaeology. However, an initial phase with a systematic mapping of the subsoil would help the researcher to focus the following phases with corings and excavations. This leads to the main objective of this thesis: the development of a geophysical survey methodology for investigating wetland environments carrying an archaeological background.

This thesis tries to deconstruct some of the preconceptions about the ‘impossibility’ of wetland geophysical survey, and suggests that geophysical prospection might also be a useful tool in helping wetland archaeology answering major criticisms that have emerged in the last 15 years.

Geophysical prospection may have a key role as a site and landscape investigation tool in wetland archaeology, but only if it can meet the challenges that peatland environments pose. As mentioned above the archaeological remains, correlated with Palaeolithic and Mesolithic contexts, are of the order of a few centimeters in size which is often less than the resolution of the most commonly applied geophysical methods. A focused investigation of these features is almost impossible.

Palaeoenvironmental reconstruction of wetland development is therefore, the most important tool that geoarchaeologists own to understand human occupation during the late Glacial periods and the Mesolithic. This investigation depends, critically, on knowledge of the peatland stratigraphy including the thickness of the peat deposit, within-peat layering and the underlying lake sediments (gyttja). Depending on the site conditions, peats and gyttjas can vary in their organic matter and this factor may thus influence the mechanical and hydrological properties (Becker et al., 2004). Within the peat deposits, the degree of decomposition has an influence too, organic matter content decreases and bulk density increases with the degree of decomposition (Heller and Zeitz, 2012). The understanding of these characteristics is also important for figuring out how well preserved the layers are.

This leads to the second objective of this thesis, which is to present two case studies that show how a multimethod approach is used to reconstruct ancient landscapes to identify possible locations for human activities. We investigated a small kettle hole at Tyrsted, south of Horsens (Denmark) with the aim to determine the extension and depth of this feature using geophysical methods (Corradini et al., in review). A former excavation at Tyrsted at a neighboring site revealed Late Palaeolithic flint of the Bromme type and worked reindeer antlers (Borup and Nielsen, 2017; Eriksen et al., 2018). This connection in a Late Glacial horizon is unique not only in a Danish context and it can help to improve and clarify the dating of the Bromme culture. The second investigated site is the early Mesolithic camp-site at ancient lake Duvensee, schleswig-Holstein (Germany) (Bokelmann, 2012; Groß et al., 2018). This area is very well known and several geoarchaeological research has been conducted in the past 100 years providing 23 different locations of Early Mesolithic hunter-gatherer groups and Neolithic farmers located on small sand banks that formed multiple islands (called islets by K. Bokelmann) in the prehistoric lake (Corradini et al., 2020; Corradini et. al., submitted).

We show how different methods image the stratigraphy of former lakes and identify key targets for further test excavations. Moreover we illustrate how a three-dimensional reconstruction of the investigated area

can help to elucidate where hunter-gatherers could settle and move from a location to another, following the shorelines of an overgrowing lake. Moreover, integrating geophysical measurements with corings and soil analysis allows a differentiation within the same sediment: high and low degraded peat, fine and coarse detritus gyttja, for instance.

Synthetically, this thesis examines four different research questions in the context of a landscape reconstruction using multi method geophysical surveys in wetland environments. Besides the methodical geophysical aspect each question aspire to bring new knowledge for the archaeological research:

- How can we provide a stratigraphic description of a kettle hole using non-invasive methods? Are we able to identify the depth of the Bromme horizon using geophysical methods on a way to plan further test excavations?
- Can we reconstruct the landscape to identify the location of five former islands with Mesolithic camps using geophysical investigation at ancient lake Duvensee (Germany)? Can we understand how people moved through those islands during the Mesolithic?
- How can we map the main stratigraphic units filling the ancient lake Duvensee for a better understanding of the former basin evolution? Under which conditions can we identify peat and gyttja layers in terms of geophysical parameters (e.g. electric resistivity, shear wave velocity and dielectric permittivity)?
- How suitable are GPR, ERT and SH-wave seismics to detect peat properties, paying particular attention to the identification of different gyttja layers and different degrees of peat decomposition?

Beside these research questions the geophysical properties have been analyzed and compared with soil parameters to understand if they are correlated and therefore possible to differentiate.

For palaeoenvironmental researchers or archaeologists with limited time and budget for conducting extended drilling campaigns, this study provides a very important planning tool for future investigations. A further aim of this research is to make the researchers able to map large areas with geophysical surveys, enabling the geoarchaeologist to reduce the time consuming drilling procedure. The direction would be using geophysics in a way to extrapolate the coring results from single point to large areas. However, the comparison with corings will be always necessary because of the site-specific conditions which affect these kinds of environments.

And most importantly, this prospective will enable the archaeological and palaeoenvironmental research groups to reconstruct palaeolandscapes and to identify possible areas of interest.

1.2 Archaeo-Geophysics in wetlands

Gaffney and Gater define archaeological geophysical survey as ‘The examination of the Earth’s physical properties using non-intrusive ground survey techniques to reveal buried archaeological sites, features and landscapes’.

Archaeological geophysics typically makes use of the following techniques; magnetometry, electrical resistivity tomography (ERT), ground penetrating radar (GPR), and electromagnetic surveys (EMI). Less frequently, and usually in response to specific issues or environments, seismics might be employed too, and has lately been intensified (Stümpel et al., 1988; Gaffney & Gater, 1993; Rabbel et al., 2004; Wunderlich et al., 2015; Schwardt et al., 2020; Corradini et al, in review).

A surprisingly large number of people besides archaeologists are interested in peat environments. Engineers need to know how it behaves for construction projects, like oil pipelines (Jol & Smith 1995); ecologists need to examine the nutrient loadings and hydrology (Comas et al., 2004) and they have been using geophysical means to investigate these environments for some time, principally GPR and ERT though with some seismic work as well (Theimer et al., 1994; Plets et al., 2007).

Despite the interest in investigating these kinds of environments, there is a general scepticism in the academic and commercial archaeological community about the usefulness of geophysics in wetland archaeology (Milton, 2018).

The nature of the deposits themselves also makes surveys difficult. They are wet and not magnetically enhanced (Thompson & Oldfield, 1986; Weston, 2004). Contrasts, in physical and chemical terms, between the waterlogged archaeology (where the targets are wooden structures, for example), and the waterlogged peat are very low, potentially outside the limits of detection for current equipment. There are also very few recorded uses of EMI surveys in these environments.

The numerous studies carried out in different bogs and peatland show the potential of geophysics, but no general trend or rules have been established.

Ground penetrating radar (GPR) has been widely used to analyze peat deposits (Warner et al. 1990; Theimer et al., 1994; Slater and Reeve, 2002; Comas et al, 2005; Persico et. al., 2010; Corradini et al., 2020) providing strong reflections for excellent geophysical imaging (Lowry et al. 2009). Moreover, several studies have related peat internal reflections to layers of different decomposition-degree, different peat types or pieces of wood (Warner et al. 1990; Slater and Reeve, 2002; Comas et al., 2015). The same is observed, if we consider the interfaces between peat and gyttja layers. Comas et al. (2004) for instance, illustrated a distinction between peat and organic gyttja layer, whereas Plado et al. (2011) could not. A few researchers have trialled GPR in wetlands, usually prospecting for prehistoric wooden trackways known to lie beneath the peat (Clarke et al., 1999; Utsi, 2003; Utsi, 2004) but varying degrees of success are claimed for these surveys also because of the resolution between the methods and the investigated features.

ERT and seismic measurements have been applied in such environments less frequently although both methods may deliver important complementary information. Electric resistivity profiling can assist peatland studies as it can provide stratigraphic information from beneath the mineral soil contact (Theimer et al., 1994; Slater and Reeve, 2002). However, little is known still about the relationship between electrical conductivity (which is the reverse of resistivity) and peat properties in differing site conditions (Walter et al., 2016). Comas et al. (2004) and Walter et al. (2015) found that the total amount of solutes in the pore fluid and the cation exchange capacity are the most appropriate properties to describe electrical conductivity of poorly decomposed *Sphagnum* peat. Moreover, they claim that water content and cation exchange capacity are mainly correlated with electrical conductivity.

Although SH-wave sounding can identify and differentiate soft soils such as fine grained lake sediments or swampy organic deposits (Corradini et al., in review), this method is even less applied than ERT in these

environments. It is directly sensitive to the rigidity of soil layers and capable of resolving stratigraphic interfaces at much larger depths than GPR (Wunderlich et al., 2018; Lamair, 2019).

The geophysical surveys presented in this thesis can make contributions to the understanding of archaeological sites, particularly by contextualising them, both in a wider landscape. Very few of previous surveys in wetlands have employed more than one technique to the same area, making it hard to comparatively evaluate the results produced. We propose, therefore a methodology in surveying these environments, which can be developed for future investigations. Furthermore, the case studies show the benefits of using multiple techniques, and the key role ground truthing has to play.

1.3 Interpretation of the surveys based on ground-truthing

The investigation of peatland stratigraphy by geoarchaeological surveys in wetlands, require integrated multidisciplinary and scale overlapping approaches including surveys and geophysical prospecting, as well as medium-, small- and micro-scale drilling campaigns and excavations to ground truth the results (Comas et al., 2005; Hadler et al., 2018; Zielhofer et al., 2018).

In this context, the calibration of geophysical data by stratigraphic information deduced from outcrops or sediment cores is an important component of data interpretation (Fischer et al, 2016; Wunderlich et al., 2018).

Drilling as well as EC-DP logging provide detailed information about the vertical stratigraphy but usually with a low lateral sampling density due to the time consuming character of this method. Additionally, inter-drilling point sections have to be interpolated, resulting in an unknown uncertainty about small-scale changes in the stratigraphy. This disadvantage can be improved by combining drilling with non-invasive geophysical methods, ground penetrating radar (GPR), electrical resistivity tomography (ERT) and SH-wave seismics, which allow a laterally continuous mapping of the lithological change (Corradini et al., in review; Wunderlich et al., 2018). To improve the results, a comparison with stratigraphic information is needed. Therefore, we can improve the geophysical outputs by constraining the computation with depth information from drillings (Fischer et al., 2016; Wunderlich et al., 2018).

The waterlogged nature of wetland environments can also create some problems with excavations and drillings. Therefore, geophysical mapping of the subsurface soil is the first step in evaluating focused ground truthing operations.

For the presented case studies, corings were conducted using an Usinger piston corer (Mingram et al., 2007), proceeding with 1 m increments. This methodology produces compaction of the organic sediments (peat in particular) in the first meter below the surface. Sedimentary units with a distinct minerogenic or calcareous component are only marginally affected. Understandably, sediment compression affects the measurements of stratigraphic transitions and the estimation of the compression is important also for ground truthing. This thesis presents also an attempt to determine the compaction of the peat depending on the degree of decomposition by comparing the GPR reflections depth with the coring information (Corradini et al., submitted).

1.4 Structure of the thesis

The thesis presents the following structure: first the two site-specific landscape reconstructions using geophysical methods are described.

I first introduce the kettle hole reconstruction at the Palaeolithic site of Tyrsted (Denmark) using different geophysical methods (Corradini et al., in review). I compare the results of GPR and electromagnetic induction (EMI) to determine the horizontal extension of the feature; ERT and SH-waves seismic enable the detection of the depth and the shape of the kettle hole. After the non invasive investigation, a location for an open excavation was chosen in a way to ground-truth the geophysical results allowing the direct comparison with the stratigraphy. Due to this comparison, GPR and seismic are the best solution to identify the Bromme horizon. Both show indeed reflectors whose depth can be directly correlated with the (late) Allerød and early Younger Dryas deposits, allowing a rough identification of such cultural layers. Focused excavations would be therefore planned on the investigation of a possible find horizon belonging to the Bromme culture in a way to improve the dating information collected so far. Due to the unfavourable, partly muddy, conditions of the subsurface, this exemplary study also shows how seismic measurements can be useful where the common methods do not.

The second site-specific landscape reconstruction belongs to the Early Mesolithic site of Duvensee (Schleswig Holstein, Germany) (Corradini et al., 2020). I present the GPR investigation of 64 ha of today's bog which delivered the location of five former islands hosting Mesolithic hunter-gatherers camps. The depth maps of the three most important sedimentary facies interfaces of the ancient Lake Duvensee are presented. In particular, using Interface3, which marks the top of the basal sand deposits at the lake bottom and stratigraphic information, the creation of a palaeolandscape 3D model of the Duvensee bog during the Mesolithic was possible. The islands locations and their estimated dive-up times agree with the spatio-temporal pattern of the previous archaeological finds. The model shows where hunter gatherers could settle and move from one island to another following the shorelines of the overgrowing lake. Besides, it provides a basis for a sustainable groundwater management needed for heritage preservation.

Finally, the multi-geophysical methods approach is applied at the Early Mesolithic site of Duvensee. GPR, ERT and SH-Seismics were carried out at a reference profile close to the shoreline where also corings and DP-EC logs were performed for comparison. This study allows a more comprehensive interpretation of the basin evolution and enables to determine under which conditions peat and gyttja layers can be identified and distinguished in terms of geophysical parameters. Resistivity measurements and borehole guided wave analysis of electromagnetic waves have been carried out and compared with soil analyses. Due to this approach we are now able to distinguish between high and low decomposed peat layers and different gyttjas. GPR and SH-Seismics present different resolutions confirming that the latter allows measurements which are more focused on determining the extension of the basal sand deposits, whose depth is difficult to reach with GPR. Values concerning electrical resistivity, dielectric permittivity, and shear wave velocity have been determined for each sediment and are therefore available to complete and improve the investigation of wetland environments.

Chapter 3 summarizes the results of these studies and a conclusion is given. In chapter 4 subsequent studies and possible methodical improvements for both investigated sites are illustrated.

Chapter 2

Publications

2.1 List of publications

The following publications are part of this cumulative dissertation and can be found in the appendix:

Paper I

Corradini, E., Valentin Eriksen, B., Fischer Mortensen, M., Krog Nielsen, M., Thorwart, M., Krüger, S., Wilken, D., Pickartz, N., Panning, D., Rabbel, W., **in review**. Investigating lake sediments and peat deposits with geophysical methods - a case study from a kettle hole at the Late Palaeolithic site of Tyrsted, Denmark. *Quaternary International*

Paper II

Corradini, E., Wilken, D., Zanon, M., Groß, D., Lübke, H., Panning, D., Dörfler, W., Rusch, K., Mecking, R., Erkul, E., Pickartz, N., Feeser, I., Rabbel, W., 2020: Reconstructing the palaeoenvironment at the early Mesolithic site of Lake Duvensee: Ground-penetrating radar and geoarchaeology for 3D facies mapping. *The Holocene*. DOI: <https://doi.org/10.1177/0959683620902234>

Paper III

Corradini, E., Dreibrodt, S., Erkul, E., Groß, D., Lübke, H., Panning, D., Pickartz, N., Thorwart, M., Vött, A., Willershäuser, T., Wilken, D., Wunderlich, T., Zanon, M., Rabbel, W., **submitted**. Understanding wetlands stratigraphy: geophysics and soil parameters for investigating ancient basin development at lake Duvensee. *Geosciences*

2.2 Contributions

Paper I

I contributed to this paper planning and supervision of the measurement campaign, processing and interpretation of the data; concept of all Figures and the initial version of the manuscript (except sections ‘Landscape and geological setting’, ‘Archaeological research at Tyrsted (site10)’, ‘ Electromagnetic Induction’)

Paper II

I contributed to this paper processing and interpretation of the data, all Figures and the initial version of the manuscript (except section ‘Stratigraphy of the basin from drilling’)

Paper III

I contributed to this paper planning and supervision of the measurement campaigns, processing (except seismics) and interpretation of the data; concept of all Figures and the initial version of the manuscript (except section ‘Acquisition of stratigraphic data by drilling and laboratory analyses’)

2.3 Other Contributions

Paper IV

Groß, D., Piezonka, H., **Corradini, E.**, Schmöcke, U., Zanon, M., Dörfler, W., Dreibrodt, S., Feeser, I., Krüger, S., Lübke, H., Panning, D., Wilken, D. 2019. Adaptations and transformations of hunter-gatherers in forest environments: New archaeological and anthropological insights. *The Holocene* 29 (10). Fuchs, K., Kirleis, W., Müller, J. (Guest eds.) Special Issue: Scales of Transformation – Human-Environmental Interaction in Prehistoric and Archaic Societies, 1531-1544. DOI: <https://doi.org/10.1177/0959683619857231>

I contributed to this paper writing section ‘Ancient lake Duvensee’ and Figure 1, Figure 2, Figure 3.

Paper V

Pickartz, N., **Corradini, E.**, Kahn, R., Panning, D., Rassmann, K., Müller-Scheeßel, N., Furholt, M., Wilken, D., Wunderlich, T., Rabbel, W., forthcoming 2020. Extending archaeological documentation from 2D to 3D: The benefits of geophysical on-site measurements in excavations. In Furholt, M., Cheben, I., Müller, J., Bistáková, A., Wunderlich, M. and Müller-Scheeßel, N. (eds.), *Archaeology in the Žitava valley I - The LBK and Želiezovce settlement site of Vráble*. Leiden, Sidestone Press. ISBN: 9789088908972

I contributed to this paper writing sections ‘Methods - Ground Penetrating Radar’, ‘Results - Ground Penetrating Radar’.

Paper VI

Müller-Scheeßel, N., Müller, J., Cheben, I., Mainusch, W., Rassmann, K., Rabbel, W., **Corradini, E.**, Furholt, M. 2020. A new approach to the temporal significance of house orientations in European Early Neolithic settlements. *PLoS ONE* 15(1).
DOI:<https://doi.org/10.1371/journal.pone.0226082>

I contributed to this paper planning the measurements campaigns, measuring and processing the data.

Chapter 3

Summary and conclusions

The thesis was focused on the development of a methodology which can provide reconstructions of ancient landscapes with the aim of defining key targets for archaeological research. Through a multi-geophysical approach, this thesis aims to highlight the potential of SH-waves seismic profiling in wetland environments and the importance of ground truthing with stratigraphic information.

For the investigated site 8 at Tyrsted (Corradini et al., in review), we delivered a graded approach which can be applied to successfully investigate kettle holes. In this regard EMI enables locating the kettle hole and its near-surface lateral extension, whereas GPR defines the upper part of the kettle hole, especially its dipping lateral boundary and near-surface stratigraphy.

The general increase in water saturation with depth led to decreasing lateral contrast between the kettle hole and surrounding as the ERT and EMI sections show (Corradini et al., in review). For the same reason GPR absorption increases strongly with depth. For these reasons EMI and GPR can be expected to line out the contours of kettle holes close to the ground surface but are much less well suited to explore the depth structure of kettle holes.

Successfully, SH-wave seismics enables exploring the kettle hole down to its full depth, in which the major shape can be found from the S-wave velocity distribution as provided by refraction tomography.

The related pronounced contrasts in shear rigidity (shear modulus) are one of the reasons why shear wave sounding turned out to be successful in determining both the full depth range of the kettle hole and its internal layering. S-wave velocity values of the organic sediments are in the range of 50 to 100 m/s, whereas the glacial tills and sands show 150 to 300 m/s, almost independently of water saturation. However, the associated resolution is less (~ 20 to 40 cm) than that of GPR (~ 12 to 14 cm) which means that the latter can help to better define the shallower stratification. The further calibration of geophysical results through a test trench confirmed that a specific GPR reflection can be associated with the transition between Late Allerød and early Younger Dryas, which is correlated to the Bromme horizon.

S-wave reflection seismics showed a possible Bromme horizon, too, but the interpretation of the shallower subsurface is affected by direct waves, source signals and ultra shallow reflections close to the surface. Therefore, GPR can reconstruct the stratigraphy of the shallow subsurface at a higher resolution, while Seismic delivers the whole shape of the kettle hole.

This study provides an important planning tool for museum archaeologists who frequently struggle with a limited budget for conducting logistically complex excavations. Moreover, this prospective planning tool will enable the archaeological and palaeoenvironmental research groups to reconstruct palaeolandscapes and to identify possible finding places of these very rare, but highly important palaeolithic remains.

For the early Mesolithic site at Duvensee we first created a 3D model (Corradini et al., 2020) which combines an aerial GPR survey with geoarchaeological information from exemplary corings. The major reflections in the GPR records were generated from interfaces between layers that differ in grain size (Interface1, Interface2, Interface3). Adding an hypothetical linear time model of the water level, we were able to identify the location and extension of five former islands. It is extraordinary that the location of the islands and their estimated times of emergence from the water agree with the spatio-temporal pattern of previous archaeological finds, which therefore support our model. With the regression of the water and the

overgrowing peat from the shore to the centre of the lake, the described islands became suitable for the settlement of new camps, as confirmed by both our topographic model and the occurrence of archaeological findings. This study delivered the base for further numerical modelling, first regarding the sedimentation in the bog area using the volumes of the organic and inorganic sediments and consequently regarding grounded water management, which is a necessary component of a comprehensive heritage preservation strategy.

Secondly, we applied a multi-methodological approach at ancien lake Duvensee which delivered additional information about the stratigraphy of the former lake (Corradini et al., submitted). We found that GPR is even able to identify the boundary between the uppermost poorly decomposed peat (“acrotelm”) and underlying well-decomposed peat (“catotelm”). Guided wave measurements provided a high resolution image of the permittivity in the subsurface which have been compared with resistivity and shear-waves velocity. Moreover, GPR together with stratigraphic information was useful to estimate the peat compaction due the extraction after drilling. It turned out that the compaction is higher for the shallower peat layer associated with the low degrad peat, while the underlying more degraded peat presents a lower compaction.

ERT is capable of distinguishing between sediments with different grain sizes, but is not able to separate between clayey to silty deposits and lake sediments. However, small scale variations, due to different degrees of peat and organic remains, in the peat layer were visible as resistivity changes. We proposed SH-Seismics as an alternative tool for investigating wetlands and it delivered promising results, the method is indeed able to distinguish between sediments with different grain sizes with a vertical resolution of about 0.2 m to 0.7 m. It’s also interesting to novice how ERT and SH-wave seismics work vice versa for detecting different interfaces. Combining geophysical properties together with soil analyses delivered more conclusions: resistivity is well correlated with water content and organic matter for distinguish between different peat degrees of decomposition and different gyttjas (calcareous/fine), moreover, seismics velocities can be correlated to bulk density.

Due to the variety of ecological conditions and stratigraphy in wetlands, the results of this study are also valuable in complementing existing case studies. The delineation of different gyttja layers is especially promising for the calculation of peatlands total carbon content.

This thesis concludes that geophysical prospection contributes to wetland archaeology as a tool for site detection, landscape reconstruction and interpretation. Future research should aim to further our understanding of the relationship between geophysical response and peatland geochemistry, alongside a more extensive programme of surveys and ground-truthing work to improve survey methodologies and archaeological interpretations.

Chapter 4

Outlook

In this chapter I describe further ideas that can extend the research aims of this thesis. The chapter is divided in two sections each of them belonging to the presented sites.

4.1 Ideas for Tyrsted

The investigation of kettle holes is not principally different from the prospection of more common archaeological/geological features. The research at Tyrsted carried out by the Horsens Museum had demonstrated several smaller ancient wetland areas (site 7, 8 and 12), but our study focused only on one of those (site 8). The unfavorable conditions at Tyrsted can hamper the measurements efficiency, therefore a first study was done. The geophysical investigation would be the faster way to validate the hypothesis of further scattered kettle holes. Next investigations would be addressed on confirming the nature of these scattered wetlands which can turn out to be new kettle holes.

We recommend using GPR and/or EMI for aerial prospection to line out the contours of possible kettle holes close to the ground surface. Based on the presented study, S-wave seismic is then recommended to explore the depth structure of kettle holes. Some improvements which can be added to a further research in the area are summarized as follow:

- (i) planning a GPR grid of profiles to generate amplitude maps (time-slices) to gain more details on the kettle hole extension (if the field condition allows that).
- (ii) using a higher separation between the transmitter and receiver coil for EMI measurements. This condition allows greater depth to define the shape of the former lake.
- (iii) measuring several S-wave profiles to perform a 3D seismic survey to reconstruct the entire shape of the pond.
- (iiii) implementing the stratigraphic information in the computation of the applied methods to create models which can quantitatively validate our measurements.

Regarding GPR, the velocity determination is an essential factor to keep in consideration in a way to improve the time-depth conversion. Velocity variations are normally present in the subsurface and defining the lateral and vertical changes can also reduce the error associated to the reflectors depth. Either GPR borehole equipment or guided waves measurements provide high-resolution velocity information that can be used to calculate permittivity profiles in the subsurface. The conversion time-to depth is the key factor for the determination of the Bromme horizon which can be verified by test excavations.

Another method which could be also tested in the feature can be the tTEM: a ground based method for transient electromagnetic data acquisition. The aim of the tTEM development has been to design a system covering the depth range from 0 – 30 m in full 3D. White et al. (2019) and Johnson et al. (2019) showed that this application improved the resolution of sand and gravel distribution within the tTEM depth of investigation.

There are plenty of possibilities to carry multi-methodological surveys with the aim to reconstruct ancient landscapes and connect them to human occupation. What is important is to always find the right compromise between the aim of the survey, the time for collecting data and the resolution we want to achieve.

4.2 Ideas for Duvensee

4.2.1 *Detecting roasting hearths*

The early Mesolithic site of Duvensee is one of the most known hunter-gatherers camp-site in northern Europe for early Holocene research. Archaeological sites on the former lake provide vivid illustrations of early Mesolithic life, with bark mats and other organic finds preserved, including evidence for hazelnut roasting in specific hearths, of about 1 m² dimension. The more ambitious task delivered to geophysics is to try to detect these features in a way to find new camp-sites. The dimension and the thickness of roasting hearths and flint concentration as well are less than the resolution of the common geophysical methods making this task very difficult. In the literature there are some attempts to recognize fireplaces using GPR and magnetic (Jones and Munson, 2005; Urban et al., 2014; Urban et al., 2019) and improvements in instrumentation and computer-processing now allow a better understanding of these ephemeral sites. Some of these studies were able to identify some fireplaces but within house-structures which can restrict the area for hearths detection. As reported in Corradini et al. (2020) the geophysical survey together with the long lasting archaeological research in this area, delivered the location of five islands in which some mesolithic-camps were investigated. Unfortunately the hearths were excavated before the measurements took place, therefore the possibility to recognize one of them in the geophysical record is impossible. In summer 2018 further archaeological investigation in an unknown area took place revealing the exceptional location of a fireplace. A small trench was opened and a hearth came out. Fortunately a transect was left and the feature runs through it allowing a surface measurement for its detection. A test was made using a GSSI dual frequency antenna (330 MHz and 800 MHz) with the aim to see if a hearth can produce a reflection on the GPR record. In Figure 1 the test measurement is reported showing the location of the GPR profiles (Figure 1a), the antenna used for the test (Figure 1b), an example of a hearth at Duvensee (Figure 1c) and the results (Figure 1d).

Focusing on Figure 1d we notice that a reflector is present at the same location of the hearth (the archaeological documentation is superimposed for comparison, red dots) delivering the condition to conclude that these features can be detected. The ambitious task is to locate these structures in space because similar reflections can occur in the same area. To develop a methodology that can enable us to recognize and map hearths is a future task not only for Duvensee but also for prehistoric research.

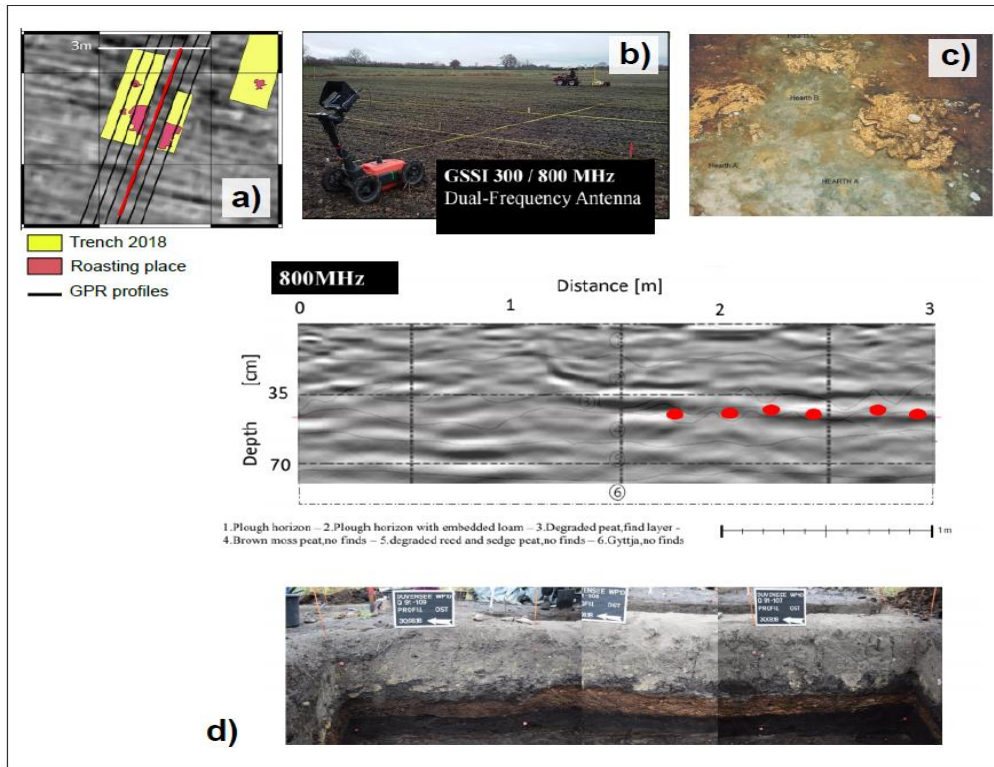


Figure 1. Test measurements aimed to detect a fire place. (a) trench carried out in August 2018 with the roasting place underneath the transect. The red line is the presented result. (b) the dual frequency antenna used for the measurements. (c) example of a roasting place (Bokelmann, 2012). (d) GPR profile with the superimposed archeological interpretation of the section (up), section of the trench (down).

For decades and worldwide, magnetic survey methods have seen extensive use in archaeology (Gaffney and Gater, 1993), including for the detection of features associated with burning, such as hearths and kilns (e.g., Jones and Munson, 2005; Urban et al., 2014). A joined application of GPR and magnetic survey can also be an approach to develop a methodology to understand these features in space.

4.2.2 Quantitative interpretation with a priori information

The study at Duvensee delivered the basis for a more quantitative interpretation of geophysical data. In this context, the calibration of by stratigraphical information deduced from outcrops or sediment cores is an important component of data interpretation (e.g. Seeliger et al., 2013; Fischer et al. , 2015).

Usually, geophysical data is analyzed with inversion, which is the concept of deriving a spatial distribution of physical subsurface parameters (synthetic measurements) that fit the actually measured data.

Geoelectric data, for instance, is analyzed in a tomographic inversion process leading to images of the subsurface in terms of electric resistivity (ERT). However, the tomographic inversion process is ambiguous, which means that different equivalent subsurface models can be found by the inversion matching with the measured data. In order to reduce this ambiguity, a priori information and constraints gained from other

methods (e.g. vibracoring, excavations, DP-EC logs) can be applied (Ellis and Oldenburg, 1994). Common examples of structural constraints are depths of layer interfaces derived from GPR or seismic measurements. A problem with this approach is that sedimentary and seismic interfaces do not necessarily represent interfaces in terms of electric resistivity, too. Therefore, one further step of improvement would be to use in-situ values of electric resistivities as constraints. Examples using DP-EC logs on geoarchaeological data sets were shown either by Fischer et al. (2016) and Wunderlich et al. (2018) using interfaces and resistivity regions derived from DP-EC logs or by Günther and Rucker (2012). In a way to improve the understanding of the stratigraphy the in-situ measurements performed with DP-EC logs and on the sediment cores can be used to constrain ERT. Moreover, the layers depth is useful to constrain seismic tomography as well to understand how far we can go with the resolution of each method. Both case studies can benefit in the geophysical interpretation by including constraints from different methods. Seismics and ERT can be constrained by GPR reflections and in-situ resistivity measurements, as well using depth interfaces from the coring information.

4.2.3 Ameliorating the methodology

Our case studies at both sites confirm the importance of including S-wave seismic in geoarchaeological research. In this regard a new tool, which may be able to resolve small-scale near surface structures even more reliably, is the Full Waveform Inversion (FWI). FWI has been introduced recently in the archaeological context by Köhn et al. (2018), Köhn et al. (2019) and Schwardt et al. (2020). As an example, at the Fossa Carolina, FWI was able to improve the definition of the canal basement and to resolve small scale velocity anomalies correlated with features in the archaeological documentation (Köhn et al., 2018).

Moreover, compressional waves (P-waves) can be a tool to test at Duvensee despite the longer wavelength and thus coarser resolution compared to shear waves. Nevertheless, P-waves are depending on the compressional modulus and this might be a parameter that is changing between sedimentary layers, too. For example, V_p increases with a decrease in porosity, and increases with an increase in density.

Combining geophysics and soil characterization is currently required to aid the rapid discovery and characterisation of buried wetland archaeology. For instance the identification of different peat degradation can be an indicator of the layers preservation which can address the archaeological research. Characterisation of the deposits prior to full survey is therefore an essential step in conducting geophysical surveys in wetlands. We presented a range of different parameters (e.g. dielectric permittivity, resistivity and SH seismics) which are connected with soil information (water content organic matter) and can therefore delineate different deposits. The dielectric permittivity is well defined using the guided wave measurements which can be improved also using a motor pulling the metal rod into the ground allowing a more detailed survey of the GPR velocity. Evaluating with more accuracy the degree of decomposition of peat for instance would help the determination of soil compressibility and porosity. Using EC-Direct Push is the most successful way to determine the conductivity/resistivity values.

As reported by Milton (2018), geochemical and borehole methods can also work together with geophysics with the aim to address the general scepticism in the academic and commercial archaeological community about the usefulness of geophysics in wetland archaeology. Focused geochemical studies on wetland sites

subject to full excavation and interpretation could drastically improve the potential of employing these techniques as a means of interpreting different deposit types.

Bibliography

Becker, A., Bucher, F., Davenport, C. & Flisch, A. (2004) Geotechnical characteristics of post-glacial organic sediments in Lake Bergsee, southern Black Forest, Germany. *Engineering Geology*, **74**, 91–102.

Bokelmann, K. (2012) Spade paddling on a Mesolithic lake - Remarks on Preboreal and Boreal sites from Duvensee (Northern Germany), In: Niekus, M.J.L.T., Barton, R.N.E., Street, M., Terberger, T. (Eds.), A mind set on flint. Studies in honour of Dick Stapert. Groningen Archaeological Studies, Groningen, pp. 369-380.

Borup, P. and Nielsen, M.K. (2017) Tyrsted – et kighul til senistiden. *Skalk* (December 2017/6), 3-9.

Brown, A.G. (1997) *Alluvial Geoarchaeology - Floodplain Archaeology and Environmental Change*. Cambridge Manuals in Archaeology. Cambridge University Press: Cambridge.

Clarke, C., Utsi, E. & Utsi, V. (1999) Ground penetrating radar investigations at North Ballachulish Moss, Highland, Scotland. *Archaeological Prospection*, **6**, 107-21.

Comas, X., Slater, L. and Reeve, A. (2004) Geophysical evidence for peat basin morphology and lithologic controls on vegetation observed in a northern peatland. *Journal of Hydrology*, **295**, 173– 184, doi:10.1016/j.jhydrol.2004.03.008.

Comas, X., Slater, L., and Reeve, A. (2005) Stratigraphic controls on pool formation in a domed bog inferred from ground penetrating radar (GPR). *Journal of Hydrology*, **315**, 40– 51, doi:10.1016/j.jhydrol.2005.04.020.

Comas, X., Terry, N., Slater, L., Warren, M., Kolka, R., Kristiyono, A., Sudiana, N., Nurjaman, D., Darusman, T., (2015) Imaging tropical peatlands in Indonesia using ground-penetrating radar (GPR) and electrical resistivity imaging (ERI): implications for carbon stock estimates and peat soil characterization. *Biogeosciences*, **12**, 2995–3007

Conneller, C. (2004) Becoming deer. Corporeal transformations at Star Carr. *Archaeological Dialogues*, **11**, 37-56.

Corradini, E., Wilken, D., Zanon, M., Groß, D., Lübke, H., Panning, D., Dörfler, W., Rusch, K., Mecking, R., Erkul, E., Pickartz N., Feeser, I., Rabbel, W. (2020) Reconstructing the palaeoenvironment at the early Mesolithic site of Lake Duvensee: Ground-penetrating radar and geoarchaeology for 3D facies mapping. *The Holocene*. <https://doi.org/10.1177/0959683620902234>

Corradini, E., Eriksen, B.V., Fischer Mortensen, M., Krog Nielsen, M., Thorwart, M., Krüger, S., Wilken, D., Pickartz N., Panning, D., Rabbel, W. (**in review**) Investigating lake sediments and peat deposits with geophysical methods - a case study from a kettle hole at the Late Palaeolithic site of Tyrsted, Denmark. *Quaternary International*

Corradini, E., Dreibrodt, S., Erkul, E., Groß, D., Lübke, H., Panning, D., Pickartz, N., Thorwart, M., Vött, A., Willershäuser, T., Wilken, D., Wunderlich, T., Zanon, M., Rabbel, W., (**submitted**) Understanding wetlands stratigraphy: geophysics and soil parameters for investigating ancient basin development at lake Duvensee. *Geosciences*

-
- Dietze, E., Theuerkauf, M., Bloom, K. et al. (2018) Holocene fire activity during low-natural flammability periods reveals scale-dependent cultural human-fire relationships in Europe. *Quaternary Science Reviews*, **201**, 44–56.
- Doran, G.H. (2013) Excavating wet sites. In F. Menotti, A. O'Sullivan (Eds.), *The Oxford Handbook of Wetland Archaeology*. Oxford University Press: Oxford, pp. 483-494.
- Ellis, R.G., Oldenburg, D.W. (1994) Applied geophysical inversion: *Geophysical Journal International*, **116**, no. 1, 5–11.
- Eriksen, B.V. (2002) Reconsidering the geochronological framework of Lateglacial hunter-gatherer colonization of southern Scandinavia. In: B.V. Eriksen & B. Bratlund (eds), *Recent studies in the Final Palaeolithic of the European plain. Jutland Archaeological Society Publications Vol. 39*. Højbjerg, pp. 25-41.
- Eriksen, B.V., Krüger, S., & Wild, M. (2018) Tyrsted – a Late Palaeolithic Christmas gift. *Zentrum für Baltische und Skandinavische Archäologie, Jahresbericht 2017*, pp. 78-79.
- Fischer P, Meurers-Balke J, Gerlach R, Bulla A, Peine, et al. (2015) Accepted for publication. Geoarchaeological and archaeobotanical investigations in the environs of the Combining ERT, DP-EC Logs and Coring as New Approach in Geoarchaeology 227 Copyright © 2016 John Wiley & Sons, Ltd. *Archaeol. Prospect.* **23**, 213–228 (2016) DOI: 10.1002/arp Holsterburg lowland castle (North Rhine-Westphalia) – evidence of landscape changes and saltwater upwelling. *Zeitschrift für Geomorphologie. N.F. Supplementary Issue*. http://dx.doi.org/10.1127/zfg_suppl/2015/S-00186
- Fischer, P., Wunderlich, T., Rabbel, W., Vött, A., Willershäuser, T., Baika, K., Rigakou, D., Metallinou, G. (2016) Combined Electrical Resistivity Tomography (ERT), Direct-Push Electrical Conductivity (DP-EC) Logging and coring - A new methodological approach in geoarchaeological research. *Archaeological Prospection*, **23**, 213-228 doi: <https://doi.org/10.1002/arp.1542>
- Gaffney, C., & Gater, J. (1993) Development of remote sensing, part 2 - Practice and method in the application of geophysical techniques in archaeology. In: Hunter, J & Ralston, I, (eds). *Archaeological resource management in the UK: An introduction*. Stroud: Sutton.
- Gaffney, C & Gater, J. (2003) *Revealing the buried past: geophysics for archaeologists*. Stroud: Tempus.
- Groß, D., Lübke, H., Schmölcke, U., and Zanon, M. (2018) Early Mesolithic activities at ancient lake Duvensee, northern Germany. *The Holocene* **29** (2), 197-208
- Groß D, Piezonka H, Corradini E et al. (2019) Adaptations and transformations of hunter-gatherers in forest environments: New archaeological and anthropological insights. *The Holocene* **29** (10). Special Issue: Scales of Transformation – Human-Environmental Interaction in Prehistoric and Archaic Societies, DOI: 1531-1544. DOI:10.1177/0959683619857231ola
- Günther, T., Rücker, C. (2012) Boundless Electrical Resistivity Tomography (BERT) v.2.0 Open Access Software for Advanced and Flexible Imaging, in C. Herve, A. Adler, B. Lionhart, eds., *100 Years of Electrical Imaging: Workshop*, 9-10 July 2012, ISBN : 978-2-911256-87-5.

-
- Hadler, H., Vött, A., Newig, J., Emde, K., Finkler, C., Fischer, P., Willershäuser, T. (2018) Geoarchaeological evidence of marshland destruction in the area of Rungholt, present-day Wadden Sea around Hallig Südfall (North Frisia, Germany), by the Grote Mandrenke in 1362 AD. *Quaternary International* **473 A**, 37-54.
- Heller, C., Zeitz, J. (2012) Stability of soil organic matter in two northeastern German fen soils: the influence of site and soil development. *Journal of Soils Sediments*, **12**, 1231–1240.
- Jol, H & Smith, D. (1995) Ground penetrating radar surveys of peatlands for oilfield pipelines in Canada. *Applied Geophysics*, **34**, 109-23.
- Johnson, C., White, E.A., Maurya, P., Kress, W., Kelly, D.B., Lane, J.W. tTem, a towed electromagnetic induction system - an example from the Mississippi alluvial plain. SAGEEP 2019 - 32nd Annual Symposium on the Application of Geophysics to Engineering and Environmental Problems
- Jones, G., Munson, G. (2005) Geophysical survey as an approach to the ephemeral campsite problem: case studies from the northern plains. *Plains Anthropol*, **50**, (193), 31e43. <https://doi.org/10.1179/pan.2005.006>.
- Köhn, D., Wilken, D., Wunderlich, T., De Nil, D., Rabbel, W., Werther L. , Schmidt J., Zielhofer C., and Linzen S. (2018) Seismic SH full waveform inversion as new prospecting method in archaeo-geophysics., 80th Conference and Exhibition, EAGE.
- Köhn, D., Wilken, D., De Nil, D., Wunderlich, T., Rabbel, W., Werther, L. et al. (2019) Comparison of time-domain SH waveform inversion strategies based on sequential low and bandpass filtered data for improved resolution in near-surface prospecting. *Journal of Applied Geophysics*, **160**, 69–83.
- Lamair, L., Hubert-Ferrari, A., Yamamoto, S., Fujiwara, O., Yokoyama, Y., Garret, E., De Batist, M., Heyvaert V.M.A., et al. (2019) Use of high-resolution seismic reflection data for paleogeographical reconstruction of shallow Lake Yamanaka (Fuji Five Lakes, Japan). *Palaeogeography, Palaeoclimatology, Palaeoecology*, **514**, 233-250
- Lowry , C.S., Fratta, D., Abdreson M.P. (2009) Ground penetrating radar and spring formation in a groundwater dominated peat wetland. *Journal of hydrology*, **373**, 68-79
- Menotti, F., O'Sullivan, A. (2013) *The Oxford Handbook of Wetland Archaeology*. Oxford University Press.
- Milton, C.J. (2018) Geophysics and geochemistry: an interdisciplinary approach to archaeology in wetland contexts. *Journal of archaeological Science: Reports*, **18**, 197-212
- Mingram, J., Negendank, J.F.W., Brauer, A., Berger, D., Hendrich, A., Köhler, M., Usinger, H. (2007) Long cores from small lakes—recovering up to 100 m-long lake sediment sequences with a high-precision rod-operated piston corer (Usinger-corer). *Journal of Paleolimnology* **37**, 517–528.

-
- Persico, R., Soldovieri, F., & Utsi, E. (2010) Microwave tomography for processing of GPR data at Ballachulish. *Journal of Geophysics and Engineering*, **vol. 7, no. 2**, pp. 164–77.
- Plado, J., Sibul, I., Mustasaar, M., Jõelet, A. 2011 Ground-penetrating radar study of the Rahivere peat bog, eastern Estonia. *Est. Journal of Earth Science*, **60**, 31–42.
- Plets, R, Dix, J & Best, A. (2007) Characterization of buried inundated peat in seismic (chirp) data, inferred from core information. *Archaeological Prospection*, **14**, 261-72.
- Rabbel, W. Stümpel, H., and Woelz, S. (2004) Archeological prospecting with magnetic and shear wave surveys at the ancient city of Miletos (western Turkey): The Leading Edge, 23, 690-703.
- Seeliger M, Bartz M, Erkul E, et al. (2013) Taken from the sea, reclaimed by the sea: the fate of the closed harbor of Elaia, the maritime satellite city of Pergamon (Turkey). *Quaternary International*, **312**, 70–83
- Schwardt M., Köhn D., Wunderlich T., Wilken D., Seeliger M., Schmidts T., Brückner H., Başaran S., Rabbel W. (2020) Characterisation of silty to fine-sandy sediments with SH-waves: full waveform inversion in comparison to other geophysical methods. *Near Surface Geophysics* **18** (3): 217-248 DOI:[10.1002/nsg.12097](https://doi.org/10.1002/nsg.12097)
- Slater, L., Reeve, A. (2002) Understanding peatland hydrology and stratigraphy using integrated electrical geophysics. *Geophysics*, **67**, 365–378.
- Stümpel, H., Rabbel, W., & Schade, J. (1988). Oberflächennahe geophysikalische Untersuchungen im Mündungsgebiet des Río de Vélez und des Río Algarrobo. *Madrider Beiträge*, 14, 60-72
- Theimer, B.D., Nobes, D.C., Warner, B.G., (1994) A study of the geoelectrical properties of peatlands and their influence on ground-penetrating radar surveying. *Geophys. Prospect.* **42**, 179–209.
- Thompson, R & Oldfield, F. (1986) Environmental magnetism. London: Allen & Unwin
- Trinks, I., Hinterleitner, A., Neubauer, W., Nau, E., Löcker, K., Wallner, M., Gabler, M., Filzwieser, R., Wilding, J., Schiel, H. and et al. (2018) Large-area high-resolution ground-penetrating radar measurements for archaeological prospection. *Archaeological Prospection*, **25**, 171–195.
- Urban, T.M., Vella, C., Bocancea, E., Tuttle, C.A., Alcock, S.E. (2014) A geophysical investigation of a newly discovered Early Bronze Age Site near Petra, Jordan. *Journal of Archaeological Science*, **42**, 260e272.
- Urban, T.M., Rasic, J.T., Alix, C., Anderson, D.D., Chisholm, L., Jacob, R.W., Manning, S.W., Mason, O.K., Tremayne, A.H., Vinson, D. (2019) Magnetic detection of archaeological hearths in Alaska: A tool for investigating the full span of human presence at the gateway to North America. *Quaternary Science Reviews*, **211**, 73-92
- Utsi, E. (2003) Sinking into old ground: Ground probing radar in the Scottish wetlands. In: Jones, R, Going over old ground: perspectives on archaeological geophysical and geochemical survey in Scotland;

proceedings of a conference held at the Department of Archaeology, University of Glasgow, Scotland, August 2003. Oxford: Archaeopress

Utsi, E. (2004) Ground-penetrating radar time-slices from North Ballachulish Moss. *Archaeological Prospection*, **11**, 65–75.

Van de Noort, R & O'Sullivan, A. (2006) Rethinking wetland archaeology. London: Duckworth.

Walter, J., Lück, E., Bauriegel A., Richter, C., Zeitz, J. (2015) Multi-scale analysis of electrical conductivity of peatlands for the assessment of peat properties. *European J. of soil science*, **66**, 639-650

Walter, J., Hamann, G., Klingenfuss, C., Zeitz, J. (2016) Stratigraphy and soil properties of fens: Geophysical case studies from northeastern Germany. *Catena*, **142**, 112-125.

Warner, B.G., Nobes, D.C., Theimer, B.D. (1990) An application of ground penetrating radar to peat stratigraphy of Ellice Swamp, southwestern Ontario. *Canadian Journal of Earth Science*, **27**, 932–938.

Weston, DG. (2004) The influence of waterlogging and variations in pedology and ignition upon resultant susceptibilities: a series of laboratory reconstructions. *Archaeological Prospection*, **11**, 227-35.

White, E.A., Johnson, C.D, Maurya P.K., Kress, W., Kelly D.B., and Lane J.W., Use of a towed electromagnetic induction (tTEM) system for shallow aquifer characterization – an example from the Mississippi alluvial plain. Symposium on the Application of Geophysics to Engineering and Environmental Problems 2019 <https://doi.org/10.4133/sageep.32-016>

Wunderlich T., Wilken D., Erkul E., Rabbel W., Vött A., Fischer P., Hadler H., Ludwig S., and Heinzelmann M. (2015) The harbour(s) of ancient Ostia. Archaeological prospection with shear-wave seismics, geoelectrics, GPR and vibracorings. *Archaeologia Polona*, vol 53: 2015, Special theme: *Archaeological prospection*, ISSN 0066-5924

Wunderlich, T., Wilken, D., Erkul, E., Rabbel, W., Vött, A., Fischer, P., Hadler, H., Heinzelmann, M. (2018) The river harbour of Ostia Antica - stratigraphy, extent and harbour infrastructure from combined geophysical measurements and drillings. *Quaternary International*, **473**, 55-65.

Zielhofer, C., Rabbel, W., Wunderlich, T., Vött, A., Berg, S. (2018) Integrated geophysical and (geo)archaeological explorations in wetlands. *Quaternary International*, **473** A, 1-2.

Eidesstattliche Erklärung

Hiermit versichere ich, die vorliegende Arbeit selbstständig verfasst und keine anderen als die angegebenen Quellen und Hilfsmittel benutzt sowie die Zitate deutlich kenntlich gemacht zu haben.

Ich erkläre weiterhin, dass die vorliegende Arbeit in gleicher oder ähnlicher Form noch nicht im Rahmen eines anderen Prüfungsverfahrens eingereicht wurde.

Die Arbeit entstand unter Einhaltung der Regeln guter wissenschaftlicher Praxis der Deutschen Forschungsgemeinschaft.

Desweiteren wurde mir kein akademischer Grad entzogen.

Kiel, den 26. Juni 2020

Erica Corradini

Appendix A

Publications

A.1 Paper I

The following version was submitted to the Journal *Quaternary International* on February 2020 and is currently in the review process.

Investigating lake sediments and peat deposits with geophysical methods - a case study from a kettle hole at the Late Palaeolithic site of Tyrsted, Denmark

Erica Corradini ¹, Berit Valentin Eriksen ², Morten Fischer Mortensen ³, Martin Krog Nielsen ⁴, Martin Thorwart ¹, Sascha Krüger ², Dennis Wilken ¹, Natalie Pickartz ¹, Diana Panning ¹, Wolfgang Rabbel ¹

Keywords:

Late Palaeolithic, SH seismics, applied- geophysics, geoarchaeology, kettle holes

Highlights:

SH-wave seismics enables exploring the kettle hole down to its full depth

The detection of the Bromme horizon is possible with geophysical methods

Ground truthing the results with corings allows the reconstruction of the stratigraphy to plan test excavations

Abstract:

Kettle holes are common ice decay features in formerly glacial landscapes like those in Southern Scandinavia and Northern Germany. Here the kettle holes are represented either as dry depressions, wetland areas or lakes. However, the majority of these features are silted and part of the present farmland. We investigated a small kettle hole at Tyrsted, near the township of Tyrsted, south of Horsens (Denmark) with the aim to determine the extension and depth of this feature using geophysical methods. A former excavation at Tyrsted carried out from the Horsens Museum in 2017 at a neighboring site revealed Late Palaeolithic flint of the Bromme type and worked reindeer antlers. This connection in a Late Glacial horizon is unique not only in a Danish context and it can help to improve and clarify the dating of

¹ *Institute of Geoscience, Christian-Albrechts-University Kiel, Germany*

² *Centre for Baltic and Scandinavian Archaeology (ZBSA), Schleswig-Holstein State Museums Foundation Schloss Gottorf, Schleswig, Germany*

³ *National Museum of Denmark, Environmental Archaeology and Materials Sciences, I.C. Modewegsvej, 2800 Kongens Lyngby*

⁴ *Horsens Museum, Archaeology, Fussingsvej, 8700 Horsens, Denmark*

the Bromme culture. We used ground penetrating radar (GPR), electromagnetic induction (EMI) and electrical resistivity tomography (ERT) to estimate the extension of the kettle hole (~16 mx25m). Shear wave reflection and refraction seismics (SH Seismics) were able to detect the bottom sediment of the former lake at about ~5 m depth. Furthermore a seismic event at about 1.30 m depth is visible which can be associated to the transition between the Allerød and Younger Dryas sediment making the detection of the Bromme horizon possible. After the non invasive investigation, a location for an open excavation has been chosen in a way to groundtruth the geophysical results allowing the direct comparison with the stratigraphy. These results allow the archaeologists to identify key excavation areas focused on the investigation of the Allerød and Younger Dryas layers in a way to improve the dating information about the Bromme horizon collected so far. Furthermore geophysical investigations together with excavations will enable the archaeological and palaeoenvironmental research groups to search large scale palaeolandscapes for these very rare, but highly important finds.

1. Introduction

In Northwestern Europe most wetland areas have excellent preservation conditions for organic material and have provided us with some of the most spectacular archaeological finds from the prehistory. The very rich finds from the Mesolithic and onwards is in sharp contrast to the Late Glacial period. Here organic materials with human traces are extremely rare. An obvious reason is of course that the population during the Late Glacial was much smaller than during the following periods. However, this is most likely not the only reason; we also lack efficient tools to locate potential find layers in waterlogged sediments. Today it is often done by systematic corings followed by test pits, before an excavation is made. However, an initial phase with a systematic mapping of the subsoil would help us to focus the following phase with coring and test pits. As a case study we investigate a small kettle hole next to the Palaeolithic site of Tyrsted in Denmark, using different geophysical methods in combination with excavations.

Kettle holes are melt-out features associated with glacial and glaciofluvial landforms. They develop mainly as a consequence of disintegrating glaciers and the subsequent burying of ice blocks (dead ice) by glaciofluvial sediments (Carlson et al. 2005; Kalettka and Rudat 2006; Benn and Evans 2010;). Maizels (1977) carried out laboratory experiments on kettle-hole formation showing that the size of the resulting depression in glacial outwash depends on the degree of burying and the size of the dead ice block. Depending on the retention potential of the underground, they may turn into lakes or wetlands becoming a location for species diversity.

Kettle holes and lakes which formed along the retreating Fennoscandian ice sheet (Germany, Denmark, Poland and Estonia) have been studied in detail and different context, including paleo-climatic, ecologic and hydrologic as well as habitat investigations (Kalettka and Rudat, 2006; Gerke et al. 2010; Mortensen et al. 2011; Karasiewicz et al., 2014, Mortensen et al. 2014a). In 2017 the Horsens Museum excavated a kettle hole (Tyrsted, site 10) near Horsens (Denmark) and the excavation revealed Late Palaeolithic Bromme type flints and worked reindeer antlers (Borup and Nielsen 2017; Eriksen et al. 2018). This connection between Bromme findings and worked reindeer antlers in a Late Glacial horizon is unique.

Throughout southern Scandinavia, Late Palaeolithic finds are almost exclusively known in the form of lithic inventories, many of which come from surface sites or, in case of excavations, from sites lacking a proper stratigraphy. Thus, the organic artefact inventory from the Bromme culture is largely unknown – apart from some stray finds of Late Palaeolithic appearance. Likewise, faunal remains that may be attributed to Bromme settlements are hardly ever present. Accordingly, due to the scarcity of organic remains and the general lack of proper stratigraphic observations the absolute dating of the Bromme culture is a genuine research desideratum. The available dates concentrate in the (late) Allerød and early Younger Dryas chronozones, but unfortunately most of these dating are tentative only (Eriksen 2002; Fischer et al. 2013; Mortensen et al. 2014b).

The investigated kettle hole at Tyrsted is only one out of millions of small sediment traps, scattered over the area once covered by the Fennoscandian glaciers. Our present scientific approach therefore combines predictive modelling based on an inspection of existing archives and systematic surveys to locate such kettle holes in relation to known archaeological sites. We aim then to develop a non invasive, fast and cheap methodology to pinpoint the most promising areas for further archaeological excavation. Archaeologists and geophysicists work together to reconstruct the past landscape for understanding the human occupation. Geophysical methods such as GPR (ground penetrating radar) and ERT (electrical resistivity tomography) have been applied to investigate kettle holes with geological implications (Thompson, 1978; Koszinski 2013; Götz et al. 2018) but rarely in archaeological contexts. Seismic reflection and refraction measurements using shear waves were successfully applied in archaeological prospection occasionally as well (Woelz et al. 2009; Rabbel et al., 2004; Wilken et al., 2015a), because its resolution is regarded to be insufficient to image small-scale archaeological features, but in the past years improvements have been made.

The aim of this study is to provide a stratigraphic description of a kettle hole using non invasive methods providing the horizontal extension, the shape and depth of the pond to the archaeological research, using the surrounding landscape of the Tyrsted site as our research area. We compare the results of GPR and electromagnetic induction (EMI) to determine the horizontal extension of the feature; ERT and shear waves (SH) seismic enable us to examine the depth of the kettle hole. After the non invasive investigation, a location for an open excavation was chosen in a way to ground truth the geophysical results allowing the direct comparison with the stratigraphy. This result permits to plan archaeological excavations focused on the detection of sediment of Allerød age and a possible find horizon belonging to the Bromme culture in a way to improve the dating information collected so far. Due to the unfavourable, partly muddy, conditions of the subsurface, this exemplary study also shows how seismic measurements can be useful where the common methods do not. After the geological and archaeological background of the investigated area we present the geophysical measurements done during different campaigns. In the last section, focusing on the seismic results, we compare the final outcome from different methods allowing a reconstruction of the kettle hole and an estimation of its depth and extension.

2. Landscape and geological setting

The area under investigation is part of a young morainic landscape that was formed in the Late Weichselian by the East Jylland re-advance of ice that reached its maximum extension c. 10 kilometres further west some 19-18.000 years ago (Houmark-Nielsen, 2011). The glaciers left a landscape that today is characterized by numerous small in filled kettle holes. These form where blocks of “dead ice” are left behind by a retreating glacier and become buried under insulating layers of morainic sediments. As the ice melts, the ground gradually sinks in, and often a small lake or a pond develops. They stand out as water- or peat-filled hollows with often quite steep sides and usually with no in- or outlets. In the present case, various palaeo-environmental analyses (sedimentology, palynology, macrobotanical remains, etc.) indicate that the melting progressed relatively fast, and that the sedimentation and infilling of the kettle hole started at least 14.000 years ago (no later than the Allerød period). Very often, the ice will melt gradually and the water depth increases accordingly, creating the steep sides. This development along with the influence of different disturbances evidently may create a highly complex stratigraphy (Mortensen, 2007). The excavated kettle hole (Tyrsted, Site 10) measures ~15x25 m, covering about 325 m². The original pond was c. 3.5 m deep (measured from present day surface to the bottom of the Allerød-layer) and had no in- or outlet. Sedimentation started in the early late glacial and continued throughout the early postglacial where peat started forming. The stratigraphy shows – from the bottom – the complex organogenic (pre-Allerød and) Allerød layers, followed by the 60 cm thick clay gyttja layer of the Younger Dryas, and a 10 cm thick Preboreal deposit on top. Younger peat layers are not preserved. In the late Bronze Age or early Iron Age, these peat layers were exploited by nearby villagers – leaving the peat extraction pits that gave rise to the initial archaeological excavation. The East Jylland morainic soils are very fertile and during the past couple of hundred years most of the area was farmland (as evidenced by historic maps). Thus, the top layer is ploughed, colluvial soil. Due to the ongoing construction work, Site 10 was excavated as a rescue excavation and the excavated area was then sealed (now there is a bicycle path).

However, in the immediate vicinity a previous test excavation survey carried out in 2016 by the Horsens Museum (red boxes in Figure 1) had demonstrated several smaller ancient wetland areas below the plow soil (sites 7,8 and 12 in Figure 1). In some of these areas the test trench had shown that the peat layers also here were removed in prehistory. Furthermore, it was likely that some of the wetland areas represented regular kettle holes with Late Glacial sediments, however, this could not be definitively concluded from the test excavation. The geophysical investigation was therefore the faster solution to validate the hypothesis of scattered kettle holes. After a first GPR Survey which took place during the summer of 2017 (where site 7,8 and 12 have been investigated), another campaign was carried out in summer 2018 with the aim to apply other methods to improve the understanding of these features. Unfortunately, site 7 and 12 presented unfavorable conditions for a geophysical survey (presence of grass and water scattered at the surface), therefore we decided to focus the geophysical investigation on site 8 after the first survey in 2017.

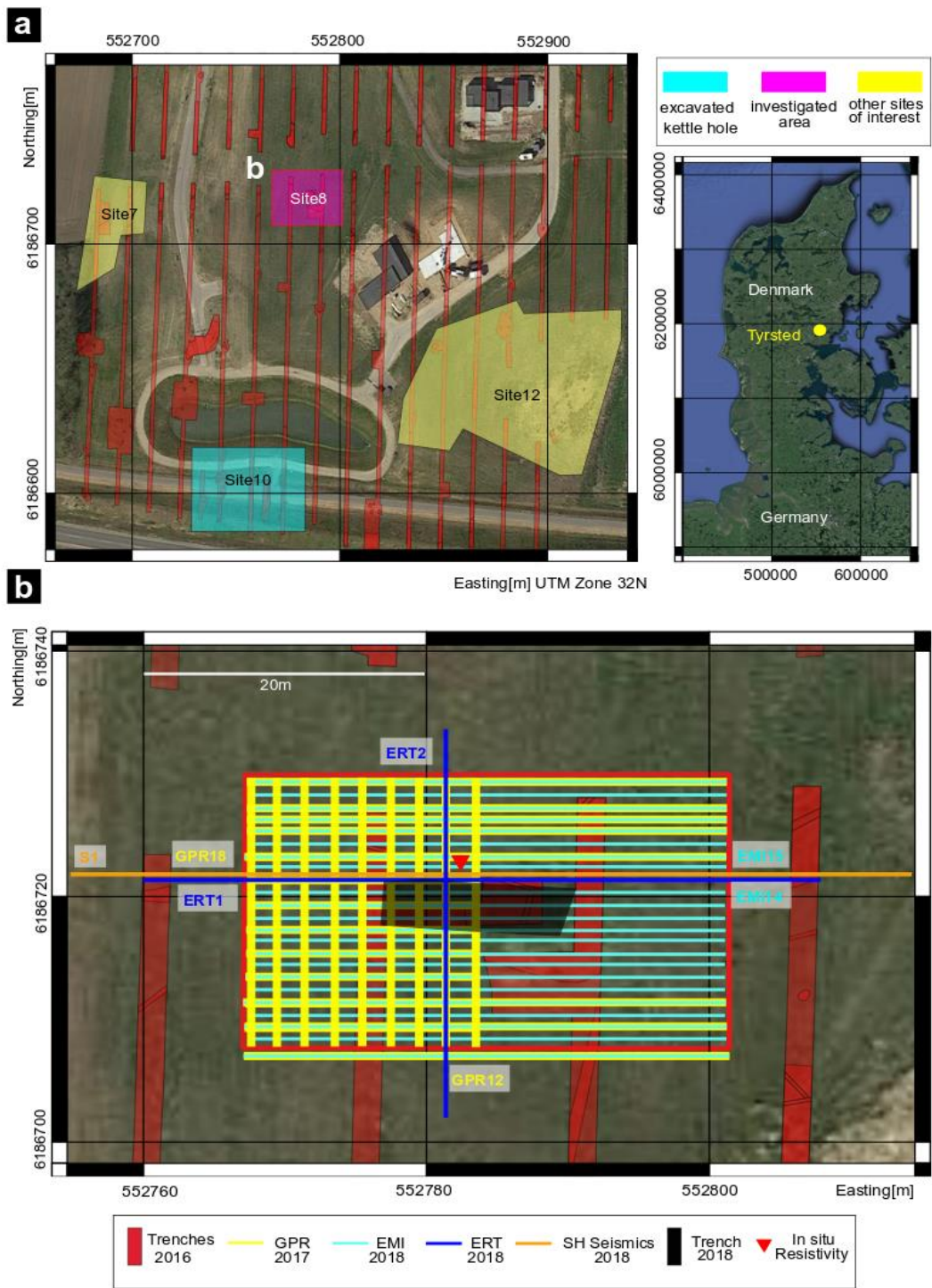


Figure 1: Location of the sites of interest in Tyrsted and geophysical measurements carried out at site 8. a) Location of the Tyrsted area and the overview of the archaeological investigation (trenches and sites of interests); b) Focus on area 8 indicating the geophysical measurements (color coded) presented in this study and carried out in different campaigns.

3. Archaeological research at Tyrsted (site 10)

In 2016 an extended archaeological excavation survey (transects in Figure 1) was made in advance of construction work to detect areas with prehistoric activities. In accordance with the Danish law, areas with significant prehistoric activity should be kept free of construction work or such areas must be excavated prior to construction work. In late December 2016, archaeologists from Horsens Museum excavated the kettle hole at Site 10 (cyan square in Figure 1). This excavation was caused by the construction of a new road. The investigation of some prehistoric peat extraction pits in a small kettle hole had been successfully completed, and the only thing yet remaining was to extend the excavation to the bottom of the kettle hole in order to have a look at the deeper subsurface sediments (Borup & Nielsen 2017; Eriksen *et al.* 2018). The kettle hole proved to have exquisite conditions for organic preservation. In the deep gyttja layers the almost complete skeleton of a pike was soon accompanied by a wealth of very well preserved floral macro-remains, a Late Palaeolithic Bromme type tanged point (c. 13.000 – 12.500 calBP), more Late Palaeolithic flint artefacts, and five very well preserved reindeer antlers. Unfortunately none of the antlers were found in situ. Due to the scheduled construction work, the excavation had to be resumed in the dead of winter under quite challenging circumstances (Figure 2a).



Figure 2: Excavated kettle hole and archaeological finds at site 10. a) The kettle hole (Tyrsted site 10) during excavation in February 2017. View towards the Southwest. Photo © Horsens Museum. b) Late Palaeolithic flint artefacts found during the excavation of Tyrsted site 10. Photo © Horsens Museum. c) One c. 14,000 year old jaw of pike (*Esox lucius* sp.). Photo © Morten Fischer Mortensen. d) One c. 14,000 year old birch stem with tooth marks from beaver gnawing. Photo © Horsens Museum.

Accordingly, the scheduled construction work was put on hold to allow for a rescue excavation of the small kettle hole. This was completed in February and March 2017. Due to the challenging circumstances,

the focus of the excavation was placed on the documentation of the find-context of the anthropogenic objects, and on securing the scientific potential with respect to dating the find horizon(s) and establishing the palaeoecological background for the Late Palaeolithic settlement at the kettle hole. During the excavation, numerous Late Palaeolithic flint artefacts were recovered from the gyttja and peat layers (Figure 2b). These sediments also produced ample remains of fish (in part very well preserved complete specimens of pike (Ritchie, 2018), but most likely naturally embedded) (Figure 2c) as well as floral macro-remains, e.g. birch and poplar stems (with tooth marks of beaver), branches, twigs and even well-preserved leaves (Figure 2d).

Archaeologists depend on high-resolution stratigraphic data in order to contextualise prehistoric human behaviour within an environmental setting that was very different from modern landscapes and biotopes. In this respect, the importance of the small kettle hole at Tyrsted for our understanding of the timing and nature of the colonization of Southern Scandinavia following the end of the Weichselian Ice Age is manifest. It represents a sediment trap where outstanding conditions for preservation of organic remains allow us a rare glimpse of the organic artefact inventory from the Bromme culture. The sediments are partly disturbed and therefore, the archaeological finds were partly relocated and cannot be dated stratigraphically.

4. Methods

In the following section we report the geophysical measurements (Figure 3) we carried out in different campaigns between 2017 and 2018.



Figure 3: picture from the field during the different geophysical campaigns. a) GPR measurements done pulling the 200 MHz antenna on the ground in 2017; b) Geophones on the ground during the seismic

measurements done in 2018. c) *In-situ acquisition of the resistivity values during summer 2018*; d) *ERT profile carried undertaken during summer 2018*.

4.1 Ground penetrating radar and electrical resistivity tomography

2D ERT and GPR were used to investigate the kettle hole of site 8. Common to both methods is the inverse relationship of data resolution and penetration depth, which has to be taken into account.

4.1.1 Ground penetrating radar

An electromagnetic pulse is emitted by a transmitter, the amplitude and phase of the reflected part of the pulse is recorded by a receiver after a measured time. The reflections are caused by contrast in dielectric permittivity whereas depth of investigation is controlled by electric conductivity, antenna frequency and by geometrical spreading due to the propagation of a spherical wave (Davis and Annan, 1989). Both signal strength and center frequency of radar signals decrease during wave propagation due to energy absorption (e.g. Wunderlich and Rabbel, 2013). This leads not only to a limitation of depth penetration but also to a decrease in spatial resolution with depth. A subsurface characterized by a high water content and clay sediment strongly attenuates the radar signal and reduces the depth of investigation (Davis & Annan, 1989). Penetration depth and resolution are also influenced by the GPR antenna frequency. Lower antenna frequencies are favourable for greater penetration but result in a decrease in resolution which is approximately defined as a quarter of the GPR wavelength and ranges from 0.08 m for saturated sands with 200 MHz antennas to 0.04 m for dry sands with 100 MHz antennas (e.g Van Dam, 2000). However, the best vertical resolution that can be reached is about one quarter of the dominant wavelength (e.g. Neal, 2004; Sheriff, 1977). Regarding sedimentological interpretation, this means that the lower stratification can be poorly imaged compared to the upper stratification. In this context drilling or excavation trenches enable the understanding of the stratigraphy and facies patterns in the radargrams and is very important for ground truthing.

A GSSI GPR unit with a 200 MHz center frequency antenna was used to perform the measurements at site 8 (the antenna was pulled on the ground using markers along measuring tapes and the acquisition settings are the following: sampling frequency 4273 MHz and interpolation to 0.01 m trace spacing; number of samples 512; number of stacked scans 8; time window 100 ns). The GPR campaign took place in June 2017 with the aim to have a first look at the area and to identify the location and the dimension of the wetland area. The measurements were carried out by pulling the GPR antenna on the ground following the natural topography of the subsurface. The field conditions in some locations of site 8 were difficult for the application of GPR because part of the surface was covered with water. We avoided that part during the GPR survey, therefore some profiles were carried out only in the first half of the area and are 16 m long (yellow lines, Figure 1). Due to the mentioned unfavorable field conditions we decided to undertake the NS profile only in the west side of area 8. Therefore, a rectangular grid of GPR profiles with 2 m spacing in both directions was performed, covering an area of 575 m² of the total 750 m².

The GPR processing sequence included:

- Timezero correction which adjusts the GPR traces to a common time-zero position (t0 time shift to -7ns)
- Subtract mean trace which filters out continuous flat reflections caused by multiple reflections between 0 and 100 ns
- Spreading correction enhancing signals located at greater depths
- Time-depth conversion using a constant velocity of 0.065 m/ns, derived from diffraction hyperbola fitting

In order to ensure the quality of the data, we performed spectrum analysis on these GPR data. The spectral maximum is at 130 MHz, the signal frequency band ranges from 0 to 500 MHz, ensuring a sharp wave form. Considering the quarter wavelength ($\lambda/4$) criterion and the average velocity reported above, the expected vertical resolution is of the order of 0.10 to 20 m. After the processing of the profiles the interpretation of the GPR images was performed visually, picking the reflections from different sediments using the Kingdom IHS Software. This software allows the visualization of GPR profiles together with the stratigraphy from drillings and wells. Using the stratigraphic information coming from the small trenches done in 2016 we tried to follow the reflectors coming from the sediment filling the kettle hole (grey-black clay gyttja). The picked reflections were then interpolated and a contour map as well as a 3D model were created using the Surfer Software. The interpolation for the 3D model was set up applying the Nearest Neighbor Method (<https://support.goldensoftware.com>).

4.1.2 Electrical resistivity tomography

A geoelectric measurement is made with four electrodes, the current flows between the two outer electrodes and the potential difference is measured between the two inner ones. Electrode spacing and penetration depth increases during the survey until the maximum spacing is reached, which provides the deepest resistivity information (Loke, 2016). Geoelectric profiling is conducted by repeating these four-electrode measurements densely spaced along the survey line. Zones of different resistivity are an indication for different compositions of the subsurface including a variation of the water content. Geoelectric data is always analyzed in a tomographic inversion process leading to images of the subsurface in terms of specific electric resistivity (Electric Resistivity Tomography, ERT). To improve the results, a comparison with stratigraphic information is needed. Therefore, we can improve the ERT results by constraining the tomographic computation with depth information from drillings (Wunderlich et al., 2018).

In summer 2018 we performed two intersecting ERT profiles (ERT1 and ERT2, blue lines Figure 1). A RESECS (Geoserve) system was used to carry out the measurements. Wenner-Alpha, and Dipole-Dipole array configurations were used, providing better resolution of horizontal subsurface structures and lateral

variations of the resistivity (Loke, 2016). ERT1 (47.5 m long) consists of 96 electrodes with 0.5 m spacing whereas ERT2 is 31.5 m long and made of 64 electrodes with 0.5 m spacing. Electrode locations were determined by Differential GPS (Trimble R10). The inversion was carried out using the BERT software (Boundless Electrical Resistivity Tomography, Günter et al.(2006)), a finite-element (FE) inversion software. The model of the subsurface is made of triangular cells that are small at the surface and become larger with depth indicating a decreasing of the structural resolution of ERT. A regularization parameter of $\lambda=20$ was applied in the inversion, that was selected based on the L-curve method (L2-NORM) (Loke, 2003; Hansen and O'Leary, 1993).

An earth resistivity meter was used to measure the resistivity on the vertical profile of the excavation trench. The resistivity meter is equipped with four electrodes in Wenner-Alpha configuration (5 mm long and 5 mm distant with 1 mm diameter). This quadrupole was inserted in the soil ensuring the contact between the electrodes and the ground. The surface contact area of the electrodes is about 1 mm^2 . Due to the varying soil conditions the electrodes had different penetration depths in different layers. This was compensated by applying correspondingly varying geometry factors considering that the electrodes are nearly punctiform. We measured a vertical profile 5 cm point spacing and compared the measured values with those coming from the other methods to better understand the change of each property in the sediments in the kettle hole.

4.2 Electromagnetic induction

Electromagnetic Induction (EMI) is a more mobile sounding method than ERT, making it attractive for resistivity mapping. However, it shows less resolution in depth sounding than ERT. EMI measurements allow to deduce a three-dimensional distribution of the electric conductivity of the subsurface. EMI devices emit an oscillating electromagnetic (EM) field from a transmitter coil. The EM field induces eddy currents in the subsurface, which in turn induce a secondary magnetic field depending on the electric conductivity distribution. Receiver coils record the ratio of the primary and secondary magnetic field whose out-of-phase component is directly proportional to the apparent conductivity (see e.g. Bonsall et al., 2013). The in-phase component is sensitive to the magnetic susceptibility (which is not further considered here). The depth of investigation depends on the separation of transmitter and receiver coil, the frequency and the orientation of the coils with respect to surface and each other and subsurface properties. Even though the measurements are usually assigned to a distinct depth interval, the values are affected by the subsurface volume through which the EM field propagates. Via inversion computations fitting the measured apparent conductivities values, subsurface models consisting of conductivity depth functions are derived (e.g. De Smedt, 2011). These are stitched together and form a three-dimensional data cube.

We used the CMD Mini-Explorer by GF Instruments and conducted measurements in vertical (VCP) and horizontal coplanar (HCP) configuration. The device is operating at 30 kHz with three receiver coils in 0.32 m, 0.71 m and 1.18 m distance to the transmitter. The manufacturer gives approximate values of sounding depth. Corresponding to the three coil separations these are 0.25 m, 0.5 m and 0.9 m in VCP configuration and double in HCP configuration. The area was covered with parallel profiles in east-west direction and 1

m separation (see Figure 1, cyan lines). The sample frequency was 10 Hz. To reduce noise, we applied a lowpass butterworth filter (third order, cutoff. wavenumber = 0.7 m^{-1}). Finally, the inversion was performed with the software IX1D by Interpex. We derived 'smooth models' (Constable et al., 1987) with ten layers from 0.1 m depth to 1.8 m depth with a starting conductivity of 50 mS/m.

4.3 Seismics

Seismic waves are radiated from natural or artificial tremor sources and propagate through the solid earth as short-time pulses or continuous waves depending on the source type. There are two groups of seismic waves: compressional waves (P-waves) and shear waves (S-waves). The propagation velocities of both P- and S-waves depend on soil composition, fabric, effective ambient pressure and temperature. S-waves have two properties that make them for many near-surface applications more suitable than P-waves: (1) In water-saturated unconsolidated sediments S-wave propagation velocities are much slower than P-wave velocities (up to a factor of 10). In this case S-wave imaging of geological structure shows much higher spatial resolution than P-wave imaging (Stümpel et al., 1984), and (2) in contrast to P-waves, S-wave velocity and reflection strength are only very little influenced by water saturation. Therefore, in these conditions, S-wave velocities often can be more directly correlated with lithology than P-wave velocities. In contrast, P-wave velocities are strongly influenced by pore fluids, that is in near-surface applications by the ground water level (Schön, 2015). For these two reasons, we preferred to apply SH waves (polarized horizontally, perpendicular to the propagation direction) for studying the Tyrsted kettle hole. Stümpel et al. (1988) were the first to apply S-wave profiling for a geoarchaeological study of an estuary at Río Vélez (Spain). But the use of this technique is not wide-spread and has only lately been intensified (e.g. Obrocki et al. 2018; Rabbel et al. 2015; Krawczyk, 2012 ; Beilecke and Krawczyk, 2011; Polom et al., 2010; Stucchi, 2017).

The seismic reflection method and ground-penetrating radar (GPR) are both important geophysical tools based on wave propagation and reflection, but wavelength ranges, and, consequently, resolution and penetration depths differ significantly. Seismics has a larger depth penetration but in most cases a lower resolution than GPR. The reflections conform to images of the geological deposits and are caused by major changes in seismic impedance. Stacks of thin layers can cause constructive and destructive interference of the wave trains, which may alter the layer appearance and decrease resolution. (Mayer 1980; Van Dam, 2000).

Seismic resolution is the ability to distinguish between two features from one another. Vertical resolution represents the distance between two interfaces as separate reflectors while horizontal resolution recognizes two lateral displaced features on the single interface (Kallwait, 1982). The widely accepted limit of vertical resolution is a quarter of the dominant wavelength. The lateral resolution refers to how close two reflecting points can be recognized as two separate points rather than one in the horizontal direction. Corresponding to optics the horizontal resolution is often identified with the 1st Fresnel zone depending on both target depth and the wavelength. However, digital data processing can improve the horizontal resolution by applying a migration filter leading to the same quarter wavelength limit as for vertical resolution (e.g. Yilmaz, 2001).

4.3.1 Reflection Seismics

Reflection seismics deals with the use of seismic waves (S-waves in our case), which reflect at geological interfaces separating layers with different seismic impedance. Seismic impedance is the product of density and seismic wave velocity. For near-surface prospecting seismic waves can be generated with hammer blows on a metal plate at the surface. The emitted and reflected waves are recorded along the survey line with a set of equally spaced receivers (geophones). The hammer blows are repeated at a set of equally spaced source points for sounding the subsurface most uniformly. The results are seismograms showing the amplitudes of the emitted and reflected arrivals as a function of geophone location and travelttime. From these distance-traveltime functions of the relevant reflections can be derived for determining the location and depth of the geological interfaces. Digital amplitude processing, such as so-called common-midpoint (CMP) processing and seismic migration, is used to convert seismograms into seismic reflection images showing depth sections of the stratigraphy in a more direct way. The theory and analysis of seismic reflection data is well documented (e.g. Yilmaz, 2001).

For studying the kettle hole we conducted a 61 m long S-wave profile almost in the middle of site 8 (orange line in Figure 1). Table 1 shows the acquisition parameters (a) and the processing parameters (b). The data were recorded with 3 Geometrix Geode seismographs placed in line, equipped with 72 10-Hz horizontal geophones oriented perpendicular to the profile line. The seismograms were digitized with 0.125 ms sampling interval and 0.5 s recording time. We excited horizontally polarized S-waves (SH-waves) by horizontal hammer blows against the sides of a steel bar, which was coupled to the ground by steel spikes mounted at the bottom of the bar. The use of a horizontal force perpendicular to the profile line generates dominantly SH-waves. Therefore, P-waves were not observed in the data. The source points were located midway between the receivers and the steel bar and blows oriented perpendicular to the profile line.

The acquired data covers a frequency band from 10 Hz to 90 Hz. In the processing of the reflection data we followed the standard procedure of the CMP-method. It includes steps of editing headers, binning, editing the tracks, calculating static corrections, applying frequency-wave-number filtering, and various band-pass filters. Aim of the processing flow is to suppress surface waves (ground roll) and to enhance the reflections. In case of SH-seismics the surface waves are Love waves, which are a superposition of over critically reflected SH-waves, which occur at larger offsets, meaning in our case at offsets > 5m. However, for seismic reflection imaging the SH-wave reflections need to be separated from the Love waves. Therefore, we included only records with offset < 5 m in the reflection processing.

After the processing a sequence of trial CMP stacks was created as part of a velocity analysis, and finally the migration of the stack section was performed. The seismic data were processed with the VISTA software (<https://www.software.slb.com>), processing flow see Table 1. The comparison between the raw and processed data is shown in Figure 4.

Seismic acquisition parameters		Seismic processing flow	
<i>Item</i>	<i>Specification</i>	<i>Process</i>	<i>Processing parameters</i>
Profile length	61 m	Geometry	n. a.
Receiver type	Horizontal geophone 10 Hz	Trace edit	n. a.
Receiver number and spacing	122, 0.5 m	Ormsby bandpass filter	10-15-90-120 Hz
Source type	Horizontal sledge hammer, 2-fold vertical stacking	Spreading correction	n. a.
Source point number and spacing	123, 0.5	Spike deconvolution	Operator 40 ms
Source-receiver offset min-max	0.25 m, 35.75 m	FK-filter	Pie slice 222 m/s
CMP number and spacing	244, 0.25 m	CMP velocity analysis	3-fold super gather
CMP maximum coverage	125	NMO correction	30% stretch mute
Recording unit channel number	72	FD time migration	RMS velocity model
Sampling rate, record length	0.125 s, 0.5 s	Time-to-depth conversion	Interval velocity model

Table 1: Acquisition and processing parameters of the SH-wave seismic reflection profile.

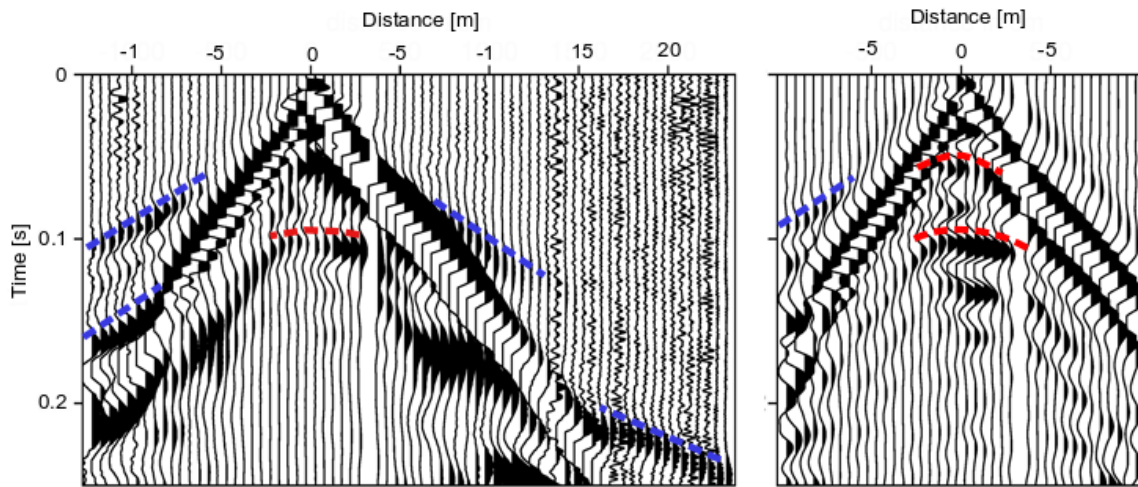


Figure 4: data section of the raw (left) and preprocessed (right) data. The red dashed lines indicate the reflections, while the blue dashed lines indicate the refracted waves.

4.3.2 Refraction Seismics

Refraction seismic data interpretation aims at determining the spatial distribution of seismic wave velocity as a characteristic of sediment type. This is accomplished by analyzing the arrival times of the waves transmitted through interfaces and refracted through the lying layers and back to the earth's surface. The refraction effect depends on the ratio of the seismic velocity of the layers above and below the refracting interface. The method is typically used, inter alia, to localize major bedding boundaries, and to characterize the degree of weathering.

Seismic refraction interpretation requires the identification of refracted arrivals in the seismograms, first arrivals mostly, and picking of their traveltimes as a first step. From these a simplified seismic velocity model of the subsurface is generated, which serves as a starting model for a tomographic inversion computation. The result of the refraction tomography is a 2D distribution of the wave velocities representing a depth section underneath the profile line. For traveltimes picking we used the interactive analysis tool PASTEUP for wide-angle seismic data (Fujie et al., 2008). Thereafter, a tomographic inversion software (tomo2D from Korenaga et al., 2000) was applied to determine the S-wave velocity model. Since the S-wave velocities increase very strongly in the uppermost few meters, we followed an inversion scheme where the tomographic velocity model was updated sequentially from top to bottom in separate steps. This was necessary in order to obtain a numerically stable and physically reasonable tomographic solution. The steps were as follows:

1. Estimating a 1D linear two gradient model: strong gradient for the upper 2 m (100 m/s -> 200 m/s). Below a lower gradient was used, with increasing velocity is up to 280 m/s at 10 m depth.

2. Inversion of first arrival traveltimes with maximum source-receiver distances of 6 m to determine the velocity model close to the surface,
3. Inversion of first arrival traveltimes with maximum source-receiver distances of 15 m using the result of step 1 as starting model,
4. Inversion of all traveltimes picks using the result of step 2 as starting model,
5. Application of a smoothing filter to the result of step 3 with 10 m horizontal and 2 m vertical operator length for suppressing numerical artefacts .
6. Inversion of all traveltimes picks using the result of step 4 as the starting model.

Each inversion run (1 to 3 and 5) showed convergence within 5 iterations with a RMS final of 2.83 ms. In each iteration step a maximum velocity update of 40% was allowed.

4.4 Stratigraphic analysis

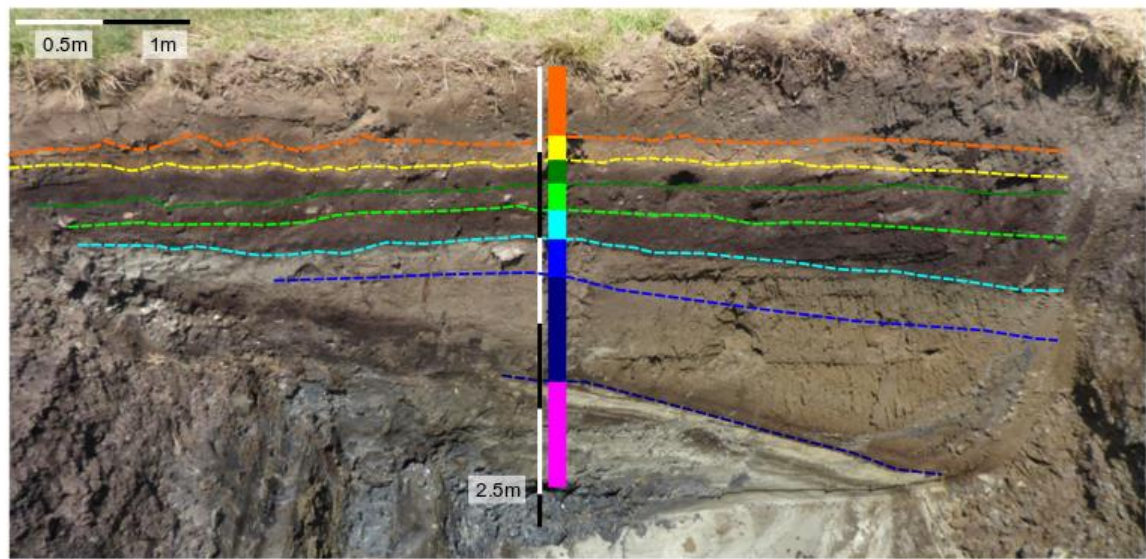
The first transects, made in 2016 prior to the geophysical survey (red boxes in Figure 1), were about 2 meters wide and 15 meters apart from each other. They were excavated with a machine to a depth of 0.5 m and locally 0.70 m all over the field to enable detection of prehistoric activity. These transects also gave first indications of the ancient wetlands/possible kettle holes below the plow layer.

For investigating and comparing the stratigraphy with the geophysical results from site 8, in summer 2018 a test trench of 13 m by 4 m was excavated with a machine to a depth of approximately 3.5 m. Based on the GPR survey (Figure 1) the position of the trench was chosen to enable ground truthing of the geophysical results regarding the location of the supposed kettle hole. The stratigraphy of the sediment was described in the field (Figure 5) following the Troels-Smith system (Troels-Smith, 1955).

5. Results

5.1 Stratigraphy of the investigated kettle hole

In summer 2018 a trench at site 8 was excavated to ground truth the geophysical measurements. The resulting stratigraphic profile serves as a reference for the interpretation of the geophysical data and is, therefore, presented first. The sediments consist apart from the upper plow layer and disturbed sediments (0 - 0.83 m) of peat and gyttja. The description of the lithology and the main stratigraphic units are shown in Figure 5. The peat (0.83 m - 0.91 m) has a distinct brown/black and is highly decomposed. Stones and pottery in the sediment are the remains of a ritual deposition made during the Iron Age in the peat extraction pits. The peat itself most likely formed during the Boreal, Atlantic and Subboreal periods. Underneath the peat layer the sediments consist of gyttja (0.91m - 1.03 m) probably formed in the early Holocene. Below is a highly minerogenic clay-gyttja (1.03 m - 1.22 m) which are typical for the Younger Dryas sediments in this region. The main components in the underlying sediments are gyttja (1.22 to >1.82 m) with an increasing content of lime and most likely belongs to the Allerød period. The Bromme layer would be then expected to be located between the Late Allerød layer and the oldest part of the Younger Dryas layer as shown with the dashed red line in Figure 5.



	Depth [cm]	Sediment	T-S-log
Orange	0-50	Grey-brown plowed soil, from 30 cm darker due to increased water content. Clay, containing sand, gravel and pebbles.	2As,1Ag,1As
Yellow	50-65	Yellowish clay deposition, presumably applied. Contains smaller stones	3As,1Ag +Ga,+Gs
Green	65-83	Grey-brown gyttja containing some sand	4Ld ³ ,+Ga
Light Green	83-91	Strongly decomposed peat containing several larger stones and fragments of pottery The layer is disturbed by Iron Age peat digging	4Dg
Cyan	91-103	Grey-black clay gyttja (EARLY HOLOCENE)	3Ld ² ,+1As
Blue	103-122	Grey clay / sandy deposition that eroded into the lake. Contains large flint block (YOUNGER DRYAS)	2Ag,2Gs
Dark Blue	122-182	Grey-green gyttja, that in the deeper part of the kettle hole continues to approximately 350cm (LATE ALLERØD)	4Ld ¹
Magenta	> 182	Lime gyttja (EARLY ALLERØD)	

Figure 5: simplified lithology of the investigated kettle hole. The different sediments are color coded.

5.2 Ground penetrating radar and electrical resistivity tomography

The GPR and ERT surveys at area 8 are presented in Figure 6. The GPR investigation carried out in June 2017 was performed under non-optimal weather conditions because of large water puddles located in the center of the investigation area. Several profiles are therefore shorter than the total length of the area avoiding the part covered by water.

GPR12 (Figure 6c) and GPR18 (Figure 6d) are two profiles intersecting in the center of the area approximately at the location of the supposed kettle hole (Figure 6e). Both profiles show a first shallow

reflector at the top of the profile (~0.5 m) correlated to the topsoil. At the crossing point an interface with a round shape is visible presenting a depth of ~1.5 m. This feature fits with the shape of a pond, but from the stratigraphic information we know that this interface does not correspond to the complete profile of the kettle hole. It is indeed associated with the transition between the grey-clay/sandy deposition that eroded into the small lake and the Grey-green gyttja (white line in Figure 6e). In this transition it would be possible to find the cultural layer of the Bromme culture and, therefore, it was used to create the contour map in Figure 6b. An interpolation between the measured profiles gives us a first overview of the horizon distribution. Referring to Figure 6b a dipping interface down to 1.6 m depth is then visible in the north-east part of the area.

In the eastern portion of GPR18 a dipping reflection is visible only until ~1.8 m depth (white arrow in Figure 6e). This interface indicates a reflector which probably goes deeper and can be correlated to the transition Grey-green gyttja and Lime Gyttja sediment (Figure 6e). The depth of investigation is not enough to follow this limit because below 2 m the radargram shows no clear reflection. In general, we can recognize that below 1 m depth the reflections become less visible.

The red squares indicate the location of the test trenches done in 2016 and the radargram presents some disturbances at the same position confirming the shallow work done in this area. The depth of investigation of GPR is unfortunately less than 2 m. The high water content and the gyttja sediments of the subsurface attenuate the radar waves making the detection of the bottom not possible. The topography also helps to identify a small depression almost in the middle of the area showing almost 1 m of elevation difference between the start and the end of the ERT profiles (Figure 6c and Figure 6d). The GPR section did not need a topographical correction because the surface was sufficiently plane and flat.

The geoelectric survey at site 8 delivered corresponding 2D resistivity tomographies shown in Figure 6c/d. ERT1 shows rms residuals of only 1 to 3% after 4 iterations. Minimum resistivity values of ~15 Ωm are found underneath the depression at the location of the supposed kettle hole. Maximum values of ~150 Ωm are found in the topsoil of the elevated parts of the profile. The high resistivity layer on top seems to stop around 23 m and it starts again (but less strong) at about 32 m (red dashed lines in Figure 6d), below this first interface, a layer with lower resistivity occurs. Locally the resistivity increases with depth but almost in the middle of the profile a low resistivity area is visible. The same is found on profile ERT2 (rms 2 to 3%, lower resistivity value ~15 Ωm and higher resistivity value ~120 Ωm) in which a topsoil layer with high resistivity is present and a low resistivity area almost in the middle of the profile is visible. According to the topography the blue area corresponds to the location of the kettle hole filled with gyttja sediments characterized by a low resistivity (~ 15/20 Ωm) (red squares figure 6d and 6e). The presence of clayish sediment in the kettle hole associated with a high water content in that part creates a low resistivity condition compared to the surrounding area favorable for the detection of the kettle hole. The depth of investigation (DOI) is about ~5 m but it is not possible to understand the whole shape of the feature, particularly the bottom of it, because of too little resistivity contrasts.

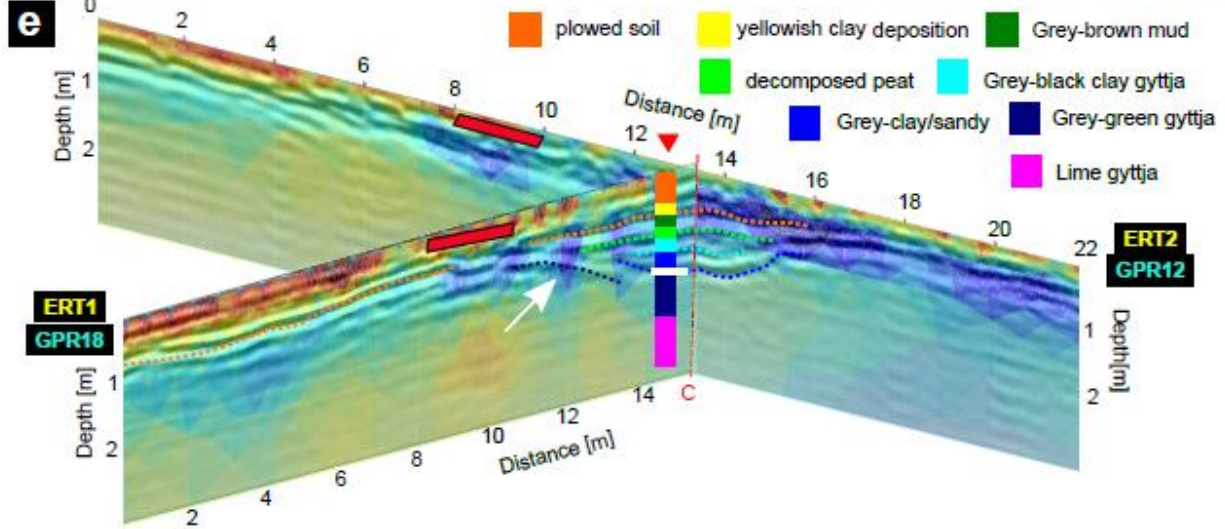
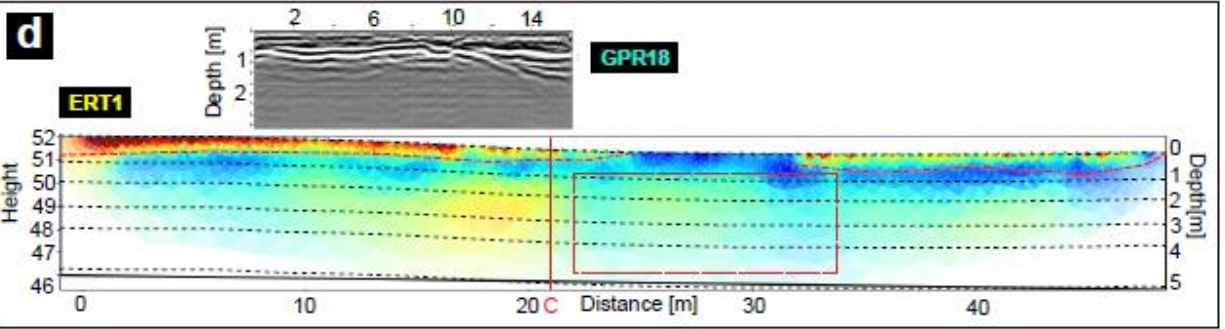
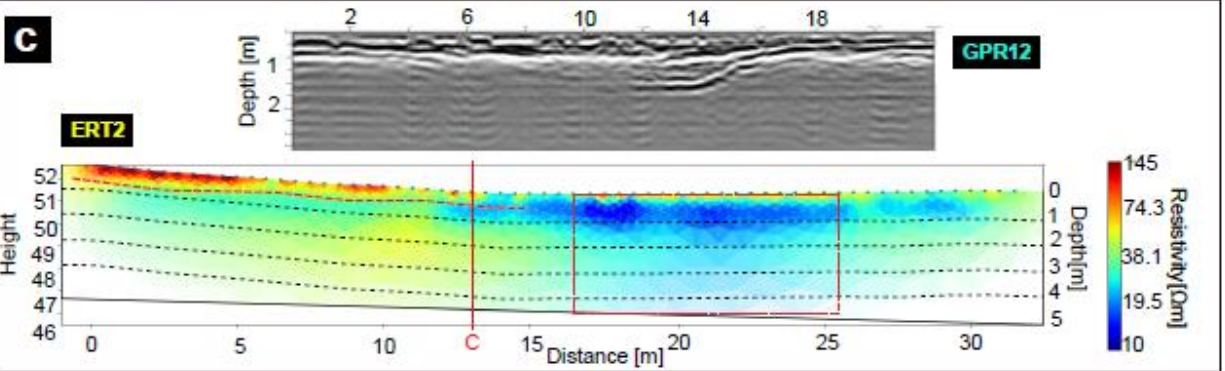
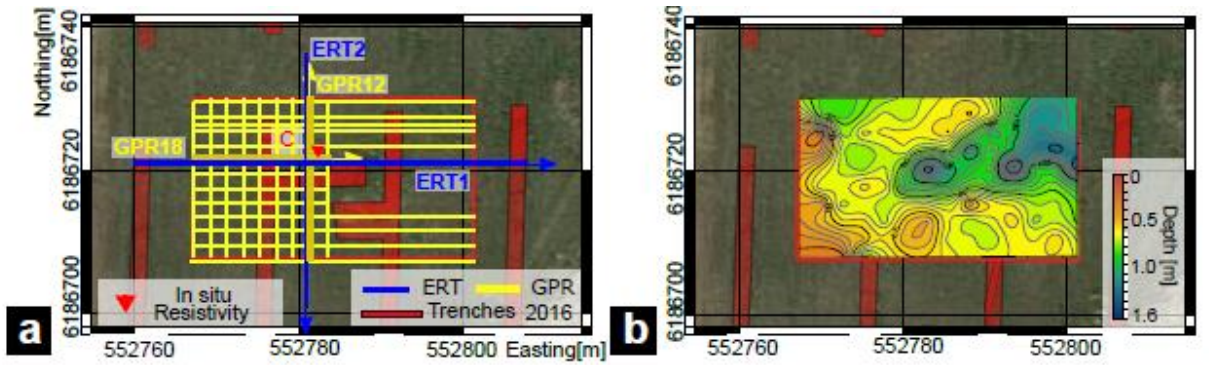


Figure 6: Results from the GPR and ERT measurements in area 8. a) Location of the measured profiles. b) Depth contour map of the GPR reflection from the transition between grey-clay/sandy deposition and the grey-green gyttja. The color scale indicates the depth of this interface in the investigated area. c) GPR12 in comparison with ERT; the red square indicates the location of the supposed kettle hole. d) GPR18 in comparison with ERT; the red square indicates the location of the supposed kettle hole. e) GPR profiles together with the ERT profiles crossing the middle of area 8 at the location of the supposed kettle hole. The orange and cyan dashed lines indicate the top-soil interface and the grey-black clay gyttja/grey-clay sandy deposition associated with the transition of the shallow layers of the kettle hole (see stratigraphy in Figure 5). The crossing point is indicated with a red line. The red triangle indicates the location of the in-situ resistivity measurements and the red squares the trenches made in 2016.

5.3 EMI

For comparison with ERT (Figure 6d), we show vertical sections of the EMI inversion crossing the location of the kettle hole in Figure 7a. In the inverted EMI resistivity/conductivity model the uppermost layer shows high resistivity values ($85 \Omega\text{m}$) at the top underlain by decreasing resistivity values down to $30 \Omega\text{m}$. At 20 m distance, in both profiles a feature marked by low resistivity values appears in agreement with the supposed location of the kettle hole. The horizontal distribution of the resistivity values is presented in Figure 7b, where some separate low resistivity areas are found at shallow depth, which appear to merge at larger depths. The total lateral dimension of this anomaly extends with increasing depth. This is somewhat surprising because a narrowing with depth might be expected for a depression filled by conductive sediments. However, it has to be considered that the EMI slices of Figure 7 show only the very near-surface structure down a depth of ~ 1.5 m depth. This is indeed the depth where the kettle hole reaches its maximum extension as will become apparent in the seismic section (see Figure 8 below). Underneath this level the sides of the pod converge again and become steeper, but the EMI method is not able to resolve it. The depth of the layers are subject to a certain method-inherent ambiguity. Therefore, to determine absolute depths from EMI a calibration is needed, which can be performed through drilling or excavation. Still, the lateral dimensions and vertical sequence can be derived from the EMI inversion results alone.

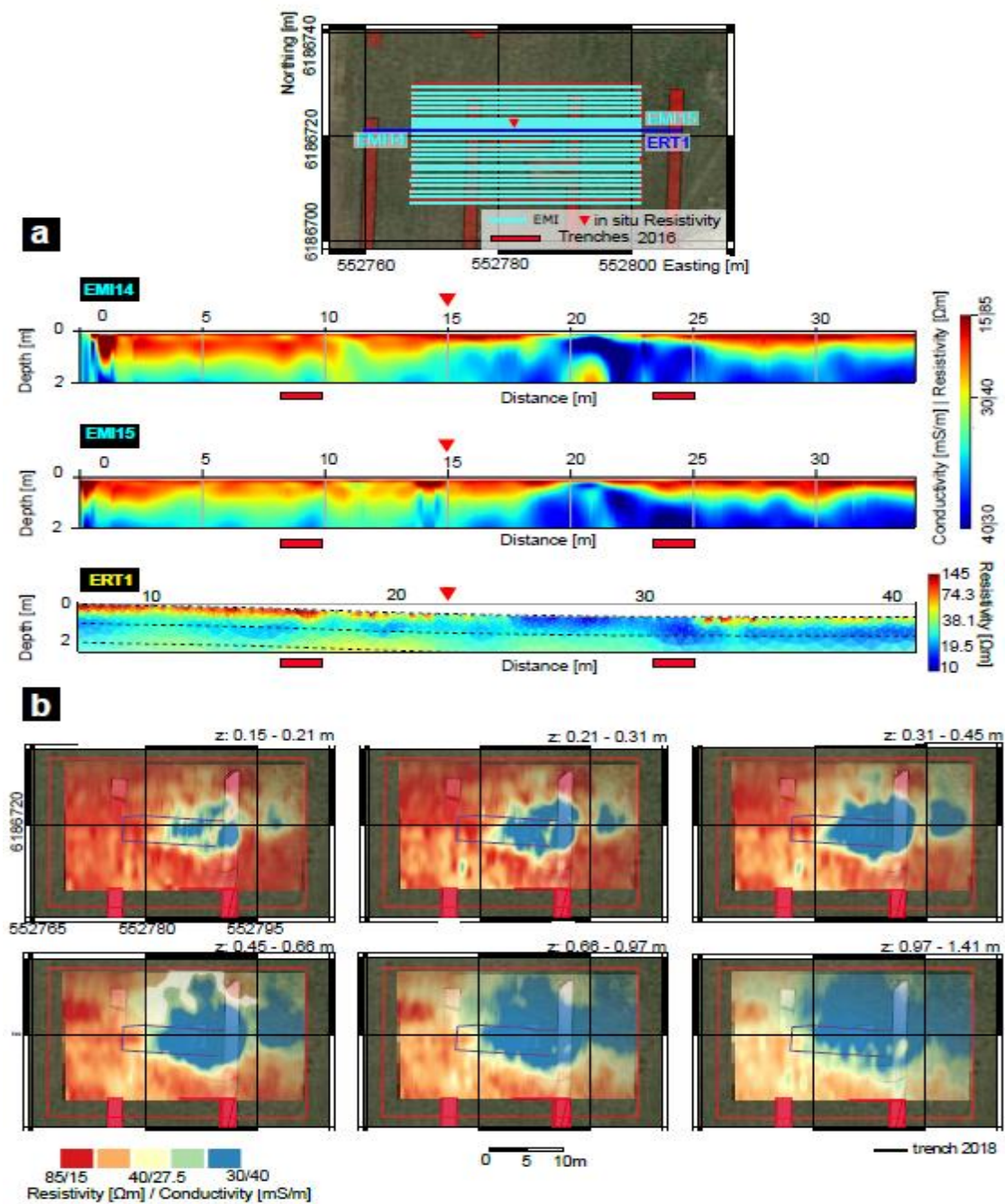


Figure 7: results from the EMI measurements after inversion. a) Results of the EMI inversion from Profile EMI14 and EMI15. EMI15 is compared with ERT1 at the same location (the ERT is cut on the external parts to help the comparison of both methods). EMI14 also shows a probable inversion artefact (at approx. 21 m, below 1.5 m depth) characterized by high resistivity values concentrated in a restricted area. b) Resistivity/electric conductivity distribution from the inversion of EMI measurements from different layers. The red triangle indicates the location of the resistivity in-situ measurements.

5.4 SH-wave seismic

The seismic profile crosses the location of the supposed kettle hole in W-E direction. Both reflection and refraction profiling provide structural information down to about 8 m depth (Figure 8). The bulk seismic structure can be recognized easily from the comparison of the first-arrival travel-time tomography (FATT) and the reflection depth section of shear-wave seismics. (Figure 8b). It allows a qualitative characterisation of the sediments. In general, the shear-wave velocities increase toward depth, with values ranging between 60 and 300 m/s. Between 25 and 55 m along the profile a distinct ~5 m deep depression is visible filled with soil with a velocity of ~100 m/s and even less. These low velocity values are in strong contrast to the surrounding and confirm the presence of a soil volume which is mechanically significantly weaker than its surrounding. The observed velocity values < 100 m/s indicate soft soil such as fine grained lake fills or swampy organic material. It can be interpreted as the filling of a small lake consisting of peat and fine grained organic enriched sediments like gyttja. Therefore, the observed decrease in S-wave velocity can be regarded as a clear indication of the kettle hole.

At about 7 m depth an interface appears, below which a velocity of ~300 m/s is found. The values of 150 to 300 m/s are typical for unconsolidated sediments of varying grain size, basically silt, sand and gravel (c.f. Wunderlich et al., 2017; Gomberg et al., 2003; Xia et al., 1999).

The spatial resolution of the reflection images can be evaluated using the depth-converted reflection section, from which we can determine the effective wavelengths (black-white wiggle, Figure 8b). In the upper 2.5 m of the section we notice that the wavelength is ~0.4 to 0.9 cm, while at deeper levels it becomes wider, ~1.6 m at approximately 5 m depth. This variation is caused by the dominant frequencies changing with depth due to absorption. The higher frequencies are still in effect at shallowest depths and get increasingly absorbed with depth. This consideration shows that the resolution is ~0.20 to 0.40 cm order of magnitude.

Considering Figure 5 we notice that most of the layers have a thickness which is less than 0.25 m, which is comparable to the calculated resolution. Therefore, the interpretation of the internal structure of the kettle hole is possible only regarding major structure, but it remains challenging in the uppermost part where fine layering occurs (see below).

The image of the SH-wave reflection section is shown in Figure 8a and 8b, in the latter superimposing the S-wave velocity structure. It allows a further detailed structural interpretation. Focusing first on the profile segment between 25 and 55 m, we can recognize a series of reflections which form a bowl shaped reflector down to 5 depth that coincides with the velocity interface described above (feature A). We interpret this reflection as the main contour describing the shape of the kettle hole. Moreover, other dipping reflection elements are found that represent the internal structure of the kettle hole. We will come back to this set of layers below in the context of the trenching.

Outside the supposed kettle hole a sequence of strong-amplitude subhorizontal reflections is found in the uppermost 2.5 m and then again, locally, at depth >~6 m (feature B, Figure 8b). They are mostly correlated

with the structural changes of the S-wave velocity distribution. From this we can conclude that these reflections are caused most probably by layering of sediments with changes in grain size.

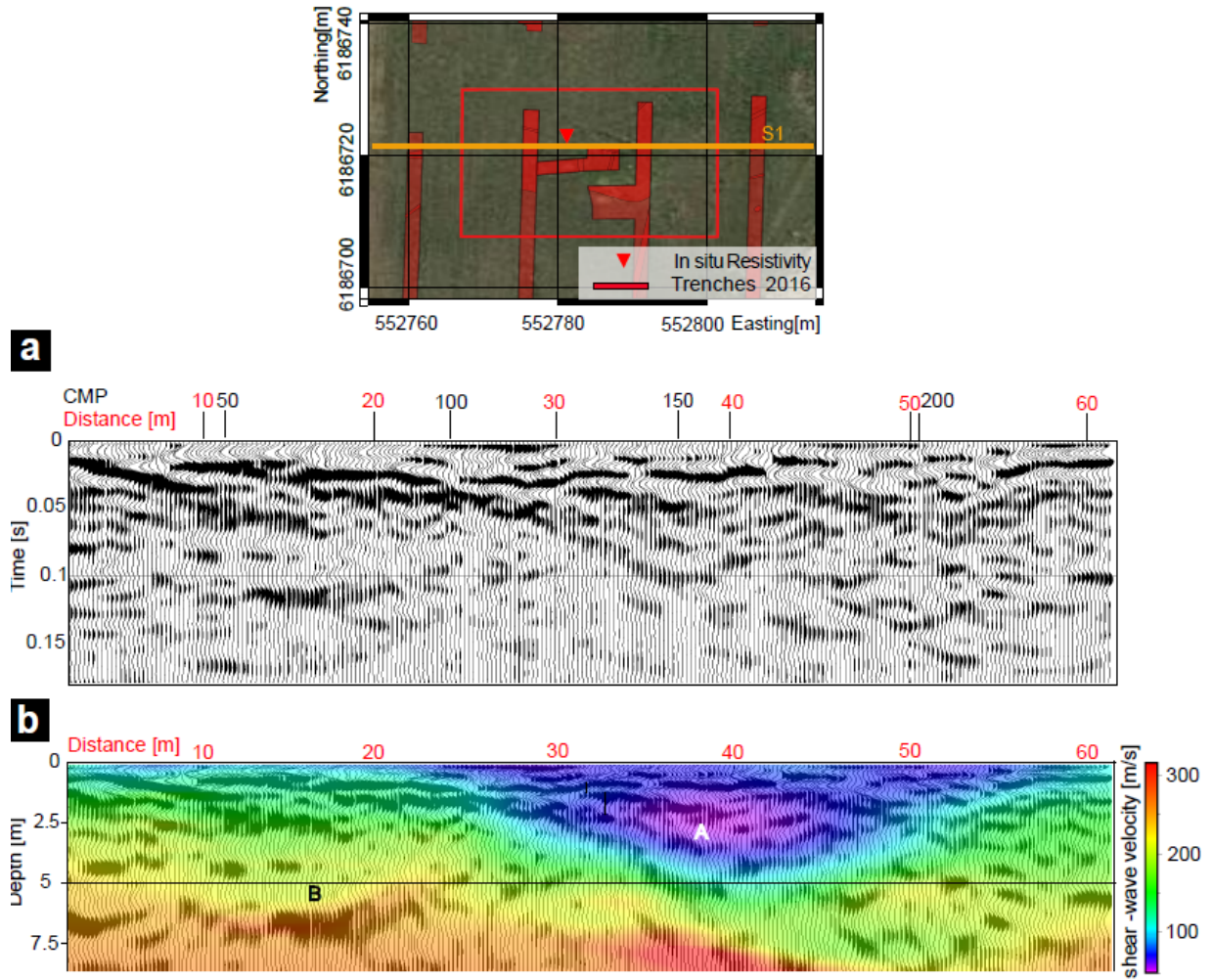


Figure 8: Shear-wave reflection seismic section of the profile crossing the location of the kettle hole a) Stack; b) time migrated and depth converted section, overlain by color-coded shear-wave velocities from the tomography (FATT). Feature A indicates the low velocity body associated with the kettle hole, while feature B corresponds to a deeper reflector located at a boundary with changing velocity. (CMP=common midpoint).

5.5 Comparison and Interpretation

Figure 9 shows a comparison between the stratigraphy excavated in the 2018 trench and the results of all geophysical prospection methods at the same location. Figure 9a shows the stratigraphy and the dashed lines indicate the main transitions between sediments. Figure 9b shows the corresponding seismic reflection section, in which we can recognize some shallow signals that can be correlated to the stratigraphy. The dashed blue lines indicate where the transition should be located in the seismic profile according to the stratigraphy. The first marks the transition between Younger Dryas and Late Allerød (where the Bromme horizon is supposed to be) and the second is the boundary between Late Allerød and Early Allerød deposits. This dipping interface is of special importance because it marks the boundary of the kettle hole. The geophysical results agree that all of them show it. According to the quarter-wavelength criterion the vertical structural resolution of the seismic reflection section is of the order of 20 to 40 cm. Since the stratigraphic layer thicknesses are partly less, or of the same order, the basic structure of the layer sequence is imaged well but all the interfaces as such are not resolvable. In particular the interpretation of the first meter is very difficult because of different factors, for instance it is difficult to separate direct waves, source signals and ultra shallow reflections close to the surface. Therefore, GPR can help to reconstruct the stratigraphy of the shallow subsurface at a higher resolution (see below). Figure 9d shows the GPR profile connected with the stratigraphy and some reflections have been recognized. The depth of investigation of GPR was however influenced by the high water content, visible with a high attenuation of the radar waves, thus the maximum information we got was less than ~2 m. Maximum amplitude values are visible from the top of the section until about 0.45 m depth; below this limit, the amplitude decreases (Figure 9f). In this part of the radargram, a series of interfering reflections is visible coming from narrow interfaces, making the interpretation of topsoil difficult. Between 0.45 m 0.65 m the amplitude decreases, indicating lower contrast and attenuation of the radar waves. The comparison with the stratigraphy shows a clayish deposition corresponding to this part. A variation occurs also at 0.80 m depth, which corresponds to the peat deposits. Below this limit the amplitude decreases through the gyttja sediment.

For estimating the vertical resolution of the GPR survey, the combination of stratigraphic column and depth-converted radargram can be used too (Figure 9d). Considering the frequency spectrum of the GPR trace (Figure 9g) at the same location we see that the center frequency is ~110 MHz which means that the dominant wavelength is ~0.5 m. Using the quarter-wavelength criterion, the resolution limit can be estimated from 12 to 14 cm layer thickness, which agrees with the visual appearance of the GPR section. Due to the absorption the transition between the green-gyttja and lime gyttja is not possible, therefore the complete shape of the former lake is missing. If we compare the thicknesses of the layers in Figure 5 with the calculated resolution we can conclude that this method is able to detect all the units but one. The Grey-black clay gyttja and the decomposed peat are considered like one layer (Figure 9d and Figure 9f).

The amplitude of the reflection depends on the reflection coefficient, which is related to the contrast in dielectric permittivity. Typically, the values of dielectric permittivity in wet environments are around 80 for peat (Neal, 2004), 2-5 for dry clay and 42-46 for wet clay (Conyers, 2013). The corresponding reflection

coefficients for the clay-peat and peat-gyttja interfaces are about 0.9 and 0.5 and it explains why the transition between clay and peat looks more pronounced as compared to the gyttja transitions. This conclusion comes using the values from the literature, therefore more GPR velocity and permittivity measurements are important to ground truth this statement.

However dealing with GPR can produce some depth errors. Velocity variation can happen in all directions and through different sediments. Unfortunately these effects can easily change the lower boundary of a structure/layer by more than 30% (Leckebusch, 2007). These pull-up/pull-down effects can only be corrected if the wave velocity is continuously determined along the profiles. Since velocity profiling is rarely conducted in GPR sounding ground truthing with drillings is needed for a calibration of the measured data.

The ERT results are shown in Figure 9c and the interface associated with the topsoil is well recognizable marked with high resistivity values but the other horizons are not clear. Referring to Figure 9e, which shows the in-situ resistivity measurements, we can notice that below 0.5 m ($\sim 55/70 \Omega\text{m}$) the resistivity values do not have visible changes and this is a factor that can make the detection of the kettle hole difficult. Considering the resistivity variation it is difficult to distinguish between different sediments because the values are about $\sim 15 \Omega\text{m}$ and $19 \Omega\text{m}$ from 0.5 m depth until the end of the section. Locally a variation occurs but these are caused by small sand patches contained in the grey-clay deposition. If we compare these results with the ERT inversion (Figure 9c) at the same location, we notice a difference between them, in particular below the topsoil. At this position the inversion shows a range of values between $\sim 19 \Omega\text{m}$ and $\sim 40 \Omega\text{m}$, while Figure 9e points out a range between $15 \Omega\text{m}$ and $19 \Omega\text{m}$ locally $35 \Omega\text{m}$ but only associated with a sand inclusion in the sediment.

The difference depends on different factors, for instance the correct contact between the small electrodes and the soil. Test measurements pointed out that the different depth of penetration of the electrodes in the soil can affect the results. Locally the coupling between the ground and the small electrodes was different because of the different nature of the sediments. The main focus was to identify the variation of the resistivity along the kettle hole section, future work will be focused on the improvements of in-situ resistivity measurements with different probes. Moreover, the presence of sand patches in the gyttja can be the reason for creating inversion artefacts which can differ from the expected resistivity distribution. In any case, the measured resistivities seem to agree with the values described above for the internal structure of the kettle hole.

To sum up, the ERT profiles show only a low resistivity value according to the location of the kettle hole, the shape and the bottom are however not clear. The reason can be attributable to the low contrast in the resistivity between the sediment surrounding the anomaly. The water at the surface could have affected the superficial measurements but below 1 m the resistivity values are changing, defining an area with lower values. The variation at about 1.10 is caused by a sand patch in the grey-clay deposition.

5.6 Mapping the horizontal extent of the kettle hole

Based on the results presented so far, we can conclude that all applied methods showed evidence of the suspected kettle hole, but with different clearness and at different depth levels. Shear wave seismics has shown to be capable of lining out the kettle hole over the whole depth range due to the major contrast in S-wave velocity of the fill compared to its surrounding. However, seismics is the most expensive of the considered prospection methods and cannot be applied for areal mapping in a cost effective way. In contrast, GPR and EMI are suitable for mapping whereas the penetration depths are restricted to very near surface depth.

To find out the areal signature of the kettle hole in terms of GPR and EMI we compare the contouring map from GPR (Figure 6b) and the EMI slice (Figure 7b) belonging to ~1.5 m depth in Figure 10. The mapped GPR reflection corresponds to the interface associated with the transition between the Younger Dryas and Late Allerød sediments (Grey clay / sand deposition filling the kettle hole and grey-green gyttja). It shows a depression extending from the center to the east part of the area (3D in Figure 10b). The contoured horizon can be identified with the Bromme Horizon, which is the deepest interface visible with 200 MHz GPR. The same structure is visible in the EMI map where it extends approximately 16 m in the N-S direction and ~ 25 m in E-W direction. These values agree with the dimension of the excavated kettle hole at area 10. Considering the shape of the kettle hole as determined from the seismic depth section, it might be expected that the diameter of the associated electric conductivity anomaly should shrink with depth, but the opposite is the case. The EMI depth slice shows that the anomaly diameter increases continuously with depth. This is most probably caused by the increase of the water content of the sediment with depth, which overprints the horizontal sedimentary contrasts in terms of electric conductivity.

Besides the depression associated with the main kettle hole, EMI shows a second depression close to the kettle hole, which can be interpreted as a second small pond with the same genesis. Seismics instead does not confirm this hypothesis because the tomography shows clearly only one body with different properties. However, more detailed stratigraphic information is required to validate this scenario. Referring to the 3D reconstruction in Figure 10b we can recognize the two features close to each other.

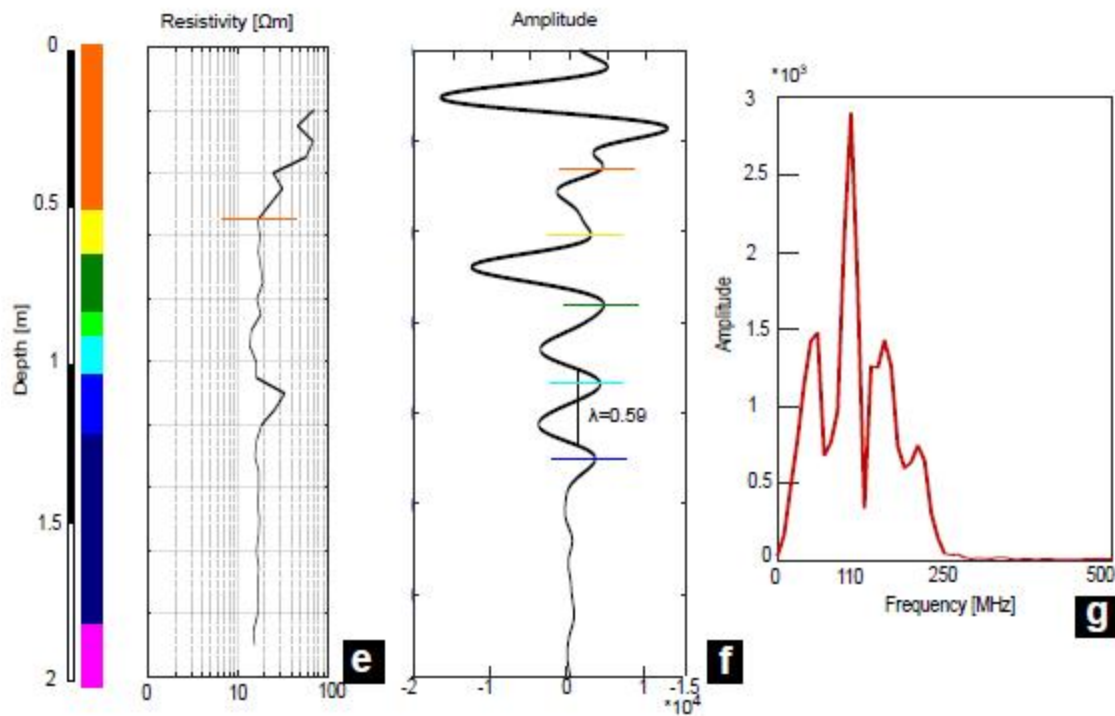
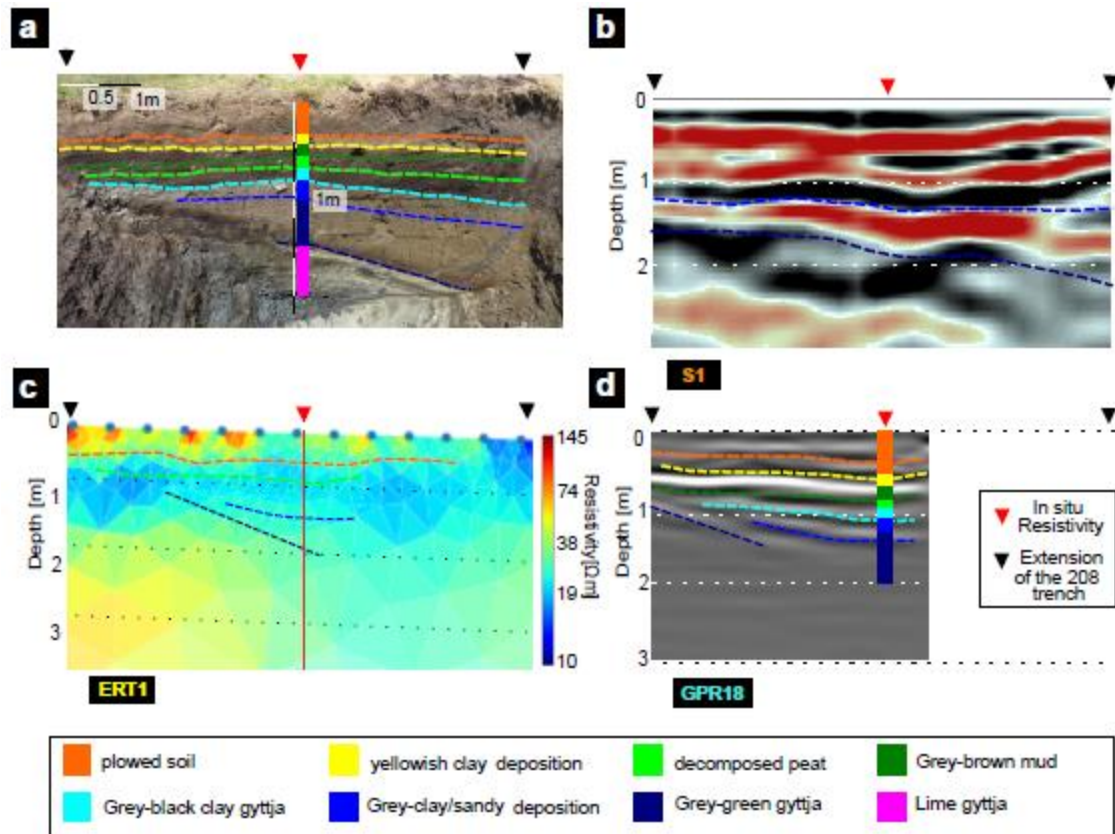


Figure 9: a) Comparison between the GPR profile and the stratigraphy at the location of the test trench made in summer 2018. a) stratigraphy from the trench, the main transitions between sediments are

color coded. b) seismic profile at the trench location compared with the stratigraphy. c) ERT results at the trench location, the main transitions between sediments are color coded and the red line indicates the location of the in-situ electric resistivity values measured on the vertical section of the trench in summer 2018; d) GPR results at the trench location, the main reflections are compared (color coded dashed lines) with the main sediments transitions. e) lithological depth profile and in-situ electric resistivity values measured on the vertical section of the trench in summer 2018. f) amplitude of the GPR trace at the location of the in-situ measurements g) frequency spectrum associated to the GPR trace at the location of the in-situ-electric resistivity measurements.

5.7 Geoarchaeological stratigraphic assessment of depth sounding results

The main aim of the present study was to define a methodology for the non-invasive investigation of small kettle holes in prehistoric glacial environments. In Tyrsted we see a strong connection between Late Glacial Horizon and the Late Paleolithic Bromme culture. SH-wave seismic measurements gave us the best results in defining the gross structure of the kettle hole and we can now try to connect the visible signals with the stratigraphy and to compare them with GPR and ERT amongst each other and along a stratigraphic column (Figure 11). GPR can trace the boundary of the kettle hole down to 2 m depth (Figure 11a) and the internal reflections correlate well with the sediments filling the kettle hole (Grey-brown mud, decomposed peat grey-black clay gyttja and grey-clay/sandy deposition). But the depth of investigation is not enough to detect the interfaces below. The interesting sediments for archaeological research are between the Allerød Grey-Green gyttja and the Younger Dryas layers; the GPR can give us a rough idea of where this horizon can be located because the last transition visible in the radargram corresponds to this interface. In ERT (Figure 11b) this most interesting interface is difficult to recognize. Due to the limited resolution of ERT and weak contrasts in electric resistivity, stratigraphic units can be distinguished only coarsely and at few segments of the profile. Down to 2 m depth the best resolved stratigraphic results came from GPR, which was able to distinguish between the internal layers filling the former small lake. The seismic reflection profile also shows a correlation with the stratigraphic boundaries found in the trench. In any case it may appear somewhat surprising that the resolution of the SH-wave section is comparable to GPR. This is caused by the low wave velocity of ~100 m/s and lower as the signal frequencies generated by the hammer beats are only the typical range of 20 to 80 Hz order of magnitude. This enables us to associate the interface Younger Dryas / Late Allerød with a visible seismic event. In Figure 11c we show the interpretation of the seismics profile and a line-drawing of the shape of the kettle hole. Here the Bromme horizon can be located from 1.10 m up to ~1.8 m depth moving to the shoreline to the deeper part of the kettle hole. This horizon is clearly visible with a horizontal signal in the seismic profile. The bottom of the investigated feature seems to be at about ~5 m depth defining the known shape of a kettle hole with steep sides.

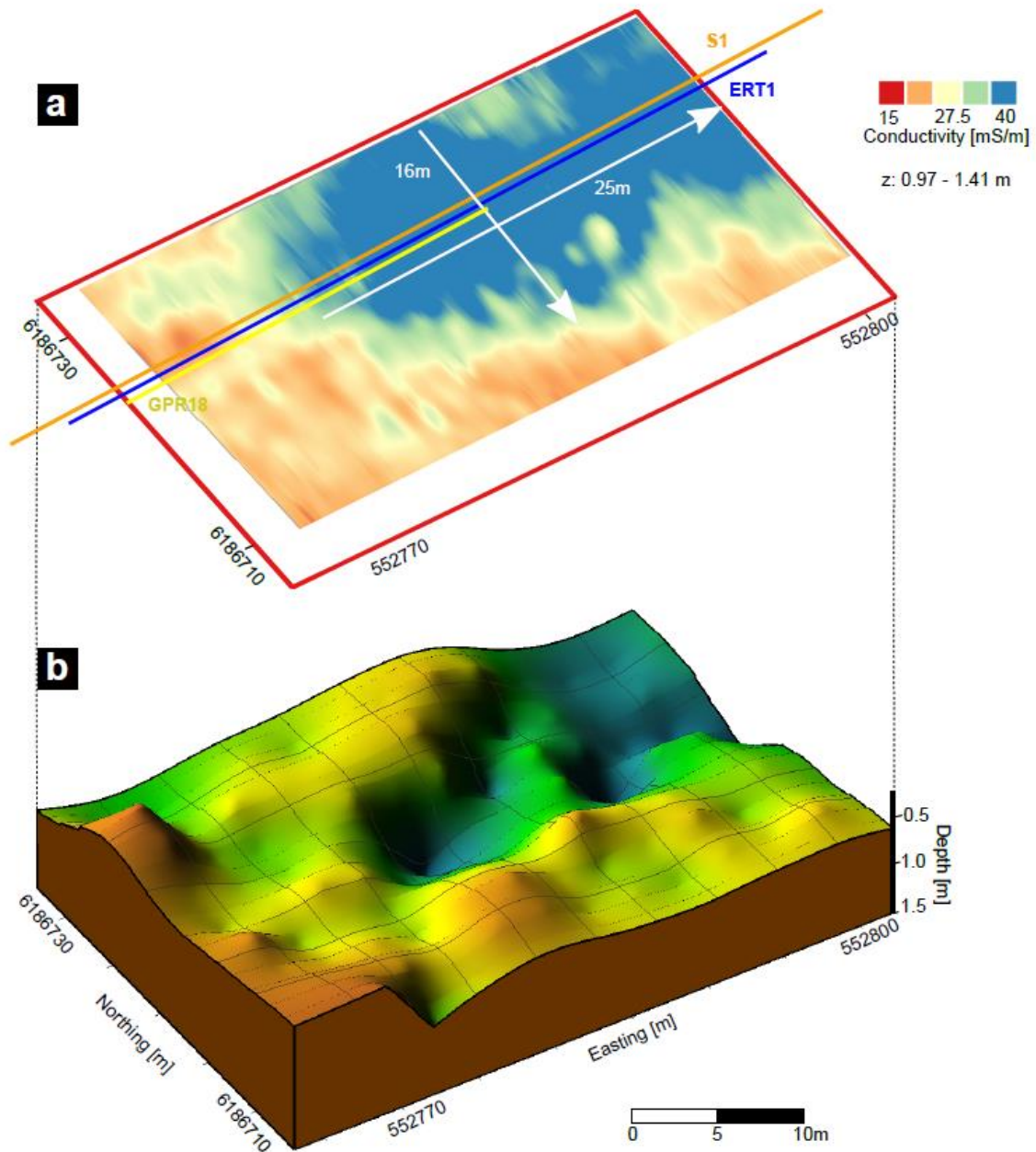


Figure 10: Comparison between the applied geophysical methods at site 8. a) Horizontal map of EMI results at a depth of ~ 1.5 m together with the location of the measured profiles (GPR, ERT and seismic) b) 3D reconstruction using the contour map in Figure 6b allowing a visualization of the depth associated with the transition between grey-clay/sandy deposition grey-green gyttja. This reconstruction allows an approximate depth of the Bromme horizon.

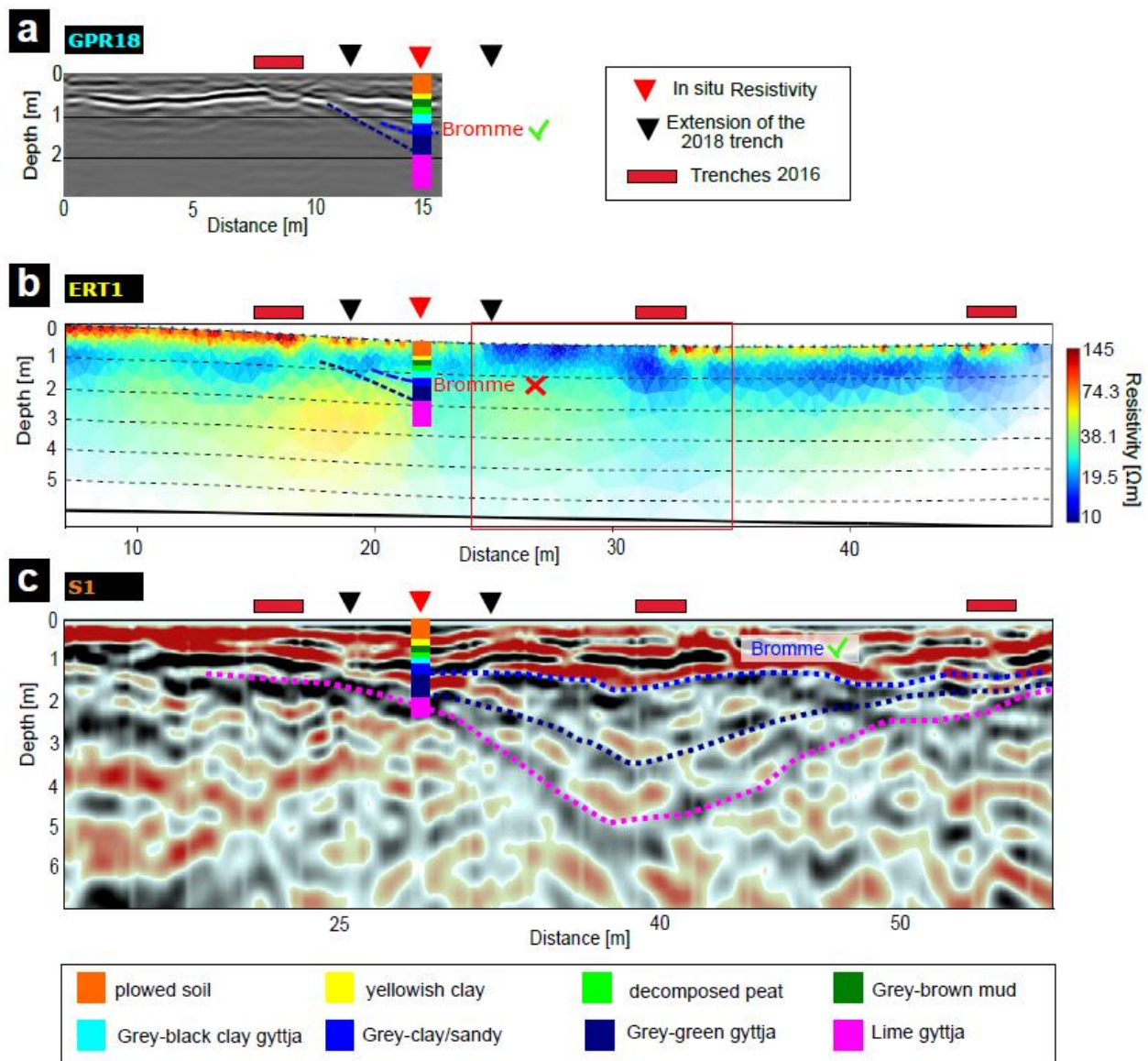


Figure 11: comparison between GPR, ERT and SH-seismic. a) GRP Profile compared with the stratigraphy from the trench. The transition between grey-caly/sandy deposition and grey -green gyttja is visible making the estimation of the Bromme horizon possible. b) ERT profile compared with the stratigraphy from the trench. The sediment transitions are not clearly defined, therefore the estimation of the Bromme horizon is not possible. A region with low resistivity is visible (red square) locating the kettle hole. The profile is cut in the external parts to permit an easier comparison. c) Seismic profile compared with the stratigraphy of the trench. A signal is visible at the location of the transition between grey-caly/sandy deposition and grey-green gyttja allowing an estimation of the Bromme horizon. The bottom of the kette hole is also possible to define (pink dashed line) following a visible reflector up to ~5 m depth. The profile is cut in the external parts to permit an easier comparison.

6. Discussion

6.1 Prospection concept for kettle holes

Kettle hole prospection is not principally different from the prospection of more common archaeological targets in so far as it requires a four-step approach consisting of

1. An areal screening based on the analysis of air photographs, airborne remote sensing or micro-topography to identify generally suspect terrain and narrow down the target area,
2. An areal prospection of the target area based on mobile geophysical methods to contour the target,
3. High-resolution depth sensitive measurements to explore the target structure in detail
4. Drillings or test pits for ground truthing and calibration of the geophysics.

Step 1 has not been considered in this article as we regard it as a theme on its own. Regarding steps 2 and 3 it has to be considered that kettle holes are characterized by organogenic sediments, especially gyttja and peat, which determine the physical properties of the internal layering and the parameter contrast to the surrounding. The gyttja is fine-grained, not much different from fine-grained non-organic sediments. But the organic matrix as such is mechanically weaker than the matrix of inorganic sandy and silty soils. The related pronounced contrasts in shear rigidity (shear modulus) are one of the reasons why shear wave sounding turned out to be successful in determining both the full depth range of the kettle hole and its internal layering. The second reason is that the shear wave velocity, which is proportional to the square root of rigidity, is determined mainly by the matrix and is not affected by the pore fill. Therefore S-wave contrasts are maintained independently of the degree of water saturation. This is very much in contrast to electric conductivity and dielectric permittivity, which are essentially determined by the soil water content. For kettle hole prospection this means that the electric parameter contrast not only depends on the soils, in which the kettle hole is embedded, but also on the groundwater situation. In our field example the general increase in water saturation with depth led to decreasing lateral contrast between kettle hole and surrounding as the ERT sections show. For the same reason GPR absorption increases strongly with depth. For these reasons EMI and GPR can be expected to line out the contours of kettle holes close to the ground surface but are much less well suited than S-wave seismic to explore the depth structure of kettle holes. Therefore, based on the presented experience, we recommend using GPR and/or EMI in step 2 and S-wave seismic in step 3. In this context ERT plays a certain role for cross checking results from other methods to a certain extent, especially from EMI, but it appears less likely to provide reliable information on the deeper parts of a kettle hole than S-wave seismics.

Our present results can be compared to a number of studies, which investigated targets in similar geological situations. In contrast to our example the studies of Götz et al. (2018) and Koszinski et al. (2013) present field examples, in which ERT turned out to be a useful tool for investigating kettle holes, but these kettle hole had a very different composition from the surrounding sediments making the resistivity

contrast high enough to create a visible anomaly. Corradini et al. (2020) demonstrated that GPR is capable of lining out former islands in the bog area of an ancient lake. This lake can also be regarded as a sort of mega kettle hole. But it is embedded in basal sands that create a significant contrast in the dielectric permittivity enabling GPR to record the internal structure clearly even in wet environments.

The comparison of these studies to the present one show that the application of different geophysical methods in a test phase is advantageous in any case as it enables us to find out which combination of methods is most suitable to locate a kettle hole and to define its lateral extension and depth.

6.2 Improving the future work

Considering the presented work as a case study, the investigation of future wetland areas can be improved. The topography is the first indicator of depressed areas and this is the first factor that has to be taken into account. The horizontal extension of a kettle hole can be estimated using either GPR or EMI. If the field conditions are similar to Tyrsted, the faster solution would be to start the investigation with EMI because carrying GPR on uneven and wet subsurfaces can negatively influence the measuring procedure and bring bad quality data.

To gain more information about the bottom of the kettle hole a GPR antenna with a significantly lower central frequency than 200 MHz would be needed, but the DOI would be always affected by the water content of the investigated area and the resolution would decrease as well. If we want, for instance, to increase the DOI by a factor of two, the central frequency should be lowered by a factor of four, which is 50 MHz. This frequency would produce a decrease of the resolution by a factor of four too, making the GPR resolution worse than the S-waves reflections. In these conditions it would be (again) better to apply SH-seismics for these environments. Moreover, in a way to improve the GPR survey, in general, it would be useful to plan a grid of profiles to generate amplitude maps (time-slices) to gain more details. The stratigraphic information can also be useful to constrain the computation of the applied methods to create models which can quantitatively validate our measurements. The radar velocity is also an important factor to keep in consideration in a way to improve the time-depth conversion. Velocity variations are normally present in the subsurface and defining the lateral and vertical changes can also reduce the error associated to the reflectors depth. These measurements can be improved using GPR borehole equipment which gives high-resolution velocity information that can be used to calculate permittivity profiles in the subsurface.

EMI can also be improved using a higher separation between the transmitter and receiver coil. This condition allows to reach greater depth important to define the shape of the former lake. ERT can also be applied differently, for example using a higher electrode spacing providing more depth information. The electrodes distance of 0.5 m has been chosen to have more resolution on the detection of the kettle hole and referring to the excavation which took place in area 10, the bottom was within 3.5 m. However, the test trench done in 2018 revealed that the bottom of the feature was deeper than expected, therefore the complete profile of the kettle hole is not possible to follow in the ERT profile.

We propose to use SH-wave seismic as the main tool to investigate the depth of such environments. The contrast in seismic impedance is the physical property to differentiate these features from their surroundings. However, some improvements can also be planned. The distance between the receivers can be reduced to 0.25 m but the time of measurements will increase, losing the cost-effective character of the survey. The compromise between time of acquisition and data quality is also an important component to consider when dealing with local authorities and museum archaeologists. Another remark to make would be about the source used for seismic waves. A higher frequency source would produce waves with smaller wavelength and therefore the resolution would be higher, but in the SH-wave case the higher frequencies would be quickly attenuated and difficult to measure. A step forward can also be to perform 3D seismics and try to reconstruct the entire shape of the pond using more profiles.

Our case study confirms the importance of including S-wave seismic in geoarchaeological research. In this regard a new tool, which may be able to resolve small-scale near surface structures even more reliably, is the Full Waveform Inversion (FWI). FWI has been introduced recently in the archaeological context by Köhn et al. (2018, 2018a, and 2018b) and Schwardt et al. 2020. As an example, at the Fossa Carolina, FWI was able to improve the definition of the canal basement and to resolve small scale velocity anomalies correlated with features in the archaeological documentation (Köhn 2018b).

Another method which could be also tested in the feature can be the tTEM: a ground based method for transient electromagnetic data acquisition. The aim of the tTEM development has been to design a system covering the depth range from 0 – 30 m in full 3D. White et al. (2019) and Johnson et al. (2019) showed that this application improved the resolution of sand and gravel distribution within the tTEM depth of investigation.

There are plenty of possibilities to carry multi-methodological surveys with the aim to reconstruct ancient landscapes and connect them to human occupation. What is important is to always find the right compromise between the aim of the survey, the time for collecting data and the resolution we want to achieve.

7. Conclusions

Kettle holes such as found in Tyrsted are characterized by organic sediment fill, especially gyttja and peat, surrounded by silty sediment left from the glacier activity. Based on our field study we found that kettle holes prospection can successfully performed in a graded approach of three steps where:

1. EMI enables locating the kettle hole and to give its near-surface lateral extension. Lateral contrasts in the electric conductivity of the kettle hole fill and the surrounding glacial sediments can be expected to be significant in the vadose zone but may decrease strongly already at shallow depth due to increasing water or clay contents of the country rock.
2. GPR serves for defining the upper part of the kettle hole in dm-scale resolution, especially its dipping lateral boundary and near-surface stratigraphy. Radar penetration depth is restricted due to the clay and water content of the glacial sediments, in our case to about 2 m depth.

3. SH-wave seismics enables exploring the kettle hole down to its full depth (~5 m in our case), in which the major shape can be found from the S-wave velocity distribution as provided by refraction tomography. The lateral boundary and internal stratigraphy of the kettle hole can be determined at 0.5 m-scale resolution through S-wave reflection imaging. S-wave velocity values of the organic sediments are in the range of 50 to 100 m/s, whereas the glacial tills and sands show 150 to 300 m/s, almost independently of water saturation.

The geophysical results should be calibrated through drills or test pits. In case of the investigated Tyrsted site the accompanying geoarchaeological investigations showed that GPR reflections could be identified with the transition between Late Allerød and early Younger Dryas and the major Bromme horizon. S-wave reflection seismics showed a possible Bromme horizon, too, and the Gyttja layering down to the bottom of the hole.

The multi-geophysical approach presented in this study confirms the importance to apply different methods in geoarchaeological research and highlights the potential of SH-wave profiling. The combination of these measurements with corings allows us to understand and reconstruct the stratigraphy and plan test excavation in the most promising areas. For museum archaeologists with a limited budget for conducting logistically complex excavations these measurements will provide a very important planning tool. And most importantly, this prospective planning tool will enable the archaeological and palaeoenvironmental research groups to reconstruct palaeolandscapes and to identify possible finding places of these very rare, but highly important palaeolithic remains.

Acknowledgements

We are grateful to the German Research Foundation (DFG) grant 2901391021 (SFB 1266) for funding the presented research. We want to thank the Horsens Museum for the support in the field and the opportunity to open a small trench to ground truth the geophysical measurements. We would also like to thank Tobias Burau, Philipp Leineweber, Ines Budde for their help during fieldwork and Tina Wunderlich for the support during the review of this paper. Moreover, we would like to thank the two anonymous reviewers for their valuable comments on the text. The current study is part of an interdisciplinary project (which is part of the CRC 1266 `scales of transformation`, Kiel University) that focuses on investigating kettle holes against the background of its archaeological importance through prehistory.

8. References:

Aaris-Sørensen, K.; Mühldorff, R.; Petersen, E.B. 2007. The Scandinavian reindeer (*Rangifer tarandus* L.) after the last glacial maximum: time, seasonality and human exploitation. *J Archaeol Sci.* 34:914–923. doi:10.1016/j.jas.2006.09.014.

Annan AP. 2009. Electromagnetic principles of ground penetrating radar. In *Ground Penetrating Radar: Theory and Applications*, Jol HM (ed). Elsevier: Amsterdam; 3–40.

Beilecke, T., Krawczyk, C.M., 2011. Versatile shear-wave reflection seismic system enables high-resolution near-surface aquifer imaging in urban areas. *Physics and Chemistry of the Earth, Special Volume on Urban Geophysics*, submitted for publication.

Benn, DI., Evans, DJA. 2010. *Glaciers and glaciation*. Hodder Education. New York: Taylor & Francis.

Bonsall, J., Fry, R., Gaffney, C., Armit, I., Beck, A., and Gaffney, V., 2013. Assessment of the CMD Mini-Explorer, a New Low-frequency Multi-coil Electromagnetic Device, for Archaeological Investigations. *Archaeological Prospection*, 20 (3), 219–231.

Borup, P. and Nielsen, M.K. 2017. Tyrsted – et kighul til senistiden. *Skalk* (December 2017/6), 3-9.

Carlson, A.E., Mickelson, D.M., Principato, S.M., Chapel, D.M., 2005. The genesis of the northern kettle Moraine, Wisconsin. *Geomorphology*. 67:365–374.

Constable, S.C., Parker, R.L., and Constable, C.G., 1987. Occam’s inversion: A practical algorithm for generating smooth models from electromagnetic sounding data. *Geophysics*, 52 (3), 289–300.

Conyers, Lawrence B., 2013. *Ground-penetrating Radar for Archaeology*, 3rd Edition. Altamira Press, Rowman and Littlefield Publishers, Lantham, Maryland.

Corradini, E., Wilken, D., Zanon, M., Groß, D., Lübke, H., Panning, D., Dörfler, W., Rusch, K., Mecking, R., Erkul, E., Pickartz N., Feeser, I., Rabbel, W., 2020. Reconstructing the palaeoenvironment at the early Mesolithic site of Lake Duvensee: Ground-penetrating radar and geoarchaeology for 3D facies mapping. *The Holocene*. <https://doi.org/10.1177/0959683620902234>

Davis, J.L., Annan, A.P., 1989. Ground-penetrating radar for high- resolution mapping of soil and rock stratigraphy. *Geophys. Prospect.* 3, 531–551.

De Smedt P., Van Meirvenne M., Meerschman E., Saey T., Bats M., Court-Picon M., De Reu J., Zwertvaegher A., Antrop M., Bourgeois J., De Maeyer P., A.Finke P., Verniers J., Crombé P., 2011. Reconstructing palaeochannel morphology with a mobile multicoil electromagnetic induction sensor. *Geomorphology*. Volume 130, Issues 3–4, 136-141

Eriksen, B.V., 2002: Reconsidering the geochronological framework of Lateglacial hunter-gatherer colonization of southern Scandinavia. In: B.V. Eriksen & B. Bratlund (eds), *Recent studies in the Final Palaeolithic of the European plain*. Jutland Archaeological Society Publications Vol. 39. Højbjerg, pp. 25-41.

Eriksen, B.V., Krüger, S. & Wild, M. 2018: Tyrsted – a Late Palaeolithic Christmas gift. *Zentrum für Baltische und Skandinavische Archäologie, Jahresbericht 2017*, pp. 78-79.

- Fischer, A., Mortensen, M.F., Henriksen, P.S., Mathiassen, D.R. and Olsen, J., 2013. *Dating the Trollesgave site and the Bromme culture – chronological fix-points for the Late glacial settlement of Southern Scandinavia*. Journal of Archaeological Sciences. Vol 40 p.4663-4674.
- Fujie, G., Kasahara, J., Murase, K., Mochizuki, K. and Kaneda, Y.: Interactive analysis tools for the wide-angle seismic data 440 for crustal structure study (Technical Report), Explor. Geophys., 39. doi:10.1071/EG08006, 2008.
- Gerke, H.H., Koszinski, S., Kalettka, T., Sommer, M., 2010. Structures and hydrologic function of soil landscapes with kettle holes using an integrated hydrogeological approach. Journal of Hydrology 393, 123e132.
- Gomberg, J., Waldron, B., Schweig, E., Hwang, H., Webbers, A., R. van Arsdale, Tucker, K., Williams, R., Street, R., Mayne, P., Stephenson, W., Odum, J., Cramer, C., Updike, R., Hutson, S., Bradley, M., 2003. Lithology and shear-wave velocity in Memphis, Tennessee. Bulletin of the Seismological Society of America, 93 (3), pp. 986-997
- Götz J., Salcher B., Starnberger R., and Krisai R., 2018. Geophysical, topographic and stratigraphic analyses of perialpine kettles and implications for postglacial mire formation. Geografiska Annaler: Series A, Physical Geography, 100:3, 254-271, DOI:10.1080/04353676.2018.1446638
- Günter, T., Rücker, C., 2006. A general approach for introducing information into inversion and examples from dc resistivity inversion: 10th Annual European Meeting of Environmental and Engineering Geophysics, EAGE. extended Abstract P039
- Hansen, P. C., and O'Leary, D. P., 1993, The use of the L-curve in the regularization of discrete ill-posed problems, SIAM Journal on Scientific Computing, 14, 1487-1503.
- Houmark-Nielsen, M. 2011: Pleistocene Glaciations in Denmark: A Closer Look at Chronology, Ice Dynamics and Landforms. In: J. Ehlers, P.L. Gibbard & P.D. Hughes (eds.): *Quaternary Glaciations – Extent and Chronology: A Closer Look*. Developments in Quaternary Sciences, Volume 15. Elsevier, pp. 47-58.
- Loke, M.H., Acworth, I., Dahlin, T., 2003. A comparison of smooth and blocky inversion methods in 2D electrical imaging surveys. Exploration Geophysics 34, 182e187. <http://dx.doi.org/10.1071/EG03182>
- Johnson, C., White, E.A., Maurya, P., Kress, W., Kelly, D.B., Lane, J.W. tTem, a towed electromagnetic induction system - an example from the Mississippi alluvial plain. SAGEEP 2019 - 32nd Annual Symposium on the Application of Geophysics to Engineering and Environmental Problems
- Kalettka T., Rudat C. 2006. Hydrogeomorphic types of glacially created kettle holes in North-East Germany. Limnol – Ecol Manage Inland Waters. 36:54–64. doi:10.1016/j.limno.2005.11.001.
- Kallweit R. and L. Wood, 1982. The limits of resolution of zero-phase wavelets. Geophysics, 47. No. 07, 1035-1046.

- Karasiewicz M.T., Hulisz P., Noryśkiewicz A.M., Krześlak I., Świtoniak M. 2014. The record of hydroclimatic changes in the sediments of a kettle-hole in a young glacial landscape (north-central Poland). *Quat Int.* 328–329. doi:10.1016/j.quaint.2013.09.045.
- Korenaga, J., W. S. Holbrook, G. M. Kent, P. B. Kelemen, R. S. Detrick, H.-C. Larsen, J. R. Hopper, and T. Dahl-Jensen. 2000 Crustal structure of the Southeast Greenland margin from joint refraction and reflection seismic tomography. *J. Geophys. Res.*, 105, 21,591-21,614
- Köhn, D., Wilken, D., DeNil, D., Wunderlich, T., Rabbel, W., and L. Werther, 2018a, 2D full waveform inversion applied to a strongly-dispersive Love wave field dataset: 80th Conference and Exhibition, EAGE.
- Köhn, D., Wilken, D., Wunderlich T., De Nil D., Rabbel, W., Werther L. , Schmidt J., Zielhofer C., and Linzen S., 2018b Seismic SH full waveform inversion as new prospection method in archaeo-geophysics,. 80th Conference and Exhibition, EAGE.
- Köhn, D., Wilken, D., DeNil, D., Wunderlich, T., Rabbel, W., Werther, L., Schmidt, J., Zielhofer, C., and S. Linzen, 2018. Comparison of time-domain SH waveform inversion strategies based on sequential low and bandpass filtered data for improved resolution in near-surface prospecting: *Journal of Applied Geophysics*, 160, 69-83.
- Koszinski S., 2013. Geophysical-based Modeling of a kettle hole catchment of the Moranic soil landscape. Special Section: Frontiers of Hydropedology in vadose Zone Research. *Vadose Zone J.* doi:10.2136/vzj2013.02.0044.
- Krawczyk, C. M., Polom, U., Trabs, S., & Dahm, T., 2012. Sinkholes in the city of Hamburg - New urban shear-wave reflection seismic system enables high-resolution imaging of subsrosion structures. *Journal of Applied Geophysics*, pp. 133-143.
- Leclerc, R.F., Hickin, E.J., 1997. The internal structure of scrolled floodplain deposits based on ground-penetrating radar, North Thompson River, British Columbia. *Geomorphology*. 21:17–38.
- Leckebusch, J., 2007. Short Report Pull-up/Pull-down Corrections for Ground-penetrating Radar Data. *Archaeol. Prospect.* 14, 142–145
- Loke, M.H., 2016. Tutorial: 2D and 3D electrical imaging surveys. www.geotomosoft.com.
- Maizels, J.K., 1977. Experiments on the origin of kettle holes. *J Glaciol.* 18:291–304.
- Mayer, L.A. (1980) Deep-sea carbonates: physical property relationships and the origin of high-frequency acoustic reflectors. *Mar. Geol.*, 38, 165±183.
- Mortensen, M.F., Henriksen, P.S. and Bennike, O. 2014a. *Living on the good soil: relationships between soils, vegetation and human settlement during the late Allerød time period in Denmark*. *Vegetation History and Archaeobotany*. 23:3 p. 195-205.

Mortensen, M.F., Henriksen, P.S., Christensen, C., Petersen, P.V. and Olsen, J. 2014b. *Vegetation development in southeast Denmark during the Weichselian late Glacial – palaeoenvironmental studies close to the Palaeolithic site of Hasselø*. Danish Journal of Archaeology Vol.3. Nr.1. 48-66.

Mortensen, M.F., Birks, H.B., Christensen, C., Holm, J., Noe-Nygaard, N., Odgaard, B.V., Olsen, J., Rasmussen, K.L., 2011. Lateglacial vegetation development in Denmark - new evidence based on macrofossils and pollen from Slotseng, a small-scale site in southern Jutland. Quaternary Science Reviews 30, 2534e2550.

Mortensen, M.F., 2007. *Biostratigraphy and chronology of the terrestrial late Weichselian in Denmark: New investigations of the vegetation development based on pollen and plant macrofossils in the Slotseng basin*. Aarhus Geoscience – Ph.D. thesis; vol. 30. Aarhus Universitet.

Neal A., 2004. Ground-penetrating radar and its use in sedimentology: principles, problems and progress earth-Science Reviews , 261-330.

Obrocki, L., Vött, A., Wilken, D., Fischer, P., Willershäuser, T., Koster, B., Lang, F., Papanikolaou, I., Rabbel, W., and Reicherter, K., Tracing. 2018 Tracing tsunami signatures of the AD 551 and AD 1303 tsunamis at the Gulf of Kyparissia (Peloponnese, Greece) using direct push in situ sensing techniques combined with geophysical studies. Sedimentology (October) .DOI: [10.1111/sed.12555](https://doi.org/10.1111/sed.12555)

Polom, U., Hansen, L., Sauvin, G., L'Heureux, J.-S., Lecomte, I., Krawczyk, C.M., Vanneste, M., Longva, O., 2010. High-resolution SH-wave seismic reflection for characterization of onshore ground conditions in the Trondheim harbor, central Norway

Miller, R.D., Bradford, J.D., Holliger, K. (Eds.) 2010 SEG Geophysical Developments Series No. 15: Advances in Near-Surface Seismology and Ground-Penetrating Radar, SEG, Tulsa, pp. 75-92

Rabbel W., Wilken D., Wunderlich T., Bödecker S., Brückner H., Byock J., von Carnap-Bornheim C., Kalmring S., Karle M., Kennecke H., Messal S., Schmidts T., Seeliger M., Segschneider M., and Zori D., 2015. Geophysikalische Prospektion von Hafensituationen – Möglichkeiten, Anwendungen und Forschungsbedarf. *Häfen im 1. Millennium A.D. – Bauliche Konzepte, herrschaftliche und religiöse Einflüsse*, eds. T. Schmidts and M. Vučetić. Romano-Germanic Central Museum Press (RGZM), Mainz. ISBN 978-3-79543-039-9

Sheriff, R.E., 1977. Limitations on resolution of seismic reflections and geologic detail derivable from them. In: Payton, C.E. (Ed.), *Seismic Stratigraphy—Applications to Hydrocarbon Exploration*. AAPG Mem. 16, 3–14.

Rabbel, W. Stümpel, H., and Woelz, S., 2004, Archeological prospecting with magnetic and shear wave surveys at the ancient city of Miletos (western Turkey): The Leading Edge, 23, 690-703.

Ritchie K., 2018: Zooarchaeological analysis of fish material from HOM3370, Tyrsted (unpublished report, Moesgaard Museum, pp. 1-26)

Schön, J. H. (2015). *Physical Properties of rocks: Fundamentals and principles of petrophysics* (Vol. 65). Elsevier.

Schwardt M., Köhn D., Wunderlich T., Wilken D., Seeliger M., Schmidts T., Brückner H., Başaran S., Rabbel W. (2020) Characterisation of silty to fine-sandy sediments with SH-waves: full waveform inversion in comparison to other geophysical methods. *Near Surface Geophysics* **18** (3): 217-248 DOI:[10.1002/nsg.12097](https://doi.org/10.1002/nsg.12097)

Stucchi E, Tognarelli A., and Ribolini A. 2017. SH-wave seismic reflection at a landslide (Patigno, NW Italy) integrated with P-wave. *Journal of Applied Geophysics* 146 (2017) doi.org/10.1016/j.jappgeo.2017.09.011

Stümpel, H., Kähler, S., Meissner, R., & Milkereit, B., 1984. The use of seismic shear waves and compressional waves for lithological problems of shallow sediments. *Geophysical Prospecting*, pp. 662-675.

Stümpel, H., Rabbel, W., & Schade, J. (1988). Oberflächennahe geophysikalische Untersuchungen im Mündungsgebiet des Río de Vélez und des Río Algarrobo. *Madrider Beiträge*, 14, 60-72

Thompson, R., 1978. Resistivity Investigation of fan infilled Kettle Hole. *Quaternary Research* 9, 231-237

Troels-Smith, J., 1995. "Characterization of unconsolidated sediments," DGU. RæIV Bind 3 (Nr.10):1-73

Van Dam, RL, Schalger W., 2000. Identifying causes of ground-penetrating radar reflections using time-domain reflectometry and sedimentological analyses. *Sedimentology* 47, 435±449

White, E.A., Johnson, C.D., Maurya P.K., Kress, W., Kelly D.B., and Lane J.W., Use of a towed electromagnetic induction (tTEM) system for shallow aquifer characterization – an example from the Mississippi alluvial plain. *Symposium on the Application of Geophysics to Engineering and Environmental Problems 2019* <https://doi.org/10.4133/sageep.32-016>

Wilken, D., Wunderlich, T., Andersen, J., and W. Rabbel, 2015a, Geophysical investigation of past harbors: challenges and application examples: *Proceedings of the 11th International Conference on Archaeological Prospection*, 161-163.

Woelz, S., Rabbel, W., & Mueller, C., 2009. Shear waves in near surface 3D media—SH—wavefield separation, refraction time migration and tomography. *Journal of Applied Geophysics*, 68(1), 104-116.

Wunderlich, T., and Rabbel, W., 2013. Absorption and frequency shift of GPR signals in sandy and silty soils: empirical relations between quality factor Q, complex permittivity and clay and water contents. *Near Surface Geophysics*, 11(2), 117-127.

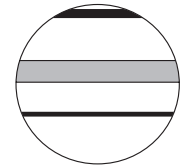
Wunderlich, T., Wilken, D., Erkul, E., Rabbel, W., Vött, A., Fischer, P., Hadler, H., Heinzemann, M., 2017. The river harbour of Ostia Antica - stratigraphy, extent and harbour infrastructure from combined geophysical measurements and drillings. *Quaternary International*, 2017, 1-11

Wunderlich T., Fischer P, Wilken D., Hadler H. Erkul E Mecking R. Guenther T., Heinzelmann M., Voett A., Rabbel W., 2018. Constraining E electric resistivity tomography by direct Push electric conductivity logs and vibracores: an exemplary study of the fiumeMorto silted riverbed (ostia Antica, western Italy) *Geophysics* 83(3):1-58 DOI:10.1190/geo2016_0660.1

Xia, J., Miller, R.D. , Park, C.B. , 1999. Estimation of near-surface shear-wave velocity by inversion of Rayleigh waves . *Geophysics*, 64 (3), pp. 691-700

Yilmaz, Ö., 2001 . *Seismic data analysis (Vol.1)*. Tulsa: Society of Exploration Geophysicists.

A.2 Paper II



Reconstructing the palaeoenvironment at the early Mesolithic site of Lake Duvensee: Ground-penetrating radar and geoarchaeology for 3D facies mapping

The Holocene
1–14

© The Author(s) 2020




Article reuse guidelines:

sagepub.com/journals-permissions

DOI: 10.1177/0959683620902234

journals.sagepub.com/home/hol



Erica Corradini,¹  Dennis Wilken,¹ Marco Zanon,²  Daniel Groß,³ 
Harald Lübke,³  Diana Panning,¹ Walter Dörfler,²
Katharina Rusch,¹ Rebekka Mecking,¹ Ercan Erkul,¹
Natalie Pickartz,¹  Ingo Feeser²  and Wolfgang Rabbel¹

Abstract

We investigate the landscape development of the early Mesolithic hunter-gatherer sites of Duvensee (10000–6500 cal. BCE). Based on ground-penetrating radar (GPR) and geoarchaeological drillings, we present for the first time a three-dimensional (3D) reconstruction of the palaeoenvironment of 63 ha covering subarea of the former lake during the Mesolithic. The archaeological aims were (1) to detect the location of former islands possibly hosting hunter-gatherer settlements and (2) to reconstruct the ancient landscape development for understanding prehistoric land use. The research in Duvensee lasts almost 100 years, providing vivid illustrations of early Mesolithic life. Clusters of Mesolithic camps have been found located on small sand hills that formed islands in the prehistoric lake. For this environment, we present depth maps of the three most important sedimentary facies interfaces of the ancient Lake Duvensee. Interface 1 represents the transition between coarse organic sediments (peat and coarse detritus gyttja) and fine-grained organic sediments (fine detritus gyttja, calcareous gyttja), Interface 2 represents the transition to the underlying clayish-loamy sediments, and Interface 3 marks the top of the basal sand deposits at the lake bottom. From Interface 3, we identified the location and extent of five former islands with Mesolithic camps. Stratigraphic information from the corings enabled us to create a 3D model of the spatio-temporal development of the Duvensee bog. The locations of the islands and their estimated dive-up times agree with the spatio-temporal pattern of the previous archaeological finds. The model shows where hunter-gatherers could settle and move from one island to another following the shorelines of the overgrowing lake. The 3D stratigraphic model provides growth and shrinking rates of the island and lake areas in the Mesolithic, and volumes of organic and non-organic deposited lake sediments. Besides, it provides a basis for a sustainable groundwater management needed for heritage preservation.

Keywords

3D reconstruction, archaeo-geophysics, corings, GPR, Mesolithic, settlement archaeology

Received 23 October 2019; revised manuscript accepted 29 November 2019

Introduction

The evolution of a landscape is important for understanding human behavior within it. Aspects like geomorphology and anthropogenic influences have to be taken into account for a full comprehension of palaeolandscapes. The conventional techniques to figure out the stratigraphy of sites and their surroundings include coring and near-surface geophysical surveys (e.g. De Smedt et al., 2011 or Gourry et al., 2003). Drilling allows a detailed registration of the vertical layering but usually with a low lateral sampling density due to the time-consuming character of this method. This limitation in the interpretation of lateral variation can be improved using non-invasive geophysical methods like ground-penetrating radar (GPR) which allow a more continuous mapping of the lithological change.

In particular, GPR has been extensively used in archaeological studies for mapping and imaging subsurface objects. The application of this method is based on detecting the contrast in electromagnetic properties (dielectric permittivity) and on recognizing the different signatures between man-made and natural features

(Campana and Piro, 2008; Conyers, 2012; Zhao et al., 2013). GPR has been employed for the investigation of sedimentary geometries, stratigraphic units (e.g. Davis and Annan, 1989; Jol and Smith, 1991; Neal, 2004; Stern, 2008), facies analysis (e.g. Carreon-Freyre et al., 2003; Grant et al., 1998; Heinz and Aigner, 2003; Mellet, 1995; Pipan et al., 2000; Ruffell et al., 2004), and peatland stratigraphy (e.g. Doolittle and Butnor, 2009; Holden et al., 2002; Lowry et al., 2009; Menotti and O’Sullivan, 2013;

¹Institute of Geoscience, Christian-Albrechts-University Kiel, Germany

²Institute of Pre- and Protohistoric Archaeology, Christian-Albrechts-University Kiel, Germany

³Centre for Baltic and Scandinavian Archaeology (ZBSA), Schleswig-Holstein State Museums Foundation Schloss Gottorf, Germany

Corresponding author:

Erica Corradini, Institute of Geoscience, Christian-Albrechts-University Kiel, Otto-Hahn-Platz 1, 24116 Kiel, Germany.

Email: erica.corradini@ifg.uni-kiel.de

Warner et al., 1990), but it has also some limitations. Clay layers and a high level of water saturation produce a strong attenuation of GPR signals, which especially restricts the application of this technique on alluvial deposits (Ferring, 2001; Moorman, 1990; Toksdorf et al., 2013).

In this paper, we present a geophysical investigation of the Duvensee palaeolake in south-eastern Schleswig-Holstein, Germany, which is one of the most relevant micro-regions for early Mesolithic hunter-gatherer archaeology on the Northern European Plain (Groß et al., 2018). The former lake occupies a depressed area within late Pleistocene sandy moraines that was formed by melting dead-ice after the retreat of the last Weichselian glaciation. Its irregular topography resulted in several islands scattered along the ancient water body, which were used by early Mesolithic hunter-gatherers groups to establish temporary camps.

The current study is part of an interdisciplinary project (which is part of the CRC 1266 ‘scales of transformation’, Kiel University) that focuses on reconstructing the environmental evolution of ancient Lake Duvensee against the background of its archaeological importance through prehistory. The main goal of the geophysical investigation is to find the location of former islands hosting early Mesolithic camps, enabling an evaluation of their relevance impact in the human occupation. It is very likely that in a transforming environment, the hunter-gatherers changed the locations of their camps from an island to another, following the lakeshore of the overgrowing lake. Thus, recreating the situation during that period by means of GPR and geoarchaeology is our goal. Following the background of intensive research in the Northern European Plain (Groß, 2017; Groß et al., 2018, 2019; Hartz et al., 2014; Lübke et al., 2011; Schmölcke, 2016; Schmölcke and Nikulina, 2015), this paper provides a first reconstruction of the paleotopography and stratigraphy of parts of the bog during the early Mesolithic using geophysics.

After giving a geological and archaeological background of the investigated area, we describe the geophysical survey carried out with GPR, its interpretation, and how it contributes to build a new picture of the lake development connected to human occupation. In the last section, we propose a three-dimensional (3D) model of the lake using the depth information of the different facies from GPR and stratigraphic information from corings. This allows to trace the extension of five former islands where hunter-gatherers’ settlement has been discovered. Based on the topographic information of the lake bottom in ancient time, the accessibility of the different islands could be inferred, explaining how people moved across the islands during the early Mesolithic.

Geological setting

The landscape surrounding the Duvensee basin was modeled by late Pleistocene glacial activity (source: Geologische Übersichtskarte 1:200.000, www.bgr.bund.de). The basin itself is the result of melting dead-ice blocks following the retreat of the Weichselian glacier front. Past stratigraphic investigations revealed a complex basin topography, characterized by numerous deeps and sand banks (Averdieck, 1986). Lacustrine sedimentation began approximately in the Older Dryas, while maximum areal extension was achieved during the early Holocene (Averdieck, 1986; Günther, 1986). The gradual infilling of the basin was accompanied by a general decrease in water level over time. By the 19th century CE, most of the basin was occupied by a bog. Two remnant open-water areas were drained in 1850 CE to facilitate peat extraction and agricultural activities (Averdieck, 1986). A simplified model of the gradual sediment deposition in the lake area is shown in Appendix S1 (available online). The various stages of sedimentation show characteristic profiles in connection with the construction of Mesolithic camps in the organic layer.

Archaeological background

In 1923, the first archaeological finds in the 4.3-km² large Duvensee bog were made by the geologist Karl CJ Gripp who found early Mesolithic artifacts in drainage ditches during an excursion (Schwantes et al., 1925, 1939). Subsequently, the archaeologist G Schwantes, started the first investigation on record concerning the area and identified four different sites which he named Wohnplatz (abbreviated WP), meaning dwelling site. The result of this first investigation was that only two of the discovered sites (WP 2 and WP 5) provided informative material in terms of flint assemblage and a paddle made of pine wood (Bokelmann, 1971; Schwantes et al., 1925). In 1946, H Schwabedissen (1951) excavated another site (WP 1) and further intensive research was done by K Bokelmann whose work lasted in 1966–1967 (Bokelmann, 1971, 1991) and lasted until 2001.

Nowadays 23 different locations of early Mesolithic hunter-gatherer groups and Neolithic farmers are known in the Duvensee bog and 17 of them have been partly excavated. While the duration of each camp was rather limited in time, the full extent of the Mesolithic occupation at Duvensee spans a few millennia and has witnessed several landscape transformations. Radiocarbon dating sets the establishment of the earliest known Mesolithic camps within the Preboreal time period (WP 8-9; ca. 9000 cal. BC), whereas the youngest Mesolithic evidence is dated to the early Atlantic period (WP 19; ca. 6500 cal. BC). In addition, one site belongs to the northern early Neolithic Funnel Beaker culture (WP 17) and one to the late Neolithic Single Grave culture (WP 15; Figure 1b).

Coherent overviews of the research of ancient Lake Duvensee have been given by Bokelmann (2012) and Groß et al. (2018). All of the sites investigated so far are located on small sand banks that formed multiple islands (called islets by K Bokelmann) in the prehistoric lake. The archaeological layers are not directly located on the mineral soils, but within the overlaying organic sediments, because these islands started to be overgrown with peat already during the early Holocene. Island 1 (Figure 2b), for instance, is located closest to the western shore of the former lake. The known Boreal sites WP 1-6 as well as WP 11 and 12 are located at 150 m to the east on island 2, a sandy island, which was exposed by a lowering of the lake water level during the Boreal. A thin gyttja layer shows that it must have still been under water in the Preboreal (Bokelmann, 1971; Groß et al., 2018). Two other islands – island 3 and island 4 – are also known to be occupied during the Boreal and the early Atlantic periods. From the distribution of surface finds, at least two more islands (5 and 6) are expected (Figure 1a and b): island 5 in the south and island 6 in the north (the area including island 6 is not part of this study).

At a few sites, specific fireplaces were excavated, defining the main anthropogenic feature of a camp, which can be connected with hazelnut roasting and other subsistence activities (Figure 7 in Bokelmann, 2012). These hearths, however, were not constructed following a uniform design scheme, probably this may be connected with different purposes of the features or chronological differences (Bokelmann, 2012). In several cases, the base of the roasting hearths in Duvensee consisted of a loamy/clayey layer which was interpreted as remnants of specially constructed clay plates (Lage, 2011). But in some cases, a compact layer of loam directly on a layer of non-heated sand was detected (Bokelmann, 2012), giving the impression that the loam layer was not heated on gleaming charcoal. Generally, it has to be assumed that several hearths were used for hazelnut processing but different construction techniques are present. Nevertheless, this makes a detection of anthropogenic features of the camps very difficult in terms of geophysics because the single remains are below the resolution of any technique. We thus focused on the detection and investigation of the island features as a whole.

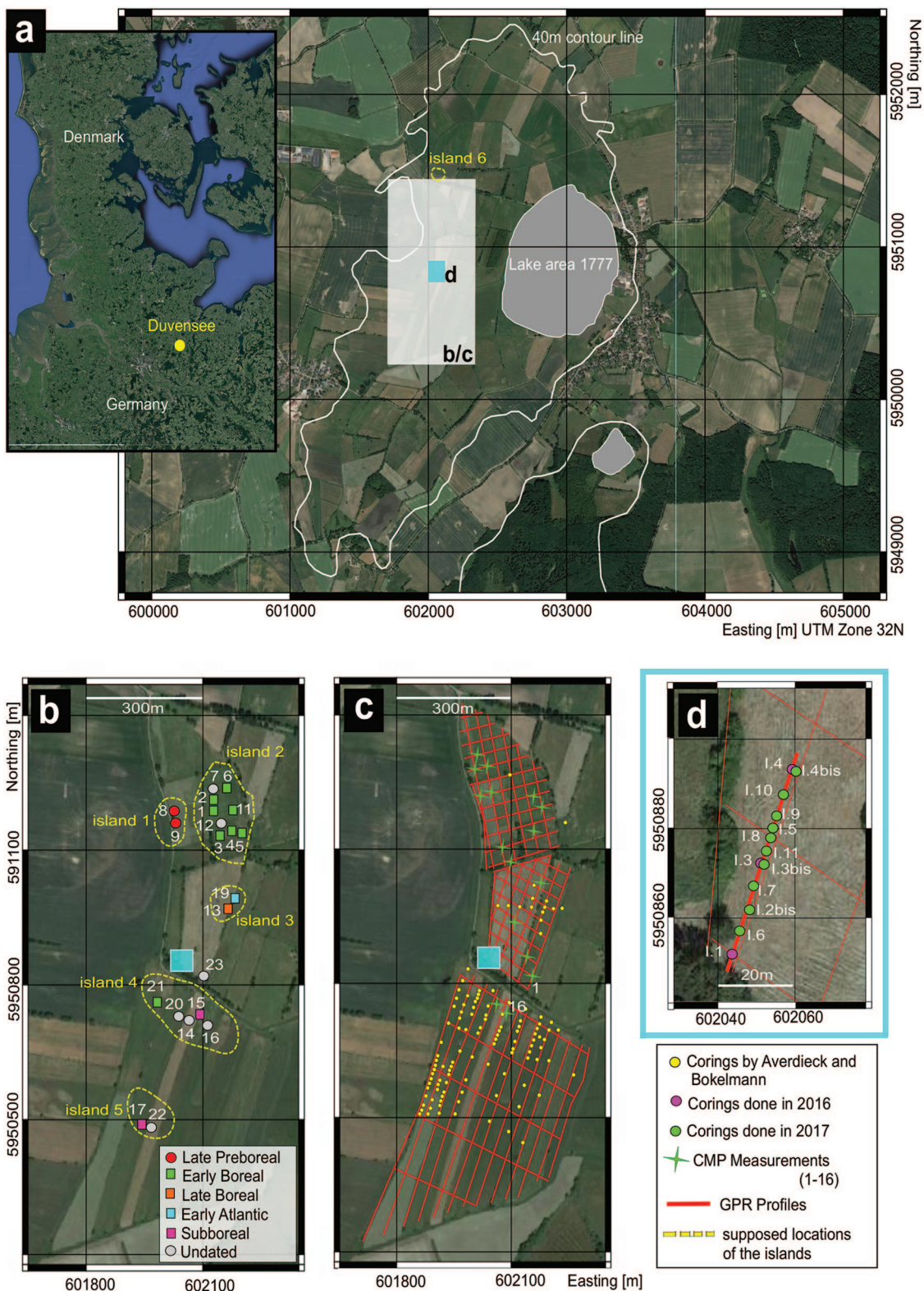


Figure 1. Area of investigation including the archaeological and geophysical research. (a) Location of the Duvensee area considering also the maximum extent of the lake in the early Holocene (Groß et al., 2018). (b) Dating, location of the sites and the supposed positions of the islands (yellow dashed lines) in the western part of the ancient Lake Duvensee. (c) Ground-Penetrating Radar Survey (red lines), CMP measurements (green stars), and corings done in the area of interest (color-coded dots). (d) Locations of the corings done in 2016 and 2017 along the reference profile.

Methodology

GPR is a non-invasive geophysical technique that can be used to detect electrical discontinuities in the shallow subsurface. The theory and methodology of GPR are comprehensively explained, for example, in Davis and Annan (1989). The electrical properties (dielectric permittivity and electric conductivity) of the different

sediments associated with changes in water and clay content determine the electromagnetic wave propagation velocity and the amount of energy which is absorbed and back-reflected at the interfaces between different lithologies (Davis and Annan, 1989; Doolittle et al., 2007). In a medium with uniform moisture content, the conversion of reflection traveltim to interface bottom can be done using one average velocity without introducing errors in depth

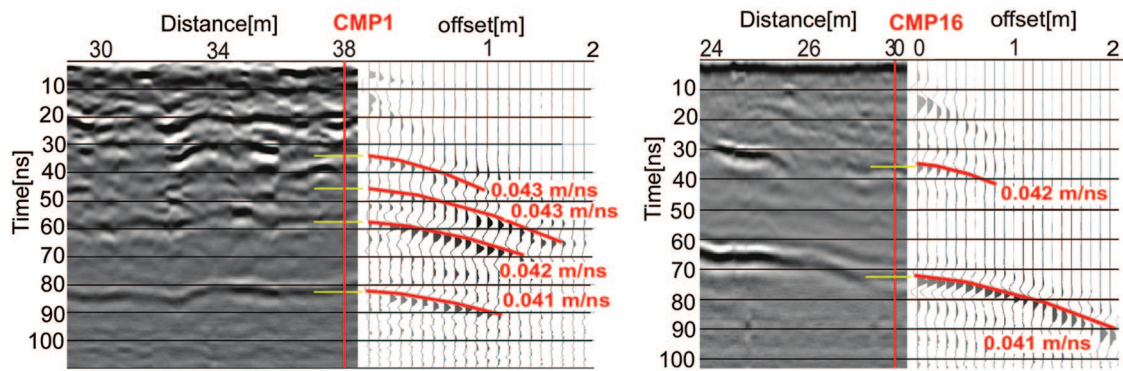


Figure 2. Velocity calculation. Example of two different CMP measurements and NMO velocity determination.

determination. This condition is rarely encountered in the field and using one average value may cause errors (Boll et al., 1996). Identifying the correct velocity distribution of electromagnetic waves in the subsurface is essential for accuracy and precision of the depth of investigation in a way to locate an archaeological object, feature or layer, and crucial for any imaging method applied to the data. Knowledge of subsurface GPR velocity is also crucial for guiding intensive probing and excavations that may follow a GPR survey or, in our case, to ground truth the geophysical results with the stratigraphy coming from the corings.

Numerous sedimentological studies have used GPR to reconstruct past depositional environments, but often with open questions regarding the resolution of the investigation (Neal, 2004). The vertical resolution increases with the used GPR center frequency, enabling the detection of thinner layers. From theory, we know that the best structural resolution that can be reached is about one quarter of the dominant wavelength (Neal, 2004; Sheriff, 1977). Due to energy absorption, both signal strength and center frequency of radar signals decrease during wave propagation (e.g. Wunderlich and Rabbel, 2013), leading not only to a limitation of depth penetration but also to a decrease in structural resolution with depth. For sedimentological interpretation, this implies that the lower stratification can be poorly imaged compared to the upper stratification. If the subsurface incloses layers that are thin compared to the dominant wavelength, the accuracy of the stratigraphic interpretation of GPR sections can be greatly improved by incorporating information from drillings. In this context, drilling enables the recognition of major interfaces and facies patterns in radargram and serve thus for ground truthing.

GPR profiling and interpretation procedure

A GSSI GPR unit with a 200 MHz center frequency antenna was used to investigate the Duvensee area (for acquisition settings and processing sequence, see Appendix S2, available online). In monostatic mode, this antenna enables the acquisition of profiles with a constant, close to zero, offset between transmitter and receiver. A rectangular grid of GPR profiles was established to investigate the palaeolandscape with 30-m spacing in the northern part of the area. In the southern sector, the profile spacing is ca. 100 m in NS direction and 30 m in WE direction (Figure 1c). For deriving a 3D stratigraphic subsurface model, it was necessary to recognize and pick in every radargram the reflections associated with the interfaces between the main sedimentary units identified in the drill cores (yellow dots in Figure 1c): basal sands, fine minerogenic sediments, fine and coarse organic deposits. The description of each sediment unit will be presented in Section 5.1. Picking was performed using the Kingdom IHS Software for the entire survey area. This Software was chosen because it allows to display GPR data together with drillings. During the picking procedure, a two-dimensional (2D) and 3D view of the dataset is

possible comparing anytime the GPR reflectors with the stratigraphic information for each picked profile.

Kingdom enabled then the comparison between the GPR profiles with the stratigraphic information from the corings in order to understand which interfaces and facies units could be identified uniquely. The picked reflectors were finally interpolated and a map showing the depth of each interface was created. The interpolation was carried out using the Flex Gridding algorithm (more information is available in the IGS Kingdom online manual, <https://kingdom.ihs.com>) with a cell size of 25 m. For converting reflection time to depth, we used velocity-depth functions determined from common-midpoint (CMP) measurements that had been carried out separately. In this way, a specific wave velocity was attributed to each layer. At the locations of the corings, we compared the waveforms of the GPR traces to the drilled stratigraphic sequences in order to evaluate the resolution of the GPR section and to identify the wave patterns indicating the main stratigraphic transitions and facies (e.g. Figure 5c). The resulting 3D model of the investigated area was finally created and visualized using the Surfer software. The grid for the 3D model was set up by applying the Nearest Neighbor Method (<https://support.goldensoftware.com>).

GPR velocity model

For the determination of the velocity-depth functions, the local CMP method was applied as described, for example, in Annan (2004) or Jol (2009).

The CMP soundings were performed with two GSSI GPR antennae with 200-MHz center frequency at 16 CMP sample locations. The CMP gathers were measured up to 2-m transmitter-receiver distance with a spacing of 0.1 m per record (Figure 1, green stars). The two-way traveltimes of the major reflected arrivals were picked and the normal-moveout (NMO) velocity determined from the curvature of the respective reflection hyperbolae by least-squares fitting (Figure 2). Using Dix's formula (Yilmaz, 1988), we then converted the NMO velocity values into interval velocity values for each layer.

As the stratification of the subsurface is not strictly horizontal, the effect of dip on the NMO velocity needs to be estimated (Jacob, 2016). It turned out that the average interface dip is 8°. The corresponding error in NMO velocity is about 1%, and is thus negligible.

Acquisition of stratigraphic data by drilling

The extraction of stratigraphic information from surface geophysical measurements is a task that should be preceded by calibration through actual lithological data. For this reason, the sedimentary infilling of Duvensee was probed with a series of cores along a 50-m long transect (Figure 1d). This transect has been taken as

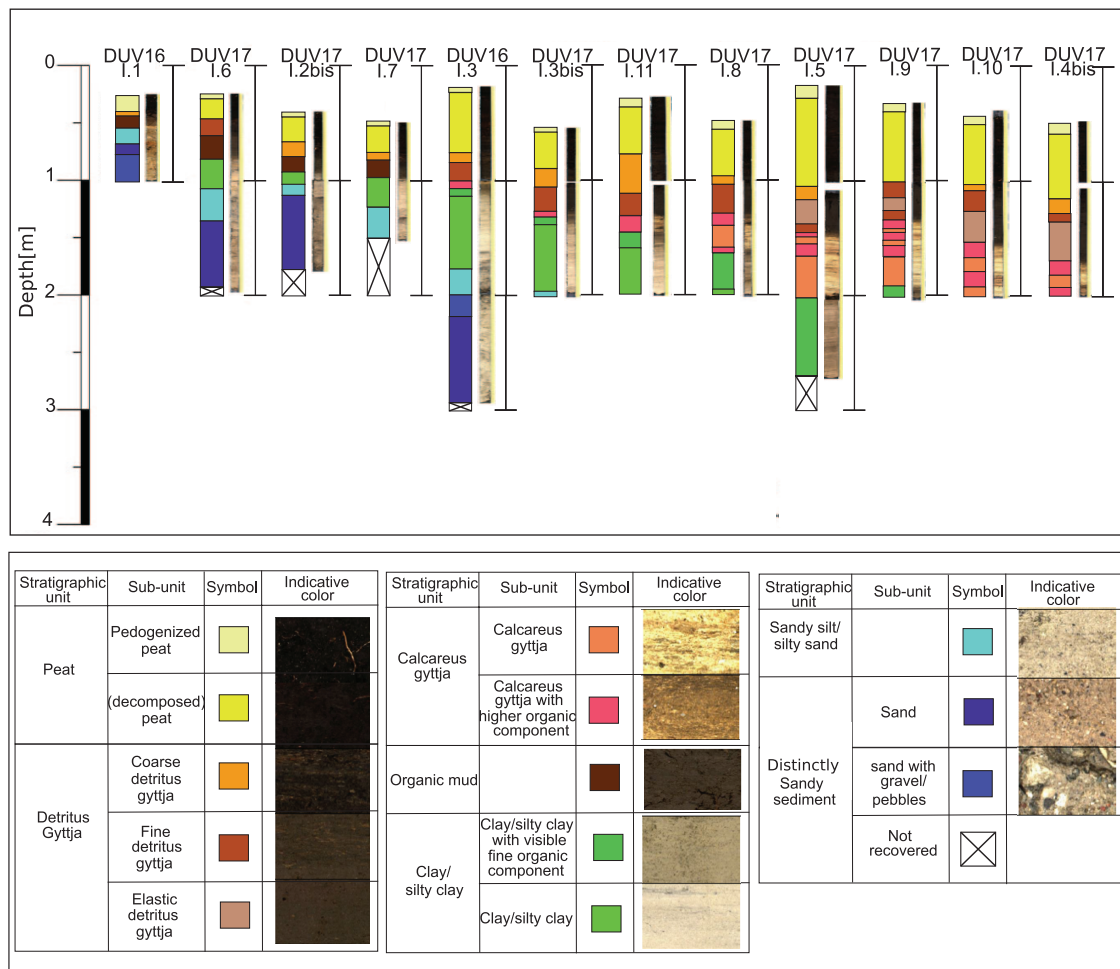


Figure 3. Stratigraphy of the reference profile. Simplified lithology of the cores presented in Figure 1d. The different sediments are indicated with different colors.

reference profile to verify the stratigraphy close to the shoreline. A total of 12 cores was extracted with an Usinger piston corer (Mingram et al., 2007), proceeding at 1-m increments in depth. During the years of research at the Duvensee bog area, other corings had been done previously by Bokelmann and Averdick (internal unpublished report), and their results were incorporated in our study, too.

Results

Stratigraphy of the basin from drilling

The simplified lithology of all cores extracted along the 50-m transect (Figure 1d) is shown in Figure 3. The most distinctive stratigraphic units are peat, detritus gyttja, calcareous gyttja, organic mud, clay/silty sediments and sand. The distinction between these sediment types is primarily based on tactile/visual field observations and on loss in ignition data (LOI, Heiri et al., 2001).

Peat deposits present a distinct dark brown/black color. Distinguishable plant remains are generally limited to modern roots or sparse decomposed fragments. The structure of this sedimentary unit depends on its degree of decomposition and pedogenization, ranging from loose blocks of compact and rather homogeneous plant matter (decomposed peat) to sub-centimetric granules (pedogenized peat). Detritus gyttja is finer and more elastic than peat. It retains a predominant organic component (LOI values between 60% and 90%; carbonates are limited to ca. 1–5%) and is generally lighter in color than peat (brown to dark brown). It can be separated in fine, coarse and elastic detritus gyttja. The term fine detritus gyttja refers to a sediment composed by a rather homogeneous

fine organic matrix, with elastic and compact texture. An increase in coarser plant remains, still encased in a predominantly fine and rather elastic matrix, determines the transition to coarse detritus gyttja. The term elastic detritus gyttja is used to describe sections of fine detritus gyttja with more accentuated elastic properties and visibly lacking recognizable plant macroremains. Calcareous gyttja is composed by fine and plastic sediments with a distinctly high carbonate component (LOI values between 20% and 35%). LOI values for organic matter are generally between 15% and 20%, although bands of irregular thickness with higher organic content are present (LOI values up to 45–55%). Organic mud is a sediment characterized by a high fine organic content (brown, dark brown color), visible but sparse plant tissue remains and higher clay/silt content compared to fine detritus gyttja. This sediment has been recorded in cores that lack a calcareous gyttja unit and represents a transitional element between clayish/silty sediments and fine detritus gyttja. Accordingly, its silt/clay content appears to decrease gradually from bottom to top, together with an increasing fine organic component. Clay/silty clay sediments have a predominant fine minerogenic component (organic matter between 1% and 10%; carbonates between 6% and 12%).

Although coring operations proceeded at 1-m increments in depth, the uppermost segments of the cores are sometimes shorter than 1 m (Figure 3). This discrepancy results from sediment compression produced by the extrusion of the sediment out of the Usinger corer barrel. Notably, these compression issues appear to affect only organic layers in the first meter below the surface. Sedimentary units with a distinct minerogenic or calcareous component are only marginally affected. Understandably, sediment compression affects the measurements of stratigraphic transitions.

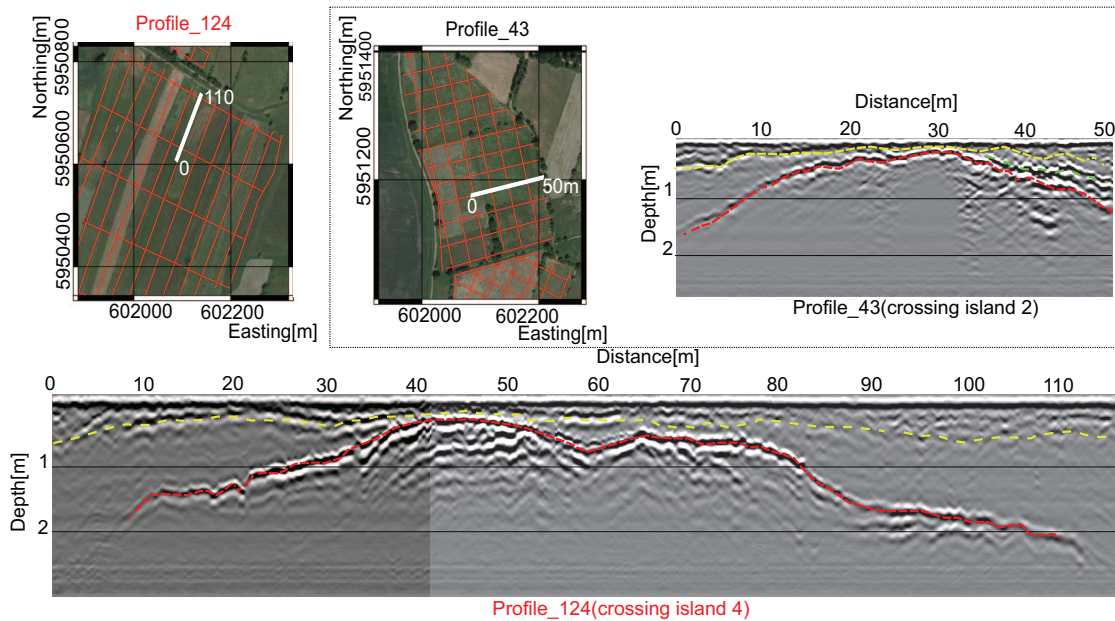


Figure 4. GPR Profiles crossing two different islands. The red line indicates the reflection coming from the transition between clay and sand (Interface3), green and yellow lines indicate Interface2 and Interface1. The only location with the best stratigraphic information was in correspondence of the reference profile because of the large number of coring in that area (Figure 1d). The estimation of the depths in the surrounding area, where few corings were available, could be then affected by an error due to the interpolation between the picked horizons of the entire survey. Also where the location of one drilling was not at the same position of a GPR profile, the estimation of the main transition could be approximated.

For this reason, we focus primarily on the stratigraphy below the superficial detritus gyttja/peat layer. The relation between GPR readings and gyttja/peat transitions are discussed as well, although with a higher degree of caution.

GPR survey

After the processing of the GPR data (see Appendix S2, available online), the picking of the main horizons was performed. This procedure was carried out in feedback with the comparison of the radargrams with the provided stratigraphy from the corings. The location of some corings was not always exactly on a GPR profile; however, this information was still helpful to understand the reflection in the GPR. Figure 4 shows two examples of different profiles crossing two islands. Clearly, a reflection correlated to this feature is indicated with a round shape that becomes deeper on the sides. From the corings at the investigated area, we know that the sediment below this reflection is the basal sand. The detection of this transition was easy because the associated reflection was clearly visible in the radargrams. The shallowest interface identifiable (called Interface1 from now on) separates the top of the stratigraphy peat and coarse detritus gyttja from the underlying fine organic deposits (calcareous gyttja, fine detritus gyttja), whereas the second interface (Interface2) marks the limit between these fine organic sediments and clay. Below these two transitions we find Interface3 defining the change between clay and the basal sands. The dashed lines in Figure 4 indicate, respectively, Interface1 (yellow line), Interface2 (green line), and the red line is Interface3, marking the clay/basal sands limit. To gain more information about the reflections visible in the survey, we compared several radargrams with the stratigraphy from the drillings available in the surrounding area. The dashed lines have been set considering the stratification along the profile, although sometimes the coring was few meters distant from the profile. Considering the entire survey, we recognize five locations in which we found reflections clearly indicating the former islands.

GPR velocity model

Using the 16 CMP measurements together with the stratigraphic information from the corings (Figure 2, Table 1), we could define an average interval velocity and its standard deviation for each layer: $v_1 = 0.045 \pm 0.005$ m/ns for coarse sediments (peat and coarse detritus gyttja), $v_2 = 0.039 \pm 0.003$ m/ns for the fine organic sediments (fine detritus gyttja and calcareous detritus gyttja), $v_3 = 0.037 \pm 0.003$ m/ns for the clay layer. From the evaluation of the CMP measurement, we obtained 14 values for v_1 , 9 for v_2 , and 7 for v_3 and the relative standard deviation was calculated. The velocity associated to the basal sand is $v_4 = 0.038 \pm 0.004$ m/ns coming from three values of the CMP.

These interval velocities were then used to convert the travel time to interface depth.

Knowing the travel time from the picked horizons in the radargrams and the three calculated interval velocities, the depth of each interface has been computed. The radargram in Figure 5a shows the fit of this conversion to the stratigraphic column. Maximum amplitude values are visible from the top of the section until about 0.5 m depth; below this limit, the amplitude decreases. In the first 0.5 m of the radargram, a series of reflections are visible coming from different reflectors, making the interpretation of the peat on top difficult. To better understand each reflections a more detailed stratigraphy is needed. Between 0.5 and 1.10 m the amplitude decreases, indicating lower contrast and attenuation of the radar waves. The comparison with the stratigraphy shows that this part of the radargram is correlated to the fine organic sediments (fine detritus gyttja and clay). A new increase of the amplitude appears at about 1.10 m depth. It is caused by the strong dielectric parameter contrast connected with the stratigraphic change from fine organic sediments to the sand forming the core of the island.

In summary, we can correlate the observed amplitude changes with the transitions between the following major units: the fine organic sediments (fine detritus gyttja and calcareous gyttja) below the coarse sediments (peat and coarse detritus gyttja), followed by the basal sand. For estimating the vertical resolution of

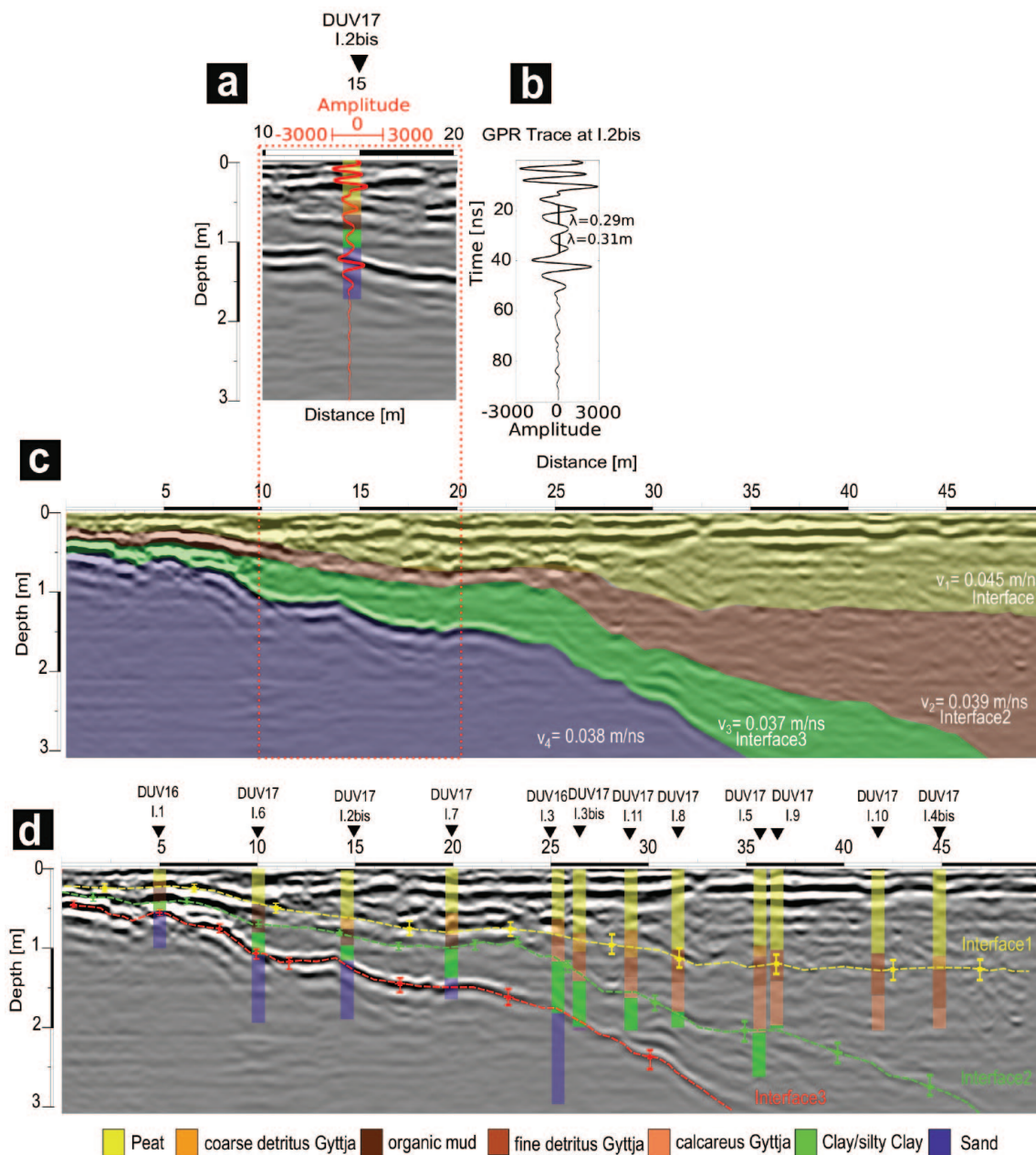


Figure 5. Comparison between GPR results and the stratigraphy. (a) 1D trace from the reference profile in the same position of the Coring I.2bis already converted using three different velocities from the CMP measurements, (b) single GPR trace and λ determination, (c) velocity distribution associated with the reference profile, (d) reference profile together with the stratigraphy and the estimation of the error for the depth calculation. The transitions between the sediment layers are indicated with dashed lines and the sediment with different colors. The yellow line (Interface1) indicates the transition between coarse organic sediments (peat, coarse detritus gyttja) and more fine organic sediments (fine detritus gyttja and calcareous gyttja). The green line (Interface2) indicates the transition between fine organic sediments (fine detritus gyttja and calcareous gyttja) and clay sediments. The third reflection (Interface3) represents the transition between clay and basal sands.

the GPR survey, the combination of stratigraphic column and depth-converted radargram can be used too (Figure 5b). Given a radiated center frequency of 200 MHz and an average wave velocity of $\sim 0.04\text{ m/ns}$, the dominant wavelength is $\sim 0.2\text{ m}$, which shifts toward $\sim 0.3\text{ m}$ at deeper levels due to absorption. Using the quarter-wavelength criterion, the resolution limit can be estimated 5- to 8-cm layer thickness, which agrees with the visual appearance of the GPR section.

Taking the reference profile (Figure 1d) as a starting point, we visualize the velocity distribution in 2D (Figure 5c) by extrapolating the velocity value along the respective stratigraphic units. The stratigraphy together with the radargram and the associated standard deviation are shown in Figure 5d. The effect of the errors in the depth determination increases with depth. Accordingly, the standard deviation of the depths of the interfaces increases from

6–8 cm in the shallower parts to 25–30 cm in the deepest parts of the section.

As evident from Table 1 and Figure 5c, the velocity decreases from the upper to the lower layers by about 10%. This is caused by an interplay of the content of fine-grained clayish sediments and water saturation. The peat on top of the stratigraphy is indeed characterized by a high water content ($\sim 70\%$ by weight), but the velocities are also attenuated by clay, the volume portion of which increases below the gyttja deposition.

Regarding the intensity of the reflections visible in the reference profile, we can recognize that the most visible reflection belongs to the clay/basal sand transition. From the theory it is known that when a propagating electromagnetic wave encounters a significant discontinuity with respect to the dielectric permittivity, some energy is reflected. The amplitude of the reflection

Table 1. Results from CMP measurements.

TWT (ns)	V_{NMO} (m/ns)	V_{RMS} (m/ns)	V_{INT} (m/ns)	ϵ_r	Depth (m)
CMP1					
33.75	0.043	0.043	0.043	49	0.73
45.40	0.043	0.042	0.041	54	0.97
57.18	0.042	0.042	0.039	59	1.20
82.93	0.041	0.041	0.039	59	1.71
CMP16					
34.92	0.042	0.042	0.042	51	0.75
72.66	0.041	0.040	0.039	59	1.48

CMP: common-midpoint.

TWT indicates the two-way reflection time and ϵ_r is the relative permittivity value.

depends on the reflection coefficient, which is related to the contrast in dielectric permittivity. Typically, the values of dielectric permittivity in wet environment are around 26 for wet sand and 46 for wet clay (Conyers, 2013). This latter value agrees qualitatively with the value of 59 (3.9 cm/ns), which we found for the clayish bottom layer. The resulting reflection coefficient at the bottom interface is 0.2 (59 from this study vs 26 from Conyers, 2013).

The permittivity values of the gyttja and peat layers resulting from the velocity values of Table 1 are 54 (4.1 cm/ns) and 49 (4.3 cm/ns), respectively. The corresponding reflection coefficients for the peat–gyttja and gyttja–clay interfaces are about 0.025 both. In comparison with the observed reflection amplitudes, this calculation obviously underestimates the reflection coefficients (cf. Figure 5), which may effectively get enhanced by intercalated thin layers and related tuning effects. Yet, it explains why the transition between peat and clayish-loamy sediments looks less pronounced as compared to the clay–sand transition. This conclusion holds as well if permittivity values from the literature are used (e.g. 37 and 46 for loam and peat, following Conyers, 2013). Between the different organic sediments like calcareous and fine detritus gyttja, the variation of the dielectric permittivity is not big enough to create an evident reflection which can clearly distinguish them. Also, more gradual than abrupt transitions can occur between fine detritus gyttja and organic mud and also between silty sand and sand. Changes in the amount and type of fluid occupying pores, changes in grain shape and grain type give also significant reflections

To verify the calculated velocity from the CMP measurements, we used the known depths of Interface2 and Interface3 from the cores and the traveltime of each interface from the GPR. The results are (for core I.2bis) $v_2 = 0.042$ m/ns for interface2 and $v_3 = 0.039$ m/ns for Interface3. The values are similar to the obtained from the CMP ($v_2 = 0.039 \pm 0.003$ m/ns and $v_3 = 0.037 \pm 0.003$ m/ns) and they are in the range of uncertainty.

In summary, considering these conditions, GPR is able to detect the three major transitions presented above due to a change in the characteristics of the sediments. Interface1 delimits the change between coarse and fine organic sediment, Interface2 indicates the boundary between fine organic sediment and clay and Interface3 is associated with the clay–sand transition. The step from fine detritus gyttja to calcareous gyttja is not immediately recognizable in the GPR profiles despite the difference in composition.

Development of the Duvensee landscape and settlement places as derived from the GPR subsurface model

Using the Kingdom Software, it was possible to visualize all the GPR profiles and compare them with the stratigraphy from the corings. Locally clear rounded reflections coming from the transition clay/basal sand (Interface3) were visible, defining easily the location of former islands in the ancient landscape. From the

comparison of the GPR profiles and the stratigraphy, it turned out that the visible reflectors correspond to the transitions between coarse and fine sediments described in the section, ‘GPR survey’. Interface2 belongs indeed to the transition between the fine gyttja sediments and the Lateglacial clay deposited at the bottom of the ancient lake. This transition was easy to follow through the profiles despite the smaller amplitude of the radar back-reflections. The interface was weaker in the radargrams than Interface3, but possible to follow. Interface1 represents the transition from the fine gyttja and the coarse gyttja and peat sediments which filled the lake. Recognizing this transition was difficult because the radargrams somewhere did not present a clear reflection associated with this layer. The stratigraphic information was helpful to detect this reflector though the survey and the visualization at the same time of the picked horizons and stratigraphy allowed to find Interface1 in the GPR profiles also where it was not clear. Because of an error due to the interpolation, the depth estimation of this layer should be considered with caution. Nevertheless, it does not impact the general result of this study, whose primary focus is on the detection of ancient islands. The time to depth conversion of the three main interfaces was carried out using the velocity values presented in the section, ‘GPR velocity model’ with the aim to create 2D maps showing the bottom of each layer. The interpolation between the profiles was finally done allowing the creation of 2D contour maps shown in Figure 6a–c. If we focus on Interface3, we recognize at least five areas characterized by brown colors, meaning that the reflections associated with the basal sands are at shallower depths with respect to the blue areas, in which they are deeper. This means that the brown features are supposed to represent the islands.

Now we can compare the map of Interface3 with the positions of the dwelling sites already known. Referring to Figure 6c, we notice a very good correspondence between the likely locations of the islands as obtained from the GPR survey and the archaeological evidence. The Mesolithic camps are indeed concentrated in the brown areas (islands 1 to 5) in accordance with the archaeological field studies performed so far (Groß et al., 2018).

Based on the new data, the extension of each island can be determined: island 1, for instance, has an extension of 35 m in the east-west direction and 65 m in the north-south direction, hosting the oldest excavated sites (WP 8 and WP 9). Leaving island and moving approximately 100 m to the east, we find island 2, which was ~175-m long and ~85-m wide. Here, we find the early Boreal sites (WP 1, 2, 5, 6, 11, and 12). Moving 100 m to the south, almost in the middle of the investigated area, island 3 shows up with an extension of ~42 m in EW direction and ~74 m in NS direction carrying WP 13 and WP 19. Further south, 200 m from island 3, two more islands are found: island 4, about 85-m long and ~80-m wide, and island 5, about 82-m long and ~150-m wide. These islands are hosting early Neolithic settlements.

Figure 7 shows the three major interfaces and radar velocities of the corresponding layers in a 3D visualization using Surfer.

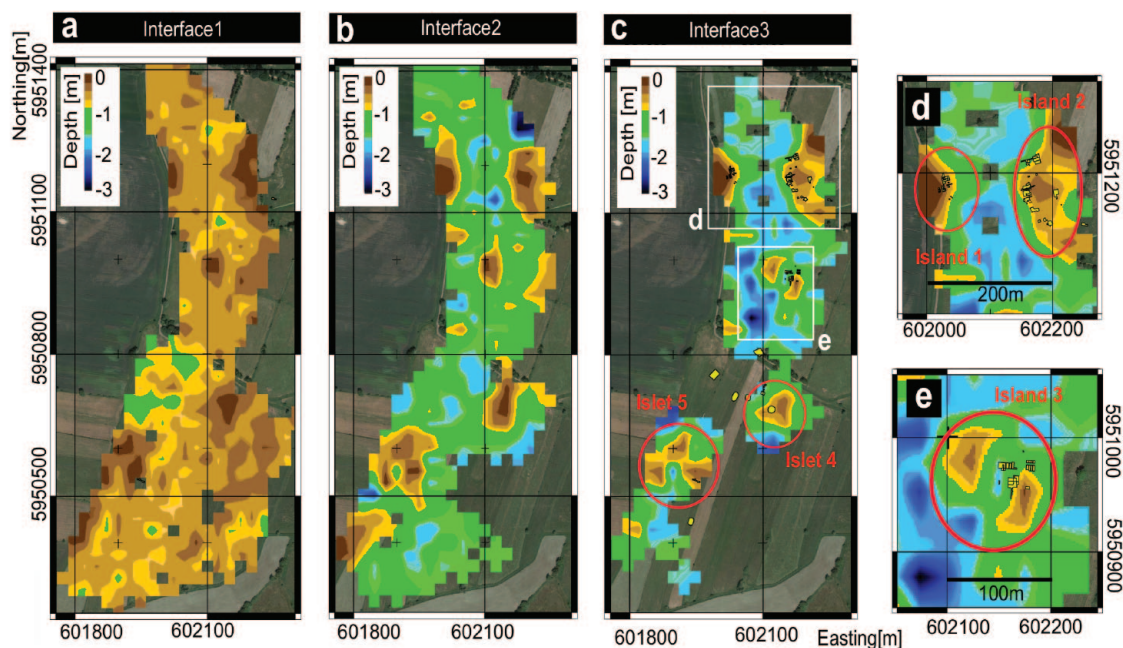


Figure 6. Maps of the transition between the main sediments visible in the GPR Survey: (a) Interface1 indicates the transition between coarse sediments and fine organic sediments, (b) Interface2 indicates the transition between fine organic sediment and clay, whereas (c) Interface3 shows the transition between clay and the basal sand associated with the bottom of the lake. Furthermore, in boxes (d) and (e), the match between the brown areas (associated with the islands) and the Mesolithic camps (the yellow squares) is presented.

Each velocity is shown with a different color and the depth of the equivalent interface is color coded. Maximum depths are about 3 m, showing the penetration depth of the GPR in this case study. The island topography shows up clearly in the exemplary vertical sections of Figure 7b.

Taking into account each layer, the volume occupied by sediment unit could be estimated.

The coarse sediments (peat and coarse detritus gyttja) on top occupy a volume of $\sim 30.8 \times 10^6 \text{ m}^3$, the fine organic sediments (fine detritus gyttja and calcareous gyttja) $\sim 23.8 \times 10^6 \text{ m}^3$, the clay $\sim 37.6 \times 10^6 \text{ m}^3$ and the basal sand (down to 3-m depth) $\sim 68.6 \times 10^6 \text{ m}^3$. These results are important for a first estimation of the water reduction at the ancient Lake Duvensee because of the sedimentation. The fish supply of the hunter-gatherers could have been indeed influenced by this factor. We used these results to calculate the area of the islands between the first late Preboreal occupation and the Neolithic for estimating the growth rate of each island, which corresponds to an average value of $\sim 0.50 \text{ m}^2/\text{yr}$. The hypothesis at this point is that people moved probably southward to the deeper part of the lake where water was still available. This can be the reason why the oldest Mesolithic camps are concentrated in the northern part of the surveyed area earlier covered by sediments.

For investigating the evolution of the lake environment as living space of moving hunter-gatherers and the occupation of the area with time, we have to consider the changing water table of the lake. Using the new 3D model of the lake area, we can hypothetically simulate the regression of the water between the late Preboreal and the Subboreal.

Assuming a continuous decrease of the water level from the late Preboreal to Sub-Boreal, we obtain a spatio-temporal model of the landscape evolution showing the growth of the habitable island areas and the shrinking of the lake areas over time. From the archaeological research, we know that the early Mesolithic camps were located within the overlaying organic sediments and not on the mineral soils forming the islands; therefore, the model shown in Figure 8 includes Interface3, Interface2 and a changing water level. Its maximum depth is about 3 m, corresponding to the penetration depth of GPR. The stratigraphy visible in the corings

shows that the transition clay/basal sand is in the eastern part of the lake below 3 m depth. Therefore, the model has to be considered with some care at the boundaries. Figure 8 shows clearly that the oldest Mesolithic camps (9000 cal. BC) are concentrated in the northern part of the ancient lake (WP 8 and WP 9). The 3D reconstruction suggests that island 1 was indeed a lone emerged area at that time. This may be the reason why it became the place of the first colonization during the lowering of the water level in the Preboreal. During the early Boreal, island 2 and island 4 became the location for new hunter-gatherer camps and further in time also islands 3 and 5 were chosen as a place to settle, even for Neolithic groups (WP 15 and WP 17).

Discussion

General assessment

In this paper, we presented the results of a spatio-temporal landscape transformation based on a GPR survey and coring analysis. For the first time the results allow a reconstruction of the development of parts of the Lake Duvensee landscape during its hunter-gatherers occupation. The derived four-dimensional (4D) model (3D spatial plus time) shows the growth of the habitable area on the islands over time, the development of pathways between the islands, the shrinking of the lake area, and it provides thereby estimates of organic and non-organic sediment volumes deposited in the lake depression. This may be used as an input or boundary condition for dynamic landscape modeling or to infer on the water volume hosting the fishing resources in this area. As a by-product of this archaeological investigation, the present model can be used as a tool for a sustainable groundwater management necessary in the frame of a general heritage preservation strategy.

Apart from methodical details, we see a general confirmation of the model in the agreement between the spatio-temporal pattern of the places found, areal growth of the islands and the time when they emerged. Clearly, details of the presented spatial model of the Duvensee bog are debatable because especially the organic parts of the sediment fill show complex forms of layering that could not be fully resolved in the vertical

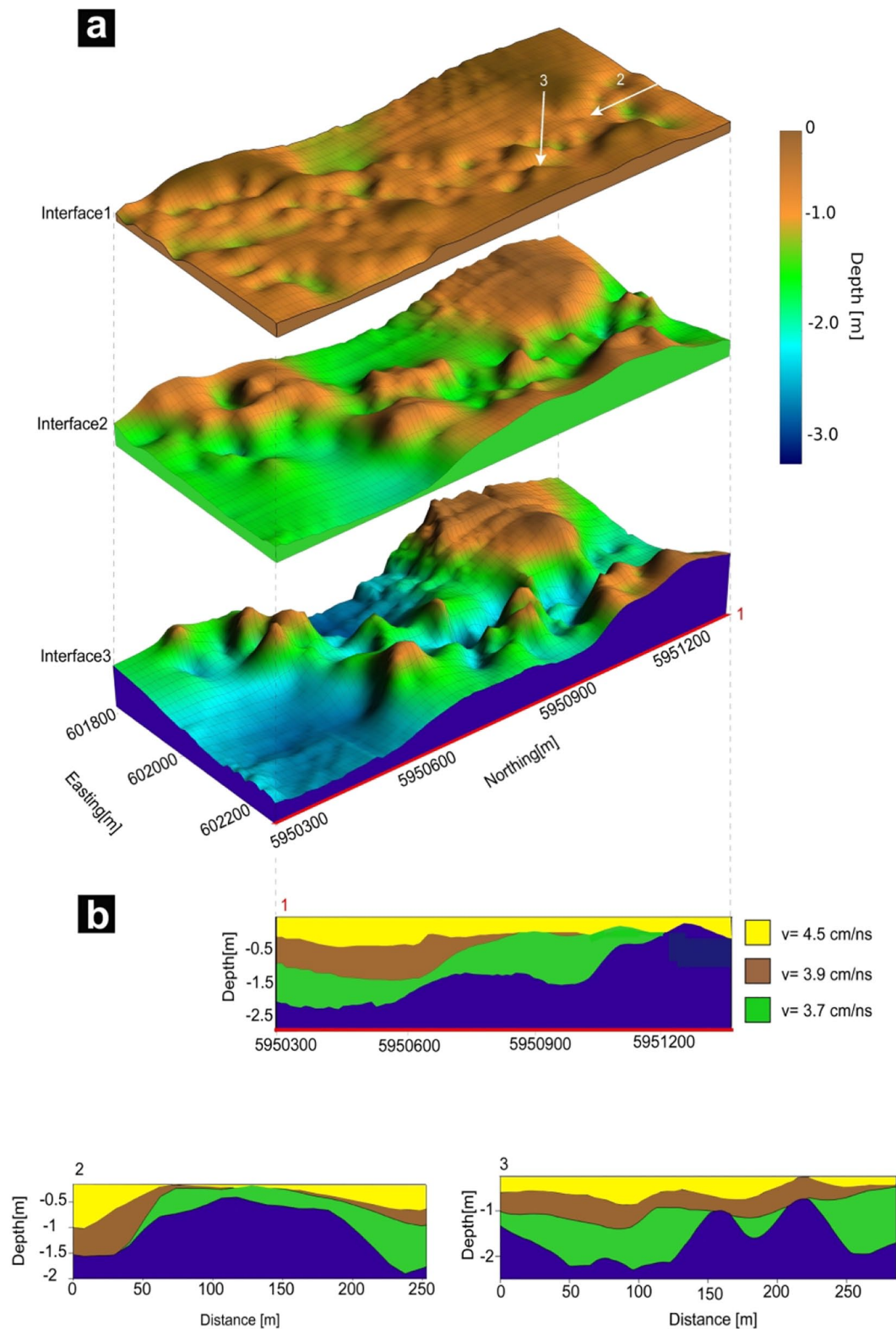


Figure 7. 3D model of the interfaces and velocity distribution. (a) 3D Visualization of the main interfaces and layers derived from the 3D GPR survey, (b) vertical sections from the 3D model, profiles 1 and 2 cross the location of two supposed islands in Figure 1b.

direction and were difficult to follow over large distances. Therefore, the interpretation had to concentrate on three major interfaces that could be traced through the whole investigation area. As to the reliability of the spatial part of the model, it has to be highlighted that these major interfaces and the included facies have multiply been checked and depth calibrated by drilling and stratigraphic analysis. We see this combination of GPR surveying and drilling as the essential part of the chosen methodology.

Core compaction

Because of their central role for ground truthing, the information obtained from drilling demands a special discussion. This is because the extrusion of the soil from the Userger core barrel can lead to a strong compaction of the core, which complicates the depth matching of the stratigraphic column and the interfaces depths detected by GPR (giving an estimation error up to 35 cm). In our case, the compaction affected only the first layer made up of peat and coarse detritus gyttja, while the minerogenic and

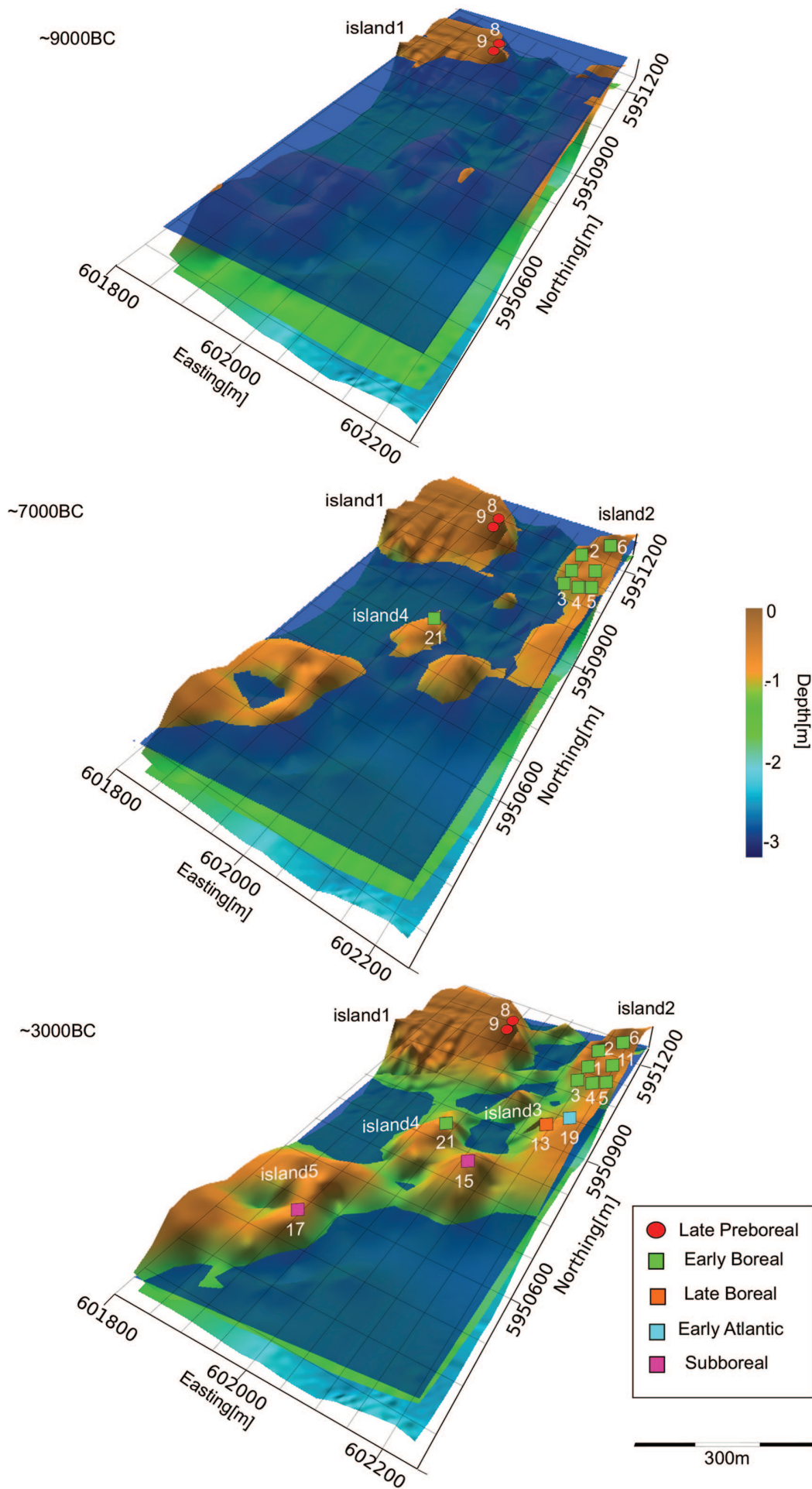


Figure 8. 3D reconstruction of the Duvensee area with a hypothetical regression of the water level and the occupation of the islands by the hunter-gatherers (color coded squares). A linear water decrease starting at 9000 BC and ending at 3000 BC.

calcareous sediment were marginally or not affected. Therefore, the compaction leads to some uncertainty regarding the depth of Interface1. The depth of the clay-to-basal sand transition (Interface3) is therefore not affected.

Although the depth of the sandy base was the major target of this study, we find it also important to estimate the compaction ratio to clarify the depth of Interface1. For this purpose, we compared the GPR depth section along the reference profile and the core catena.

Considering an average depth of the peat coming from the stratigraphy, the corresponding GPR reflector has been set and compaction has been estimated. The compaction for core I.5, for instance, is 21%, for core I.8, is 53% and for core I.4bis, it is 38% and it does not present a homogeneous behavior; therefore, each core has to be taken into consideration for this calculation.

Timing aspects

As for the timing of sedimentation, it is important to distinguish between our reconstruction and the more complex sedimentary dynamics occurring within water basins, especially in the organic sections. Our model is capable of differentiating between broad sedimentary units, yet it treats each one of them as occurring synchronously across the whole study area. In reality, the deposition of different units co-occurred in different sedimentary environments (Averdieck, 1986; Bokelmann, 2012) and only pollen analysis and radiometric dating are capable of determining the time of deposition. Despite the lack of this chronological component, we find it plausible to assume that more elevated areas emerged above the water level earlier than the more shallow ones (e.g. after a gradual lowering of the water table, or due to a gradual accumulation of organic matter), thus allowing us to model the evolution of the Duvensee landscape through time with a simple water-level model. We see the plausibility confirmed by the already mentioned agreement of the spatio-temporal patterns of the archaeological finds and the appearance and growth of island areas.

Subsidence is also a factor that should be ideally considered when modeling ancient landscapes. This phenomenon is influenced by soil/sediment porosity (Allis, 2000), and as such it might have affected the thickness of the most compressible sedimentary units within our case study (e.g. peat and gyttja deposits). Given the highly irregular topography of Duvensee and the variable thickness of its sedimentary layers, it is reasonable to assume that ground subsidence affected different areas of the basin with variable degrees of severity over time. Modeling this complex behavior is a task beyond the capabilities of the current model, and therefore – while we acknowledge its importance – it will not be addressed further in the discussion of our results.

Conclusions

To study the landscape development at the early Mesolithic sites of ancient Lake Duvensee, we derived a 3D model of the major stratigraphic units covering an area of about 63 ha.

The 3D model is based on combining an areal GPR survey with geoarchaeological information from exemplary corings. In this approach, GPR was used to detect major units in terms of dielectric permittivity contrasts and to trace the respective layer interfaces all over the area, whereas the drill cores served for identifying the units lithologically, for calibrating the layer depths determined by GPR CMP sounding and for assessing the spatial resolution of the GPR depth sections. We estimated that the depth determined via CMP measurements were accurate within $\pm 10\%$ and that the effective stratigraphic resolution (corresponding to half a wavelength) of the applied 200-MHz GPR unit was of the order of 0.10 m near the surface and 0.15 m at the maximum sounding depth of about 3 m.

We observed that the major reflections in the GPR records were generated from interfaces between layers that differ significantly in grain size. Therefore, the 3D model consists of four layers separated by the following three main interfaces (from top to bottom):

- Interface1 represents the transition between the coarse organic sediments (peat and coarse detritus gyttja) at the surface and the underlying fine organic sediments (e.g. fine detritus gyttja, calcareous gyttja);
- Interface2 represents the transition between fine organic sediments and underlying clayish-loamy sediments in the bottom of the previous lake;
- Interface3 marks the transition between clayish-loamy layer and the basal sand deposits.

Based on the 3D stratigraphic model of the Duvensee bog and a hypothetical linear time model of the height of the water level, we come to the following conclusions:

1. There were five former islands that occurred successively in the late Preboreal and early Boreal, which grew and eventually connected in the Sub-Boreal.
2. The maximum sizes of the islands before they merged was between $\sim 180,000$ and ~ 3500 m². The growth rates were of the order of ~ 0.25 to ~ 0.78 m²/yr during this period. Vice versa, the area of the surrounding lake shrunk at the same rate, thus possibly reducing the fish supply of the hunter-gatherers.
3. The locations of the islands and their estimated times of emergence from the water agree with the spatio-temporal pattern of the previous archaeological finds, which therefore support our model.
4. The growth pattern of the islands and the land bridges, which formed between them before the whole area landed up, highlights the growing extension of the hunter-gatherer occupation. With the regression of the water and the overgrowing peat from the shore to the center of the lake, the described islands became suitable for the settlement of new camps, as confirmed by both our topographic model and the occurrence of archaeological findings.
5. The 3D model enabled determining the volumes of the peat, gyttja, and clayish-loamy inorganic layers, thus providing important constraints for the numerical modeling of sedimentation in the bog area, which may be matter for future investigation.

The results show that GPR is quite a cost-effective and useful way for understanding past wetland areas. As the overgrowing processes smeared topographical information, modern remote sensing techniques present a useful way for understanding past landscapes and consequently human behavior and settlement strategies within. Even though people during the early Mesolithic were not keeping up long-term settlements, they needed an understanding of their surroundings and its potential. Therefore it is mandatory to understand how the existence of a settlement was intertwined with the surrounding environment and which potentials it provided.

Besides archaeological considerations, the developed 3D stratigraphical model can be used as an input for modeling software applied for sustainable groundwater management (Beall et al., 2011), which is a necessary component of a comprehensive heritage preservation strategy.







Acknowledgements

We would like to thank the longtime excavator and researcher of the Duvensee bog sites, Klaus Bokelmann, for detailed information. Furthermore, we thank the two reviewers for their valuable comments on the text.

Funding

The author(s) disclosed receipt of the following financial support for the research, authorship, and/or publication of this article: We are grateful to the German Research Foundation (DFG) grant 2901391021 (SFB 1266) for funding the presented research.

ORCID iDs

Erica Corradini  <https://orcid.org/0000-0003-4266-8589>
 Marco Zanon  <https://orcid.org/0000-0001-6146-5379>
 Daniel Groß  <https://orcid.org/0000-0002-1328-1134>
 Harald Lübke  <https://orcid.org/0000-0003-0451-0588>
 Natalie Pickartz  <https://orcid.org/0000-0002-3290-7032>
 Ingo Feeser  <https://orcid.org/0000-0002-9618-5139>

Supplemental material

Supplemental material for this article is available online.

References

- Allis RG (2000) Review of subsidence at Wairakei field, New Zealand. *Geothermics* 29: 455–478.
- Annan JP (2004) *Ground Penetrating Radar: Principles, Procedures and Applications*. Mississauga, ON, Canada: Sensors and Software Inc.
- Averdieck F-R (1986) Palynological investigations in sediments of ancient lake Duvensee, Schleswig-Holstein (North Germany). *Hydrobiologica* 143: 407–410.
- Beall A, Fiedler F, Boll J et al. (2011) Sustainable water resource management and participatory system dynamics. Case Study: Developing the Palouse basin Participatory Model. *Sustainability* 3(5): 720–742.
- Bokelmann K (1971) Duvensee, ein Wohnplatz des Mesolithikums in Schleswig-Holstein, und die Duvensee gruppe. *Offa* 28: 5–26.
- Bokelmann K (1991) Duvensee, Wohnplatz 9: Ein präborealzeitlicher Lagerplatz in Schleswig-Holstein. *Offa* 48: 75–114.
- Bokelmann K (2012) Spade paddling on a Mesolithic lake – Remarks on Preboreal and Boreal sites from Duvensee (Northern Germany). In: Niekus MJLT, Barton RNE, Street M et al. (eds) *A Mind Set on Flint. Studies in Honour of Dick Stapert*. Groningen: Groningen Archaeological Studies, pp. 369–380.
- Boll J, Van Rijn RPG, Weiler KW et al. (1996) Using ground-penetrating radar to detect layers in a sandy field soil. *Geoderma* 70: 117–132.
- Campana S and Piro S (eds) (2008) *Seeing the Unseen – Geophysics and Landscape Archaeology*. London: Taylor & Francis.
- Carreon-Freyre D, Cerca M and Hernandez-Marin M (2003) Correlation of near-surface stratigraphy and physical properties of clayey sediments from Chalco Basin, Mexico, using ground penetrating radar. *Journal of Applied Geophysics* 53: 121–136.
- Conyers LB (2012) *Interpreting Ground-Penetrating Radar for Archaeology*. Walnut Creek, CA: Left Coast Press.
- Conyers LB (2013) *Ground-Penetrating Radar for Archaeology*. 3rd Edition. Lanham, MD: Altamira Press, Rowman and Littlefield.
- Davis JL and Annan AP (1989) Ground-penetrating radar for high-resolution mapping of soil and rock stratigraphy. *Geophysical Prospecting* 3: 531–551.
- De Smedt P, Van Meirvenne M, Meerschman E et al. (2011) Reconstructing palaeochannel morphology with a mobile multicoil electromagnetic induction sensor. *Geomorphology* 130(3–4): 136–141.
- Doolittle JA and Butnor JR (2009) Soils, peatlands, and biomonitoring. In: Jol HM (ed.) *Ground Penetrating Radar Theory and Applications*. Amsterdam: Elsevier, pp. 179–202.
- Doolittle JA, Minzenmayer FE, Waltman SW et al. (2007) Ground-penetrating radar soil suitability map of the conterminous United States. *Geoderma* 141(3–4): 416–421.
- Ferring CR (2001) Geoarchaeology in alluvial landscapes. In: Goldberg P, Holliday VT and Ferring CR (eds) *Earth Sciences and Archaeology*. New York: Springer US, pp. 77–106.
- Gourry JC, Vermeersch F, Garcin M et al. (2003) Contribution of geophysics to the study of alluvial deposits: A case study in the Val d’Avaray area of the River Loire, France. *Journal of Applied Geophysics* 54: 35–49.
- Grant JA, Brooks MJ and Taylor BE (1998) New constraints on the evolution of Carolina Bays from ground-penetrating radar. *Geomorphology* 22: 325–345.
- Groß D (2017) *Welt und Umwelt früh mesolithischer Jäger und Sammler. Mensch-Umwelt-Interaktion im Frühholozän in der nord mitteleuropäischen Tiefebene* (Untersuchungen und Materialien zur Steinzeit in Schleswig-Holstein und im Ostseeraum 8). Kiel: Ludwig.
- Groß D, Lübke H, Schmölcke U et al. (2018) Early Mesolithic activities at ancient Lake Duvensee, northern Germany. *The Holocene* 29(2): 197–208.
- Groß D, Piezonka H, Corradini E et al. (2019) Adaptations and transformations of hunter-gatherers in forest environments: New archaeological and anthropological insights. *The Holocene* 29(10): 1531–1544.
- Günther J (1986) Ostracod fauna of Duvensee, an ancient lake in Northern Germany. *Hydrobiologia* 143: 411–416.
- Hartz S, Jöns H, Lübke H et al. (2014) Prehistoric Settlements in the South-Western Baltic Sea area and development of the regional stone age economy. Final report of the SINCOS-II-subproject 4. *Bericht der Romisch-Germanischen-Kommision* 92: 77–210.
- Heinz J and Aigner T (2003) Three-dimensional GPR analysis of various Quaternary gravel-bed braided river deposits (southwestern Germany). In: Bristow CS and Jol HM (eds) *Ground Penetrating Radar in Sediments*. Geological Society Special Publication No. 211. London: The Geological Society, pp. 99–110.
- Heiri O, Lotter AF and Lemcke G (2001) Loss on ignition as a method for estimating organic and carbonate content in sediments: Reproducibility and comparability of results. *Journal of Paleolimnology* 25: 101–110.
- Holden J, Burt TP and Vilas M (2002) Application of ground-penetrating radar to the identification of subsurface piping in blanket peat. *Earth Surface Processes and Landforms* 27: 235–249.
- Jacob B (2016) Ground-penetrating radar velocity determination and precision estimates using Common_Mid_Point (CMP) collection with Hand_picking, semblance analysis, and cross-correlation analysis: A case study and tutorial for archaeologists. *Archaeometry* 58(6): 987–1002.
- Jol HM (2009) *Ground Penetrating Radar (GPR): Theory and Applications*. Amsterdam: Elsevier Science.
- Jol HM and Smith DG (1991) Ground penetrating radar of northern lacustrine deltas. *Canadian Journal of Earth Sciences* 28: 1939–1947.
- Lage W (2011) Experimental archaeological exploration of Mesolithic techniques for hazelnut roasting. *Schriften des Naturwissenschaftlichen Vereins für Schleswig-Holstein* 73: 12–22.
- Lowry CS, Fratta D and Anderson MP (2009) Ground penetrating radar and spring formation in a groundwater dominated peat wetland. *Journal of Hydrology* 373: 68–79.
- Lübke H, Schmölcke U and Tauber F (2011) Mesolithic hunter-fishers in a changing world: A case study of submerged sites on the Jäckelberg, Wismar Bay, northeastern Germany. In: Benjamin J, Bonsall C, Pickard C et al. (eds) *Submerged Prehistory*. Oxford: Oxbow Books, pp. 21–37.

- Mellet JS (1995) Profiling of ponds and bogs using ground-penetrating radar. *Journal of Paleolimnology* 14: 233–240.
- Menotti F and O’Sullivan A (2013) *The Oxford Handbook of Wetland Archaeology*. Oxford: Oxford University Press.
- Mingram J, Negendank JFW, Brauer A et al. (2007) Long cores from small lakes – Recovering up to 100 m-long lake sediment sequences with a high-precision rod-operated piston corer (Usinger-corer). *Journal of Paleolimnology* 37: 517–528.
- Moorman BJ (1990) *Assessing the ability of ground penetrating radar to delineate subsurface fluvial lithofacies*. MSc Thesis, The University of Calgary.
- Neal A (2004) Ground-penetrating radar and its use in sedimentology: Principles, problems and progress. *Earth Surface Processes and Landforms* 27: 261–330.
- Pipan M, Baradello L, Forte E et al. (2000) Ground penetrating radar study of the Cheko Lake area (Siberia). In: Noon DA, Stickley GF and Longstaff D (eds) *Proceedings of the Eighth International Conference on Ground Penetrating Radar*, vol. 4084. Bellingham: SPIE, pp. 329–334.
- Ruffell A, Geraghty L, Brown C et al. (2004) Ground-penetrating radar facies as an aid to sequence stratigraphic analysis: Application to the archaeology of Clonmacnoise Castle, Ireland. *Archaeological Prospection* 11(4): 247–262.
- Schmölcke U (2016) Die Säugetier funde vom präboreal- und boreal zeitlichen Fundplatz Friesack 4 in Brandenburg. In: Benecke N, Gramsch B and Jahns S (eds) *Subsistenz und Umwelt der Feuchtbodenstation Friesack 4 im Havelland: Ergebnisse der naturwissenschaftlichen Untersuchungen*. Zossen: Brandenburgisches Landesamt für Denkmalpflege und Archäologisches Landesmuseum, pp. 45–116.
- Schmölcke U and Nikulina E (2015) Mesolithic beaver hunting station or base camp of supra-regional Stone Age fur trade? New archaeozoological and archaeogenetic results from Dąbki 9. In: Kabaciński J, Hartz S, Raemaekers DCM et al. (eds) *The Dąbki Site in Pomerania and the Neolithisation of the North European Lowlands (C. 5000–3000 Calbc)*. Rahden: Leidorf, pp. 65–86.
- Schwabedissen H (1951) Grabungen auf dem Moorwohnplatz von Duvensee. *Germania* 29: 208.
- Schwantes G (1939) *Die Vorgeschichte Schleswig-Holsteins (Stein- und Bronzezeit)*. Neumünster: Wachholtz.
- Schwantes G, Gripp K and Beyle M (1925) Der frühneolithische Wohnplatz von Duvensee. *Praehistorische Zeitschrift* 16: 173–177.
- Sheriff RE (1977) Limitations on resolution of seismic reflections and geologic detail derivable from them. In: Payton CE (ed.) *Seismic Stratigraphy – Applications to Hydrocarbon Exploration*, vol. 16. Tulsa, OK: American Association of Petroleum Geology, pp. 3–14.
- Stern N (2008) Stratigraphy, depositional environments, and paleolandscape reconstruction in landscape archaeology. In: Bruno D and Thomas J (eds) *Handbook of Landscape Archaeology*. Walnut Creek, CA: Left Coast Press, pp. 365–378.
- Tolksdorf JF, Turner FK, Knut et al. (2013) Multiproxy analyses of stratigraphy and palaeoenvironment of the late Palaeolithic Grabow floodplain site, northern Germany. *Geoarchaeology* 28(1): 50–65.
- Warner BG, Nobes DC, Theimer BD et al. (1990) An application of ground penetrating radar to peat stratigraphy of Ellice Swamp, Southwestern Ontario. *Canadian Journal of Earth Sciences* 27(7): 932–938.
- Wunderlich T and Rabbel W (2013) Absorption and frequency shift of GPR signals in sandy and silty soils: Empirical relations between quality factor Q, complex permittivity and clay and water contents. *Near Surface Geophysics* 11(2): 117–127.
- Yilmaz Ö (1988) Seismic data processing. *Society of Exploration Geophysicists* 2: 526.
- Zhao W, Forte E, Pipan M et al. (2013) Ground penetrating radar (GPR) attribute analysis for archaeological prospection. *Journal of Applied Geophysics* 97: 107–117.

A.3 Paper III

The following version was submitted to the Journal *Geosciences* on June 2020 and is currently in the review process

Article

Understanding wetlands stratigraphy: geophysics and soil parameters for investigating ancient basin development at lake Duvensee

Erica Corradini ^{1,*}, Stefan Dreibrodt ², Ercan Erkul ¹, Daniel Groß ³, Harald Lübke ³, Diana Panning ¹, Natalie Pickartz ¹, Martin Thorwart ¹, Andreas Vött ⁴, Timo Willershäuser ⁴, Dennis Wilken ¹, Tina Wunderlich ¹, Marco Zanon ⁵, Wolfgang Rabbel ¹

¹ *Institute of geosciences, Christian-Albrechts University Kiel, Germany; erica.corradini@ifg.uni-kiel.de*

² *Institute for Ecosystem Research, Christian-Albrechts University Kiel, Germany*

³ *Centre for Baltic and Scandinavian Archaeology (ZBSA), Schleswig-Holstein State Museums Foundation Schloss Gottorf, Germany*

⁴ *Institute of Geography, Johannes Gutenberg University Mainz, Germany;*

⁵ *Institute of Pre-and Protohistoric Archaeology, Christian-Albrechts University Kiel, Germany;*

* Correspondence: erica.corradini@ifg.uni-kiel.de; +49 431 800-3901

Keywords:

Geophysics; Peatlands; Landscape development; Drillings, Geoarchaeology

Abstract:

We present an exemplary case study of a bog showing how an integrated approach of multi-method geophysical sounding and local soil sampling can be used to identify, differentiate and map organic sediments. Our study is based on ground-penetrating radar (GPR), electrical resistivity tomography (ERT) and SH-wave seismic profiling applied to the ancient lake Duvensee (Northern Germany), nowadays a bog. It is a well known find place of remains from Mesolithic hunter-gatherers occupation, which has attracted archaeological and geoarchaeological research since 100 years. The fen is embedded in low conductive glacial sand and is characterized by layers of different gyttja sediments (detritus and calcareous). The presented study was conducted in order to identify the bog morphology and the thickness of the peat body and lake sediments to understand the basin evolution. To validate the geophysical results, derived from surface measurements, drillings, soil analyses as well as, borehole guided wave analysis of electromagnetic waves and EC-Direct-Push have been carried out and used as comparison. It turned out that each method is able to distinguish between sediments that differ in grain size, in particular between peat, lake sediment (gyttjas and clay) and basal glacial sand deposits. GPR is even able to separate between high and low decomposed peat layers which is also clear considering resistivity variations in the ERT computation. From the association between geophysical properties and soil analysis (e.g. water content and organic matter) different gyttjas were distinguished (coarse and fine) and seismic velocity was correlated to bulk density. Moreover, GPR and SH-Seismics presents different resolutions confirming that the latter allows measurements which are more focused on determining the extension of basal sand deposits, whose depth is difficult to reach with GPR. Representative values of electrical resistivity, dielectric permittivity, and shear wave velocity have been determined for each sediment type and are therefore available to complete the investigation of wetland environments.

1. Introduction

From prehistoric to historic times, floodplain margins, lake shorelines and coasts have been preferential settlement areas. Sites with water-access provided favourable conditions for human activity and habitats [1-3]. Thus, wetland margins are important zones in archaeological and geoarchaeological research [4,5] despite the often difficult exploration conditions, e.g. water inflow or the groundwater impact [6]. Palaeoenvironmental reconstruction of wetland development depends critically on knowledge of the peatland stratigraphy including the thickness of the peat deposit, within-peat layering and the underlying lake sediments (gyttja). Depending on the site conditions during sedimentation, gyttjas can vary in their organic matter content and may thus be predominantly mineral or organic deposits [7,8]. The proportion of mineral and organic matter content influence the mechanical and hydrological properties [9]. Within the peat deposits, the degree of decomposition has an influence too, organic matter content decreases and bulk density increases with the degree of decomposition [10].

The investigation of peatland stratigraphy by geoarchaeological surveys in wetlands, require integrated multidisciplinary and scale overlapping approaches including surveys and geophysical prospecting, as well as medium-, small- and micro-scale drilling campaigns and excavations to ground truth the results [11-13].

Drilling provides detailed information about the vertical stratigraphy but usually with a low lateral sampling density due to the time consuming character of this method. Additionally, inter-drilling point sections have to be interpolated, resulting in an unknown uncertainty about small-scale changes in the stratigraphy. This disadvantage can be improved by combining drilling with non-invasive geophysical methods, ground penetrating radar (GPR), Electrical Resistivity Tomography (ERT) and SH-wave seismics, which allow a laterally continuous mapping of the lithological change [14, 15].

Ground penetrating radar (GPR) has been widely used to analyze peat deposits [11, 16-21] because the low electrical conductivity of the peat allows large penetration depth and the change in water content with respect to the mineral sediment provides strong reflections for excellent geophysical imaging [22]. To resolve peatland stratigraphy with GPR in more detail, several studies have related peat internal reflections to layers of different decomposition-degree, different peat types or pieces of wood [16,18,23]. The success of detecting such interfaces depends on the dielectric contrast between the different layers and is thus site-specific. The same is observed, if we consider the interfaces between peat and gyttja layers. [24] for instance, illustrated a distinction between peat and organic gyttja layer, whereas [25] could not. Gyttja deposits show variable bulk density depending on their organic matter content [26], thus the dielectric properties broadly differ too. Therefore gyttja was often not further differentiated and it is difficult to estimate whether gyttja layers were detected or not [8].

ERT and seismics measurements have been applied in such environments less frequently although both methods may deliver important complementary information. Electric resistivity profiling can assist peatland studies as it can provide stratigraphic information from beneath the mineral soil contact [17,18]. However, little is known still about the relationship between electrical conductivity (which is the reverse of resistivity) and peat properties in differing site conditions [8]. [24] and [27] found that the total amount of solutes in the pore fluid and the cation exchange capacity are the most appropriate properties to describe electrical conductivity of poorly decomposed *Sphagnum* peat. Moreover, they claim that water content and cation exchange capacity are mainly correlated with electrical conductivity.

SH-wave seismics is directly sensitive to the rigidity of soil layers and capable of resolving stratigraphic interfaces at much larger depths than GPR [28,29]. SH-wave sounding can identify and differentiate soft soils such as fine grained lake sediments or swampy organic deposits [14], which are characterized by very slow seismic velocities.

In this paper we present a multi-method geophysical survey at the Duvensee palaeolake in south eastern Schleswig-Holstein, northern Germany, which is well known for Early Mesolithic hunter-gatherer archaeology on the Northern European Plain [30]. The former lake was formed by melting dead-ice after the retreat of the last Weichselian glaciation. Its irregular topography resulted in several islands

scattered along the ancient water body, which were used by Early Mesolithic hunter-gatherers groups to establish temporary camps.

Our study has three major objectives:

1. To identify and continuously map the main stratigraphic units filling the ancient lake Duvensee for a better understanding of the former basin evolution. For this purpose, we combined sampling by drilling with geophysical profiling, especially ground penetrating radar (GPR), electric resistivity tomography (ERT) and seismic sounding with shear waves (SH-waves).
2. To evaluate the suitability of GPR, ERT and SH-wave seismics to detect peat properties, paying particular attention to the identification of different gyttja layers.
3. To determine the conditions, under which peat and gyttja layers can be identified and distinguished in terms of geophysical parameters, in particular electric resistivity, shear wave velocity and dielectric permittivity.

The geophysical results are presented for each method and compared with the stratigraphy from the drilling to ground truth measurements. Moreover physical parameters (i.e. degree of decomposition, water content, ion concentration) of the main sediment types (peat, gyttja, clay and sand) are discussed together with electrical resistivity, SH-wave velocities and electromagnetic wave velocity variations to validate the geophysical results.

Following the description of the background about the investigated area and the physical properties of the sediments we present the results of the geophysical and geoarchaeological surveys and their implications for reconstructing the deposition of the ancient lake basin. Based on this experience we finally come up with some recommendations for future work.

2. Area of investigation and landscape development

The ancient Lake Duvensee in Schleswig-Holstein (Germany) is one of the prime locations in northern Europe for early Holocene archaeological research. The ancient lake bed was formed during the older Dryas as a dead-ice hole left by the retreating Fennoscandian ice sheet [31]. Past stratigraphic investigations revealed a complex basin topography, characterized by numerous deeps and sand banks [32]. The gradual infilling of the basin was accompanied by a general decrease in water level over time. By the 19th century CE, most of the basin was occupied by a bog.

The sediment succession near the shorelines generally exhibits a gradual shallowing of the deposition environment. The majority of the deposits are typical lake sediments, such as calcareous gyttja, algal gyttja and coarse detrital gyttja. The sediment cores have shown that in spite of similar depositional conditions, strong lateral variations in sediment facies are present. The complicated alterations observed in the drillings attest multiple changes in lake level [32]. Moreover, a remote possibility exists

that the basin floor was high and artificially formed by remnant dead ice, which prevented deposition of thick sedimentary sequences [32].

This area has been the subject of archaeological research for almost 100 years showing the presence of 23 different locations of Early Mesolithic hunter-gatherer groups and Neolithic farmers. Based on GPR sounding [21] developed a 3D model of the Duvense bog and its stratigraphy including five islands, which emerged from the retreating water over time making them suitable for Mesolithic camps. These results confirmed and complemented previous archaeological surveys [33]. The estimated dive-up times of the mapped islands agree with the spatio-temporal pattern of the previous archaeological finds [33].

Coherent overviews of the research at ancient lake Duvensee have been given by [30, 33, 34]. The area has been the subject also of different geophysical campaigns aimed at improving the knowledge about the evolution of the basin. After a large-scale GPR survey carried out in November 2016, more detailed geophysical measurements have been conducted focusing on a small scale. For ground truthing the stratigraphy of the basin a reference profile close to the ancient shoreline has been chosen and different geophysical measurements have been applied between 2018 and 2019 (Figure 1). Work at Duvensee, in particular the results of GPR and coring surveys, has been described in detail in [21], and is only briefly summarized here.

The main units visible in the stratigraphy (Figure 3) are peat (pedogenized peat and decomposed peat), detritus gyttja (coarse, fine and elastic detritus gyttja), calcareous gyttja, organic mud, clay and sand sediments. The major reflections in the GPR records were generated from interfaces between layers that differ significantly in grain size. The resulting 3D model consists of four layers separated by the following three main interfaces (from top to bottom):

- Interface1 represents the transition between the coarse organic sediments (peat and coarse detritus gyttja) at the surface and the underlying fine organic sediments (i.e. fine detritus gyttja, calcareous gyttja),
- Interface2 represents the transition between fine organic sediments and underlying clayish-loamy deposits in the bottom of the previous lake, and
- Interface3 marks the transition between the clayish-loamy layer and the basal sand deposits.

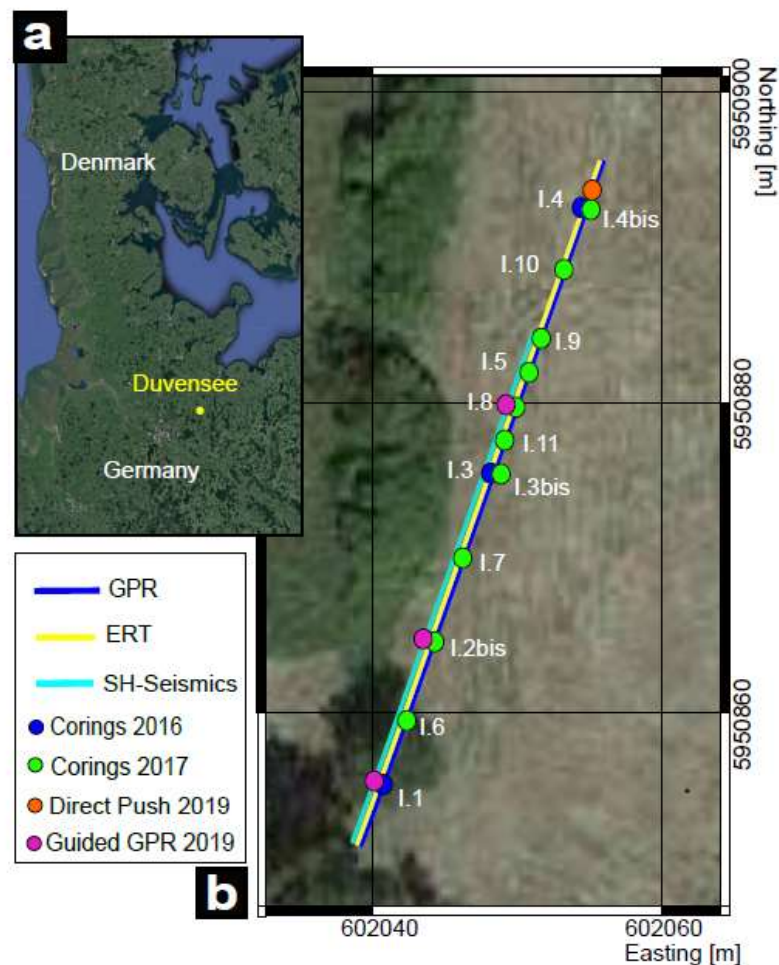


Figure 1. Area of investigation including geophysical and coring surveys. (a) Location of ancient Lake Duvensee; (b) geophysical measurements, corings and Direct Push done in the area of interest (color coded dots).

3. Physical properties of organic sediments

Peat forms through the accumulation of partially decomposed plant biomass in fens, bogs and swamps in various parts of the world [35]. The physical properties of any soil are dependent to a large degree on porosity and pore-size distribution, which in turn are related to particle-size distribution. In peat, particle size and structure and the resulting porosity are controlled primarily by the degree of decomposition. As reported in Table S1, the total porosity of peat soils often exceeds 80% [36].

Undecomposed peats contain many large pores, highly irregular and interconnected, that permit water movements. Highly decomposed peat contains smaller open pores, and also those pores that are closed or partially closed [37]. Peat is thus a dual-porosity medium that includes a ‘mobile region’ through which water moves relatively easily, and an ‘immobile region’ with negligible fluid flow velocity [38].

Peat is also a sedentary deposit which means that the degree of decomposition generally increases with depth below the ground surface, while the geometric mean pore diameter and active porosity simultaneously decrease [38,39]. For example in the Arctic tundra, the active porosity typically drops from values around 80% near the ground surface to < 50% at depths of 0.5 m [40]. Peat is a highly compressible material [41] and this property is also controlled by the structure and arrangement of its pores [42], factors that are largely controlled by the degree of decomposition [41]. Decomposed peat at greater depths typically shows lower active porosity and compressibility. The degree of decomposition is commonly assessed using the 10 classes of humification of the von Post scale [43] where H1 refers to the least, H10 the most decomposed peat. The von Post classification is based on the visual inspection of extracted soil solutions and plant residues, and is therefore particularly useful in the field.

Gyttja sediments are layers with varying organic matter content that developed in low-energy subaqueous environments. The term 'gyttja' was introduced by [44] as a combination of organic and inorganic materials precipitated from a lake water column via biochemical processes.

Organic matter that originates from aquatic life within the lake and input the lake catchment accumulates at the sediment-water interface from suspension or when its specific weight exceeds that of water. Degradation of the organic matter occurs either under anaerobic conditions or from fine/coarse pre-degraded organic materials at the surface which can be washed out in the basin. In a fresh state, gyttjas are very soft and hydrous, with a dark greenish-gray to black color depending on the organic matter content. Detritus gyttja appears similar to decomposed peat because it contains plant remains, still encased in a predominantly fine and rather elastic matrix; the fine lake sediments appear instead to have similar physical properties to clay deposits (e.g. grain size of silt and clay, and high ionic concentration of the pore water which creates high conductivities like those of clay minerals) [24].

4. Methodology

4.1 Ground penetrating radar (GPR)

4.1.1. GPR surface profiling

The GPR system consists of a transmitting and a receiving antenna. The former emits an electromagnetic wave and the latter detects the transmitted wave which is partially reflected in the subsurface at interfaces. The propagation of a radar signal depends on the dielectric permittivity (ϵ_r), which controls the propagation velocity and reflection strengths, and the electrical conductivity (σ), which mainly influences the signal attenuation.

Signal strength and center frequency of radar signals decrease during wave propagation due to energy absorption [e.g 45]. High water content and clay sediment for instance strongly attenuate the radar signal and reduce the depth of investigation [46]. Penetration depth and resolution are also influenced by the GPR antenna frequency. Lower antenna frequencies are favourable for greater penetration but result in a decrease in vertical resolution which is approximately defined as a quarter of the GPR

wavelength. This means that the lower stratification can be poorly imaged compared to the upper stratification

In order to calculate the depth of reflections from the recorded traveltimes, the radar wave velocity has to be known and thus the dielectric permittivity. [46,47] and [48] give tables of dielectric permittivity for a range of sediments and materials (Table S1). It can be seen that these values, particularly those for wetland sediments, have large ranges. [49] presents the outcome of different case studies in wetland sediments showing that dielectric permittivity can be highly variable if not waterlogged.

Due to the high permittivity of water, the bulk dielectric permittivity of sediments is mainly controlled by the water content. GPR can detect changes in water content greater than 3%, occurring within a depth interval of 15 cm [17]. The boundary between the peat and the underlying mineral sediment is identifiable because of the sharp reduction in the volumetric water content between the peat and the mineral soil below [e.g. 18,24,39]. GPR profiles within peat often show patterns of reflections and [17] suggested that these reflections strongly match variations in peat moisture content. [16] and [39] could thus identify the boundary between uppermost poorly decomposed peat (“acrotelm”) and underlying well-decomposed peat (“catotelm”).

The electrical conductivity depends linearly on the concentration of total dissolved solids in the peat pore waters. [17] found that the ionic concentration, and thus the electrical conductivity, increases linearly from the surface to basement for peat deposits. High fluid electrical conductivity in peat, or a high percentage of clay in the mineral soil, can excessively attenuate radar wave propagation, reducing the depth of penetration in peat and usually prevent recording of reflections from below the mineral soil contact underlying peat bogs [11,17].

Conductivity is strongly dependent on temperature too, which will differ depending on the season of the survey, the depth of measurement, and whether samples are measured in the field or the laboratory [17,50].

A GSSI GPR Antenna with 200 MHz frequency was used to perform common offset data acquisition in the Duvensee area. The presented profile (50 m long, blue line in Figure 1) is part of a survey made in November 2016. The measurement details and the processing steps are described in [21]. The reflections associated with the main layers visible in the cores (basal sands, fine minerogenic sediments, fine and coarse organic deposits) have been recognized and picked using the Kingdom IHS Software. The conversion from time to depth was made using the corresponding velocity values derived from CMP measurements (see [21]).

4.1.2. GPR downhole profiling using guided waves

An innovative way of measuring radar wave velocities at depth is the use of guided waves in a borehole [51], (Figure 2a). This method yields a continuous record of velocity with a regular downhole spacing of a few cm. In contrast to the familiar CMP-velocity sounding it is applicable not only to reflecting horizons but also to gradual velocity changes. Using the same principle as TDR sondes the measurement

technique uses a steel rod, which is pressed or hammered stepwise into the ground. It serves as a wave guide for the electromagnetic waves emitted by a regular GPR antenna placed next to the rod at the earth's surface. The waves travel vertically along the waveguide and are reflected at its lower end. Through knowledge of the waveguide's depth, velocities in each depth interval can be calculated and converted to permittivity values. The innovative technique applied here was developed by the Leibniz Institute for Applied Geophysics [51]. The velocity of the guided wave depends on the permittivity of the soil material, which is strongly influenced by the water content. The two-way traveltime of the reflected wave at different waveguide depths is picked and can be used to calculate interval velocities. We lowered the metal rod into the ground by hammering and recording a GPR trace every 10 cm. The travel times of the reflection at the lower waveguide end were picked and the GPR velocities were calculated. This technique was applied at the three locations of the corings (pink dots in Figure 1).

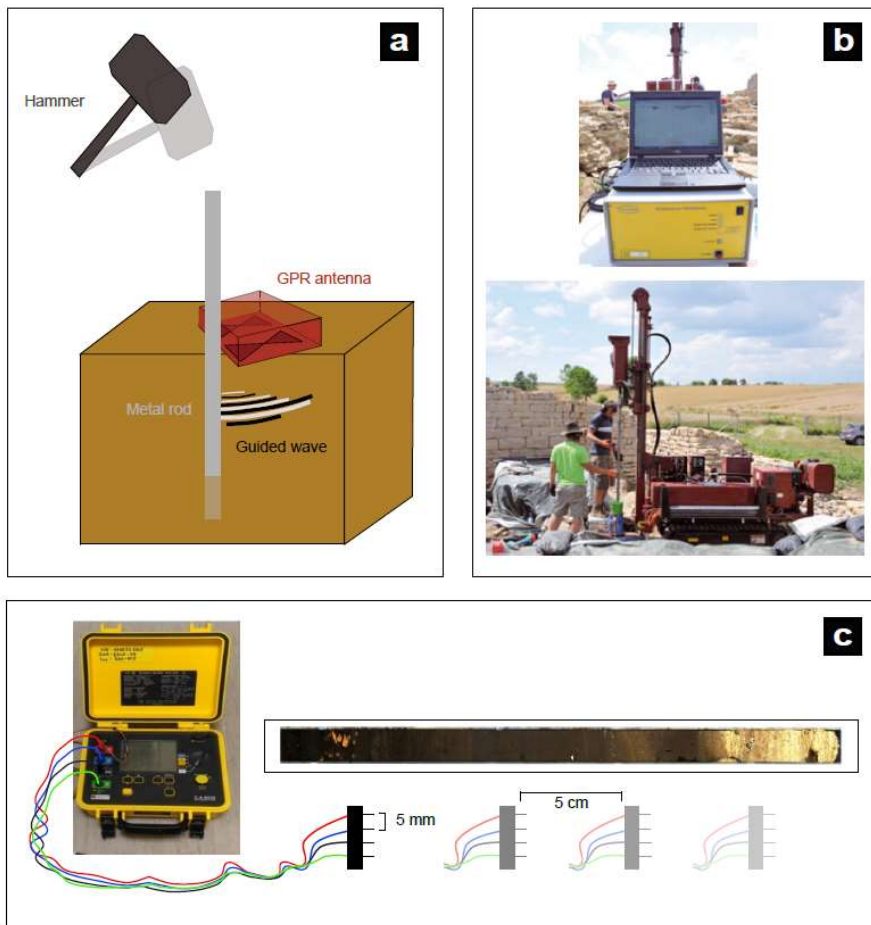


Figure 2. (a) guided GPR wave setup with 400 MHz antenna on the ground surface and waveguide lowered by hammering; (b) EC Direct Push equipment (c) Laboratory measurements of the resistivity along the cores.

4.2 Geoelectric profiling

4.2.1. Electrical resistivity tomography (ERT)

Less common are electrical resistivity measurements in wetlands but have become an important tool for geoarchaeology. Electrical conductivity is the inverse of electrical resistivity and former studies have demonstrated that peat is chargeable and is attributed to the high surface-charge density of partially decomposed organic matter [18, 52].

A geoelectric measurement is made with a set of four electrodes, the current flows between the two outer electrodes and the potential difference is measured between the two inner ones. Electrode spacing and penetration depth increases during the survey until the maximum spacing is reached, which provides the deepest resistivity information [53].

Geoelectric measurements were conducted using a PC controlled DC resistivity meter system RESECS (Geoserve) with 96 electrodes. The electrode spacing was 0.5 m (total length of the profile 47.5 m, yellow line in Figure 1) and we measured Dipole-Dipole and Wenner-Alpha arrays. Electrode locations were determined by a Differential GPS (Leica Geosystems). The inversion was carried out in 2D by applying BERT (Boundless Electrical Resistivity Tomography, [54], a finite-element (FE) inversion software. The starting model is made up using an homogeneous resistivity value of 29.84 Ωm . A regularization parameter of $\lambda=20$ was applied in the standard inversion, that was selected based on the L-curve method (L2-NORM) [55].

The quality of the fit of the resulting electrical resistivity model is given by the RRMS (relative root mean square) deviation between measured and modelled data (in %) and by the chi-squared misfit. [54] state that chi-squared values of one to five show that results are statistically reliable meaning that the data are neither overfitted nor underfitted.

4.2.2. Vertical electric profiling using Direct-Push

DP-EC logging was conducted using a Geoprobe SC520 soil conductivity probe [56], Figure 2b. The probe is composed of four electrodes in linear arrangements and was operated in a Wenner array enabling a vertical resolution of 0.02 m (www.geoprobe.com; [56, 57]). The electric current and voltage are constantly measured with depth and used for the calculation of electric conductivity in mS/m [58]. Electric conductivity is the inverse of electric resistivity. This equipment was used to measure at the location of core I.4 (orange dot in Figure 1) and the values have been compared also with the measurements carried out in the laboratory.

4.2.3 Electric resistivity measurements on drill cores

In the laboratory, the electric *resistivity* of drill core segments was measured using an earth resistivity meter connected with four electrodes in Wenner-Alpha configuration (5 mm long and 5 mm distant with 1 mm diameter, Figure 2c). The quadrupole was inserted into the sediment ensuring the contact

between the electrodes and the ground. The surface contact area of the electrodes is about 1 mm^2 . Due to the varying soil conditions the electrodes had different penetration depths in different layers. This was compensated by applying correspondingly varying geometry factors considering that the electrodes are nearly punctiform. We measured on each core with 5 cm point spacing and compared the measured values with Direct-Push and ERT to understand the change of the property in the sediments at ancient lake Duvensee.

4.3 Seismic sounding with shear (SH) waves

4.3.1 Motivation of applying SH-waves in geoarchaeology

The application of seismics for geoarchaeological research is not wide spread but has lately been intensified due to exemplary results [14, 28, 59-64].

The propagation velocities of seismic waves (P- and S-waves) depend on soil composition, fabric, effective ambient pressure and temperature. S-waves are more suitable for near surface applications in unconsolidated sediments because the propagation velocities are much slower than P-wave velocities, enabling the imaging of geological and archaeological structures with higher spatial resolution [e.g. 65]. The second aspect is that S-wave velocity and reflection strength are only very little influenced by water saturation. Therefore, S-wave velocities often can be more directly correlated with lithology than P-wave velocities.

For investigating the subsurface structure at Duvensee we applied seismic reflection imaging and seismic traveltimes tomography, which are explained in the subsections below.

For studying the stratigraphy of the ancient wetland at Duvensee we conducted a 36 m long S-wave profile (cyan line in Figure1) with receiver spacing of 0.5 m and 1 m spacing for shotpoints (for acquisition parameters see Table S2). SH waves were excited by a horizontal hammer blow. The data were recorded with three Geometrix Geode seismographs placed in line, equipped with 72 10-Hz horizontal geophones oriented perpendicular to the profile line. We excited horizontally polarized S-waves (SH-waves) by horizontal hammer blows against the sides of a steel bar, which was coupled to the ground by steel spikes mounted at the bottom of the bar. The source points were located midway between the receivers and the steel bar and blows oriented perpendicular to the profile line.

4.3.2 Seismic refraction tomography

In contrast to reflection seismics, refraction seismics data interpretation aims at determining the spatial distribution of seismic wave velocity as a characteristic of the sediment type. This is executed by analyzing the arrival times of critically the refracted waves.

The ratio of the seismic velocity of the layers above and below the refracting interface affects the refraction effect, whilst critically refracted waves only appear, if the below layer has a higher velocity than all layers above (in this case, this base is formed by sand deposits). Seismic refraction

interpretation requires the identification of refracted arrivals in the seismograms, first arrivals mostly, and picking of their traveltimes. As a first step a smooth seismic velocity model of the subsurface has to be derived. This model serves as the reference starting model for a 2D tomographic inversion computation. The result of the refraction tomography is a 2D distribution of the wave velocities representing a depth section underneath the profile line.

For traveltimes picking we used the interactive analysis tool PASTEUP for wide-angle seismic data [66]. The tomographic inversion software tomo2D [67] was used to derive the S-wave velocity model.

Tomo2D uses a combination of graphs method and binding method to calculate the raypaths and synthetic travel times. The global difference between observed and synthetic travel times is inverted for velocity perturbation in the underground by solving the linear equation system with a least squares solver. Smoothness constraints and a regularisation factor are used [67] to stabilize the inversion. Due to the non-linear nature of the tomographic problem the difference between observed and synthetic travel times are minimized by iteratively updating the underground velocity model.

The following processing steps were applied:

1. Determining a reference velocity model.

A most accurate reference model is crucial for reducing possible ambiguities of tomographic solutions and thus increasing the reliability of the tomographic result. For this purpose we followed a 3-step procedure. We first derived a velocity model of the uppermost 2 m of the underground by restricting the traveltimes inversion to source-geophone distances ("offsets") of up to 6 m. Then we extended the offsets to 15 m resulting in a velocity model of the uppermost 4 m. Finally, we took all traveltimes picks to receive the velocity model of the uppermost 6 m corresponding to maximum penetration depth of the refracted waves. We applied a Gaussian smoothing filter to the velocity model to avoid artefacts in ray paths. The halfwidth of the filter was 2 m horizontally and 1m vertically.

2. Determination of smoothing weight.

We performed a single iteration with different smoothing weights between 0.001 and 100. The roughness of the model (variance with respect to the reference model) was then plotted versus the data residuals (Chi-square function) (Figure S2a). From the resulting L-curve the regularisation factor located at the point of largest curvature (closest to the origin) was chosen as the optimum for the inversion. The obtained value is 0.4.

3. Determining the final velocity model and its dependence on the starting model

For determining the final velocity model and assessing its possible dependence on the starting model of the tomographic inversion we created 10 different starting models by altering the reference model by up to 10% (Figure S2b). For each starting model the inversion was performed separately using the same set of parameters (Table S3). Each inversion run showed convergence within 5 iterations. The minimum RMS value of traveltimes residuals was 2.9 ms. The 10 velocity models of the last iteration had a RMS

value less than 3.2. We derived the final velocity model and its uncertainty from these 10 models by determining their arithmetic mean and its standard deviation. We consider those parts of the model as being well resolved that show a standard deviation of less than 10m/s corresponding to about 5%.

4.3.3 Seismic reflection imaging

Reflection seismics deals with the use of seismic waves (SH-waves in our case), which reflect at geological interfaces separating layers with different seismic impedance (the product of density and seismic wave velocity). Seismic waves can be generated with hammer blows on a metal plate at the surface which are recorded along the survey line with a set of equally spaced receivers (geophones). The hammer blows are repeated at a set of equally spaced source points and the results consist of seismograms showing the amplitudes of the emitted and reflected arrivals as a function of geophone location and travelttime. Distance-traveltime functions of the significant reflections can be derived for determining the location and depth of the geological interfaces. To convert seismograms into seismic reflection images showing depth sections of the stratigraphy, we use digital amplitude processing (called common-midpoint (CMP) processing) and seismic migration. The theory and analysis of seismic reflection data is well documented [e.g.68].

The vertical resolution of seismic measurements can be defined as the ability to distinguish between two reflection signals from one another. It represents the distance between two interfaces as separate reflectors and it is generally determined as a quarter of the dominant wavelength (Rayleigh's criterion). The acquired data covers a frequency band from 6 Hz to 100 Hz. The seismic data was processed with the VISTA software (<https://www.software.slb.com>). The observed surface wave (Love wave) is strong. After removing noisy traces we limited our data to offset smaller than 1 m to ensure that we observe only under critical reflections and therefore no Love waves. We applied filters to enhance the reflections. To compensate the amplitude decay due to the geometrical spreading an analytic amplitude gain (linear in time) was applied. The velocity model derived in the tomography was used to determine the rms velocity model needed for the Normal-Move-Out correction. It was also used for the finite difference migration and for the conversion of the seismic image from time to depth.

Table S4 reports the acquisition parameters (left) and the processing flow with associated parameters (right) used for the seismic measurements and processing at Duvensee. A comparison between the raw and processed data is shown in Figure S1.

4.4. Acquisition of stratigraphic data by drilling and laboratory analyses

Corings were conducted using an Usinger piston corer [69], proceeding with 1 m increments in depth along a 50 m long transect (blue and green dots in Figure 1), which has been taken as a reference profile. The stratigraphy of the sediment was described in the lab and the reconstruction of the transect and a brief description of the main stratigraphic units is given in [21]. Moreover, in the laboratory the sediments were analysed as follows:

1. *Water content* and *bulk density* of the sediment samples were determined gravimetrically on small volumetric samples (ca. 2 cm³) after drying the sediment at 105 °C. The sediment of the remainder of the cores was air dried (35°C), carefully disintegrated with mortar and pestle and sieved through a 2 mm mesh sieve before additional analysis.
2. *Grain size* distribution analysis (< 2 mm) was carried out for the sediment of the cores except of the peat layers. After removal of soil organic matter (H₂O₂, 70 °C) and carbonates (acetic acid buffer, 70°C, pH 4.8) the sand fractions of the sediment were separated by sieving through meshes of 630, 200, and 63 μm. The silt fractions (2-6.3, 6.3-20, 20-63 μm) and the clay (< 2μm) were separated by sedimentation in Atterberg cylinders.
3. *The magnetic susceptibility* was measured on 10 ml samples (< 2 mm fraction) using a Bartington MS2B susceptibility meter (resolution 2*10⁻⁶ SI, measuring range 1-9999*10⁻⁵ SI, systematic error 10 %). Measurements were carried out at low (0.465 kHz) frequency. A 1 % Fe₃O₄ (magnetite) was measured regularly to check for drift and calibrate the results. Mass-specific susceptibilities were calculated [70].
4. *Loss on Ignition (LOI)* values were measured as estimates of the organic matter and carbonate contents of the sediments [71]. After drying the samples at 105°C overnight, the weight loss of the samples was determined after heating times of 2 h at 550 °C and 940 °C each.

An important remark is needed at this point: coring operations proceeded at 1 m increments in depth. However, the uppermost segments of the cores are sometimes shorter than 1 m. This discrepancy results from sediment compression produced by the extrusion of the sediment out of the Usinger corer barrel. Notably, these compression issues appear to affect only organic layers (peat in particular) in the first meter below the surface. Sedimentary units with a distinct minerogenic or calcareous component are only marginally affected. Understandably, sediment compression affects the measurements of stratigraphic transitions and the estimation of the compression is important also for ground truthing.

5. Results

In the following section we first show the results by methods starting with the laboratory analysis of cores I.2 and I.4 and continuing with GPR, ERT and shear wave seismics. At the end of the section we compare and evaluate the results of the different approaches showing their connection for the ancient basin evolution.

5.1. Electric resistivity and sediment properties

The results of the laboratory analysis of core I.2bis and I.4 are shown exemplarily in Figure 3a and Figure 3b respectively. An overview of all cores extracted along the 50 m transect (color coded dots in Figure 1 and their lithology can be found in [21]). The sediment properties that are shown are grain size, Loss on Ignition (LOI), water content, resistivity and bulk density.

Underneath the organic layers core I.2bis shows an increase of grain size between 1 m and 1.7 m depth, indicating a change from silty sediments to sands at the bottom of the core. The organic matter and water content are high (~80%) from the top of the core up to 1.2 m depth. Underneath the organic portion decreases and a corresponding increase of the bulk density occurs (~1.5 g/cm³). This boundary indicates the transition between fine sediments and sand. The electric resistivity shows higher values from the top of the core down to 0.5 m depth (~50 Ωm) where a decrease of these values down to ~1 m (~15 Ωm) occurs, too. Below 1 m, the resistivity increases again presenting local variations (~35 Ωm). Based on electric resistivity, the following transitions between sediment types can be identified: the peat on top can be separated from the fine organic mud and silty to clayey sediments underneath. The second increase in the resistivity corresponds to the presence of sand at the bottom of the core. Focusing on the peat layer an increase and a decrease (between 0.3 m and 0.6 m) of the resistivity is visible, which can be correlated with a different degree of humification [72].

Core I.4 (Figure 3b) provides information down to a depth of 4 m. The grain size distribution shows a high amount of clay in the fine organic gyttja layer between 1.5 m and 1.8 m. Below 1.8 m the grain size becomes dominated by silt, and below 3.7 m by higher amounts of sand. The organic matter (~90%) and water content (~80%) decrease from the top of the section down to ~2 m depth with little variations due to the presence of plant remains and wood. The carbonate content increases between 1.8 m and 2.5 m (~30%), indicating the deposition of a calcareous gyttja. Below 2.5 m a decrease of both components occurs (~10% for organic matter and ~30% for water content) and an increase of the bulk density (~1-2 g/cm³) is visible which is associated with the presence of a silty minerogenic mud.

The resistivity values resulting from the Direct Push measurements show variations that are correlated with different sediment transitions. A first decrease happens between ~0.4 m and 1 m depth (from ~40 Ωm down to ~20 Ωm) indicating a change in the peat degradation. Between 1.0 m and 1.3 m the values are constant indicating coarse detrytus gyttja (~20 Ωm). Between 1.3 and ~2 m the values are variable indicating internal changes in gyttja but making it difficult to pinpoint exact transition depths. Below 2.0 m the resistivity is constant (~25 Ωm) due to the silty minerogenic deposit and it shows again an increase at ~3.4 m (>40 Ωm) depth correlated to presence of sandy sediments.

In summary, we can recognize that the peat deposit thickens to the north, from 0.5 m at the south end to a maximum depth of ~1.20 m. The water content is nearly constant, between 80% and 90% and heterogeneities are marked by small decreases. The organic matter content is ~90% with some changes probably caused by the presence of wood remains. An increase of the bulk density associated with a decrease of the organic matter is also present. The resistivity increases from the top to ~0.4 m depth presenting values between 50-60 Ωm which probably correspond with the poorly decomposed peat. Below this horizon the resistivity decreases down to 20 Ωm defining the high degraded portion of the peat.

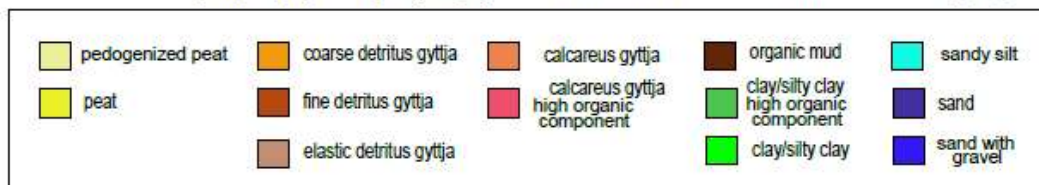
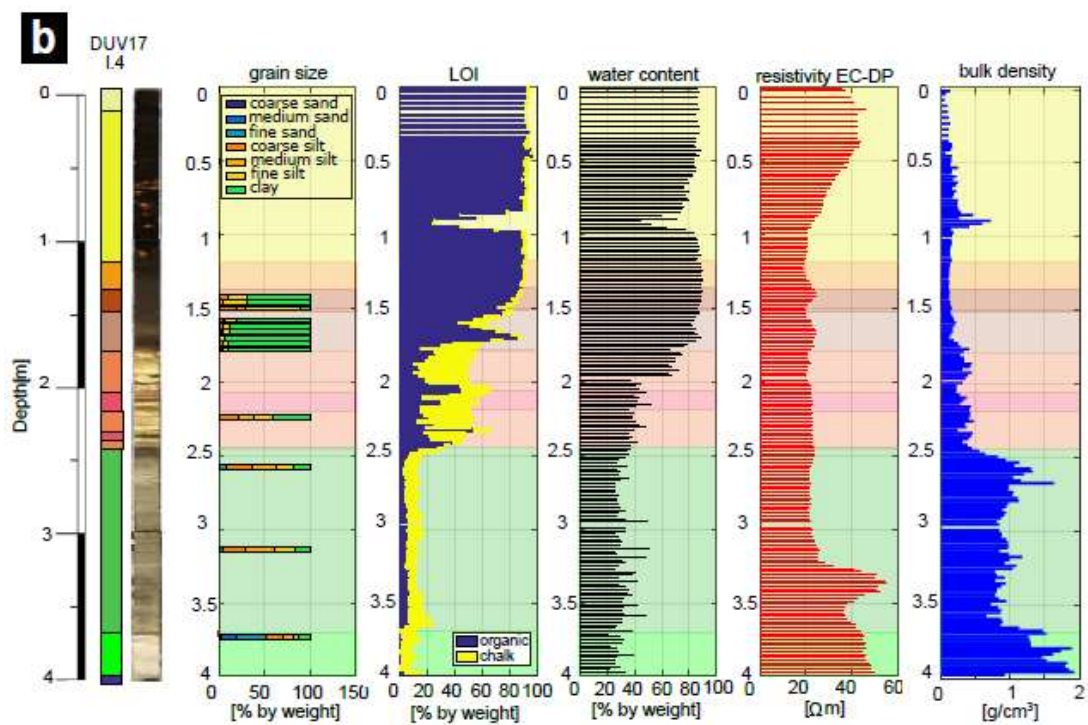
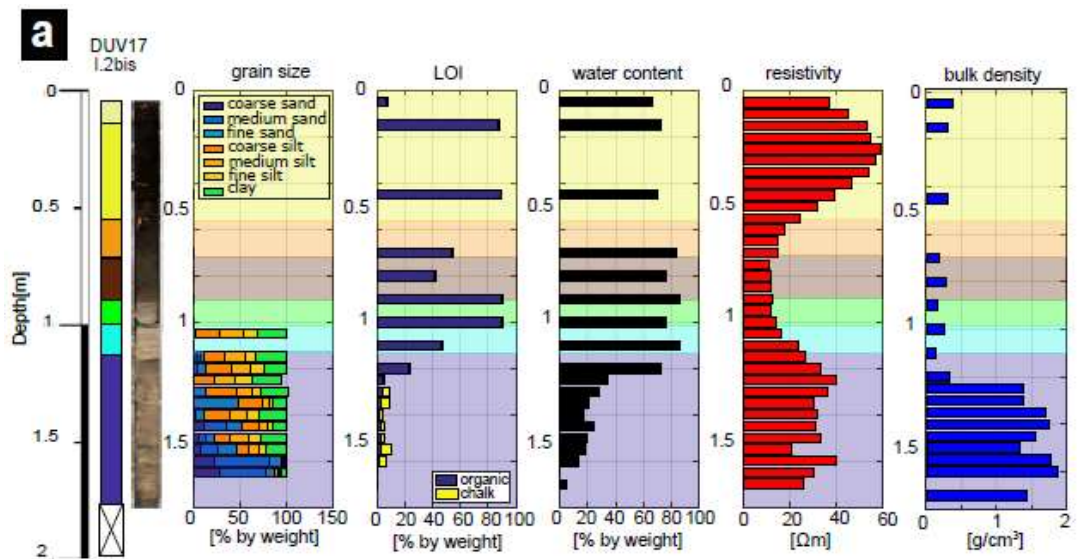


Figure 3. Laboratory analysis belonging to core I.2bis (a) and I.4 (b). The different properties are shown in comparison with the stratigraphy. The red arrows indicate the variations of the properties along the core depth.

5.2. Ground penetrating radar

5.2.1 Stratigraphy from GPR reflection profiling

In a previous study we showed that the major stratigraphic units can be traced over the whole 63 ha area of the Duvensee bog by combining drill core analysis and GPR profiling [21]. Three major stratigraphic interfaces showed up as continuous reflections (Figure 4a), which turned out to be caused by changes in grain size of the main sediment (see also section 2). In between these major interfaces, sequences of internal reflections are visible, which are partly higher, partly lower in amplitude than the reflections from the main interfaces. From the surface down to ~0.7 m depth we notice clear sub-horizontal reflections that are locally interrupted. Below 0.7 m, discontinuous, patchy sets of dipping internal reflection elements occur. An interpretation of these features is shown in form of a line drawing in Figure 4b where the shallow continuous and deeper patchy internal reflections are indicated with black and dark red colors, respectively.

The sets of strong sub-h reflections (black lines in Figure 4b) seem to be confined to the uppermost layer. The inspection of drill cores suggests that these reflections are caused by the transition between the uppermost weakly decomposed peat showing the highest porosity and the underlying well-decomposed peat showing lower porosity. The weak internal reflections of the gyttja layer (between interfaces 1 and 2, dark red lines in Figure 4b) do neither follow a clear trend in dipping, nor do they correlate systematically with visible sedimentary changes in the drill cores. Therefore, they have to be considered as scattering caused by small-scale variations of sediment composition originating from the heterogeneity of the deposition and degradation processes and the deposited organic material.

The internal reflections of the clayish-silty layer 3 basically follow Interfaces 2 and 3. The lateral continuity of these reflections indicate that the deposition of layer 3 proceeded more continuously than the deposition of layer 2.

As reported in section 5.1, the peat water content is usually >80%, which strongly influences the propagation velocity of radar waves and limits their sounding depth to a few meters, in our case due to attenuation [e.g. 73]. Using CMP measurements together with the stratigraphic depths from the corings [21] we defined an average interval velocity and its standard deviation for each main layer: $v_1=0.045 \pm 0.005$ m/ns for coarse organic sediments (peat and coarse detritus gyttja), $v_2=0.039 \pm 0.003$ m/ns for the fine organic sediments (fine detritus gyttja and calcareous detritus gyttja), $v_3=0.037 \pm 0.003$ m/ns for the clay layer. We noticed that close to the surface the velocity shows values of ~0.049 m/ns, while in the deeper humified peat the velocity is ~0.041 m/ns due to high variability of the water content in the peat sediments. The change in velocities between the gyttja sediments and clay deposits is very small, therefore the interface reflection of these sediments (Interface 2) is weaker than the peak reflection (Interface 1). The gyttja layer (between Interface1 and Interface2) shows internal layering of fine

detritus gyttja and calcareous gyttja. However, it was not possible to differentiate between these units in terms of radar velocity given the general uncertainty of the CMP measurements. Still, there must be internal velocity variation as indicated by the sporadic internal reflections. To evaluate it more refined methods such as full waveform inversion or downhole measurements have to be applied. In this regard we tested the guided wave technique to improve the velocity determination (see next section). According to the quarter-wavelength criterion the resolution of the GPR reflection images is about 5 to 8 cm layer thickness, which means that the different gyttja layers can be distinguished if they exhibit sufficient permittivity contrast [21].

As explained in section 3 the compressibility of peat depends mainly on the degree of decomposition. Figure 4c and 4d show the results of the GPR measurements and an estimation of the compaction for the first meter of the profile after extraction. Referring to [74] we can basically recognize three different degrees of decomposition starting from the top:

- 1) pedogenized peat (vermulmter Torf) visible in the first 10 cm (P1 in Figure 4c/d) ;
- 2) grounded peat (vererdeter Torf) carrying a crumb structure and locally roots (P2 in Figure 4c/d);
- 3) strongly decomposed peat (stark zersetzter Torf) with a fine grain structure and wood remains in it (P3 in Figure 4c/d).

Due to the weakness of the matrix peat layers get seriously compacted if they are sampled by drilling. As a side-product of the GPR investigation this artificial compaction can be assessed based on the visible reflections and the radar wave velocities of the layers.

Figure 4e shows the results of the compaction estimation regarding the first meter of the corings. The shallower peat (P1 and P2) show a compaction range from ~40.5 to ~70% referring to (P1), from ~35 to ~50% considering (P2), while the highly decomposed peat (P3) shows an average compaction of ~30%. According to the idea (section 3) the compaction rate decreases from the top to the bottom of the peat layer considering different degrees of decomposition. The high porosity of the top layer creates indeed a higher compaction.

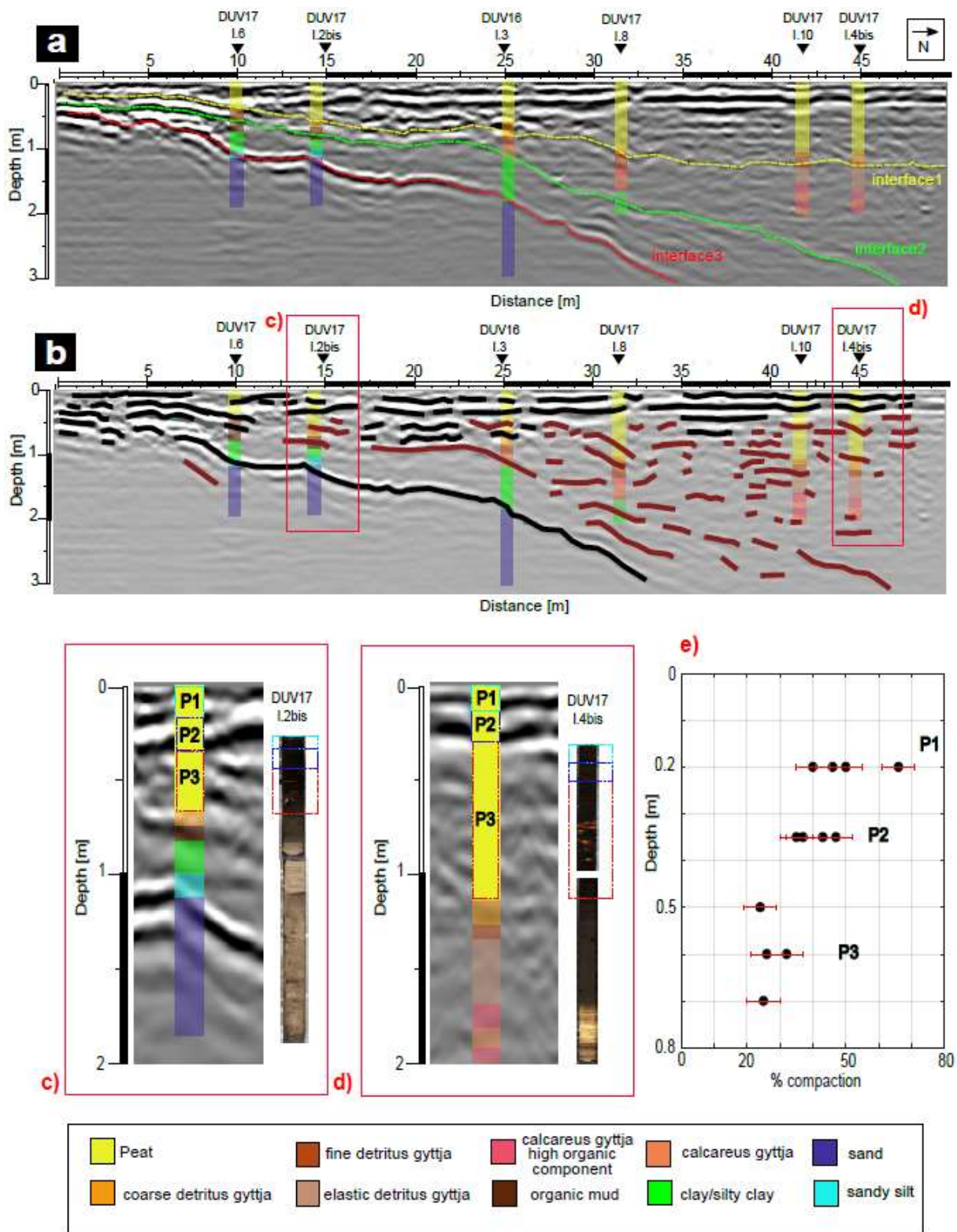


Figure 4. GPR results for the reference profile. (a) GPR profile including the recognized interfaces (after [21]); (b) GPR profile with interpretation of the visible reflections, the black lines indicate stronger

amplitude reflections and the dark red lines are the lower amplitude reflections (c) focus on core I.2bis together with GPR (d) focus on core I.10 together with GPR. In all cores the compression of the peat layer has been reconstructed using the depth of the GPR reflections. (e) Estimation of the peat compaction caused by the drilling process. The original layer thicknesses were determined from the travel times of GPR reflections, which were then compared with the compacted thicknesses measured after the extrusion on the drill core. The error interval due to the uncertainty from the GPR velocity determination

5.2.2. Guided radar waves

In this section we report the results of the guided wave measurements at the location of core I.8. The red line in the wiggle plot (Figure 5) indicates the guided wave arrival which delivered the velocities listed in the corresponding table. The radar velocity decreases with depth almost continuously with some local change. Focusing on the peat layer we can notice a higher variation compared with gyttja sediments underneath confirming the high variability of peat properties. The gyttjas show instead a very small variation of the velocity. The resulting average velocity associated with the peat layer is $\sim 0.042 \pm 0.003$ m/ns, which can be well correlated with v_1 as determined from CMP velocity analysis (section 5.2). The same applies for the gyttja which shows an average velocity of $\sim 0.037 \pm 0.002$ m/ns consistent with v_2 (section 5.2). This high resolution test focused on the determination of the GPR velocity delivered results that are consistent with the CMP measurements carried out in the same area [21] allowing the identification of small-scale permittivity variations which can be correlated with local small and weaker reflections as reported in section 5.2. Below 70 ns no arrivals are visible and therefore it was not possible to determine the velocity associated with calcareous gyttja and clay. The test at location I.1 was able to deliver the GPR velocity of the sand because the deposit is located already at 0.5 m depth ($v_4 = 0.068 \pm 0.004$ m/ns) which is consistent with the values of wet sand in the literature (Table S1). The high water content and the presence of the water table can attenuate the radar waves and make the determination of further reflections very difficult.

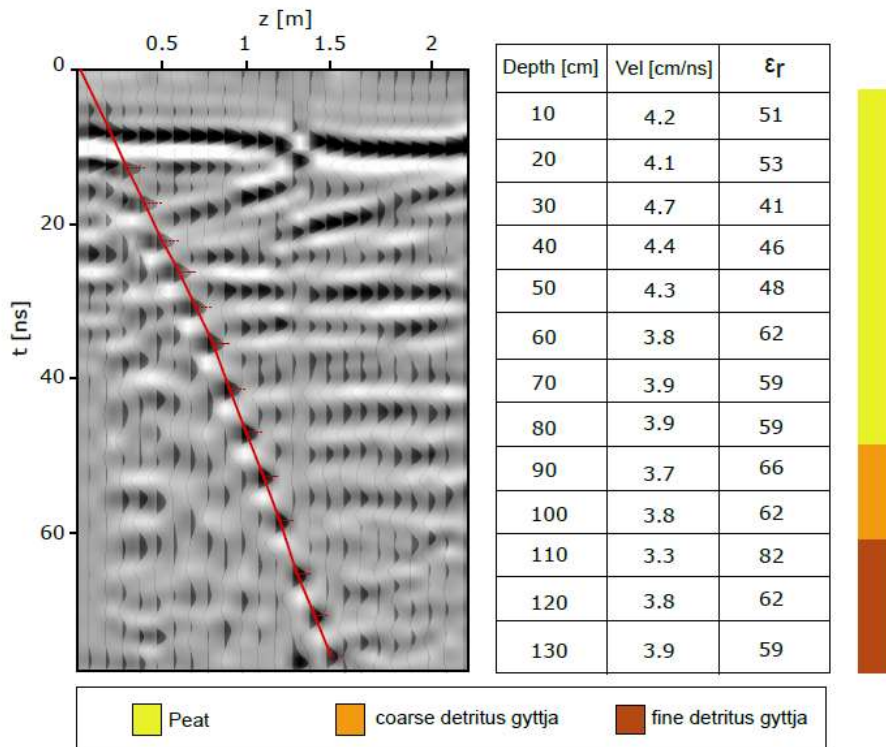


Figure 5. Field data of guided waves with picked traveltimes (red line). Z is the depth of the lower waveguide end in the hole. The table reports the GPR velocities and dielectric permittivity calculation from the guided wave measurements at core I.8. The stratigraphy is indicated with different colors for comparison.

5.3. Electrical Resistivity Tomography

The tomographic inversion of the geoelectric data delivered the electric resistivity model shown in Figure 6. The tomographic computation converged after 2 iterations showing rms residuals of 1 to 2.5%. In correspondence to the drilling results three major units can be identified in the ERT model. A uniformly resistive upper layer is visible with a maximum resistivity range of ~60 to 90 Ω m, underlain by a conductive unit of varying thickness (resistivity range ~ 20-35 Ω m). Below this layer a higher resistive unit of varying thickness is found (resistivity range ~35-50 Ω m).

The upper resistive layer correlates well with the peat deposits confirmed from corings. The relatively high resistivity of the peat is attributed to the low ionic concentration of the peat pore water. The underlying conductive layer incorporates both, the fine lake sediments (fine detritus gyttja and calcareous gyttja) and the Late Glacial minerogenic silty deposits. The high conductivity of the lake sediment is caused by the higher ionic concentration of the pore water resulting from ionic input from

the catchment mineral soils. The high conductivity of the glacio-marine deposit is primarily attributed to the high conductivity of clay minerals [e.g. 24]. The lowermost layer is defined by an increase in resistivity due to the presence of basal sandy sediments.

The GPR interfaces are superimposed for comparison (dashed yellow, green and red lines in Figure 6b). Interface3 matches very well with the top of the high resistivity area correlated with the basal sand deposit. Interface2, the top of the clayish-silt layer, is located inside the high conductive unit indicating that the gyttjas cannot be distinguished from the clayish-silt unit by geoelectric sounding from the earth surface. Interface1 correlates well with the high resistivity upper layer which distinguishes between coarse organic and fine lake sediments.

In summary, it turned out that geoelectric tomography is able to distinguish between fine lake sediments and basal sand, and between the peat deposit on top and the lake sediments underneath. To better understand up to which degree the different gyttjas can be resolved we performed the numerical modelling study reported in the supplementary material.

Figure S3a shows a simplified electric resistivity model based on the sediment layers and their depths as derived from the drill cores. To these layers typical electric resistivity values resulting from the Direct-Push measurements were attributed. For this model we calculated synthetic geoelectric data, which was then inverted again using the same parameters as for the tomographic inversion of field data. The inversion result is presented in Figure S3b overlain by the GPR-derived interfaces for comparison. The comparison shows that the two uppermost layers (depth <2 m) can be distinguished tomographically, and the tomographic image (Figure S3b) of the synthetic model (Figure S3a) matches with the tomographic image derived from the field data (Figure 6a). Moreover a model without the internal gyttja layer was inverted and the results are reported in Figure S3d. Both models agree confirming that the different gyttjas can not be distinguished from the lake sediments. The upper high resistivity layer can be well associated with the peat deposit. Within the uppermost peat layer the real data tomographic image (Figure 6a) shows some patchy localized high resistivity anomalies, which do not appear in the synthetic tomographic image. Therefore, we conclude that these patches are not an artefact of the tomographic computation process but an indication of lateral inhomogeneity of the upper layer. The gradual transition between the coarse organic sediments and the lake sediments is also visible in the modelling results. Both inversion results agree in showing a gradual transition between coarse and fine sediments probably caused by a coarse detritus gyttja layer of ~30 to 40 cm thickness in which the lowering of the resistivity is caused by the presence of higher ionic concentration. We can confirm that Interface2 is (also) not visible in the model and the sand deposit is visible but it's less precisely defined. The higher resistivity values of the last layer are more concentrated between 15 and 30 m, but they are at a greater depth and in the first meters not well defined. The model shows a linear dipping interface while the GPR interface looks more rounded, probably this approximation can create the misbalance. From the resistivity diagram we also notice any difference between coarse detritus gyttja and peat above and the lake sediments below it. This statement is also strengthened by comparing the DP-EC log with the resistivity curve extracted from the ERT results (Figure S4). The computed curve does not show a variation correlated to the coarse gyttja layer. In addition with the low

thickness of this layer and the larger size of grid cells in the ERT model at the same depth, this layer is not visible.

Therefore, we conclude that it is not possible to resolve the difference between coarse detritus gyttja and the peat and fine grained lake sediments (therefore the different gyttjas are not resolvable).

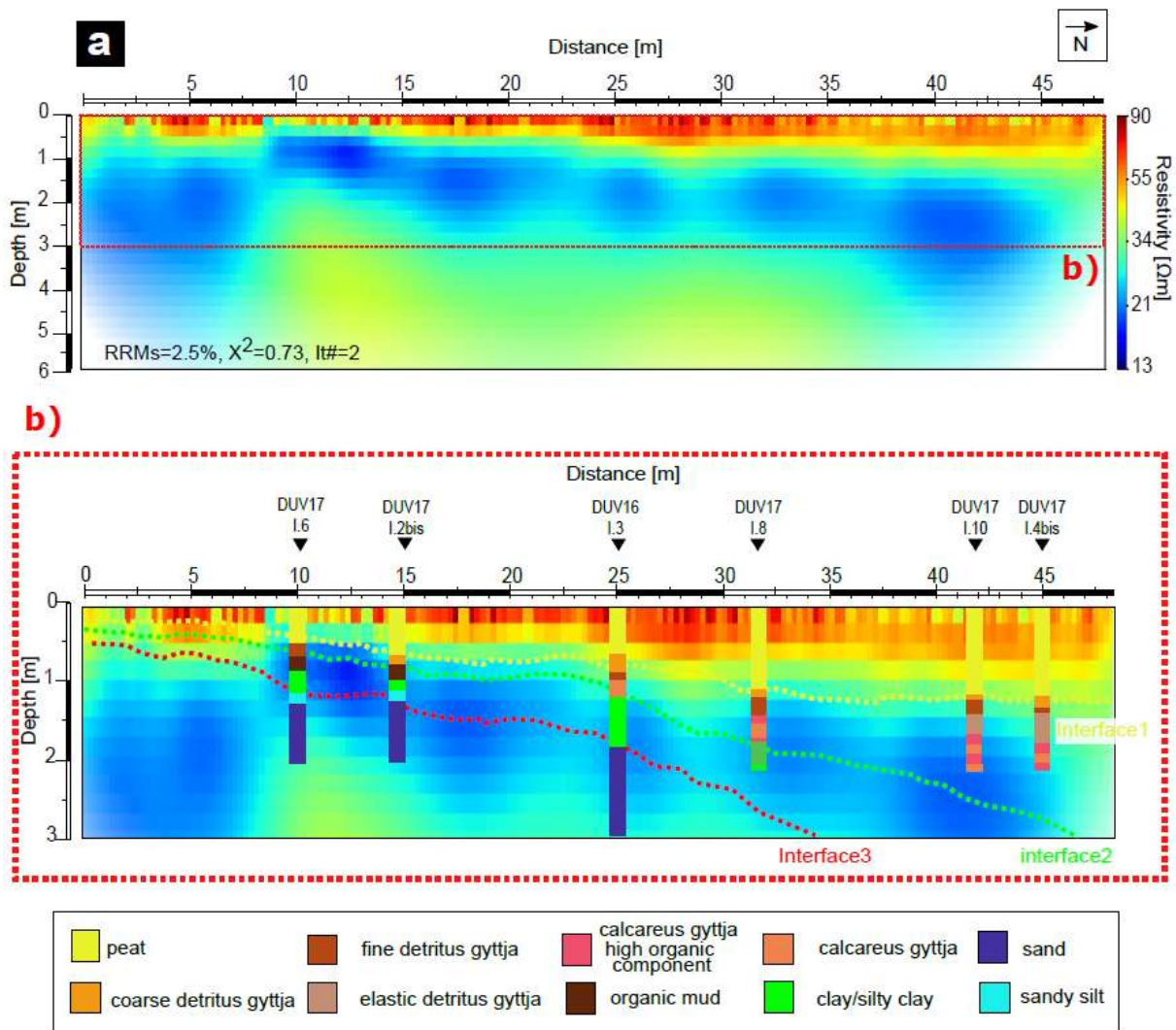


Figure 6. Results of the geoelectric measurements; (a) resistivity tomography of the reference profile (b) focus on the uppermost 3 m of the resistivity tomography together with the stratigraphy and the GPR Interfaces (Interface1, Interface2, Interface3)

5.4. Shear wave seismic

The seismic results are displayed in Figure 7. Both reflection and refraction profiling provide structural information down to about 10 m depth but for our purpose only the first 5 m are considered. The bulk seismic structure can be recognized easily from the depth section of shear-wave velocities (Figure 7a) generated by refraction tomography and from the reflection section (Figure 7b), which allows a more detailed structural interpretation of the velocity field. In general, the shear-wave velocities increase towards depth with values ranging from 40 to 250 m/s. At the first glance we can recognize an uppermost layer with velocity < 80 m/s followed by two layers with higher velocity values dipping from south to north. The first is characterized by a velocity of ~100 m/s while the lowermost layer shows velocities ~200 m/s.

The shallower low velocity values are in strong contrast to the lowermost and confirm the presence of a sediment volume at the surface, which is mechanically significantly weaker than its underlying. The observed velocity values < 80 m/s indicate soft sediment such as fine grained lake fills or swampy organic material [14]. It can be interpreted as the sediment sequence of the former lake consisting of peat and fine grained organic sediments like gyttja and the Late glacial clay.

Below this low-velocity layer the S-wave velocity increases abruptly to values of 100 to 250 m/s in the vertical direction. The values of 150 to 300 m/s are typical for unconsolidated sediments of varying grain size, basically silt, sand and gravel (c.f. [15,75]).

The spatial resolution of the reflection images can be evaluated using the depth-converted reflection section, from which we can determine the effective wavelengths (black-white wiggle, Figure 7b). In the upper 2 m of the section we notice that the wavelength is about 0.4 m, while at deeper levels it becomes wider, ~1.4 m at approximately 4 m depth. This variation is caused by the dominant frequencies changing with depth due to absorption. The higher frequencies are still in effect at shallowest depths and get increasingly absorbed with depth. This consideration shows that the resolution is about 0.20 m in the uppermost 2 m and 0.7 m in a depth > 2m order of magnitude. Considering the cores information we notice that different sediment thickness is less than 0.20 m, which is comparable to the calculated resolution. Therefore, the interpretation of the basin stratigraphy is possible regarding major deposits.

A further comparison between seismic results, GPR and corings is shown in Figure 7b, in which the major GPR Interfaces are indicated with dashed coloured lines (yellow, green and red lines). The most striking structure is a dipping reflection starting at about 1 m depth in the South and deepening down to 4 m in the North (black line, C). Obviously, it agrees with Interface3 between lake sediment and sand deposit. Interface3 matches indeed with the abrupt increase of S-wave velocity indicating the stratigraphic change at that depth.

Below this clear reflector, additional seismic events are visible presenting a similar behavior and still an increase in the shear-velocity. The comparison with the stratigraphy allows the identification of seismic events which can be correlated to Interface 2 (green dashed line from GPR). At a depth of about 1 m some reflectors are visible matching with the transition between gyttja sediment and the silty clay glacial deposit (black line, B).

Interface1, between peat deposits and gyttja, shows up in the seismic reflection section too. It coincides with the ~ 40 m/s contour line in the seismic velocity section. Within the peat layer, at a depth <0.7 m, the resolution of the seismic reflection image breaks down. This is because of interference of reflected and direct wave arrivals. However, the uppermost peat layer can still be distinguished from the underlying peat in terms of shear wave velocity as it is characterized by a velocity of ~ 40 m/s, which is the smallest value measured along the profile. Some reflectors are present too at a depth of $\sim 1/1.5$ m at the same location of interface1 confirming the possibility to detect this limit, too (black line, A). At the deeper peat levels the S-wave velocity increases to values >50 m/s due to consolidation.

Finally, we can conclude that the main interface in the reflection seismic is caused most probably by layering of sediments with changes in grain size and matrix rigidity with depth.

In Figure 7c and 7d we compare the resistivity depth curve extracted from the inversion and the shear-wave velocity depth curve from the tomography. The slope at the main interface depths can give an indication of the gradient for each property. Considering interface1 the resistivity slope is steeper than the seismic velocity for each core, which means that ERT can better resolve this layer. Interface2 is better resolved considering shear waves because the resistivity curve presents almost no slope at this depth. This is also confirmed from the ERT tomography in which Interface2 is not visible at all. The basal sand deposit is well defined by shear waves velocities but almost no slope is visible in the resistivity depth curve. In the ERT tomography it is very difficult to set a clear boundary which can define the transition to sand between 1 and 2 m (Figure 6b).

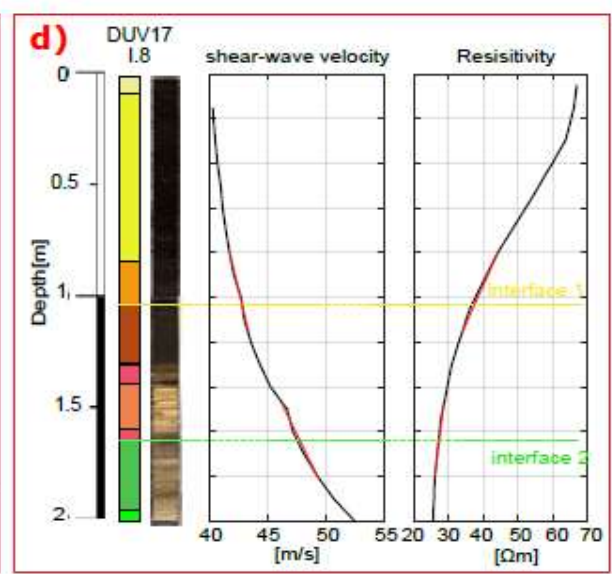
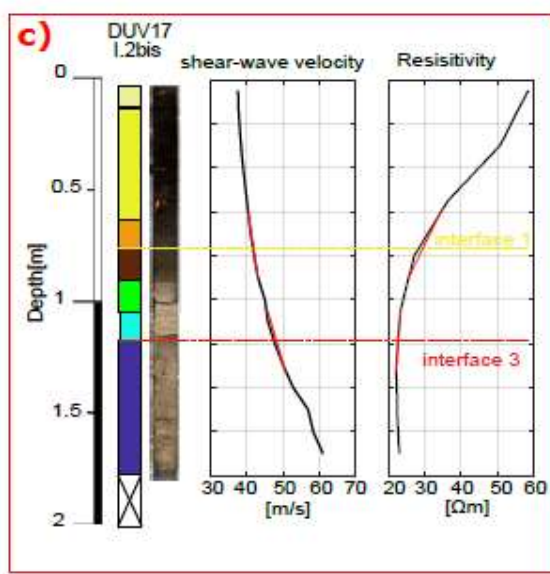
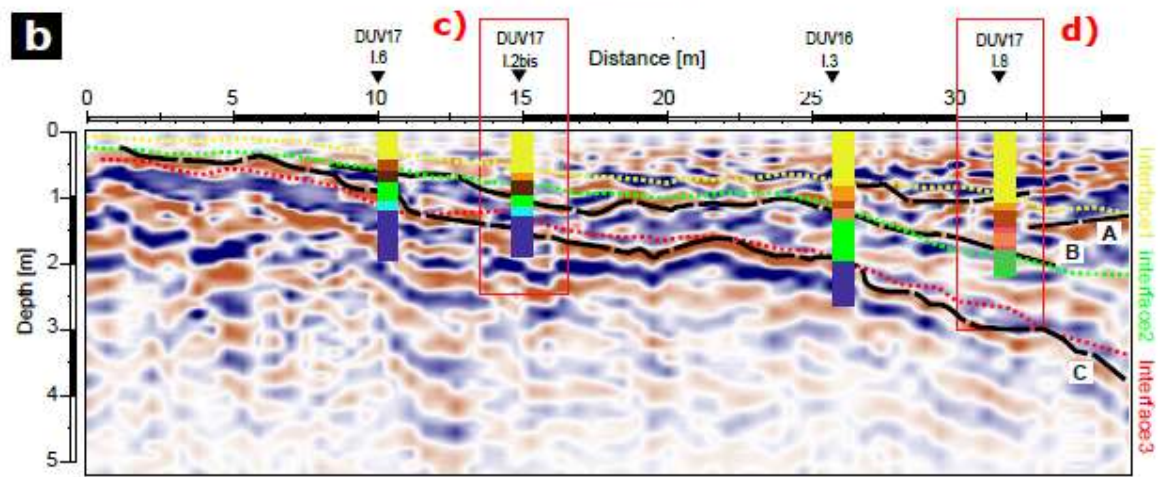
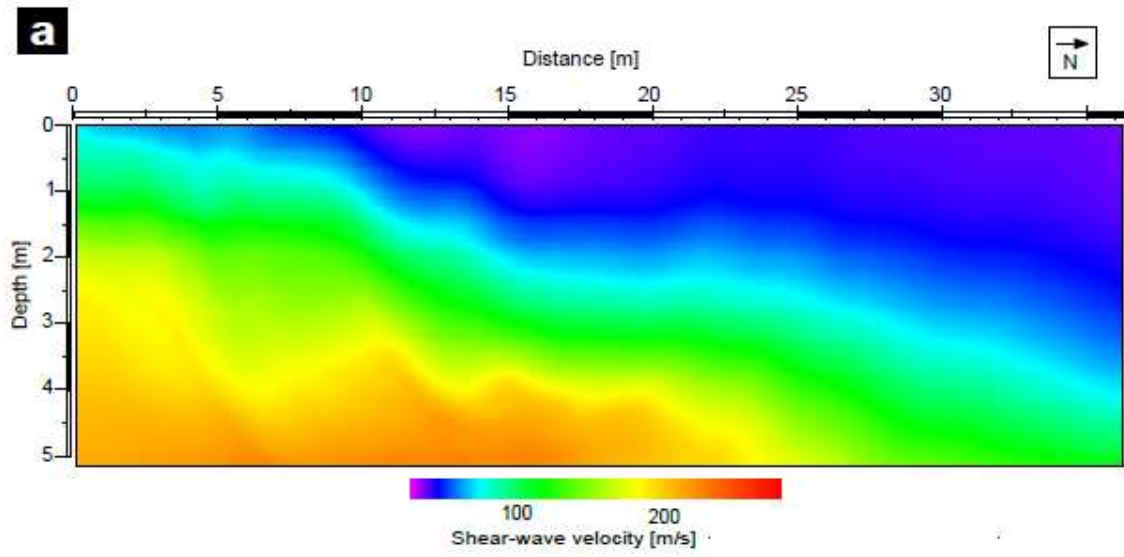


Figure 7. Shear-wave tomography and reflection seismic section of the measured profile. **(a)** color-coded shear-wave velocities tomography; **(b)** time migrated and depth converted reflection seismic together with stratigraphy, GPR Interfaces and its interpretation. The GPR interfaces are color coded (Interface 1, Interface2 and Interface3) The main reflector from the seismic reflection profile associated with GPR Interfaces are marked with black lines (A,B,C). For the legend see Figure 6. **(c)** Comparison between shear-waves velocity depth curve and resistivity depth curve at location of core I.2bis. The Interfaces from GPR are indicated with dashed lines (yellow and red). **(d)** Comparison between shear-waves velocity depth curve and resistivity depth curve at location of core I.8. The Interfaces from GPR are indicated with dashed lines (yellow and green).

5.5. Comparison of sedimentological and geophysical soil parameters

In this section we systematically compare and combine the physical sediment properties determined with the different geophysical methods and with the soil analysis in order to establish whether or not they can be used to classify bog sediments. The correlation between electrical resistivity and sediment properties is shown in Figure 8 with different symbols for each sediment. In the second part of this section we combine the physical properties resulting from the computation in Figure 9. Finally a 3D cluster analysis is presented. For a comparison we report in Table S1 the values of the sediment properties collected from the literature and in Table 1 the results from our study. Moreover [27] presented a multi-site laboratory study at various peatland sites in nord-east Germany, to highlight again the large variability of each property depending on the site conditions.

In the scatter plots of Figure 8 four different clusters are visible: peat (A), gyttja (B), clay (C) and sand (D).

Sand, clay and silty clay are easy to identify as isolated groups. Cluster D shows low water content and resistivity values between 30 and 45 Ωm , whereas cluster C presents low water content and low resistivity values (20-25 Ωm). The situation is different for peat and gyttjas. Peat sediments (Cluster A) have a high variation in resistivity values, but can be clearly separated from the gyttjas, with the exception of some outsiders, which have characteristics more like coarse detritus gyttja. The low degraded peat is also distinguishable from the high degraded peat because of its higher resistivity values. The different gyttjas are not always clearly distinguishable from each other considering the bulk density and water content, the coarse detritus gyttja, fine detritus gyttja and calcareous gyttja belong to a common cluster. The water content enables to separate the calcareous gyttja from the other gyttja types. A distinction between fine gyttjas and calcareous gyttja is possible in terms of organic matter .

To characterize the correlations between electric resistivity and the other properties of gyttja and peat in a more quantitative way we applied the Pearson correlation coefficient (r), which varies between 0 (no) and 1 (perfect correlation). Water content and organic matter have the strongest correlation with resistivity in particular for the coarse detritus gyttja ($r=0.88$ for water content and $r=0.87$ for organic matter). For peat we obtained $r=0.32$ for the water content and $r=0.58$ for the organic matter, they are weaker and probably explained by the high variability associated with this type of sediments. The high

variation of this property is site dependent and our results agree with [8]. The fine gyttjas show a value of $r=0.78$ for the water content and $r=0.67$ for the organic matter. Coarse detritus gyttja shows characteristics which are similar to high degraded peat which makes it somewhat difficult to distinguish them.

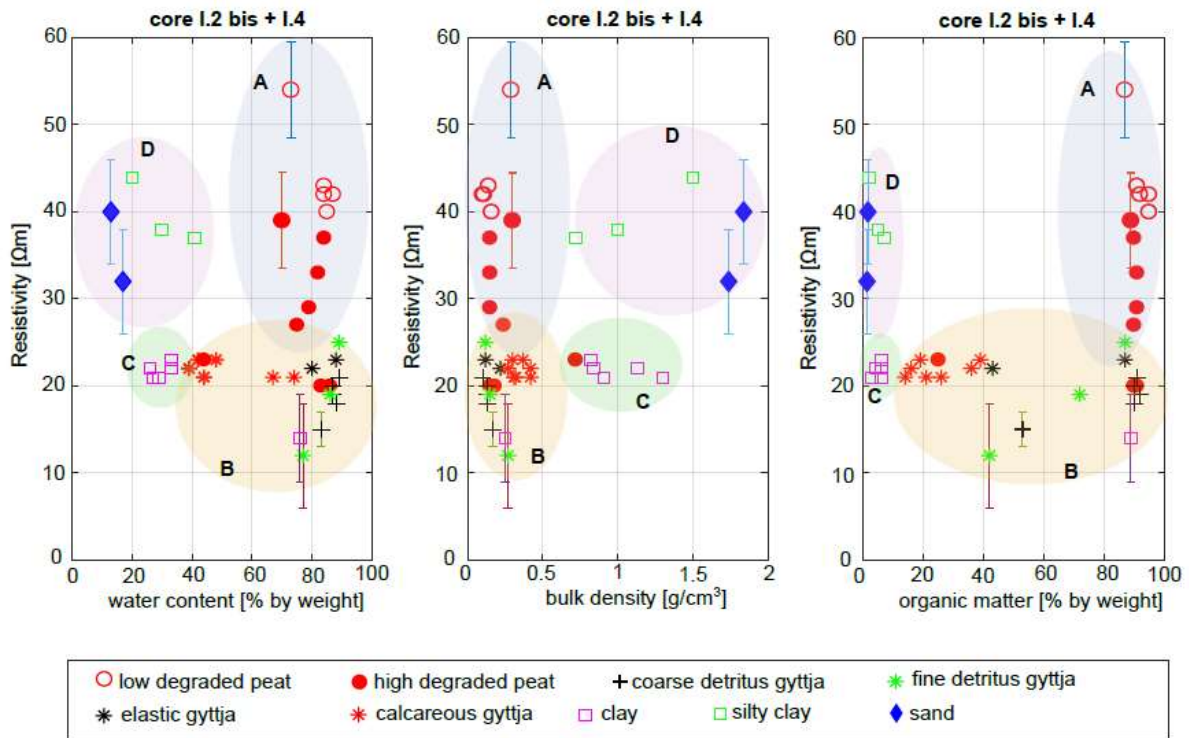


Figure 8. Relation between electrical resistivity to soil parameters for core I.2bis (upper 2m) and I.4 (upper 4 m) . The different symbols indicate the different sediments The errors associated with the laboratory resistivity measurements are indicated with bars.

Figure 9a shows scatter plots of the geophysical parameters obtained from the interpretation of the field measurements. Electrical resistivity and shear wave velocity from the tomographies (uppermost 3 m) are able to distinguish between different degrees of peat degradation (Cluster A). The gyttjas are concentrated in one cluster and show similar characteristics as clay. The plot of electric resistivity versus GPR (uppermost 2 m) velocities reveals different clusters, in particular the differently degraded peats (Cluster A). The low degradation peat is concentrated on the top of the plot (resistivity values $\sim 65 \Omega m$, GPR velocity 4-6 cm/ns) which makes its identification possible. The highly degraded peat shows a high variability of both resistivity ($\sim 40-60 \Omega m$) and GPR velocity (4-6.6 cm/ns). Despite its high variability, this sediment is well separated from the others. Some outliers are located close to the detritus gyttja which makes it difficult to well separate this sediment from the high degraded peat and fine detritus gyttja.

The sand deposit (Cluster D) and fine detritus gyttja (Cluster B) are more concentrated in separated clusters. In this regard the fine detritus gyttja could be separated from the coarse one. In the scatter plot of seismic and GPR velocity we notice that the different clusters can be identified, too, but they show some overlap. Only fine detritus gyttja seems to be concentrated within an isolated cluster (Cluster B).

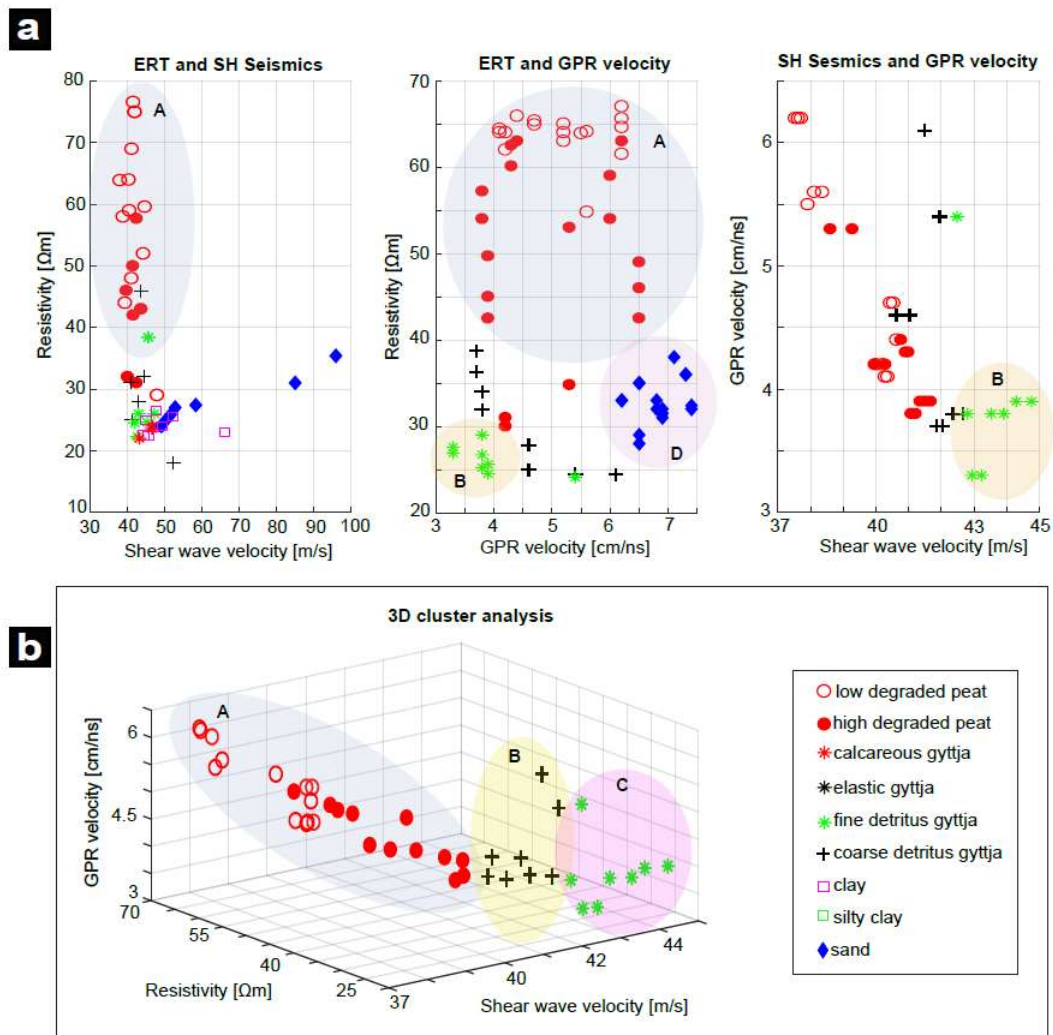


Figure 9. (a) Relation between geophysical properties resulting from the computation. From left to right: scatter plots of Resistivity vs Seismic velocity (uppermost 3 m), Resistivity vs GPR velocities derived from the guided wave measurements (uppermost 2 m), and GPR velocities vs Seismic velocity (uppermost 2 m). (b) 3D cluster analysis considering the three properties. The different sediments are displayed with different symbols and colors.

Combining the three geophysical parameters together a 3D cluster analysis was performed and the results are shown in Figure 9b. Cluster A indicates the peat deposit which can be distinguished in two

subclusters: low degraded peat and high degraded peat. Moreover, it's promising that the different gyttjas (coarse and fine) seem to belong to different groups (Cluster B and C). Unfortunately the other sediments are not possible to insert because it was not possible to measure the GPR velocity below 1.3 m depth.

Sediment	Water content (%)	Organic matter (%)	Resistivity [Ω m]	Conductivity [mS/m]	ϵ_r	SH velocity [m/s]
Low decomposed peat	66-84	89-95	37-70	27-14	41-53	~40
high decomposed peat	70-86	87-97	24-40	42-25	59-62	~40
Fine gyttja	86	72	19	52	59-82	~80
Coarse gyttja	87	92	20	50	62-66	~80
Calcareous gyttja	42	17	22	44	n.a.	~80

Table 1. Properties of the peats and gyttjas deposits delivered from this study

5.6. Peatland development

The basin stratigraphy and morphology inferred from the geophysical results can be explained in terms of the classical phases of peat bog formation confined in a basin. The initial basin was composed of glacial sands where, above it, Late Glacial clayey silt was deposited in a lake (Figure 10a). The applied geophysical methods are able to identify the glacial sands characterized by low conductivities compared with the surrounding clay sediments. During the Early Holocene warming, organic-rich lake sediments were deposited and peat formation began at the lake shore. By a rapid filling of the lake basin

that occurred already during the Early Holocene the peat covered a successively larger area of the former lake (Figure 10b/c). In the lake basin, the sequence is more complicated due to the fluctuating water levels during the Preboreal to Boreal but this sequence is (normally) the common deposition series [32]. Due to the multimethod approach we were able to identify almost all the stratigraphic units. The basal sand is very easy to identify and to map for the identification of former islands with Mesolithic occupation [21]. Figure 10a shows how this interface (Interface1) is visible in each applied method (red cross) allowing a reconstruction of the ancient basal deposits. The late glacial clayey silt and the peat unit on top were mapped as well, allowing a first reconstruction of the lake development. Figure 10a/b/c (green cross) highlights how Interface 2 was detected mainly by GPR and seismics because of the low contrast in electric resistivity between fine lake sediment and the Late Glacial clayey silt. Interface1 (yellow cross, Figure 10a/b/c) is visible in each method and it can be connected with the bottom of the peat layer often correlated with coarse detritus gyttja which presents similar properties. Between Interface1 and Interface2 different gyttja sediments (fine detritus gyttja and calcareous gyttja) are visible from the stratigraphy but not clear in the geophysical results. Some changes in the GPR amplitude are visible (cyan cross Figure 10) but without a regular behavior which allows a identification of a defined layer. The calcareous gyttja is visible only in the deep part of the ancient lake but geophysically it does not differentiate from the surrounding lake sediments. The identification of this layer would be very important also for timing aspects in a way to better understand the sequence of deposition. Soil analysis helps the distinction of this layer from the others but from the geophysical point of view it is still not defined. The transition between coarse detritus gyttja and peat is also not possible because this sediment presents some similarities with the high degraded peat. This is also visible comparing the resistivity curves from the inversion with the measured resistivities in the cores (dashed red lines in Figure 10). In this regard we can highlight the possibility to separate high degraded peat from low degraded peat (pink cross in Figure 10). This achievement would be very helpful for the archaeological research to understand how well preserved the layers are to focus further investigations (e.g. preservation conditions of organic remains). As reported in [8], gyttja layers at the base of peat deposits that can often be found in fens of north-east Germany reduce the contrast in electrical conductivity, thus the delineation of peat is not that clear anymore. The former islands started to be overgrown with peat already during the early Holocene and the Mesolithic camps are indeed not directly located on the mineral soils, but within the overlaying organic sediments. Having more detail about the first layer can be very important for further research because it hosts the archaeological evidence. Our proposed scheme of the stratigraphy is based on the detected units and not on the time of deposition, because this topic needs a specific discussion already done in [21].

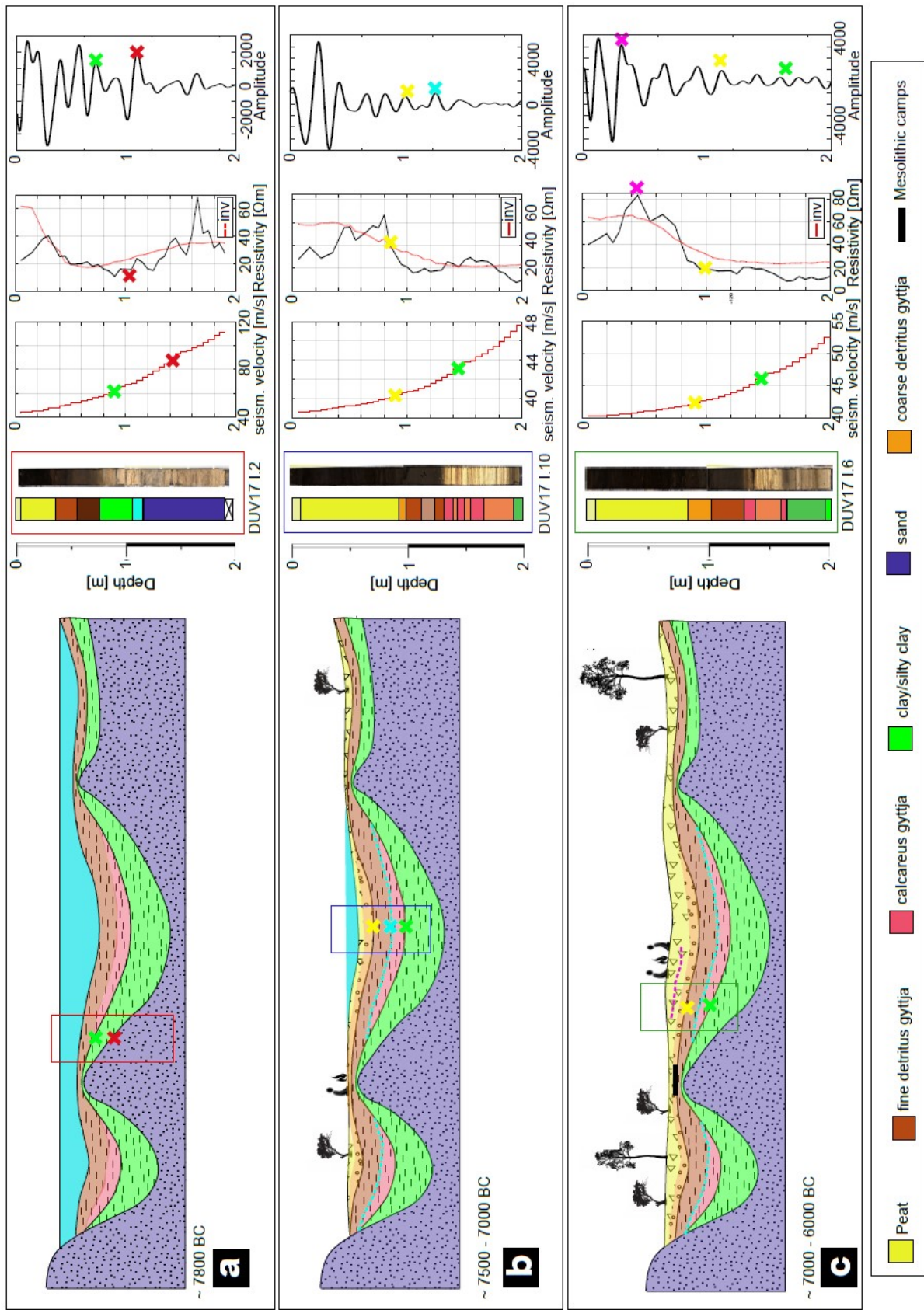


Figure 10. *Interpreted model for the Duvensee Moor development, illustrating the gradual sediment deposition within the basin during the Mesolithic period (after [32] and [76]). The 1D traces belonging to each applied geophysical method are reported on the side and the main changes are indicated with colored crosses.*

6. Discussion

6.1 Stratigraphy of bogs

6.1.1. GPR Survey

The results of the presented research together with the work of [21] provide vivid information regarding the development of the paleo-landscape at the ancient Lake Duvensee. Physical properties and geophysical investigations helped gaining more details about the characteristics of the sediments.

GPR is able to detect different layers at ancient Lake Duvensee, in particular Interface1 (transition between peat, coarse detritus gyttja and the underlying fine detritus gyttja, calcareous gyttja), Interface2 (fine detritus gyttja and underlying clayish-loamy sediments), and Interface3 (transition between clayish-loamy layer and the basal sand deposits).

Conductivity and permittivity are strongly influenced by water and clay content; these properties increase (indeed) with increasing clay and water content [77,78]. Since permittivity and velocity are indirectly proportional, an increase of those properties means a decrease in the velocity of the electromagnetic waves [77]. Clay minerals are also negatively charged and therefore able to exchange cations, if they are in solution [79]. The result is that an additional surface conductivity is present, increasing the bulk conductivity for clayey sediments.

For the reasons illustrated above Interface3 is well visible in the radargrams marking the transition between clay and sand [21]; this transition is also confirmed considering the organic matter content which decreases quickly from 30% to <5% at about 1.2 m depth in core I.2 and also considering the change in water content and bulk density. The bulk density is higher and the porosity is smaller reducing the water content, which causes a visible reflection. Organic matter influences the propagation of the radar waves too, because a high value of it enables higher water contents due to the larger surface of particles where water can adhere [80]. Therefore, the permittivity increases in sediments with high organic matter.

Interface2 is also recognizable because of a significant change in organic matter content at about ~2.5 m in core I.4 (from ~30% to ~10%) associated by a change in bulk density. The grain size distribution indicates a change in the clay content which is higher considering the gyttja than the clayey silt below this limit. The reflection is (indeed) weaker compared to Interface3, but it can be followed through the profiles.

Interface1 is instead very difficult to follow without stratigraphic information because the reflection amplitude is somewhere weak and GPR seems to encounter difficulties detecting the transition between different sediments. In the first meter of I.2bis and the first 2 m of I.4 the water and organic matter content do not present large variations. The resistivity can instead give more information about the first recognizable interface because a change of that property occurs at ~0.7m defining the transition between peat/ coarse detritus gyttja and organic mud in core I.2. and the same for I.4b. A small variation is also present concerning the grain size between coarse and fine sediments.

In the peat layer, discontinuous scattered reflections are present too, which are caused by the heterogeneous character of the peat and it poses a challenge in interpreting reflections within peatlands. Chaotic reflections can be (indeed) caused by small-scale variations in degree of decomposition, peat type or wood remains as well. The transition between fine gyttjas and calcareous gyttja has the characteristics to be detected as well, but in the radargram we can only see scattered weak reflections (Figure 4). The grain size slightly varies between the two deposits and the organic matter varies too, but more information about the GPR velocity variation would help in this direction.

Regarding GPR we confirmed that the velocity of electromagnetic waves and therefore dielectric permittivity through peat can be highly variable. Compared to former studies in wetlands our results fit well with that found by [49] and [22] for fen peats. [49] demonstrated that the degree of waterlogging does have an impact on the dielectric permittivity in fen peat, for this reason the range of variability on peat deposits is very high. Measuring in different seasons can also be a factor which can affect the results, dry conditions give a higher value of the electromagnetic wave velocity than wet conditions [49] as well as the temperature variations.

From the values found in the literature (Table S1) we know that clay- and silt-rich minerogenic sediments have lower dielectric permittivity than (any of the) peat deposits. Both peat and clay deposits are fully saturated and the peat has the capacity to hold more water than coarse grained minerogenic sediments due to the pore structure of the sediment [39]. [49] found an electromagnetic wave velocity of 0.05 m/ns (dielectric permittivity of 36) for the silty to clayey wetland sediments and they are at the upper end of the range given by [47]. Our results are even lower (velocity of 0.039-0.037 m/ns) compared to the literature, probably due to the high water content which slows down the radar waves.

The guided waves method gave results which are consistent with the CMP measurements reported in [21] and in the literature (Table S1) delivered higher resolution information about the variation of the radar velocity in the uppermost 1.3 m. this methods allowed indeed the determination of the GPR velocities every 10 cm. Unfortunately the high water content of the subsurface made it difficult to gain mode detail at a major depth. Therefore only peat, coarse detritus gyttja and fine detritus gyttja were reported.

In summary, it is evident that the ability of GPR to delineate structures within the organic deposits depends on the site-specific stratigraphy. It depends on the layer differences in peat type, degree of decomposition, water saturation, type of gyttja and small-scale variations in physical properties. Therefore, it is difficult to define general implications for other sites. A step forward would be to use

small scale information as constraints [15,56] to improve and validate the geophysical models to be able to predict the stratigraphy and (maybe) define their characteristics.

6.1.2. ERT survey

The tomographic-section of the resistivity shows regions of varying resistivity which were associated with the major sediments. Within the peat layer high resistivity regions are visible but they can not be explained by distinct layers. Interface1 was difficult to follow in the GPR profiles but with ERT it is very clear. The local variations (red spots in the uppermost 1m) are probably associated with the different peat decomposition which creates differences in the cation exchange capacity, but this is not supported by the statistical analysis of samples. Another explanation for these variations may be a different soil moisture. The statistical analysis of the sample indicates a slight correlation of water content and resistivity providing evidence for this explanation. The decrease in the resistivity within the peat layer is a good indicator of a different degree of humification of these deposits according to [36].

The transition between peat and coarse detritus gyttja is gradual considering the resistivity curve which does not show an evident change. The detection of gradual changes in property is well documented for ERT in comparison to GPR. [81] used both approaches to investigate peatland sites and he identified regions of varying resistivity within peatland which could not be resolved by GPR. Thus we concluded that a gradient layer with continuously changing dielectric permittivity was present, which cannot be detected by GPR.

With respect to the gyttja layers, ERT fails to differentiate between the different types of gyttja and the clay deposits. The resistivity of the gyttjas is not significantly higher than the resistivity of the mineral deposits.

6.1.3. SH-wave survey

The presented refraction tomography and reflection profile have shown different velocity variations and reflectors corresponding to the change in grain size of the sediments, like GPR. The identification of the silty-clay/basal sand is very clear in both methods while concerning Interface2 and Interface1 only partial reflectors are visible. The match between these seismic events is visible but further measurements would confirm this hypothesis. The very low shear wave velocity at the top of the profile indicates swampy sediments very well correlated to the organic peat deposit. The high velocities at the bottom of the section are instead clearly correlated with sand sediment. But the organic matrix as such is mechanically weaker than the matrix of inorganic sandy and silty soils. Therefore the related contrasts in shear rigidity (shear modulus) are one of the reasons why shear wave sounding turned out to be successful in determining the shape of the former island. Moreover, the shear wave velocity, which is proportional to the square root of rigidity, is determined mainly by the matrix and is not affected by the pore fill, making S-wave contrasts independent by the degree of water saturation.

This is very much in contrast to electric conductivity and dielectric permittivity, which are essentially determined by the soil water content. In our field example the general increase in water saturation with

depth led to decreasing lateral contrast between the island and the surrounding lake sediments. For the same reason GPR absorption increases strongly with depth.

Site effects primarily depend on the shear modulus of layers, which is also related to density. Attempts have been made to propose a relation between the bulk density and shear wave velocity [82,83] and our case study is in line with the literature giving a correlation factor of $r=0.85$ (Figure 11)

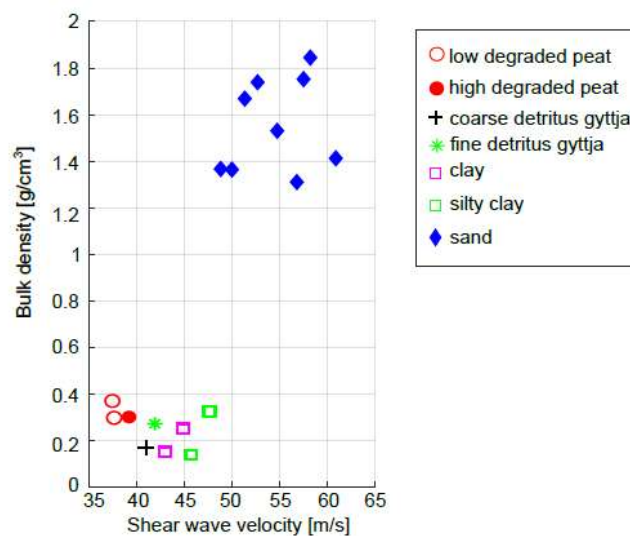


Figure 11. Shear wave velocity versus bulk density regarding core I.2bis.

Focusing on Figure 11 we can notice that the sand deposit is well isolated from the rest of the sediments. At a first glance peat presents the lower velocity values and it can be separated from the fine lake sediments and gyttja but more data would be necessary to implement that.

Efforts have been made to propose a general trend between shear wave velocities and porosity, permeability under different environmental conditions. Due to the different arrangement and composition of grains, there are differences in density, porosity and permeability as a result of differences in shear wave and compressional wave velocity. In particular the higher the density, the lower the porosity and thus the higher the wave velocity [83].

6.2. Degradation and compaction of the peat

As we presented in the paper the extrusion of the sediment from the Useringer core barrel can lead to a strong compaction of the core. In our case, the compaction affected only the first layer made up of peat

and coarse detritus gyttja, while the minerogenic and calcareous sediment were marginally or not affected. Taking the depth of the main transitions from the GPR survey in [21] a more focused estimation of the compaction has been done including also the degree of decomposition of the sediments. As we can see from our results the estimation of the compression through the peat is quite variable but combining the sediment parameters with geophysical results (GPR in our case) can give a promising methodology to understand more about this topic. In any case more tests are needed to understand how peat can be compressed during core extraction.

Another important remark about in-situ peat compaction regards its contribution to total subsidence which influences temporal and spatial sedimentation patterns.

The work of [41] found no evidence of an easy way to access peat compressibility. They argue that peat from different locations exhibited different compressibility characteristics and they concluded that more commonly and relatively easily measured sediment parameters (e.g. bulk density, state of decomposition) are no proper indicators of soil compressibility. In any case, peat is a highly compressible material and as a consequence the water storage changes produce volume changes in the peat.

Where changes in water table elevations are large, significant storage changes may arise from surface elevation changes. The nature of the surface elevation change depends on the compressibility of the peat [84].

So far, peat compaction has mainly been quantified using empirical models [85], resulting in estimated compaction rates in Holocene alluvial sequences (about < 2mm/year). However these results should be verified with field data.

[86] tried to estimate the rate of peat compaction at the Rhine-Meuse delta using bulk density and organic matter and radiocarbon dated peats. He presented a subsidence of up to 3 m in a 10 m thick Holocene sequence (0.6 mm/year) comparing the dry bulk density of compacted and uncompacted peat with an estimated error of about 15%. He also found that in two of the four cases the LOI and compaction are positively correlated but no rule is possible to define. The variability of peat compaction within the same layer derives from variations in organic content and fibre structure which is also determined by the degree of decomposition.

The degree of decomposition determines the physical properties of peat, too. Undecomposed peat has low bulk density and high fibre content [36]; therefore it contains many large pores and may have a total porosity of ~97%. During the decomposition peat becomes denser and its porosity reduces to 81-85% for highly decomposed peats [25]. In theory, if peat is fully water-saturated, the undecomposed peat has a higher water content and ϵ_r , thus the GPR velocity is lower compared to the decomposed one. In our case study the water content is almost constant in the peat deposits which means that higher velocities on the top are caused by organic undecomposed materials which can increase the velocity values. As a result of the dual-porosity character of peat the immobile region presents a negligible fluid flow velocity which can be translated in a decrease as well as the resistivity. Our study reveals this relationship, as we

can see from Figure 5, in which the lowermost peat presents lower GPR velocities indicating the more degraded part. This behaviour is also confirmed considering the electrical resistivity which decreases with depth in the same sediment according to [36]. In any case to prove this suggestion, additional GPR data against decompositional types of peat is needed.

The degree of composition of peat will also vary according to the plant species making up the peat [39]. Peats containing vascular plant remains often are more decomposable than those containing Sphagnum remains [87]. The pattern of lower and higher permeability peat in the deposit can be expected to affect the water flow through the peat which in turn may affect the patterning of vegetation. Such trends have been explored by [88] and [89], who showed that complex patterns of vegetation and of peat transmissivity may emerge from relatively simple interactions between vegetation type and water table position. However, a problem of these studies is that they have not been tested with field data and sometimes the number of boreholes are small (and not enough) to also understand horizontal variations.

To test models and to find correlations, it would be very useful if the peat could be mapped noninvasively and in detail over large areas. In these regards GPR can be the best cost-effective method to apply.

In wetland contexts also the fluctuating water table interacting with the sediments and any underlying or overlying depositional material plays a role. In our case we do not have information about the depth of the water table which would help us to understand the depth of penetration of GPR. An estimation can be done considering the geochemistry and the iron concentration which is expected at the maximum height of the water table. Below this limit the iron concentration decreases with depth due to the sensitivity to redox state and pH in bogs [90]. High concentrations of aluminium indicate a certain amount of minerogenic input into the lake basin from the catchment area. The Late Glacial to Early Holocene lake sediments of the lower part of the sequence expose clearly higher amounts of Al. This reflects a considerable minerogenic input from the catchment area, probably enabled by a sparse vegetation cover on the catchment soils. Towards the upper part of the lake sediment sequence (between 2.3 and 1.9 m) the Al content decreases dramatically, indicating a trend of stabilisation of the catchment surface by the succession of a vegetation cover in the lake catchment area. One later phase, that divides the peat deposition, is characterized by high minerogenic input, too. This might reflect a re-opening of the catchment vegetation caused by natural processes, e.g. Early Holocene climate variability [e.g. 91] or local human activity. Copper and zinc are indicative for redox processes at the water table. [49]. The high concentration of iron, associated with high values of copper and zinc at about ~1.10 m depth (Figure 12) indicates the presence of the long-term mean water table at this depth.

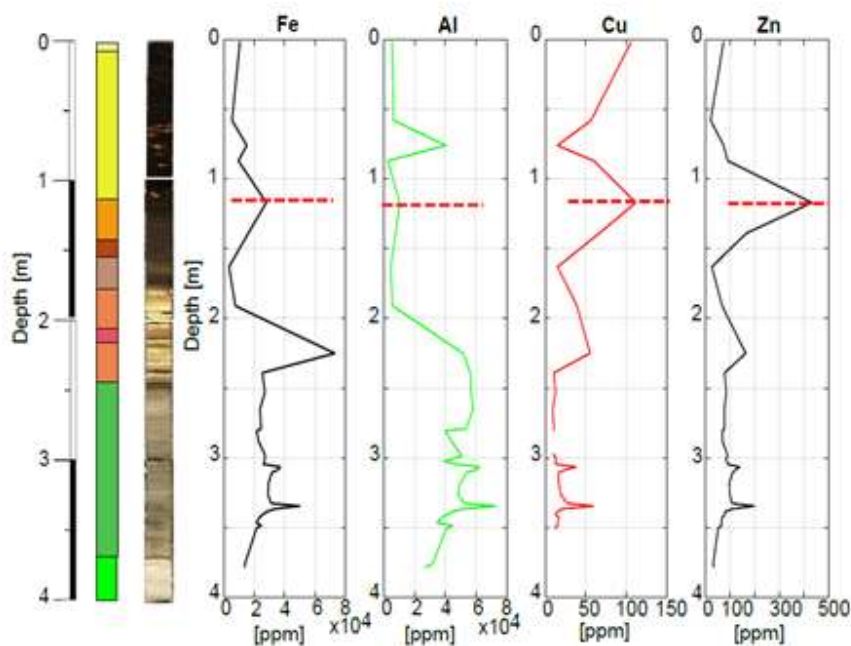


Figure 12. Geochemical and physical profile of the core I.4. The dashed red lines indicate the high values of iron, aluminium, copper and zinc [ppm].

6.3. Methodological questions

To reconstruct the stratigraphy at ancient Lake Duvensee a multi method approach has been used in a way to understand which method can deliver the best understanding of the layering.

Soil parameters have been implemented to cover small scale variations. In the following subsection we are first going to discuss which method was the most successful for the research foci and what can be improved to better define the stratigraphy. At the end of the section we will discuss what soil and petrophysical parameters are suitable for identifying different sediments. The fen basin is successfully delineated with GPR and ERT due to the high contrast in electrical properties between the organic and the surrounding mineral basal deposits. SH-seismics as well is able to recognize and separate the layers that differ in seismic impedance and grain size. GPR and Seismic tomography display sharp interfaces, whereas ERT shows gradual transitions, and these methodical differences are described by other authors as well [18,92]. The investigated peatland is embedded in low conductive glacial sands typical of fens in northern Germany [27], which means that the electrical conductivity of the organic deposits (peat and gyttja) is higher than that of the surrounding material. Delineation of peatland deposits with GPR is more achievable, and in our case we were even able to differentiate different degree of decomposition of peat and somewhere some weak reflections were correlated to different gyttjas (fine detritus gyttja and calcareous gyttja).

We propose SH-wave seismic as an alternative tool to investigate the stratigraphy of such environments. In this regard a comment about the resolution of GPR and SH-Seismic is needed. GPR shows a resolution between 5-8 cm (Section 5.2), while Seismic 20-70 cm. Concerning the goals of this research GPR would be the best method to use for reconstructing the shallow subsurface and to try to identify also internal layering concerning different gyttjas. The interpretation of the very shallow subsurface (first meter in particular) is very difficult concerning reflection seismic because of different factors, for instance, it is difficult to separate direct waves, surface waves and shallow reflections in the near field close to the source. This makes GPR more suitable for detecting shallow interfaces. However, seismics is also sensitive to sediments that differ in grain size and it provides information about the density and compaction of different deposits. The depth of penetration differs significantly making seismic more suitable for surveys focused on the ancient lake bottom. Interface3 is, indeed, very clear and it can be followed in higher depth than with GPR. In the centre of the ancient lake, for instance, the core information shows that the sand layer lies at a depth of about 6 m which is very difficult to reach with GPR. [39] used a 200 MHz antenna achieving a depth of 3 m, too enabling the extension of the different peat humifications possible. [11] and [24] used a 50 MHz, 100 MHz and 200 MHz Antenna claiming that the second was the best compromise between depth of investigation and resolution reaching a depth of about 10 m having a peat layer of about ~4m on top. Using antennae of 50 MHz or 100 MHz means that the resolution with SH-Seismics can be comparable but the depth of penetration would be always more for seismic. For this case study the best choice would be to keep measuring with a 200MHz antenna otherwise with a lower central frequency antenna we would lose resolution which could be useful for layering interpretation. However, some improvements can also be planned regarding seismics. The distance between the receivers can be reduced to 0.25 m but the time of measurements will increase, losing the cost-effective character of the survey. Another remark to make would be about the source used for seismic waves. A higher frequency source would produce waves with smaller wavelength and therefore the resolution would be higher, but in the SH-wave case the higher frequencies would be quickly attenuated and difficult to measure.

Moreover, compressional waves (P-waves) can be a tool to test in this case study despite the longer wavelength and thus coarser resolution compared to shear waves. Nevertheless, P-waves are depending on the compressional modulus and this might be a parameter that is changing between sedimentary layers, too. For example, V_p increases with a decrease in porosity, and increases with an increase in density.

The Full Waveform Inversion (FWI) is a recent tool which is able to improve the resolution of seismic data. At the Fossa Carolina FWI was able to improve the definition of the canal basement and to resolve small scale velocity anomalies correlated with features in the archaeological documentation [93]. FWI in the archaeological context has been introduced recently by [93], [94] and [95], and is becoming very important to resolve small-scale near surface structures. A further application of this tool could foster the identification of shallow structures and improve the understanding of the seismic signals visible in the reflection profile. The multichannel analysis of surface waves (MASW e.g. [95], [96]) and spectral analysis of surface waves (SASW) can also be used to improve resolution for mapping subsurface stratigraphy.

Magnetic measurements are also very common in geoarchaeological research but in our case it did not provide satisfying results. The magnetic susceptibility was measured along the core I.4 and the results are shown in Figure S4. The survey pointed out that between peat and gyttja sediments the magnetic susceptibility does not present any variation. The only visible change is the transition between the calcareous gyttja and the underlying clayey silt deposits, which is already visible with GPR. Therefore, we decided to neglect a survey of magnetic susceptibility. We tested Electromagnetic Induction instead (EMI) and the result is shown in Figure S4.

We used the CMD Mini-Explorer by GF Instruments and conducted measurements in vertical and horizontal coplanar configuration. The sample frequency was 10 Hz. To reduce noise, we applied a lowpass butterworth filter (third order, cutoff wavenumber = 0.7 m^{-1}). Finally, the inversion was performed with the software IX1D by Interpex. We derived 'smooth models' [97] with ten layers from 0.1 m depth to 1.8 m depth. The EMI inversion shows a high resistivity layer at the top of the profile which can be associated with the peat layer. Underneath this unit a high conductive area is present correlated to the lake sediments. The identification of the sand deposits is difficult because of the low depth of penetration of the instrument. For future investigations the use of EMI with higher depth penetration, e.g. by using an instrument with larger coil spacing, is promising.

Combining geophysics and soil characterization is currently required to aid the rapid discovery and characterisation of buried wetland archaeology. For instance the identification of different peat degradation can be an indicator of the layers preservation which can address the archaeological research. Characterisation of the deposits prior to full survey is therefore an essential step in conducting geophysical surveys in wetlands. We presented a range of different parameters (e.g. dielectric permittivity, resistivity and SH seismics) which is connected with soil information (water content organic matter) can delineate different deposits. The dielectric permittivity is well defined using the guided wave measurements which can be improved also using a motor pulling the metal rod into the ground allowing a more detailed survey of the GPR velocity. Evaluating with more accuracy the degree of decomposition of peat for instance would help the determination of soil compressibility and porosity. Using EC-Direct Push is the most successful way to determine the conductivity/resistivity values.

7. Conclusions

To study the landscape development of the early Mesolithic sites of ancient Lake Duvensee a multi-methodological approach has been applied. Fens of the temperate zone of central Europe are still not studied frequently with these methods. The combined use of different geophysical methods (GPR, ERT and SH Seismics) and stratigraphic information from corings helped finding additional information about the stratigraphy of the former lake. Special attention is given to the investigation of different types of gyttja, which can often be found at the base of peat deposits in this region. Based on our field survey we found that the ancient lake basin prospection can be performed with different methods each of them sensible to different variations of physical parameters:

- GPR is able to identify the main transition between sediments which differ in grain size, and the boundary between the uppermost poorly decomposed peat (“acrotelm”) and underlying well-decomposed peat (“catotelm”). Moreover the distinction between different gyttjas is locally visible with small scattered reflection but without an orientation.

Internal GPR velocity variations , which are represented with sporadic reflections, can be detected using the guided wave measurements which provide a high resolution image of the permittivity in the subsurface.

- ERT is capable of distinguishing between sediments with different grain sizes, but is not able to distinguish between clayey to silty deposits and lake sediments, therefore the different gyttja types are not detected. However, depending on site conditions ERT is able to indicate regions of gradually changing properties, such as the solutes in the pore fluid. The small scale variations, due to different degrees of peat and organic remains, in the peat layer were visible as resistivity changes.

Moreover, using GPR together with stratigraphic information was useful to estimate the peat compaction due the extraction after drilling. It turned out that the compaction is higher for the shallower peat layer associated with the low degraded peat, while the underlying more degraded peat presents a lower compaction. But no trend was observed.

We proposed SH-Seismics as alternative tool for investigating wetlands and it delivered the following results:

- SH-wave seismics enables exploring the deepest stratigraphy (up to ~19 m depth), in which the major interfaces can be found from the S-wave velocity distribution as provided by refraction tomography. The method is able to distinguish between sediments with different grain sizes. The vertical resolution is ~0.2-0.7 m through S-wave reflection imaging allowing the detection of the main interfaces as GPR. S-wave velocity values of the organic sediments are in the range of 40 to 80 m/s, whereas the glacial sands have velocities of 100 to 250 m/s. This means that sediments presenting a weaker matrix can be very easily defined and mapped

Due to the specific sensitivities of each technique on different soil properties a joint application is recommended. In this regard GPR and Seismics are able to reconstruct the stratigraphy combining high resolution and depth information. It’s also interesting to novice how ERT and SH-wave seismics work vice versa for detecting different interfaces.

Regarding the characterisation of the sediments we came to the following conclusions:

- ❖ High degraded peat presents physical parameters similar to detritus gyttja.
- ❖ Fine detritus gyttja can be distinguished from the coarse detritus gyttja
- ❖ The calcareous gyttja can be detected using a combination between physical parameters and soil analysis.

- ❖ Resistivity is well correlated with water content and organic matter for distinguish between different peat degrees of decomposition and different gyttjas (calcareous/fine)
- ❖ ERT and GPR guided waves allowed the distinction between different degrees of peat decomposition but the depth of investigation was not enough to statistically separate the different gyttjas.
- ❖ Seismics allows an estimation of sediment density.

Due to the variety of ecological conditions and stratigraphy in wetlands, the results of this study are also valuable in complementing existing case studies. The delineation of different gyttja layers is especially promising for the calculation of total carbon content of peatlands

For palaeoenvironmental researchers or archaeologists with limited time and budget for conducting extended drilling campaigns, this study provides a very important planning tool for future investigations. A further aim is to make the researchers able to map large areas with geophysics enabling the geoarchaeologist to reduce the time consuming drilling procedure. The direction would be using geophysics in a way to extrapolate the coring results from single point to large areas. However, the comparison with corings will be always necessary because of the site-specific conditions which affect these kinds of environments. And most importantly, this prospective will enable the archaeological and palaeoenvironmental research groups to reconstruct palaeolandscapes and to identify possible areas of interest.

Supplementary Materials:

Property	Material	Value	References
Total porosity	peat	~70 to 95 %	[36,72,98,99]
	gyttja	~0.90 to 0.95 %	
Compression	peat	~10 to 50 %	[38,99]
	detr. calc. gyttja	~5-35%	
Pore diameter	peat	~0.1- 5 mm	[37,40]
Organic matter	gyttja	~40-80%	[17,99]
		~30-95%	
Water content	peat	~85-95%	[8,17]
	org. gyttja	~85-88 %	
	min. gyttja	~72-75%	
Bulk density	peat	0.08-0.17 g/cm ³	[8,100]
	org. gyttja	0.13-0.22 g/cm ³	
	min. gyttja	0.27g/cm ³	

Dielectric permittivity (GPR velocity)	Air	1 (0.30 m/ns)	
	Fresh water	80 (0.033 m/ns)	[46,47]
	Clay (dry)	2.5 (0.10 m/ns)	
	Clay (wet)	5-40 (0.05-0.06 m/ns)	[49]
	gyttja	23-27(0.06-0.07 m/ns)	[77]
	Silt	5-30 (0.05-0.07 m/ns)	[22]
	Sandy clay	16.87 (0.073 m/ns)	
	Sand (dry)	2.55-7.5 (0.1-0.2 m/ns)	
	Sand (wet)	20-31.6 (0.05-0.07 m/ns)	
		40.69-34.56 (0.047-0.051 m/ns)	
	Fen peat	56.18 (0.040 m/ns)	
		40.7-73.5 (0.035-0.0479 m/ns)	
	Wood peat	57-80 (0.03-0.06 m/ns)	
	Peat		
Freshwater peat			
Conductivity/Resistivity	Sand (dry)	0.01 mS/m	[36,46]
	Silts	1-100 mS/m	
	Clays	2-1000 mS/m	
	undecomp. Peat	35-44Ωm	
	Decomposed peat	20-25Ωm	

Table S1. Range of soil parameters of different sediments from field and laboratory studies taken from literature.

Seismic acquisition parameters	
Item	Specification
Total length	36 m
Receiver type	Horizontal geophone 10 Hz
Receiver number, spacing, first and last position	72, 0.5 m
Receiver first and last position	0.5 m, 36 m
Source type	Horizontal sledge hammer
Source point number and spacing	38, 1 m
Source first and last position	0 m, 37 m
CMP number and spacing	74, 0.5 m
CMP first and last position	0 m, 36.5 m
Sampling rate, record length	0.25 ms, 0.5 s

Table S2. Acquisition parameters of the SH-wave seismic reflection profile.

Seismic Tomography processing flow	
Process	Processing parameters
Velocity smoothing	
Horizontal correlation length	0.5 m (z=0), 1m (z=12m)
Vertical correlation length	0.1 m (z=0), 0.6m (z=12m)
Smoothing weight	0.4
Velocity damping weight	0.4
LSQR tolerance	0.01
Number of iterations	5
Number of different starting models	10

Table S3. Processing parameters of the tomographic inversion.

Reflection Seismic processing flow	
Process	Processing parameters
Quality control and trace editing	Remove of noise or dead traces
Offset mute limit	1.1 m
Bandpass filter	15 - 25 - 150 - 200
NMO - Correction: velocity model	Derived from tomography
NMO - Correction: stretch mute	30%
Analytic gain	t^1
Trace normalisation	RMS - Scaling
Stack: max fold	3
FD-Migration: velocity model	Derived from tomography
FD-Migration: maximum dip	80 degrees

Time to depth conversion: velocity model	derived from tomography
--	-------------------------

Table S4. Processing parameters used in the reflection seismic.

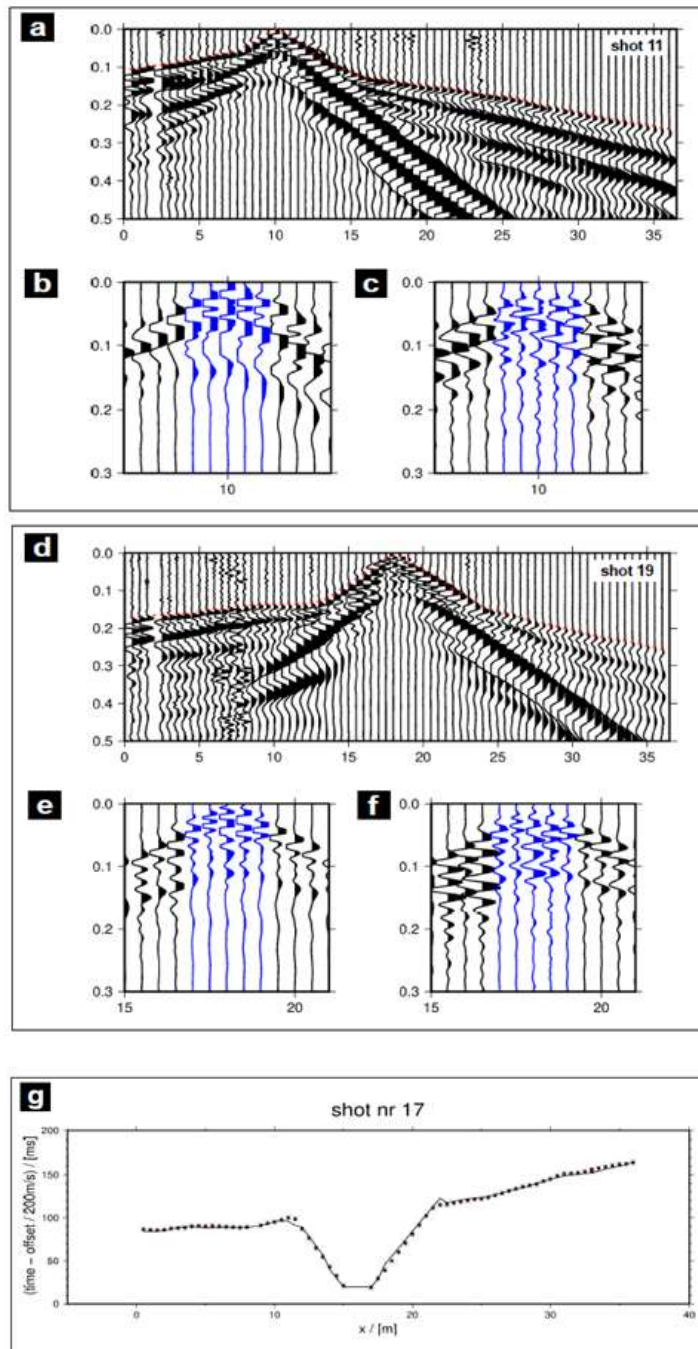


Figure S1. Examples of SH shot gather data. (a) shot 11 raw data, the red points are the pick used for the tomography; (b) focus on seismic traces used for the reflection seismic (marked with blue) before processing (c) filtered data. (d) shot 19 raw data, the red points are the pick used for the tomography; (e) focus on seismic traces used for the reflection seismic before processing (f) filtered data; (g) fit examples from seismic refraction tomography.

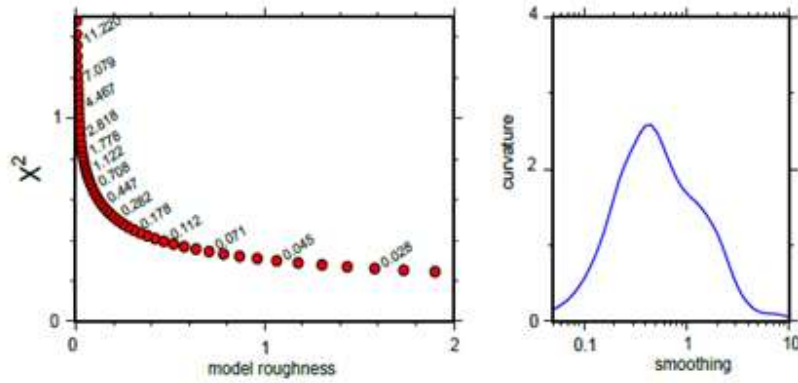
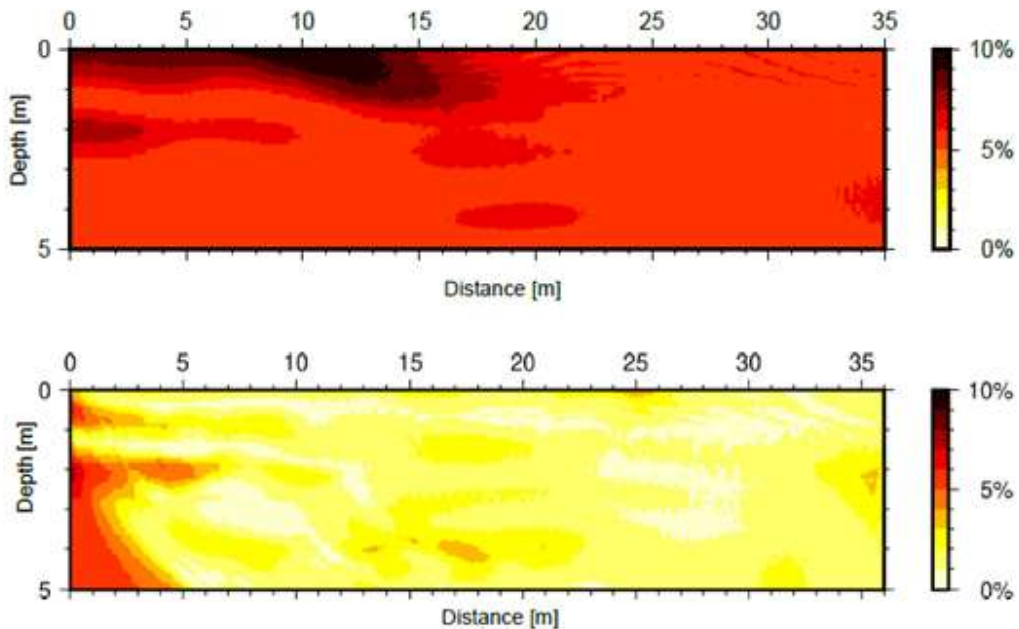
a**b**

Figure S2. (a) regularisation estimation. Left: model roughness versus data fit. Inversion was performed using a wide range of smoothing factors: 10^{-2} - 10^2 (labels at points). Right: smoothing factor versus the curvature of the graph. Optimum smoothing factor is found at the maximum curvature. (b) Standard deviation of model sets. Top: set starting models. Single starting model can be altered up to 10% from the reference model. Bottom: set of the 10 best models ($rms/rms\ best < 120\%$). Final average model is independent of the starting model used

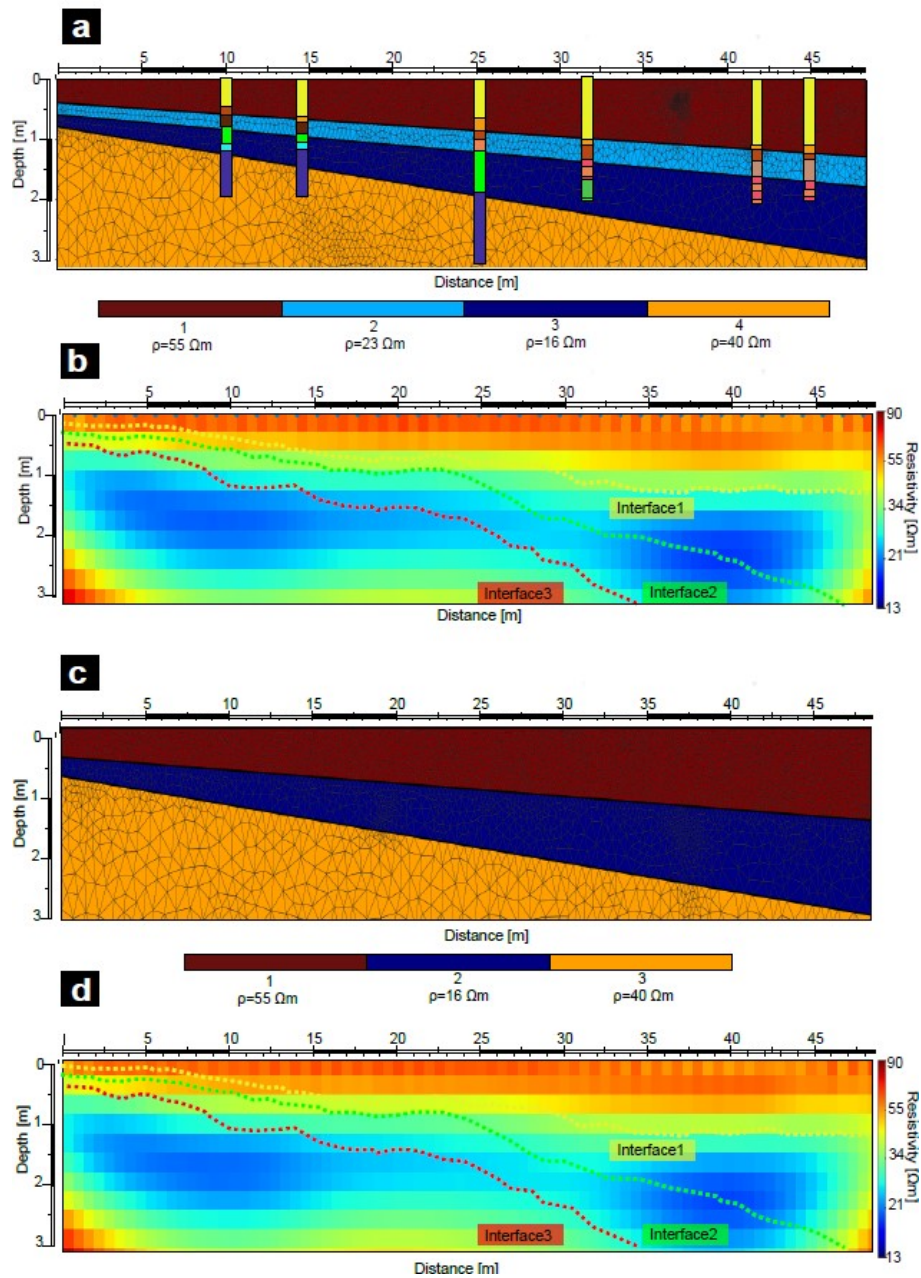


Figure S3. Numerical modelling performed for this study; (a) synthetic model built using the depth of the sediments from the core catena and typical values of the resistivity for the considered deposits. (b) tomographic image of the synthetic model with the GPR interfaces superimposed; (c) synthetic model built using the depth of the sediments from the core catena but without the fine gyttja layer and typical values of the resistivity for the considered deposits. (d) tomographic image of the synthetic model with the GPR interfaces superimposed.

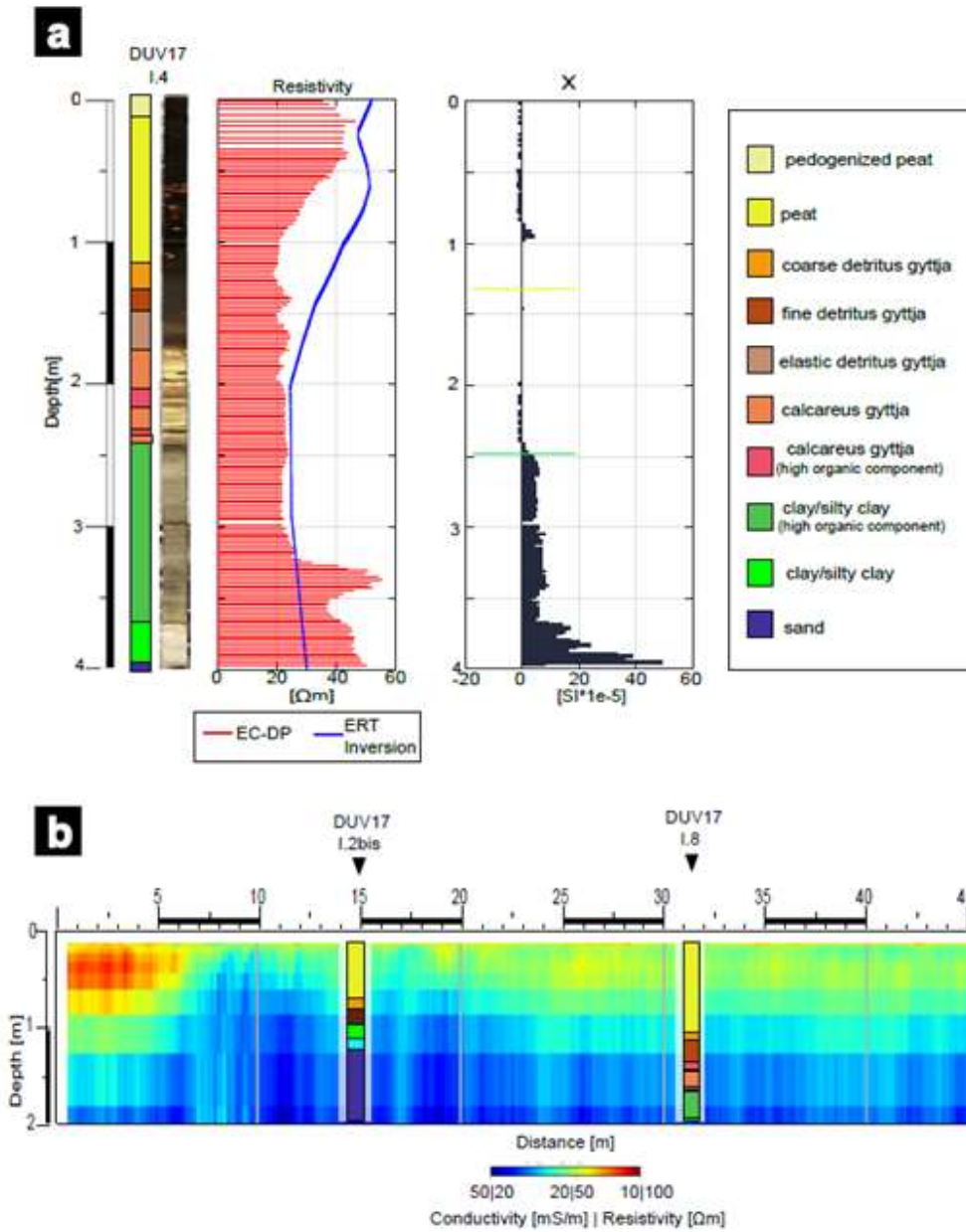


Figure S4. (a) Magnetic susceptibility measured along the core I.4 of Duvensee ; (b) Electromagnetic Induction survey along the reference profile.

Funding:

This research was funded by the German Research Foundation (DFG) grant 2901391021 (SFB 1266).

Acknowledgments:

We would like to thank the longtime excavator and researcher of the Duvensee bog sites, Klaus Bokelmann, for detailed information

References

1. Van de Noort, R., O'Sullivan, A. *Rethinking Wetland Archaeology*. Gerald Duckworth and Co. Ltd., London, 2006
2. Lillie, M., Ellis, S. *Wetland Archaeology and Environments: Regional Issues, Global Perspectives*. Oxbow Books, 2007.
3. Menotti, F. *Wetland Archaeology and Beyond: Theory and Practice*. Oxford University Press, 2012
4. Brown, A.G. *Alluvial Geoarchaeology-Floodplain Archaeology and Environmental Change*. Cambridge Manuals in Archaeology. Cambridge University Press: Cambridge 1997.
5. Utsi, E. Ground-penetrating radar time-slices from North Ballachulish Moss. *Archaeol. Prospect* **2004**, 11, 65–75.
6. Doran, G.H. Excavating wet sites. In *The Oxford Handbook of Wetland Archaeology*, F., Menotti, A., O'Sullivan, (Eds.), Oxford University Press: Oxford, 2013, pp. 483-494.
7. Stegmann, H., Succow, M., Zeitz, J. Muddearten (Types of Gytjtja). In *Landschaftsökologische Moorkunde*, M., Succow, H., Joosten, (Eds.), Schweizerbart, Stuttgart, Germany, 2001.
8. Walter, J., Hamann, G., Klingenfuss, C., Zeitz, J. Stratigraphy and soil properties of fens: Geophysical case studies from northeastern Germany. *Catena* **2016**, 142, 112-125.
9. Becker, A., Bucher, F., Davenport, C. & Flisch, A. Geotechnical characteristics of post-glacial organic sediments in Lake Bergsee, southern Black Forest, Germany. *Engineering Geology* **2004**, 74, 91–102.
10. Heller, C., Zeitz, J. Stability of soil organic matter in two northeastern German fen soils: the influence of site and soil development. *J. Soils Sediments* **2012**, 12, 1231–1240.

11. Comas, X., Slater, L., and Reeve, A. Stratigraphic controls on pool formation in a domed bog inferred from ground penetrating radar (GPR), *J. Hydrol.* **2005**, 315, 40– 51, doi:10.1016/j.jhydrol.2005.04.020.
12. Hadler, H., Vött, A., Newig, J., Emde, K., Finkler, C., Fischer, P., Willershäuser, T. Geoarchaeological evidence of marshland destruction in the area of Rungholt, present-day Wadden Sea around Hallig Südfall (North Frisia, Germany), by the Grote Mandrenke in 1362 AD. *Quaternary International* **2018**, 473 A, 37-54.
13. Zielhofer, C., Rabbel, W., Wunderlich, T., Vött, A., Berg, S. Integrated geophysical and (geo)archaeological explorations in wetlands. *Quaternary International* **2018**, 473 A, 1-2.
14. Corradini, E., Eriksen, B.V., Fischer Mortensen, M., Krog Nielsen, M., Thorwart, M., Krüger, S., Wilken, D., Pickartz N., Panning, D., Rabbel, W. Investigating lake sediments and peat deposits with geophysical methods - a case study from a kettle hole at the Late Palaeolithic site of Tyrsted, Denmark. *Quaternary International* under review
15. Wunderlich T., Fischer P., Wilken D., Hadler H., Erkul E., Mecking R., Günther T., Heinzemann M., Vött A., Rabbel, W. Constraining Electric resistivity Tomography by direct push electric conductivity logs and vibracores: an exemplary study of the fiume Morto silted riverbed (Ostia Antica, western Italy). *Geophysics* **2018**, 83(3):1-58 DOI:10.1190/geo2016-0660.1
16. Warner, B.G., Nobes, D.C., Theimer, B.D. An application of ground penetrating radar to peat stratigraphy of Ellice Swamp, southwestern Ontario. *Canadian J. of Earth Science* **1990**, 27, 932–938.
17. Theimer, B.D., Nobes, D.C., Warner, B.G. A study of the geoelectrical properties of peatlands and their influence on ground-penetrating radar surveying. *Geophys. Prospect.* **1994**, 42, 179–209.
18. Slater, L., Reeve, A. Understanding peatland hydrology and stratigraphy using integrated electrical geophysics. *Geophysics*, **2002**, 67, 365–378.
19. Persico, R., Soldovieri, F., and Utsi, E. Microwave tomography for processing of GPR data at Ballachulish. *J. of Geophysics and Engineering* **2010**, 7(2) 164–77.
20. Ruffell, A., and McKinley, J. Forensic geomorphology. *Geomorphology* 2014, 206, 14–22.
21. Corradini, E., Wilken, D., Zanon, M., Groß, D., Lübke, H., Panning, D., Dörfler, W., Rusch, K., Mecking, R., Erkul, E., Pickartz N., Feeser, I., Rabbel, W. Reconstructing the palaeoenvironment at the early Mesolithic site of Lake Duvensee: Ground-penetrating radar and geoarchaeology for 3D facies mapping. *The Holocene* 2020, <https://doi.org/10.1177/0959683620902234>

22. Lowry, C.S., Fratta, D., Abdreson M.P. Ground penetrating radar and spring formation in a groundwater dominated peat wetland. *J. of hydrology* **2009**, 373, 68-79
23. Comas, X., Terry, N., Slater, L., Warren, M., Kolka, R., Kristiyono, A., Sudiana, N., Nurjaman, D., Darusman, T. Imaging tropical peatlands in Indonesia using ground-penetrating radar (GPR) and electrical resistivity imaging (ERI): implications for carbon stock estimates and peat soil characterization. *Biogeosciences* **2015**, 12, 2995–3007
24. Comas, X., Slater, L., and Reeve, A. Geophysical evidence for peat basin morphology and lithologic controls on vegetation observed in a northern peatland. *J. Hydrol.* **2004**, 295, 173–184, doi:10.1016/j.jhydrol.2004.03.008.
25. Plado, J., Sibul, I., Mustasaar, M., Jöeleht, A. Ground-penetrating radar study of the Rahivere peat bog, eastern Estonia. *Est. J. Earth Sci* **2011**, 60, 31–42.
26. Eggelsmann, R., Heathwaite, A.L., Grosse-Brauckmann, G., Küster, E., Naucke, W., Schuch, M., Schweickle, V. Physical processes and properties of mires. In *Mires: Processes, Exploitation and Conservation*. K., Göttlich, A.L., Heathwaite, (Eds.), Wiley, New York, 1993
27. Walter, J., Lück, E., Bauriegel A., Richter, C., Zeitz, J., Multi-scale analysis of electrical conductivity of peatlands for the assessment of peat properties. *European J. of soil science* **2015**, 66, 639-650
28. Wunderlich, T., Wilken, D., Erkul, E., Rabbel, W., Vött, A., Fischer, P., Hadler, H., Heinzelmann, M. The river harbour of Ostia Antica - stratigraphy, extent and harbour infrastructure from combined geophysical measurements and drillings. *Quaternary International*, **2017**, 1-11
29. Lamair, L., Hubert-Ferrari, A., Yamamoto, S., Fujiwara, O., Yokoyama, Y., Garret, E., De Batist, M., Heyvaert V.M.A., et al. Use of high-resolution seismic reflection data for paleogeographical reconstruction of shallow Lake Yamanaka (Fuji Five Lakes, Japan). *Palaeogeography, Palaeoclimatology, Palaeoecology* **2019**, 514, 233-250
30. Groß D., Lübke H., Schmölcke U., and Zanon M. Early Mesolithic activities at ancient lake Duvensee, northern Germany. *The Holocene* **2018**, 29 (2), 197-208.
DOI:[10.1177/0959683618810390](https://doi.org/10.1177/0959683618810390)
31. Roessler, L. *Erdgeschichte des Herzogtums Lauenburg*. Ratzeburg: Albrechts, 1957
32. Averdieck, F.R. Palynological investigations in sediments of ancient lake Duvensee, Schleswig-Holstein (North Germany). *Hydrobiologica* **1986a**,143, 407-410.
33. Bokelmann, K. Spade paddling on a Mesolithic lake - Remarks on Preboreal and Boreal sites from Duvensee (Northern Germany). In *A mind set on flint. Studies in honour of Dick Stapert*.

Niekus M.J.L.T., Barton, R.N.E., Street M. et al. (Eds.) Groningen: Groningen Archaeological Studies, pp. 369-380, 2012

34. Groß D, Piezonka H, Corradini E et al. Adaptations and transformations of hunter-gatherers in forest environments: New archaeological and anthropological insights. *The Holocene* **2019**, 29 (10). Special Issue: Scales of Transformation – Human-Environmental Interaction in Prehistoric and Archaic Societies, DOI: 1531-1544. [DOI:10.1177/0959683619857231ola](https://doi.org/10.1177/0959683619857231ola)
35. Canadian System of soil Classification CSSC,1998
36. Boelter, D.H. Important physical properties of peat materials. Proceedings of the 3rd International Peat Congress, Québec, **1968**, pp. 150–154.
37. Rezanezhad F., Quinton W.L., Price J.S., Elrick D., Elliot T.R., Heck R.J. Examining the effect of pore size distribution and shape on flowthrough unsaturated peat using 3-D computed tomography. *Hydrology And Earth System Sciences* **2009**,13, 1993 – 2002.
38. Rezanezhad F., Price J.S., Quinton W.L., Lennartz, B. Structure of peat soils and implications for water storage, flow and solute transport: A review update for geochemists. *Chemical Geology* **2016**, 429, 75 – 84.
39. Kettridge, N., Comas, X., Baird, A., Slater, L., Strack, M., Thompson, D., Jol, H., and Binley, A. Ecohydrologically important subsurface structures in peatlands revealed by ground-penetrating radar and complex conductivity surveys, *J. Geophys. Res.* **2008**, 113, 1-15. doi:10.1029/2008JG000787.
40. Quinton, W.L., Gray, D.M., Marsh, P. Subsurface drainage from hummock-covered hillslope in the Arctic tundra. *J. Hydrol.* **2000**, 237, 113–125.
41. Price, J.S., Cagampan, J., Kellner, E. Assessment of peat compressibility: is there an easy way? *Hydrol. Process.* **2005**, 19, 3469–3475.
42. Kennedy, G.W., Price, J.S. A conceptual model of volume-change controls on the hydrology of cutover peats. *J. Hydrol.* **2005**, 302, 13–27
43. von Post, L. Swedish geological peat survey with the results obtained so far (in Swedish). *Sven. Mosskult. Tidskr.* **1922**, 36, 1–27.
44. von Post, H. Studier öfver nutidens koprogena jordbildningar; gyttja, dy och mylla (Studies about soil formation of coprogenic origin; gyttja, dy, turf/sod and silt/load). *Kongliga Svenska Vetenskaps-Akademiens Handlingar* **1862**, 4, 1–59 (in Swedish).

45. Wunderlich, T., and Rabbel, W. Absorption and frequency shift of GPR signals in sandy and silty soils: empirical relations between quality factor Q, complex permittivity and clay and water contents. *Near Surface Geophysics* **2013**,11(2), 117-127.
46. Davis, J.L., Annan, A.P. Ground-penetrating radar for high-resolution mapping of soil and rock stratigraphy. *Geophys. Prospect.* **1989**, 37, 531–551.
47. Conyers, L.B. *Ground-Penetrating Radar for Archaeology*. Altamira Press, Plymouth, 2004.
48. Styles, P. *Environmental Geophysics: Everything you Ever Wanted (Needed!) to Know but Were Afraid to Ask!*. EAGE, Netherlands, 2012
49. Milton, C.J. Geophysics and geochemistry: an interdisciplinary approach to archaeology in wetland contexts. *Journal of archaeological Science: Reports* **2018**, 18, 197-212
50. Wunderlich, T., Petersen, H., al Hagrey, S.A., Rabbel, W. Pedophysical Models for Resistivity and Permittivity of Partially Water-Saturated Soils. *Vadose Zone Journal* **2013**, 12, no. 4, doi: 10.2136/vzj2013.01.0023.
51. Igel, J., Stadler, S., and Günther, T. High-resolution investigation of the capillary transition zone and its influence on GPR signatures. 16th International Conference of Ground Penetrating radar (GPR), 2016.
52. Meyer, J.H. Investigation of Holocene organic sediments: a geophysical approach. *International Peat Journal* **1989**, 3, 45–57.
53. Loke, M.H. Tutorial: 2D and 3D electrical imaging surveys 2016. www.geotomosoft.com.
54. Günter, T., Rücker, C. A general approach for introducing information into inversion and examples from dc resistivity inversion: 10th Annual european Meeting of Environmental and Engineering Geophysics, EAGE. extended Abstract P039, 2006
55. Hansen, P. C., and O’Leary, D. P. The use of the L-curve in the regularization of discrete ill-posed problems. *SIAM Journal on Scientific Computing* **1993**, 14, 1487-1503.
56. Fischer, P., Wunderlich, T., Rabbel, W., Vött, A., Willershäuser, T., Baika, K., Rigakou, D., Metallinou, G. Combined electrical resistivity tomography (ERT), direct-push electrical conductivity logging (DP-EC) and coring – a new methodological approach in geoarchaeological research: *Archaeological Prospection* **2016**, doi: 10.1002/arp.1542.
57. Harrington G.A., Hendry M.J. Using Direct-Push EC Logging to delineate heterogeneity in a clay-rich aquitard. *Ground Water Monitoring & Remediation* **2006**, 26, no. 1, 92-100.
58. Direct Image, Electric Conductivity (EC) Logging. Standard Operating Procedure. Kansas, 2008

59. Rabbel, W. Stümpel, H., and Woelz, S. Archeological prospecting with magnetic and shear wave surveys at the ancient city of Miletos (western Turkey). *The Leading Edge*, **2004**,23, 690-703.
60. Rabbel W., Wilken D., Wunderlich T., Bödecker S., Brückner H., Byock J., von Carnap-Bornheim C., Kalmring S., Karle M., Kennecke H., Messal S., Schmidts T., Seeliger M., Segschneider M., and Zori D. Geophysikalische Prospektion von Hafensituationen – Möglichkeiten, Anwendungen und Forschungsbedarf. *Häfen im 1. Millennium A.D. – Bauliche Konzepte, herrschaftliche und religiöse Einflüsse*, eds. T. Schmidts and M. Vučetić. Romano-Germanic Central Museum Press (RGZM), Mainz. , 2015. ISBN 978-3-79543-039-9
61. Wunderlich T., Wilken D., Erkul E., Rabbel W., Vött A., Fischer P., Hadler H., Ludwig S., and Heinzelmann M. The harbour(s) of ancient Ostia. Archaeological prospection with shear-wave seismics, geoelectrics, GPR and vibracorings. *Archaeologia Polona* **2015**, vol 53. Special theme: Archaeological prospection, ISSN 0066-5924
62. Obrocki, L., Vött, A., Wilken, D., Fischer, P., Willershäuser, T., Koster, B., Lang, F., Papanikolaou, I., Rabbel, W., and Reicherter, K. Tracing tsunami signatures of the AD 551 and AD 1303 tsunamis at the Gulf of Kyparissia (Peloponnese, Greece) using direct push in situ sensing techniques combined with geophysical studies. *Sedimentology*, **2018** DOI: [10.1111/sed.12555](https://doi.org/10.1111/sed.12555)
63. Köhn, D., Wilken, D., De Nil, D., Wunderlich, T., Rabbel, W., Werterh, L., Schmidt, J., Zielhofer, C., Linzen, S. Comparison of time-domain SH waveform inversion strategies based on sequential low and bandpass filtered data for improved resolution in near-surface prospecting. *Journal of Applied Geophysics* **2018**, 160, 69-83
64. Schwardt M., Köhn D., Wunderlich T., Wilken D., Seeliger M., Schmidts T., Brückner H., Başaran S., Rabbel W. Characterisation of silty to fine-sandy sediments with SH-waves: full waveform inversion in comparison to other geophysical methods. *Near Surface Geophysics* **2020**,18 (3): 217-248 DOI:[10.1002/nsg.12097](https://doi.org/10.1002/nsg.12097)
65. Stümpel, H., Kähler, S., Meissner, R., & Milkereit, B. The use of seismic shear waves and compressional waves for lithological problems of shallow sediments. *Geophysical Prospecting* **1984**, pp. 662-675.
66. Fujie, G., Kasahara, J., Murase, K., Mochizuki, K. and Kaneda, Y. Interactive analysis tools for the wide-angle seismic data 440 for crustal structure study (Technical Report), *Explor. Geophys.* **2008**, 39. doi:10.1071/EG08006, 2008.
67. Korenaga, J., W. S. Holbrook, G. M. Kent, P. B. Kelemen, R. S. Detrick, H.-C. Larsen, J. R. Hopper, and T. Dahl-Jensen. Crustal structure of the Southeast Greenland margin from joint refraction and reflection seismic tomography. *J. Geophys. Res.* **2000**, 105, 21,591-21,614
68. Yilmaz, Ö. Seismic data analysis (Vol.1). Tulsa: Society of Exploration Geophysicists, 2001.

69. Mingram, J., Negendank, J.F.W., Brauer, A., Berger, D., Hendrich, A., Köhler, M., Usinger, H. Long cores from small lakes—recovering up to 100 m-long lake sediment sequences with a high-precision rod-operated piston corer (Usinger-corer). *J Paleolimnol* **2007**, 37, 517–528.
70. Dearing, J. *Environmental Magnetic Susceptibility: Using the Bartington MS2 System*. 2nd ed. (Bartington Instruments Ltd.), 1999.
71. Dean, W.E. Determination of Carbonate and Organic Matter in Calcareous Sediments and Sedimentary Rocks by Loss on Ignition: Comparison with Other Methods. *Journal of Sedimentary Petrology* **1974**, 44, 242–48.
72. Boelter, D.H. Physical properties of peat as related to degree of decomposition. *Soil Sci. Soc. Am. J.* **1969**, 33, 606–609.
73. Conyers, L.B. *Ground-Penetrating Radar for Archaeology*. Third edition. Altamira Press, Lanham, MD, 2013.
74. Deutsche Bundesstiftung Umwelt, Steckbriefe moorsubstrate. Hochschule für nachhaltige Entwicklung (FH), 2011.
75. Gomberg, J., Waldron, B., Schweig, E., Hwang, H., Webbers, A., van Arsdale, R., Tucker, K., Williams, R., Street, R., Mayne, P., Stephenson, W., Odum, J., Cramer, C., Updike, R., Hutson, S., Bradley, M. Lithology and shear-wave velocity in Memphis, Tennessee. *Bulletin of the Seismological Society of America* **2003**, 93 (3), pp. 986-997
76. Bokelmann, K. Duvensee, Wohnplatz 9: Ein präboreal-zeitlicher Lagerplatz in Schleswig-Holstein. *Offa* 48: 75–114. 1991
77. Neal, A. Ground-penetrating radar and its use in sedimentology: principles, problems and progress *earth-Science Reviews* **2004**, 261-330.
78. Curtis, J.O. Moisture effects on the dielectric properties of soils. *IEEE transactions on geoscience and remote sensing* **2001**, 39(1), 125-128. <https://doi.org/10.1109/36.898673>
79. McNeill, J. D. *Electrical conductivity of soils and rocks*. Geonics Limited. 1980.
80. Gustavsen, L., Cannell, R.J., Nau, E., Tønning, C., Trinks, I., Kristiansen, M., and Poscetti, V. Archaeological prospection of a specialized cooking-pits at Lunde in Vestfold, Norway. *Archaeological Prospection* **2018**, 25(1), 17-31
81. Groß, R. Untersuchung zur Ausbreitung elektromagnetischer Wellen in wassergesättigt Medien und Kartierung von Mooren mit dem EMR-Verfahren (Investigation of the dispersion of electromagnetic waves in water-saturated media and mapping of peatlands with the EMR-techniques). (PhD-thesis) University of Münster, Germany, 1997

82. Anbazhagan, P., Uday, A. SR Moustafa, S., S N Al-Arifi, N. Correlation of densities with shear wave velocities and SPT N values. *Journal of Geophysics and Engineering* **2016**, 13, 320-341
83. Garia, S., Pal, AK., Ravi, K., M Nair, A., A comprehensive analysis on the relationship between elastic wave velocities and petrophysical properties of sedimentary rocks based on laboratory measurements. *Journal of petroleum Exploration and Production Technology* **2019**, 9, 1869-1881
84. Price, J.S., Schlotzhauer, S.M. Importance of shrinkage and compression in determining water storage changes in peat: the case of a mined peatland. *Hydrol. Process.* **1999**, 13, 2591–2601.
85. van Asselen, S., Stouthamer, E. and van Asch, Th.W.J. Effects of peat compaction on delta evolution: a review on processes, responses, measuring and modeling. *Earth Sci.Rev.*, **2009**, 92, 35-51.
86. van Asselen, S. The contribution of peat compaction to total basin subsidence: implications for the provision of accommodation space in organic-rich deltas. *Basin research* **2011**, 23, 239-255. doi: 10.1111/j.1365-2117.2010.00482.x
87. Frolking, S., N. T. Roulet, T. R. Moore, P. J. H. Richard, M. Lavoie, and S. D. Muller Modeling northern peatland decomposition and peat accumulation. *Ecosystems* **2001**, 4, 479–498, doi:10.1007/s10021-001-0105-1.
88. Swanson, D. K., and Grigal, D. F. A simulation model of mire patterning. *Oikos* **1988**, 53, 309–314, doi:10.2307/3565529.
89. Couwenberg, J., and Joosten, H. Self-organisation in raised bog patterning: The origin of microtope zonation and mesotope diversity *J. Ecol.* **2005**, 93, 1238– 1248, doi:10.1111/j.1365-2745.2005.01035.x.
90. Mighall, T.M., Dumayne-Peaty, L., Cranstone, D. A record of atmospheric pollution and vegetation change as recorded in three peat bogs from the Northern Pennines Pb-Zn *Orefield. Environ. Archaeol.* **2004**, 9, 13–38.
91. Dreibrodt, S., Lomax, J., Nelle, O., Lubos, C., Fischer, P., Mitusov, A., Reiss, S., Radtke, U., Grootes, P.M., Bork, H.-R. Are mid Latitude slope deposits sensitive to climatic oscillations? – Implications from an Early Holocene sequence of slope deposits and buried soils from Eastern Germany. *Geomorphology* **2010**, 122, 351-369.
92. Comas, X., Slater, L., and Reeve, A. Pool patterning in a northern peatland: geophysical evidence for the role of postglacial landforms . *J. Hydrol* **2011**, 399, 173-184

93. Köhn, D., Wilken, D., Wunderlich, T., De Nil, D., Rabbel, W., Werther L., Schmidt J., Zielhofer C., and Linzen S., 2018 Seismic SH full waveform inversion as new prospection method in archaeo-geophysics,. 80th Conference and Exhibition, EAGE.
94. Köhn, D., Wilken, D., De Nil, D., Wunderlich, T., Rabbel, W., Werther, L. et al. Comparison of time-domain SH waveform inversion strategies based on sequential low and bandpass filtered data for improved resolution in near-surface prospecting. *Journal of Applied Geophysics* **2019**, 160, 69–83.
95. Schwardt M., Köhn D., Wunderlich T., Wilken D., Seeliger M., Schmidts T., Brückner H., Başaran S., Rabbel W., 2020. Characterisation of silty to fine-sandy sediments with SH-waves: full waveform inversion in comparison to other geophysical methods. *Near Surface Geophysics* 18 (3): 217-248 DOI:[10.1002/nsg.12097](https://doi.org/10.1002/nsg.12097)
96. Socco, L., Foti, S. and Boiero, D. Surface-wave analysis for building near-surface velocity models – established approaches and new perspectives. *Geophysics*, **2010** 75, A83–A102.
97. Constable, S.C., Parker, R.L., and Constable, C.G., Occam’s inversion: A practical algorithm for generating smooth models from electromagnetic sounding data. *Geophysics*, **1987**, 52 (3), 289–300.
98. Schwärzel, K., Renger, M., Sauerbrey, R., Wessolek, G., Soil physical characteristics of peat soils. *J. Plant Nutr. Soil Sci.* **2002**, 165, 479–486.
99. Malloy, S., and Pice, JS., Consolidation of hyttja in a rewetted fen peatland: Potential implications for restoration. *Mires and peat* 19. Article 05, 1-15
100. Walter, J., Lück, E., Bauriegel A., Richter, C., Zeitz, J., 2019. Multi-scale analysis of electrical conductivity of peatlands for the assessment of peat properties. *Eur J. Soil Sci* 66, 639-650

Acknowledgement

I'd like to thank my supervisor Wolfgang Rabbel for the support and motivation during the PhD. Moreover, I'd like to thank all my colleagues of the applied Geophysics group for the support and the patience during these three years, and in particular for the nice moments together at the institute and in the field.

I thank the colleagues of the SFB 1266 for the fantastic opportunity to be part of such a big interdisciplinary project. Thank for the support during field work , writing and discussing.

Tanks to all of you.

